

Continental to Shallow Marine Transition in a Tide-Dominated, Low Accommodation Basin - Controlling Factors and Depositional Architecture

Valentin Zuchuat



Faculty of Mathematics and Natural Sciences
Department of Geosciences
University of Oslo Norway

A thesis submitted for the degree of
Philosophiae Doctor (PhD)
November 2018

Preface

This doctoral thesis has been submitted to the Department of Geosciences at the University of Oslo (UiO) for the attainment of degree of *Philosophiae Doctor* (PhD). The candidate has been enrolled as a PhD research fellow at this institute between August 2015 and January 2019. The work presented herein was funded by the Norwegian Research Council's COPASS grant 244049. Associate Professor Ivar Midtkandal was the main supervisor of this thesis, and Professor Alvar Braathen has acted as co-supervisor.

It is important to note that the work of four UiO's master students was also partially incorporated in the published and submitted manuscripts. This work also involved collaborations with the scientific institutions: The departments of geology at Western Colorado University and Utah State University, the Utah Geological Survey, and the University of Keele's Basin Dynamics Research Group.

This thesis collects and combines the results of these three and a half years of study. It is articulated as two parts: The first section provides the necessary *a priori* and introductory knowledge to the results presented in the second part, which is a compilation of the three first authored articles and constitutes the main body of the thesis. The first manuscript was published in *Geology of the Intermountain West* in 2018, and the two other manuscripts, submitted to *The Journal of Sedimentary Research*, and to *The Depositional Record* respectively, were in still in review at the time of this thesis' submission. The appendix section of this thesis includes: (i) Five first authored abstracts submitted to international conferences (International Meeting of Sedimentology (IMS), Toulouse, 2017; British Sedimentological Research Group (BSRG) annual meeting, Newcastle 2017; International Sedimentological Congress, Québec-City, 2018; BSRG annual meeting, Edinburgh, 2018; Winter Conference, Bergen, 2019), (ii) three co-authored extended abstracts (International Conference on Greenhouse Gas Control Technologies (GHGT), Lausanne, 2017; GHGT, Melbourne, 2018), and five co-authored abstracts (IMS, Toulouse, 2017; Winter Conference, Copenhagen, 2018; GHGT, Melbourne, 2018). The appendix section also lists a number of side-projects in which in which the candidate has also participated during the PhD period, which are not related to the COPASS project.

Valentin Zuchuat

Oslo, November 2018

Abstract

Modern tide-dominated, regressive shorelines featuring deltas estuaries and lagoons are well characterised and distinctive from wave or fluvial dominated systems. However, some ancient tide-dominated basins and their associated sedimentary successions do not relate well to any of the above-mentioned, present-day systems. The Utah-Idaho Trough a semi-enclosed, narrow, and shallow foreland basin flooded during the Upper Jurassic by the Curtis Sea is one of these exceptions. The main target of this doctoral thesis is the Upper Jurassic, tide-dominated Curtis Formation, which outcrops in east-Central Utah, where it overlies the Middle Jurassic, aeolian deposits of the Entrada Sandstone. The Curtis Formation is defined at its base by the J-3 Unconformity and is conformably overlain by supratidal sabkha deposits of the Summerville Formation.

The Entrada-Curtis-Summerville is subdivided into eight facies associations (FA 1-8), with six sub-facies associations (FA 1a, 1b, 3a, 3b, 4a, 4b). Based on the specific three-dimensional arrangement of these facies associations, it is proposed to separate the Curtis Formation into three informal sub-units: The lower, middle and upper Curtis. The lower Curtis, which consists of upper shoreface to beach deposits (FA 2), mud- (FA 3a) and sand-dominated heterolithic subtidal flat sediments (FA 3b), sand-rich sub- to supratidal flat deposits (FA 4a) and correlative tidal channel infill (FA 4c). The lower Curtis recorded the development of three parasequences separated by traceable flooding surfaces. These parasequences are related to relative sea-level variations within this 800x150 km basin. The succeeding middle Curtis coincides with FA 5, well-sorted, very-fine- to fine-grained, sub- to intertidal channel-dune-flat complex. Its lower boundary corresponds to a transgressive/ravinement surface of regional extent, identified as the Major Transgressive Surface (MTS). This surface's extent suggests a potential correlation between the middle and the upper Curtis and the neighbouring Todilto Member of the Wanakah Formation or Todilto Formation in the "Four Corners" area. The middle Curtis is also characterised by a lack of traceable stratigraphic surfaces. The upper Curtis conformably overlies the middle Curtis, and consists of heterolithic upper sub- to intertidal flat deposits (FA 6). Towards the Utah-Colorado border in the east of the study area, FA 6 is replaced by FA 7 aeolian dunes, which corresponds to the Moab Member of the Curtis Formation. The Moab Member recorded the development of five aeolian sequences, separated by supersurfaces. The Curtis Formation is conformably overlain by the supratidal, rusty red to dark brown, evaporite-rich, sabkha deposits of Summerville Formation (FA 8), which also recorded cyclical variations, as suggested by preliminary petrophysical data.

The exhumed J-3 Unconformity displays eight different relief expressions, including; (i) angular unconformity, (ii) paraconformity, (iii) steep incisions, (iv) undulating relief, (v) irregular relief, which comprises fault-plane- and erosion-related relief irregularities, (vi) circular collapsed structures, (vii) hydroplastic sagging, and (viii) sedimentary loading. The relief's types i-v were generated by erosion-related processes, such as aeolian deflation, and water-induced erosion, whereas categories vi-viii were driven by brittle and plastic deformational processes. Thus, the J-3 Unconformity is a poly-genetic and heterochronous surface. The various processes that shaped this bounding surface did not only interact in a three-dimensional space, but also in time. Further, the J-3 Unconformity is a non-

unique bounding surface, as similar relief geometries can be produced by different processes, and one single process can generate different geometries. Because the aeolian Entrada and shallow-marine lower Curtis systems coexisted as the Utah Idaho Trough was being transgressed, the composite flooding-ravinement surface separating the two depositional systems is time-transgressive. Consequently, the regionally-extended, composite, heterochronous, non-unique J-3 Unconformity does not match with the classic unconformity-as-time-barrier definition, which states that such surfaces of erosion or nondeposition must separate older strata below from younger strata above them, and encapsulate a significant hiatus. Consequently, the marginal marine earthy facies of the Entrada Sandstone is regarded as forming a syn-transgressional unit to the shallow-marine lower Curtis, whereas the Moab Member of the Curtis Formation's aeolian dune field, as well as the supratidal deposits of the Summerville Formation must have co-existed with the middle- and the upper Curtis.

The poly-genetic and heterochronous nature of the J-3 Unconformity, as well the lower Curtis parasequences, the Moab Member's aeolian sequences, and the apparent cyclicity recorded by the Entrada Sandstone and the Summerville Formation suggest that neighbouring continental and shallow-marine systems were contemporaneous and predominantly responded to allocyclicly-driven relative sea-level variations, with the exception of the middle Curtis. Indeed, as the middle Curtis was deposited, autocyclic processes have erased any allocyclic processes' signature and associated traceable stratigraphic surfaces. The transition from a shallow marine, tide-dominated system, predominantly impacted by allocyclic processes, to a tide-dominated basin in which autocyclic behaviours overprinted any evidence of allocyclic forcing, reflects the onset of a tidal resonant stage, as the Curtis basin reached the optimal length-to-width configuration.

This work highlights the significant amount of information the study of stratigraphic surfaces can contribute to the understanding of a basin's dynamic history. It also emphasises on the importance of extending the research focus to neighbouring and contemporaneous sedimentary systems, in order to compensate for any potential intraformational signal loss.

Acknowledgments

First and foremost, I would like to acknowledge my principal supervisor, Associate Professor Ivar Midtkandal (UiO), for allowing me to join his team with this amazing PhD opportunity and field experiences. You truly helped me sailing through this academic journey, which has not always been straight forward. You showed me the ropes, and helped me grow, not only as a young and critical researcher, but also as a member of the scientific community, always encouraging external collaborations. And nothing would have been possible without your academic and/or moral support. I learned a lot from you, except enjoying telemark skiing, and your practical approach to research will remain a great example to follow. I further would like to thank my co-supervisor, Professor Alvar Braathen (UiO). You always kept your door open when I had questions. You taught me to be bold, and your sharp mind, your good old field stories, and your excellent humour were always much appreciated.

I want to extend my gratitude to all the nice people I worked with and met through this project, both in the field, and at conferences. A special mention goes to Dr Elizabeth Petrie, Moncrief Chair in Petroleum Geology, Western Colorado University. Thank you for speaking the much appreciated sarcasm language I do love! I want to thank Nate the Legend Cote for coming out of the closet, and admitting his love and admiration for the sedimentary ripple. It was a great pleasure being there for such a touching moment. I really want to thank all the lovely people working at La Pasadita in Green River, you made my stay in Utah absolutely unforgettable!

I would like to extend my sincere regards to my friends and colleagues, in Oslo and elsewhere, who really helped me, maybe without noticing it, going through my PhD. I first want to thank my office mates Anna and Arve. Despite your impeccable work ethics, you never judged my more Mediterranean approach to office hour and/or lunch. You were always keen on repeating your stories once I arrived in the office, besides allowing me to interrupt your work to talk about surfaces and other important gossips. I also need to say thank you to Dr Anja, and her imaginary boat. Thank you for being the most social Norwegian out there, and for joining me for a couple of weeks camping in Utah's wilderness, even if I snored a little! A special high five/fist bump has to be thrown at Dr Miquel and Dr Mark. You guys are two of the most impressive and inspirational young scientists I have ever met, on top of being some of the sharpest mind around! Extreme John is also to be strongly acknowledged. You always kept on joining whatever spontaneous plans we had, and that was awesome!

I also want to say thank you to my friends and lover of the good food here in Oslo: Bjarki, Bruce, and Ruben! You were always up for a nice meal, a good inappropriate laugh, and sharing some unforgettable wedding stories, especially once the wine and the whisky started flowing! Mr Scott is also not to be forgotten, as you are my favourite skiing buddy out there, even though you also appreciate "å gå på ski". I can't write these acknowledgements without mentioning my best friends Nathaniel, Daniele, Mathieu, Mats, and Gareth. You guys were always willing to come and say hello to Oslo when I couldn't travel to see you. I <insert swear word> love you guys! I also want to thank all the amazing people who visited me in Norway: the team école de ski, with Caro and Chantal, the

Garlic Surprise Crew, with Anna, Dori, Pauline, and Michael, as well as Caro and Thibaud from Team Fribourg. Seeing you up here meant a lot to me.

This list wouldn't be complete without thanking Rebecca. You are one of the first people who truly understood me, and really got me going through this journey, wherever you were on the planet. Your free spirit will always inspire me! There is a special and extraordinary person I want to thank, after she grabbed my attention in Québec: Dr Hannah Louise Brooks. You were the little extra spark I needed to finish this thesis in time. Thank you so much!

Finally, I would like to most sincerely thank my family in Switzerland, Marcel, Marie-Noëlle, Marie and Lucien. Going back home is always a pleasure when you know people like you. Et tout ce que j'ai achevé jusqu'ici n'aurait simplement pas été possible sans votre soutien inconditionnel! Merci du fond du cœur pour tout ce que vous avez fait pour moi! Je vous aime!

List of articles

Article I – Published in *Geology of the Intermountain West*

Zuchuat, V.¹, Sleveland, A.R.N.¹, Sprinkel, D.A.², Rimkus, A.¹, Braathen, A.¹, and Midtkandal, I.¹ (2018). New Insights on the Impact of Tidal Currents on a Low-gradient, Semi-enclosed, Epicontinental Basin – the Curtis Formation, East-Central Utah, USA. *Geology of the Intermountain West*, 5, 131-165. DOI: <https://doi.org/10.31711/giw.v5i0.24>.

¹*Tectonostratigraphic Research Group, University of Oslo, Sem Sælands Vei 1, 0371 Oslo, Norway*

²*Utah Geological Survey, PO Box 146100, Salt Lake City, Utah 84114*

Article II – Submitted to *The Journal of Sedimentary Research*

Zuchuat, V.¹, Midtkandal, I.¹, Poyatos-Moré, M.¹, Da Costa, S.¹, Halvorsen, K.¹, Cote, N.², Sundal, A.¹, and Braathen, A.¹ (in review). Composite Unconformities in Low-Gradient, Transitional Settings: the J-3 Unconformity and the Curtis Formation, East-Central Utah, USA. Submitted to *The Journal of Sedimentary Research*.

¹*Tectonostratigraphic Research Group, University of Oslo, Sem Sælands Vei 1, 0371 Oslo, Norway*

²*Natural and Environmental Sciences Department, Western State Colorado University, 600 North Adams Street, Gunnison, CO 81231*

Article III – Submitted to *The Depositional Record*

Zuchuat, V.¹, Sleveland, A.R.N.¹, Pettigrew, R.P.², Dodd, T.J.H.², Clarke, S.M.², Rabbel, O.¹, Braathen, A.¹, and Midtkandal, I.¹ (in review). Overprinted Allocyclic Processes by Tidal Resonance in an Epicontinental Basin: the Upper Jurassic Curtis Formation, East-Central Utah, USA. Submitted to *The Depositional Record*.

¹*Tectonostratigraphic Research Group, University of Oslo, Sem Sælands Vei 1, 0371 Oslo, Norway*

²*Basin Dynamics Research Group, Keele University, Keele, Staffordshire, ST5 5BG, United Kingdom*

Contents

Preface	I
Abstract	III
Acknowledgments	V
List of articles	VII
1. Introduction	1
1.1. Motivation	1
1.2. Aims, objectives, and study area	1
2. Geological Context	5
2.1. Basinal setting	5
2.2. Stratigraphy	5
3. Data and Methods	11
4. Article summaries, authorship and contribution	13
4.1. Article I: New Insights on the Impact of Tidal Currents on a Low-gradient, Semi-enclosed, Epicontinental Basin – the Curtis Formation, East-central Utah, USA.	13
4.2. Article II: Composite Unconformities in Low-Gradient, Transitional Settings: the J-3 Unconformity and the Curtis Formation, East-Central Utah, USA.	17
4.3. Article III: Overprinted Allocyclic Processes by Tidal Resonance in an Epicontinental Basin: the Upper Jurassic Curtis Formation, East-Central Utah, USA.	21
5. Discussion, application, and conclusive remarks	25
Further studies	28
6. References	29
7. Articles	35
7.1. Article I: New Insights on the Impact of Tidal Currents on a Low-gradient, Semi-enclosed, Epicontinental Basin – the Curtis Formation, East-central Utah, USA.	35
7.2. Article II: Composite Unconformities in Low-Gradient, Transitional Settings: the J-3 Unconformity and the Curtis Formation, East-Central Utah, USA.	75
7.3. Article III: Overprinted Allocyclic Processes by Tidal Resonance in an Epicontinental Basin: the Upper Jurassic Curtis Formation, East-Central Utah, USA.	111

8. Appendix	161
8.1. Abstracts, first author	161
8.1.1. <i>Zuchuat et al. (2017). International Meeting of Sedimentology, Toulouse</i>	161
8.1.2. <i>Zuchuat et al. (2017). British Sedimentological Research Group, Annual General Meeting, Newcastle upon Tyne</i>	165
8.1.3. <i>Zuchuat et al. (2018). International Sedimentological Congress, Québec City, 2018</i>	169
8.1.4. <i>Zuchuat et al. (2018). British Sedimentological Research Group, Annual General Meeting, Edinburgh, 2018</i>	173
8.1.5. <i>Zuchuat et al. (2019). Vinterkonferansen, Bergen 2019</i>	177
8.2. Extended abstracts, co-author	181
8.2.1. <i>Midtkandal et al. (2018). International Conference on Greenhouse Gas Control Technologies, Melbourne</i>	181
8.2.2. <i>Skurtveit et al. (2017). International Conference on Greenhouse Gas Control Technologies, Lausanne</i>	193
8.2.3. <i>Sundal et al. (2017). International Conference on Greenhouse Gas Control Technologies, Lausanne</i>	205
8.3. Abstracts, co-author	215
8.3.1. <i>Bromander et al. (2018). Vinterkonferansen, Copenhagen</i>	215
8.3.2. <i>Da Costa et al. (2018). Vinterkonferansen, Copenhagen</i>	219
8.3.3. <i>Halvorsen et al. (2018). Vinterkonferansen, Copenhagen</i>	223
8.3.4. <i>Midtkandal et al. (2017). International Meeting of Sedimentology, Toulouse</i>	227
8.4. External collaborations	231
8.5. Teaching and supervision	233

1. Introduction

1.1. Motivation

Subsurface reservoir characterisation requires an extensive understanding of the structural and depositional heterogeneities distributed within both the fluid bearing rock(s) and the seal unit, notably in today's perspective of frontier hydrocarbon exploration or CO₂ sequestration. As documented in several CO₂ injection projects worldwide (e.g. Eiken *et al.*, 2011; Braathen *et al.*, 2012; Sundal *et al.*, 2013; 2014; Denchik *et al.*, 2014; Sundal *et al.*, 2015; 2016), these sub-seismic scale, or marginal heterogeneities, are of pivotal importance, as they strongly impact on the flow rate and flow patterns of various fluids and fluid phases. Their detailed understanding allows for the identification of remaining uncertainties, the optimisation of geological models, the minimisation of leakage risk, and/or the improvement of fluid mobility predictions. The comprehension of such a complex geological system would then allow for distribution of these intricate heterogeneities within a realistic 4-dimensional (4D) geological framework.

Consequently, the study of outcropping reservoir analogues can grant scientists, as well as society, policy makers, and industry, important and novel knowledge on hydrocarbons, CO₂ plumes, or aquifers behaviour at relevant spatial and temporal scales. These studies provide critical data to better comprehend the inherent complexity of real geology. They help identifying which mechanisms are involved in the development of intra-reservoir trap-confining seals and flow baffles, as well as allowing for the recognition of geological factors affecting the localisation of leakage points within the system. To build these detailed models and optimised decisional tree schemes, it is essential to provide all the parties with the necessary geological background, such as the material and outcomes presented in this study.

1.2. Aims, objectives, and study area

This doctoral thesis aims at improving the sedimentological understanding of a presently exhumed Jurassic basin in east-central Utah (USA) that is naturally CO₂-charged. Strata within this basin has leaked CO₂ during several phases of its history, and continues leaking today (Kampman *et al.*, 2013; Ogata *et al.*, 2014; Skurtveit *et al.*, 2017; Sundal *et al.*, 2017). The thesis specifically focuses on the Upper Jurassic Curtis Formation (Fig. 1; Wilcox and Currie, 2008), a tide-dominated stratigraphic unit (Kreisa and Moiola, 1986; Caputo and Pryor, 1991; Article I¹) located between the underlying aeolian and marginal marine strata of the Entrada Sandstone (Gilluly and Reeside, 1928; Peterson, 1994; Hintze and Kowallis, 2009), one of the system's main reservoirs (Kampman *et al.*, 2013; Ogata *et al.*, 2014; see Fig. 2a in Article I), and the capping regional seal of the Summerville Formation's supratidal, sabkha deposits (Gilluly and Reeside, 1928; Caputo and Pryor, 1991; Peterson, 1994; Lucas, 2014).

¹ Article I refers to: Zuchuat, V., Sleveland, A.R.N., Sprinkel, D.A., Rimkus, A., Braathen, A., and Midtkandal, I. (2018). New insights on the impact of tidal currents on a low-gradient, semi-enclosed, epicontinental basin—the Curtis Formation, east-central Utah, USA. *Geology of the Intermountain West*, 5, 131-165.

Article II refers to: Zuchuat, V., Midtkandal, I., Poyatos-Moré, M., da Costa, S., Halvorsen, K., Cote N., Sundal, A., and Braathen, A. (submitted to *The Journal of Sedimentary Research*). Composite Unconformities in Low-Gradient Transitional Settings: the J-3 Unconformity and the Curtis Formation, East-Central Utah, USA.

Article III refers to: Zuchuat, V., Sleveland, A.R.N., Pettigrew, R.P., Dodd, T.J.H., Clarke, S.M., Rabbel, O., Braathen, A., and Midtkandal, I. (submitted to *The Depositional Record*). Overprinted Allocyclic Processes by Tidal Resonance in an Epicontinental Basin: the Upper Jurassic Curtis Formation, East-Central Utah, USA.

The overarching goal of this study is to develop a dynamic depositional model (Article III) which demonstrates how the system developed from an arid, continental depositional setting to a shallow-marine, tide-dominated basin, by identifying diagnostic sedimentary features for the recognition of similar transitional settings. The newly developed model, substantiated by the study of the sedimentary record (Article I), as well as the major bounding surfaces characterising the system (Article II), caters an synopsis of the spatial energy distribution and temporal energy variations recorded within a low-gradient, semi-enclosed tide-dominated basin, and their associated facies belts migration patterns. *In fine*, it helps predicting where, when, how and how much reservoir-grade sandstone and associated sedimentary baffles were deposited within similar or resembling sedimentary basins.

In order to address these points, data was collected from a 180x130 km area in the vicinity of the San Rafael Swell in east-central Utah (Fig. 1; see Chapter 3 for details about data and methods), where the Entrada-Curtis-Summerville interval is exposed. The study area extends from the Humbug Flats (1 to 5²), north of the San Rafael Swell, southward to Notom Ranch (35), 44 km southwest of Hanksville, and from Last Chance Desert (38 and 39) on the western margin of the San Rafael Swell, eastward to Big Pinto Mesa (30) on the Utah-Colorado border.

² Numbers in parenthesis following the names of places refer to locality numbers on Fig. 1.

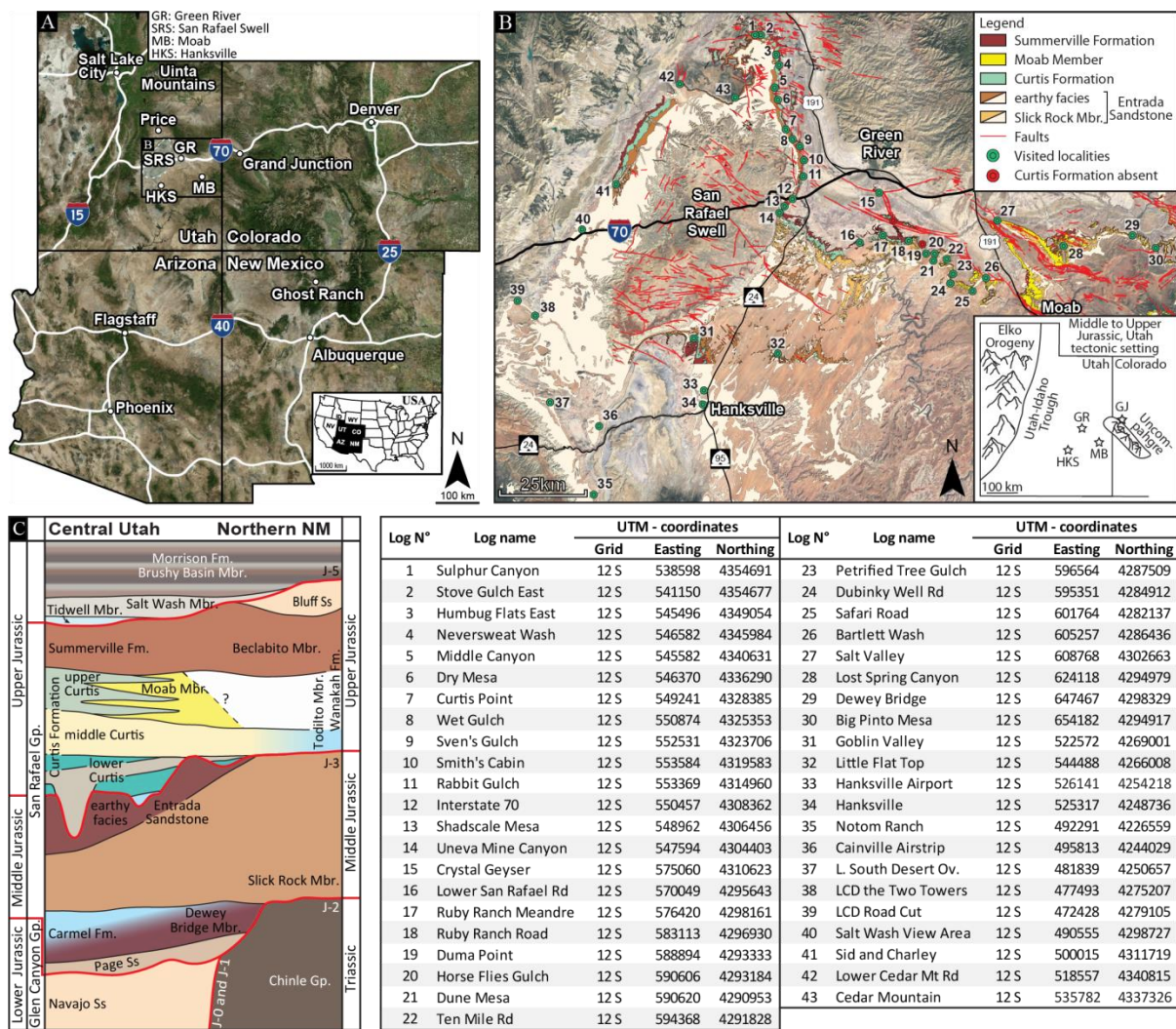


Fig. 1 – A-B. Maps of the study area, with highlighted outcropping extent of the Entrada-Curtis-Summerville interval on the map B. Green dots represent visited localities where the Curtis Formation crops out, while the red dots indicate that the Summerville Formation directly overlies the Entrada Sandstone. Each code number on the map B refers to a specific locality in the attached table (Geological units after Hintze, 1980; Witkind, 1988; Doelling, 2001; and Doelling et al., 2015; Tectonic setting after Heyman, 1983; Thorman, 2011). GJ: Grand Junction, GR: Green River, HKS: Hanksville, MB: Moab, SRS: San Rafael Swell. **C.** Schematic lithostratigraphic column showing a correlation between the San Rafael Swell area, east-central Utah, and Ghost Ranch, in northern New Mexico (Doelling, 2001; Doelling et al., 2015; Kocurek et al., in press; Article 1). Note that the contemporaneous character between the Entrada Sandstone and the lower Curtis, as well as between the middle Curtis, upper Curtis, Moab Member, and Summerville Formation is not shown in this lithostratigraphic display.

2. Geological Context

2.1. Basinal setting

Four major tectonic events impacted on Utah's geological development since the early Mesozoic, and the rise of the North American Cordillera (Hintze and Kowallis, 2009; Thorman, 2011; Anderson, 2015; Yonkee and Weil, 2015; and references therein): (i) The Nevadan Orogeny (Middle Jurassic-Lower Cretaceous), whose granitic intrusions can be observed at today's Utah-Nevada border, (ii) the Elko Orogeny (Middle Jurassic), characterised by alternating episodes of tectonic contraction and extensions, accompanied by the development of SSW-NNE-striking, stacked foreland basin development, (iii) the Sevier Orogeny (Lower Cretaceous to Paleogene), featuring thin-skinned contractional structures, and (iv) the Laramide Orogeny (Upper Cretaceous to Paleogene), associated with the development of basement-rooted monoclines, such as the San Rafael Swell (Bump and Davis, 2003).

The Stratigraphy of central-eastern Utah was also affected by diapirism and remobilisation of the Paradox Basin evaporitic strata (Trudgill, 2011), as well as by the Colorado Plateau uplift and its sub-regional to regional extensional episodes (Levander *et al.*, 2011; Murray *et al.*, 2016). The igneous intrusive complexes of the Abajo, Henry, and La Sal Mountains (Upper Oligocene) also impacted on the sedimentary strata in central-eastern Utah (Sullivan *et al.*, 1991; Nelson, 1997). The Upper Callovian to Lower Oxfordian Entrada-Curtis-Summerville lithostratigraphic sub-divisions were deposited within the Utah-Idaho Trough, a SSW-NNE-oriented retroarc foreland basin at the foot of the Elko Highlands (Thorman, 2011), which the Sundance Sea to the north flooded several times during its history (Hintze and Kowallis, 2009). In the San Rafael Swell area (Fig. 1), the Curtis Formation was buried between 2.45 km and 2.86 km (Nuccio and Condon, 1996; Petrie *et al.*, 2017).

2.2. Stratigraphy

The Middle Jurassic Entrada Sandstone of south-eastern Utah, and the overlying Upper Jurassic Curtis and Summerville formations, the coastal to shallow marine Temple Cap Formation, the aeolian Page Sandstone, and the shallow- to marginal-marine Carmel Formation comprise the San Rafael Group of the Colorado Plateau (Fig. 1C; Gilluly and Reeside, 1928; Pippingos and O'Sullivan, 1978; Peterson and Pippingos, 1979; Anderson and Lucas, 1994; Sprinkel *et al.*, 2011). These sediments represent five upward-thinning, transgressive-regressive (TR) sequences with an eastward- and southward-wedging geometry that is a consequence of deposition within the Utah-Idaho Trough (Fig. 2B; Anderson and Lucas, 1994; Brenner and Peterson, 1994; Peterson, 1994; Bjerrum and Dorsey, 1995; Thorman, 2011).

As the Middle Jurassic shallow epeiric Sundance Sea, which covered North America at this time, regressed northward during the Callovian Age, sediments of the shallow- to marginal-marine Carmel Formation (Fig. 1C) were overlain conformably by those of the marginal-marine to continental, rusty-red to light-orange, aeolian Entrada Sandstone, as warm arid conditions prevailed (Fig. 1C, Fig. 2a, 2b; Gilluly and Reeside, 1928; Peterson, 1994; Hintze and Kowallis, 2009). The Entrada Sandstone is typically divided into (i) the Slick Rock Member that comprises aeolian dune and interdune sediments,

and (ii) the overlying and partially contemporary informal unit of the 'earthy facies' (Imlay, 1952), characterised by repeated yet extraneously vegetated, mottled loess strata, interbedded with marginal-marine sabkha-like deposits (Witkind, 1988; Doelling *et al.*, 2015; and references therein). The Entrada Sandstone thickens northwards and westwards, in the direction of the Utah-Idaho Trough (Fig. 1; Witkind, 1988; Crabaugh and Kocurek, 1993; Kocurek and Havholm, 1993; Carr-Crabaugh and Kocurek, 1998; Mountney, 2012; Doelling *et al.*, 2015). The earthy facies thins out to the south and east of the study area, where the sediments of the Curtis Formation directly overlie the Slick Rock Member. Recycled fluvial sediments originating from the Appalachian Mountains are the main constituents of the Entrada Sandstone (Dickinson and Gehrels 2009, 2010). Four 'construction-destruction' sequences (*sensu* Mountney, 2006), related to regional base-level oscillations, are recognised within this coastal aeolian system (Carr-Crabaugh and Kocurek, 1998; Kocurek and Lancaster, 1999; Kocurek, 2003; Mountney, 2012), and the Entrada Sandstone is capped at its top by the regional, polygenetic, and heterochronous J-3 Unconformity (Article I, II), first defined by Pippingos and O'Sullivan (1978). The unconformity displays relief with an amplitude ranging from 0.1 m to 23 m, and a wavelength varying from decimetre to hectometre scale (Article II). Relief was generated by erosion-related processes resulting in flat angular unconformities, paraconformities, steep tidal incisions, sinuous undulations, and irregular tidal ravinement surfaces (Article II). Brittle and plastic deformational processes also impacted on the J-3 Unconformity's relief, leading to the development of circular collapse structures, sedimentary loading, and hydroplastic sagging (Article II).

The Entrada Sandstone is overlain by the lower Oxfordian Curtis Formation, originally defined by Gilluly and Reeside (1928) from exposures along the northeast margin of the San Rafael Swell (Fig. 2). The Curtis sediments comprise complexly arranged, shallow-marine, tide-dominated heterolithic (Kreisa and Moiola, 1986; Caputo and Pryor, 1991; Wilcox and Currie, 2008; Ogg *et al.*, 2016; Article I) deposited as the Curtis Sea flooded a gently dipping, shallow, and fluvially starved, epicontinental basin that developed as the rate of creation of accommodation diminished at end of the Callovian Age (Thorman, 2011; Article I). The Curtis Formation has a green to white colouration, which is due to the presence of shallow-marine glauconite and chlorite in the sediments, and it strongly contrasts with the underlying rusty-red Entrada Sandstone (Gilluly and Reeside, 1928; Caputo and Pryor, 1991; Peterson, 1994). The Curtis Sea basin reached approximately 800 km in length, and at least 150 km in width. As a result, the Curtis Formation is characterised by an east- and south-wedging geometry, with a maximum thickness of approximately 80 m at Sven's Gulch (9), in the San Rafael Swell area (Gilluly and Reeside, 1928; Caputo and Pryor, 1991; Peterson, 1994; Thorman, 2011; Anderson, 2015; see also Fig. 2 and Fig. 3 in Article I).

This study allows for the Curtis Formation is separated into three informal units based on their outcrop character: the lower, middle, and upper Curtis (Fig. 1C; Article I). The lower Curtis (Fig. 2c-g) comprises laterally restricted upper shoreface to beach deposits, grading into thinly bedded, dark-green to grey, heterolithic subtidal flat deposits in which gravel-rich, subtidal channels and dunes occur (Article I). The overlying middle Curtis (Fig. 2h) is characterised by a lighter coloured and better sorted sandstone by comparison to the underlying heterolithic lower Curtis (Article I). Its base corresponds to the regional Major Transgressive Surface (MTS, Article I, II), and consists of complex

arrangements of subtidal channels, sub-to intertidal dune and flat deposits (Article I). The dark green, upper Curtis (Fig. 2i) conformably overlies the middle Curtis, and comprises thinly bedded, sub- to intertidal deposits, which grade into the supratidal deposits of the Summerville Formation (Article I). Towards the Utah-Colorado border (Fig. 1), these deposits form lateral and contemporaneous equivalents to the aeolian deposits that form Moab Member of the Curtis Formation (Fig. 1C, Fig. 2j; Caputo and Pryor, 1991; Peterson, 1994; Doelling, 2001; Article I). The underrepresentation of wave-related structures within the Curtis Formation can be attributed to the protected nature of the Curtis Sea, as well as the elongate basin configuration, which facilitated dissipation of wave energy (Yoshida *et al.*, 2007).

Throughout the study area (Fig. 1), the Upper Curtis is overlain conformably by dark brown, sabkha deposits of the Summerville Formation (Fig. 1C, Fig. 2k; Gilluly and Reeside, 1928; Caputo and Pryor, 1991; Peterson, 1994; Lucas, 2014). However, in the unflooded neighbouring regions to the east and to the south, the Summerville Formation must have coexisted with the Curtis Formation forming a nearby coastal plain environment (Article I, II, III).

In the 'Four Corners' area, where the states of Utah, Colorado, Arizona and New Mexico meet (Fig. 1a), the Todilto Member of the Wanakah Formation is the lateral equivalent of the Curtis, while the Beclabito Member of the Wanakah Formation corresponds to the Summerville (Fig. 1c; Condon and Huffman, 1988; Kocurek *et al.*, in press; Article I, II). Further north in the Uinta Mountains area (Fig. 2a), the Curtis-Summerville interval is the lateral equivalent of the Stump Formation (Pipiringos and Imlay, 1979; Imlay, 1980; Wilcox and Currie, 2008). More regionally, it is equivalent to the Redwater Shale Member of the Sundance Formation in Wyoming (Imlay, 1947, 1980), and the Stump Formation in the vicinity of the Wyoming-Idaho border (Mansfield and Roundy, 1916; Pipiringos and Imlay, 1979; Imlay, 1980).

The Curtis-Summerville interval corresponds to Peterson's (1994) fifth (TR) cycle within the Jurassic system of the Sundance Sea and the Western Interior Basin (Pipiringos and O'Sullivan, 1978; McMullen *et al.*, 2014), and likely corresponds to the LZA-2.3 third-order TR-interval of Haq *et al.* (1987), after calibrating their out-of-date age column onto Wilcox and Currie's (2008) Curtis Formation age, and Ogg and others' (2016) timescale.

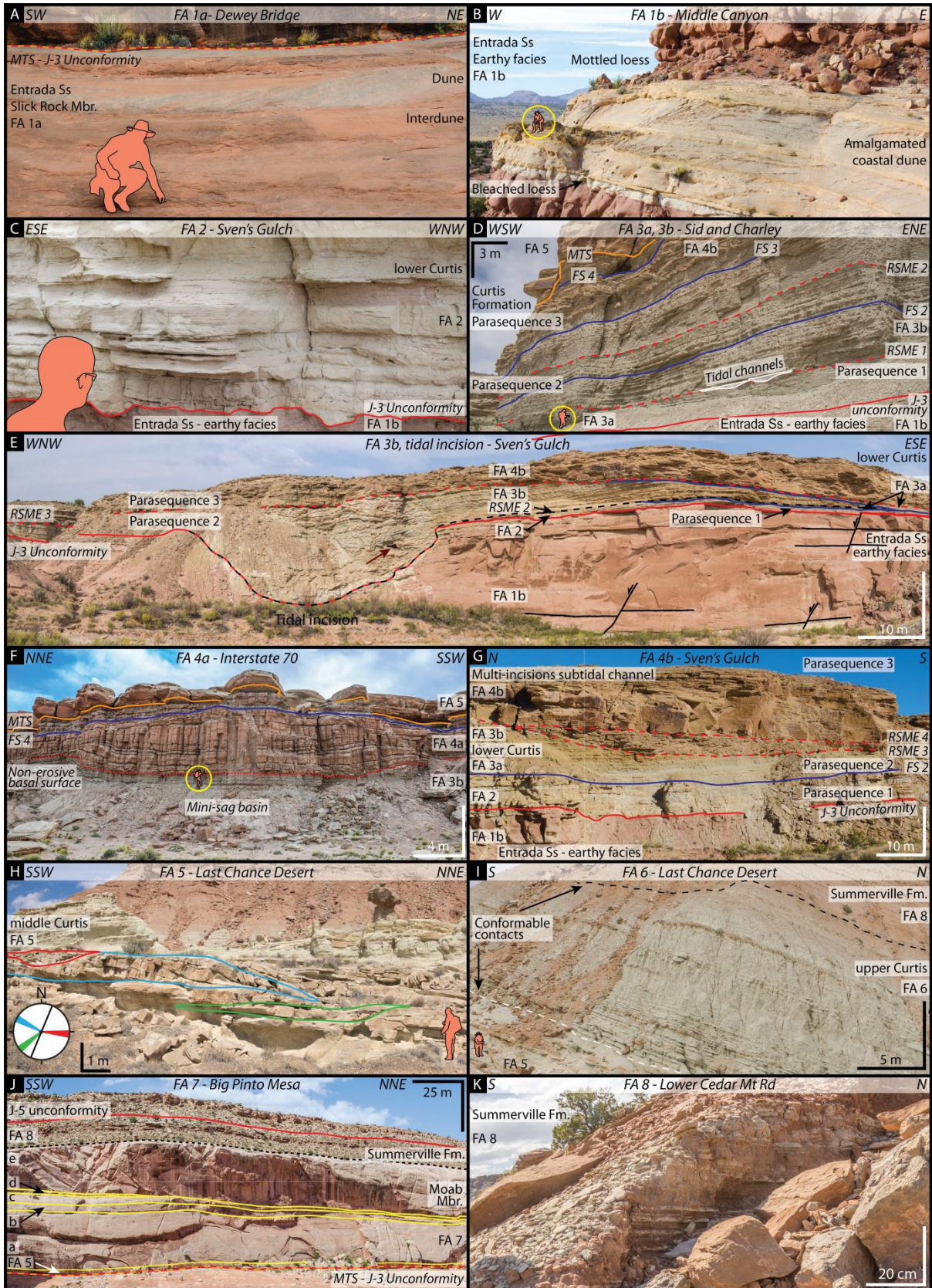


Fig. 2 (previous page; from Article III) – Summary panel of the Facies Associations (FA) cropping out with in the study area. Please refer to Article I for the detail description and interpretation of each FA. **A.** Example of wet coastal aeolian dunes of FA 1a (Entrada Sandstone, Slick Rock Member). **B.** Amalgamated aeolian coastal dunes within the fine-grained, marginal marine earthy facies of FA1b (Entrada Sandstone). Note the bleached horizon directly below the dunes. Geologist for scale. **C.** High-energy upper shoreface to beach deposits, with rip-up clasts and occasional mud-drapes. Note the loaded and eroded irregular geometry of the J-3 Unconformity. **D.** Typical stacking architecture of subtidal mud- (FA 3a) and sand-dominated heterolithic flat deposits (FA 3b). **E.** Major tidal incision observed at Sven's Gulch, carved during a short-lived regressive phase within Parasequence 2. The dark-red arrow points at a boulder of Entrada Sandstone within a matrix of FA 3b sand-dominated deposits. Note also the ravinement of Parasequence 2 deposits during the transgressive phase of Parasequence 3, followed by the by the development of a regressive and erosive, subtidal channel complex (FA 4b). **F.** Mini sag basin generated by the collapse of FA 3b deposits, as FA 4a sand-rich sub- to supratidal sandflat was being deposited. **G.** Two incision phases of FA 4b subtidal channel. **H.** Bidirectional tidal inlets (red and blue contours), and a third south-westward laterally accreting tidal channel (green contour) within a sub- to intertidal flat surrounding environment (FA 5). The respective migration direction of these three bedforms is color-coded on the rose-diagram, whereas the black line on the diagram illustrates the outcrop orientation. **I.** Conformable contact between the underlying FA 5 Sub- to intertidal channel-dune-flat complex, grading into the thinner and finer-grained FA 6 upper sub- to intertidal deposits, which are conformably overlain by FA 8 supratidal deposits of the Summerville Formation. **J.** Five aeolian sequences recorded in the Moab Member of the Curtis Formation. **K.** Close-up images of FA 8 supratidal deposits displaying regular episodes of marine flooding (white sandstone beds).

3. Data and Methods

The data necessary for this study were gathered during three field campaigns between 2015 and 2017. These have been further augmented with small-scale studies in 2018 conducted by the Basin Dynamics Research Group at Keele University. In order to cover the study area systematically along the exposure of the Entrada-Curtis-Summerville interval, forty-three localities were visited (Fig. 1). Forty-one sections were measured using contemporary field techniques to collect sedimentary, palaeocurrent and structural information, and a total of 2291 m was logged across the Entrada-Curtis-Summerville stratigraphic interval. This dataset is complemented by aerial images, as well as photographic material collected at and between the visited localities using unmanned aerial vehicles (UAV) and terrestrial techniques. Three-dimensional (3D) virtual outcrop models were produced from the collected photogrammetric material (after Westoby *et al.*, 2012), in order to document, illustrate and understand the complex 3D sedimentary architecture of the targeted interval. The models were generated using PhotoScan Pro[®] (Agisoft LLC, St. Petersburg, Russia), before being analysed and interpreted with Lime[®], a software developed by the Virtual Outcrop Geology VOG group of both Bergen and Aberdeen universities (Bonaventura *et al.*, 2017; Buckley *et al.*, 2017). To augment the sedimentary detail, 35 m of section covering the Entrada-Curtis-Summerville interval was logged using a hand-held gamma ray spectrometer in full assay mode at 20 cm intervals.

Standard facies and architectural analysis of sedimentary data permits interpretations of depositional settings. Merging sedimentary data with photogrammetric models and structural data sets provides a means of tracing key sequence stratigraphic surfaces, such as subaerial unconformities, transgressive surfaces, regressive surfaces of marine erosion, flooding surfaces, and tidal ravinement surfaces (*sensu* Catuneanu, 2006; Catuneanu *et al.*, 2009) to provide a regional sequence stratigraphic framework and interpretation.

4. Article summaries, authorship and contribution

4.1. Article I: New Insights on the Impact of Tidal Currents on a Low-gradient, Semi-enclosed, Epicontinental Basin – the Curtis Formation, East-central Utah, USA.

Key words: Curtis Formation, tidal deposits, epicontinental basin, facies associations

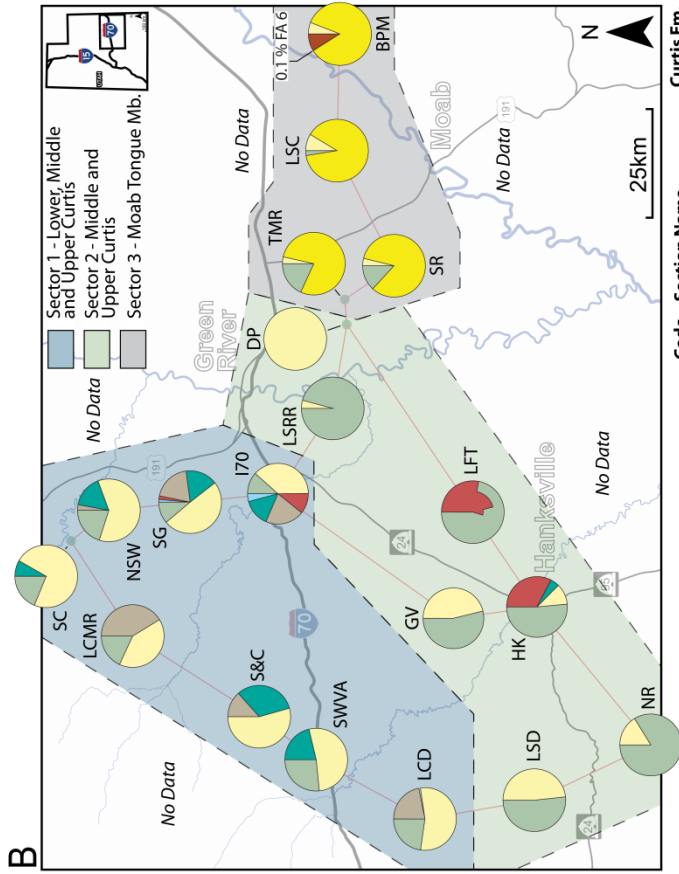
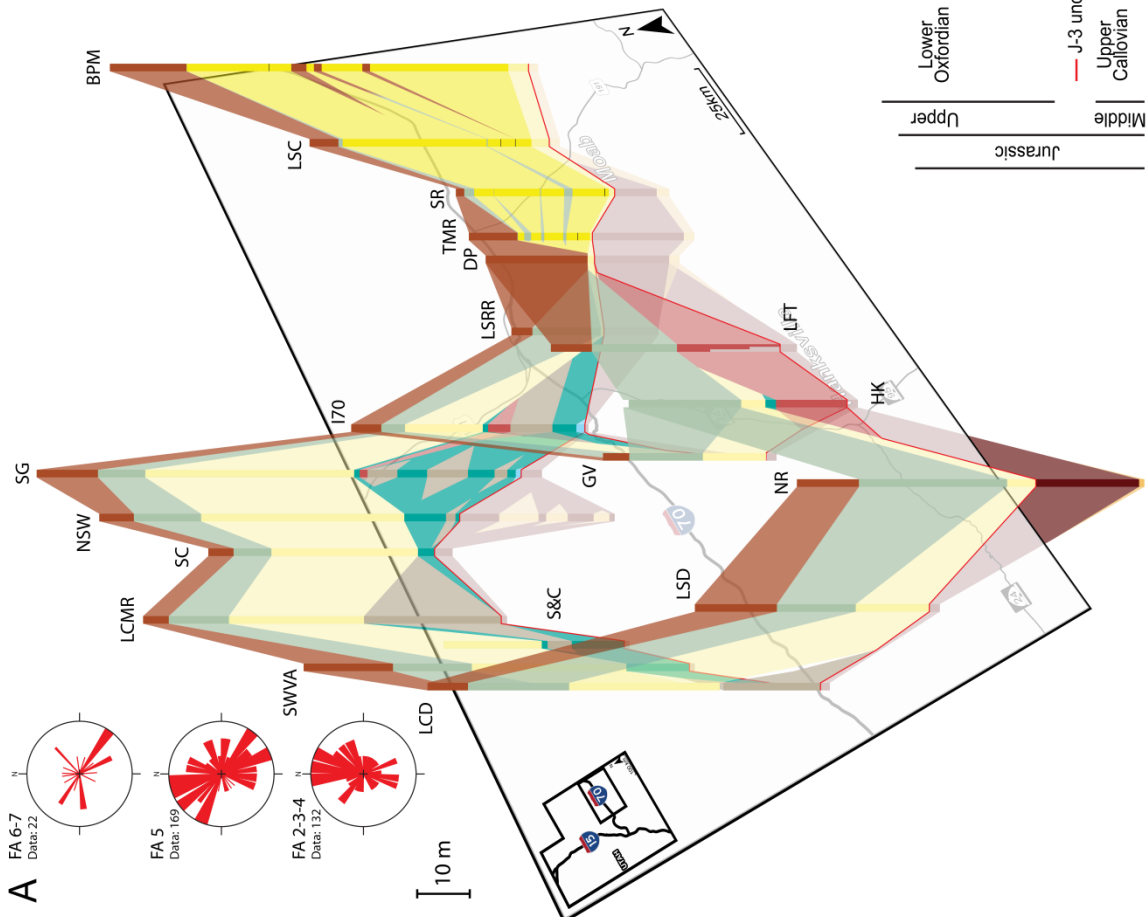
Principal author	Valentin Zuchuat
Co-authors	Arve R.N. Sleveland, Douglas A. Sprinkel, Algirdas Rimkus, Alvar Braathen, and Ivar Midtkandal
Text	Zuchuat, Sprinkel
Figures	Zuchuat, Sleveland
Concept	Zuchuat, Sprinkel, Braathen, Midtkandal
Editing	Zuchuat, Sprinkel
Data processing and interpretation	Zuchuat, Sleveland, Rimkus
Approximate contribution	Zuchuat: 80 %; Sprinkel: 10 %; Sleveland, Rimkus, Braathen, Midtkandal: 10 %
Status of the manuscript	Published in <i>Geology of the Intermountain West</i> , 5, 131-165. DOI: https://doi.org/10.31711/giw.v5i0.24 .

Based on a methodical sedimentological analysis, the Late Jurassic (Oxfordian) Curtis Formation, this paper unravels the intricate facies variability which occurs in a tide-dominated, fluviially starved, low-gradient, semi-enclosed epicontinental basin. This unit crops out in east-central Utah, between the eolian deposits of the underlying Middle Jurassic (Callovian) Entrada Sandstone, from which it is separated by the J-3 unconformity, and the conformable overlying supratidal Summerville Formation of Oxfordian age. A high-resolution sedimentary analysis of the succession led to the recognition of eight facies associations (FA) with six sub-facies associations. Based on the specific three-dimensional arrangement of these eight facies associations, it is proposed to separate the Curtis Formation into three sub-units: the lower, middle and upper Curtis. The Entrada Sandstone is separated in the Slick Rock Member and its aeolian dunes and interdunes (FA 1a), whereas the informal earthy facies of the Entrada Sandstone consists of marginal-marine, rusty-red singular coastal dunes interbedded with sabkha and loess strata displaying a varying degree of mottling (FA 1b). The J-3 unconformity defines the base of the lower Curtis, which consists of upper shoreface to beach deposits (FA 2), mud-dominated (FA 3a) and sand-dominated heterolithic subtidal flat (FA 3b), sand-rich sub- to supratidal flat (FA 4a) and correlative tidal channel infill (FA 4c). It is capped by the middle Curtis, which coincides with the sub- to intertidal channel-dune-flat complex of FA 5, and its lower boundary corresponds to a transgressive surface of regional extent, identified as the Major

Transgressive Surface (MTS). This surface suggests a potential correlation between the middle and the upper Curtis and the neighbouring Todilto Member of the Wanakah Formation or Todilto Formation. The upper Curtis consists of the heterolithic upper sub- to intertidal flat (FA 6) and coastal dry eolian dunes belonging to the Moab Member of the Curtis Formation (FA 7), and it conformably overlies the middle Curtis. The Curtis Formation is conformably overlain by the supratidal, rusty red to dark brown, evaporite-rich, sabkha deposits of Summerville Formation (FA 8). The spatial distribution of these sub-units supports the distinction of three different sectors across the study area: sector 1 in the north, sector 2 in the south-southwest, and sector 3 in the east (Fig. 3). In sector 1, the Curtis Formation is represented by its three sub-units, whereas sector 2 is dominated by the middle and upper Curtis, and sector 3 encompasses the extent of the Moab Member of the Curtis Formation.

No modern analogs exist to fully illustrate the overall Curtis Formation depositional evolution. Nevertheless, as shown in Fig. 4, the inner Gulf of California and the Wadden Sea are suggested to represent similarities to the aforementioned Curtis Formation subdivisions. The lower Curtis resembles the Bay of Las Lisas in the Gulf of California, the middle Curtis can be compared to the Wadden Sea in the Netherlands, and the upper Curtis is paralleled to the Bay of La Pinta in the Gulf of California. Such comparisons have limitations, and mainly regard spatial extent of modern environments in comparison with the size of their respective Curtis Formation counterparts, as well as basal geometry approximations. The modern analogs are not meant to represent a similar tectonic setting to the Curtis Formation foreland basin conditions.

This study also highlights the composite nature of the J-3 unconformity, which was impacted by various processes occurring before the Curtis Formation was deposited, as well as during the development of the lower and middle Curtis. Local collapse features within the lower and middle Curtis are linked to sand fluid over-pressure within a remobilised sandy substratum, potentially triggered by seismic activity. Furthermore, the occurrence of a sub-regional angular relationship between the middle Curtis and substratum implies that the area of study was impacted by a regional deformational event during the Late Jurassic, before the deposition of the middle Curtis.



Code	Section Name	Curtis Fm. length
BPM	Big Pinto Mesa	65.05 m
DP	Duma Point	1.30 m
GV	Goblin Valley	26.00 m
HK	Hanksville	41.55 m
I70	Interstate 70	38.75 m
LCD	Last Chance Desert	67.05 m
LCMR	Lower Cedar Mountain Road	63.25 m
LFT	Little Flat Top	35.80 m
LSC	Lost Spring Canyon	40.10 m
LSD	Lower South Desert Overlook	29.00 m
LSRR	Lower San Rafael Road	13.60 m
NR	Notom Ranch	33.65 m
NSW	Neversweat Wash	62.00 m
SC	Sulphur Canyon	38.23 m
SG	Sven's Gulch	80.50 m
SR	Safari Road	28.60 m
SWVA	Salt Wash View Area	56.40 m
S&C	Sid & Charley	34.40 m
TMR	Ten Mill Road	14.25 m

Facies Associations:

- FA 8 Supratidal flat
- FA 7 Coastal dry aeolian dunes Moab Member
- FA 6 Upper sub- to intertidal heterolithic flat
- FA 5 Sub- to intertidal channel-dune-flat complex
- FA 4 Sand-rich sub- to supratidal flat and correlative tidal channel infill
- FA 3b Subtidal sand-dominated heterolithic flat
- FA 3a Subtidal mud-dominated heterolithic flat
- FA 2 Upper shoreface to beach deposits
- FA 1b Earthy facies
- FA 1a Coastal dunes and Slick Rock Member

Curtis Formation

- Upper
- Middle
- Lower

Other

- Lower Oxfordian
- Upper Callovian
- J-3 unconformity
- Entrada Sandstone

Fig. 3 (previous page: from Article 1) – **A.** 3-D correlation between selected localities. As the sedimentary sections are aligned on the J-3 unconformity (red line), the Entrada Sandstone appears below the map, while the Curtis Formation remains above it. Paleo-current measurements are arranged stratigraphically from bottom to top. **B.** Pie charts representing the ratio between the different facies associations belonging to the Curtis Formation at each localities. See Zuchuat et al. (2018) for discussion of unusual pattern in Little Flat Top (LFT).

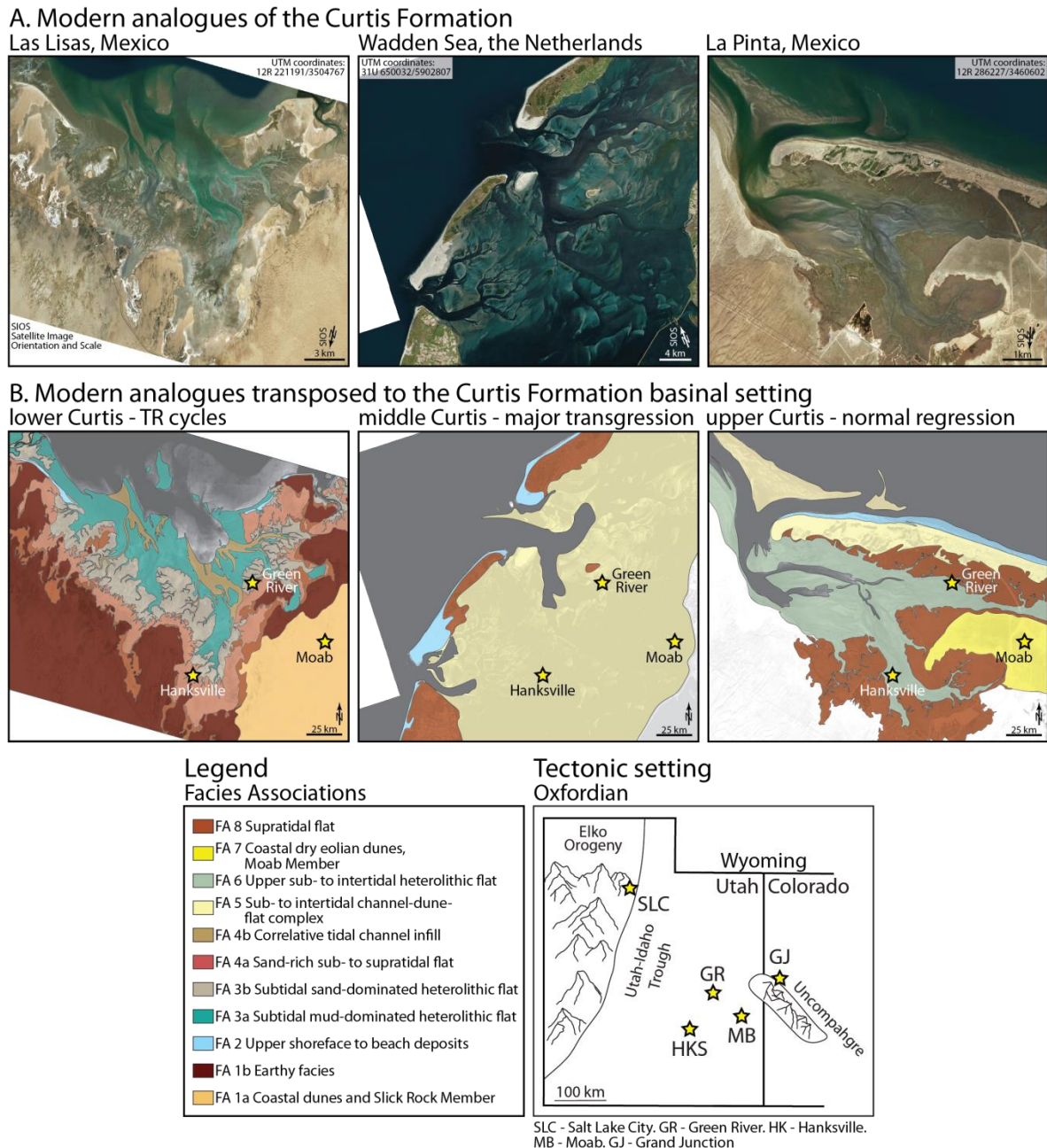


Fig. 4 (from Article 1) – **A.** Modern analogues of the lower, middle and upper Curtis, respectively. Note that these pictures are not aligned to the true north, but are rotated in a way that allows them to fit the orientation of the Curtis basin (satellite images from Microsoft Bing Maps). **B.** Modern analogues draped with the corresponding facies associations from the Curtis Formation. The change of scale between A and B illustrates how much bigger the Curtis Basin setting is with respect to the three modern analogues. TR cycles – transgressive-regressive cycles. Tectonic setting after Heyman (1983); Thorman (2011).

4.2. Article II: Composite Unconformities in Low-Gradient, Transitional Settings: the J-3 Unconformity and the Curtis Formation, East-Central Utah, USA.

Key word: Unconformity, transitional basin, composite surface, ravinement, time-transgressive

Principal author	Valentin Zuchuat
Co-authors	Ivar Midtkandal, Miquel Poyatos-Moré, Sigrid Da Costa, Kristine Halvorsen, Nathan Cote, Anja Sundal, Alvar Braathen
Text	Zuchuat, Poyatos-Moré
Figures	Zuchuat
Concept	Zuchuat, Midtkandal, Braathen
Editing	Zuchuat
Data processing and interpretation	Zuchuat, Da Costa, Halvorsen, Cote, Sundal
Approximate contribution	Zuchuat: 75 %; Poyatos-Moré: 10 %; Midtkandal: 10 %; Da Costa, Halvorsen, Cote, Sundal, Braathen: 5 %
Status of the manuscript	Submitted to <i>The Journal of Sedimentary Research</i>

Unconformities, by definition, correspond to erosive- or nondepositional surfaces, which separate younger strata below, from younger rocks above, and they can encapsulate significant time gaps. However, recent studies have highlighted the composite nature of some unconformities, as well as their heterochronous character, which challenge the use of such a definition in a four-dimensional dynamic environment. The exhumed J-3 Unconformity, separating the Middle Jurassic Entrada Sandstone from the Upper Jurassic Curtis Formation (and laterally-equivalent units) in east-central Utah, displays eight different relief expressions. These are summarised in Fig. 5, and include: (i) angular unconformity, (ii) paraconformity, (iii) steep incisions, (iv) undulating relief, (v) irregular relief, including fault-plane- and erosion-related relief irregularities, (vi) circular collapsed structures, (vii) hydroplastic sagging, and (viii) sedimentary loading.

The first five types of relief were generated by erosion-related processes, such as aeolian deflation, and water-induced erosion, whereas the three remaining ones were driven by deformational processes. Thus, the J-3 Unconformity is a composite surface (Fig. 6), with several processes that do not only interact and shape the unconformity on a differential three-dimensional space, but also in time. Results of this work therefore demonstrate the heterochronous and non-unique nature of this and potentially other surfaces interpreted as unconformities, where the same relief geometry can be produced by different processes, and one single process can generate different geometries (Fig. 7). In this particular study, with coexisting aeolian and shallow-marine systems within a transgressed basin setting, the composite flooding-ravinement surface separating the two depositional systems is time-transgressive (Fig. 8).

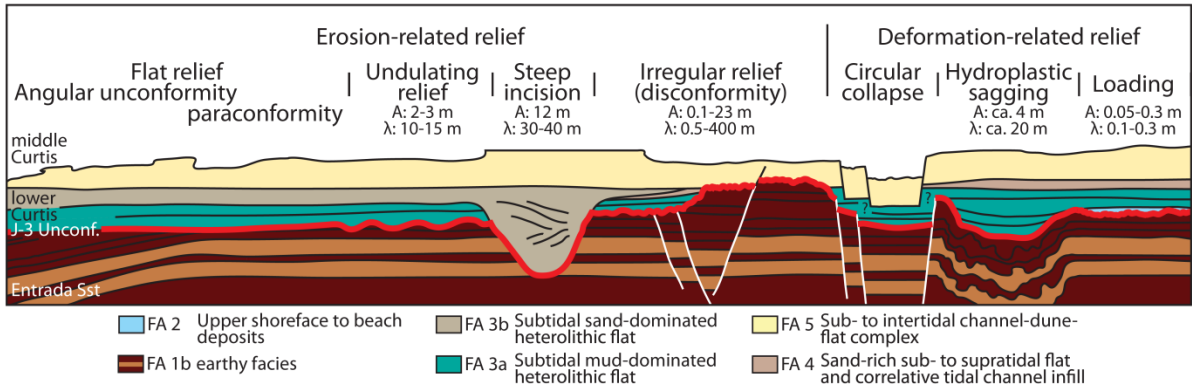


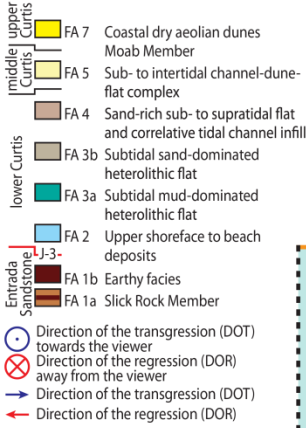
Fig. 5 (from Article II) – Diagram illustrating the five erosion-related, and the three deformation-related types of relief documented throughout the study area. The vertical- and horizontal scales are not representative of the reality.

Consequently, the regionally-extended, composite, and heterochronous J-3 Unconformity does not match with the classic unconformity definition, and should therefore not be considered as such. This outcrop example cautions against misunderstanding the subseismic complex character of these bounding surfaces, especially while conducting subsurface analyses, which may lead to inaccurate timing and sediment budget predictions, and ultimately have strong implications for basin evolution and reservoir models.

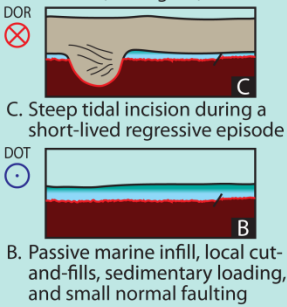
Composite J-3 Unconformity



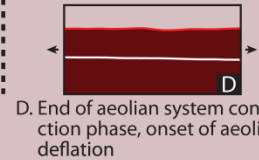
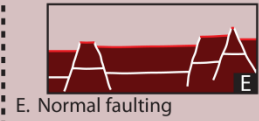
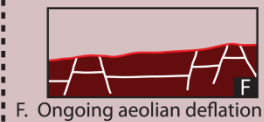
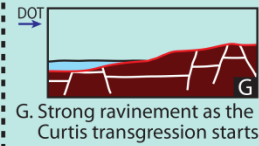
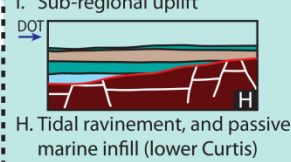
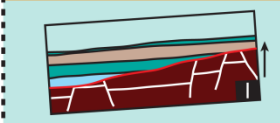
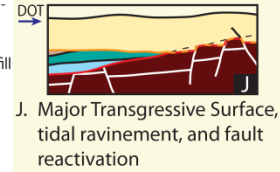
t3 Onset of the High Stand ST (HST)
 t2 Major Transgression (MTS)
 t1 The Curtis Sea starts to transgress the study area (TST)



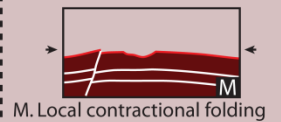
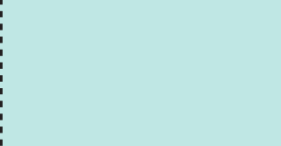
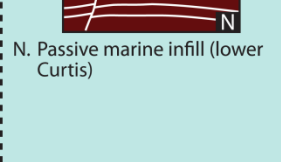
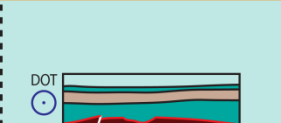
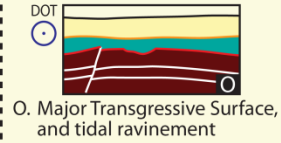
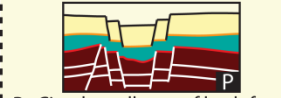
Sven's Gulch (SG) (See Fig. 4E)



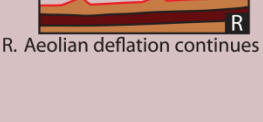
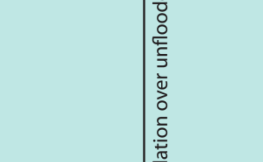
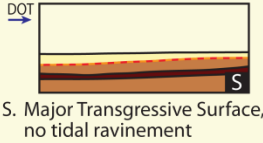
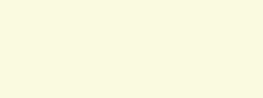
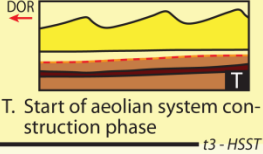
Shadscale Mesa (SM) (See Fig. 4H)



Hanksville Airport (HKA) (See Fig. 4L)



Big Pinto Mesa (BPM)



Coeval aeolian deflation over unflooded areas

Fig. 6 (from Article II) – Diagrams showing when the various processes impacted on the J-3 Unconformity at four selected localities. Note that the spacing between t1 (onset of the Curtis Sea Transgression), t2 (Major Transgression), and t3 (onset of the High Stand Systems Tract) do not hold any absolute time information, but these three lines themselves do represent fixed points in time.

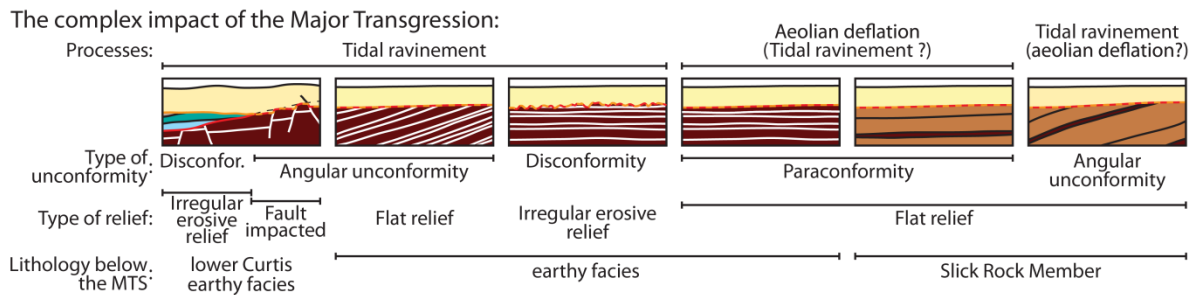


Fig. 7 (from Article II) – Diagram illustrating the non-uniqueness of the relief generated by the Major Transgression, highlighting the complexity existing in the system, between the processes involved, the types of unconformity and the types of relief they generated, as well as the underlying reworked lithology.

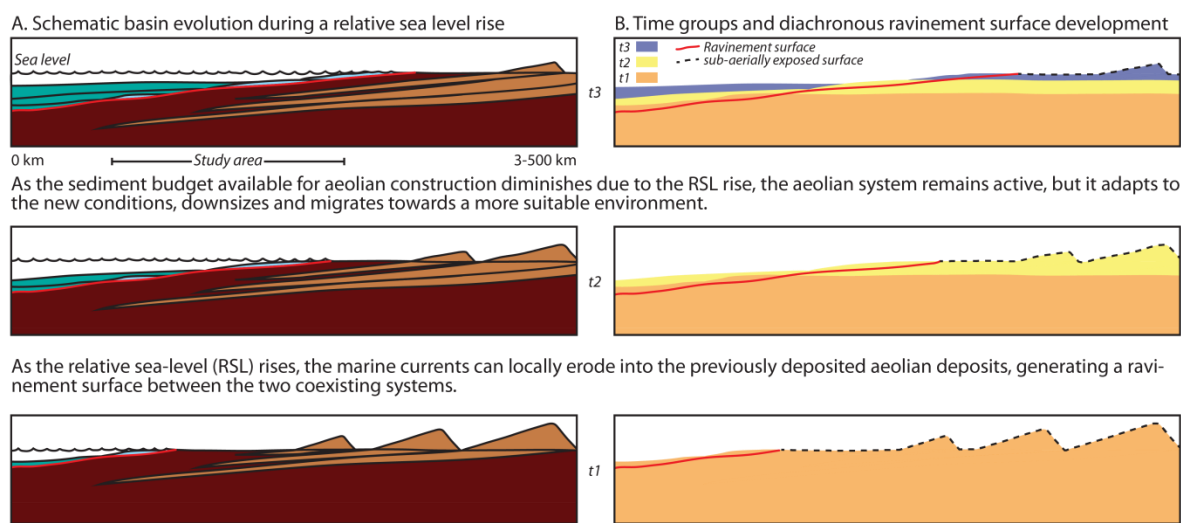


Fig. 8 (from Article II) – **A.** Model showing the evolution, over time, of an aeolian system, adjacent and coexisting with a subaqueous domain. The whole composite system undergoes a progressive climatic change towards a more humid period, a constant relative sea-level rise (RSL) and is fed by a steady sediment supply. **B.** The coexisting aeolian and subaqueous deposits are grouped according to their age, illustrating the time-transgressive nature of such a composite ravinement-flooding surface, across a transitional, continental to marine-setting. The nature of RSL rise is irrelevant to the model, and the vertical scale is not representative of the reality.

4.3. Article III: Overprinted Allocyclic Processes by Tidal Resonance in an Epicontinental Basin: the Upper Jurassic Curtis Formation, East-Central Utah, USA.

Key word: Tidal resonance, autocyclic processes, allocyclic processes, stratigraphic surfaces, aeolian sequences, Curtis Formation

Principal author	Valentin Zuchuat
Co-authors	Arve R.N. Sleveland, Ross P. Pettigrew, Thomas J.H. Dodd, Stuart M. Clarke, Ole Rabbel, Alvar Braathen, Ivar Midtkandal
Text	Zuchuat, Pettigrew, Dodd, Clarke
Figures	Zuchuat, Pettigrew, Dodd
Concept	Zuchuat, Midtkandal, Pettigrew, Dodd, Clarke
Editing	Zuchuat, Dodd, Clarke
Data processing and interpretation	Zuchuat, Sleveland, Pettigrew, Dodd, Clarke
Approximate contribution	Zuchuat: 75 %; Pettigrew, Dodd, Clarke: 15 %; Sleveland: 5 %; Rabbel, Braathen, Midtkandal: 5 %
Status of the manuscript	Submitted to <i>The Depositional Record</i>

Modern, tide-dominated and/or tide-influenced coastlines correspond to deltas, estuaries, and lagoons. However, some tide-dominated basins and related sedimentary units in the rock record, such as the semi-enclosed, shallow, Utah-Idaho Trough foreland basin of the Jurassic Curtis Sea, do not correspond to any of these modern systems. Persistent aridity caused the characteristic severe starvation of perennial fluvial input throughout this basin, in which the informal lower, middle, and upper Curtis, as well as the Summerville Formation were deposited. Wave energy was efficiently dissipated by the shallow basin's elongated morphology (approximately 800x150 km), as well as its protected nature. Consequently, the semi-enclosed, shallow marine system was dominated by amplified tidal forces, resulting in a complex distribution of heterolithic deposits.

In the early stage of the transgression, as the lower Curtis was deposited, allocyclic forcing was strongly impacting upon the system's intrinsic autocyclic processes. Short-lived relative sea-level variations, as well as uplift and deformation episodes, resulted in three parasequences, separated by traceable flooding and ravinement surfaces (Fig. 9). The subsequent transgression, which defines the base of the middle Curtis, allowed for the shallow-marine part of the system to enter into tidal resonance because the basin reached the optimal length-to-width configuration. This resonant system overprinted any evidence of allocyclic forcing and related traceable stratigraphic surfaces. However, the contemporaneous and neighbouring Moab Member's coastal aeolian dune field characterised by five stacked aeolian sequences, as well as the Summerville Formation's supratidal deposits, lingered to record allocyclic signals, as the Curtis Sea regressed (Fig. 10).

This study shows that (i) a tide-dominated basin can enter into tidal resonance as it reaches its optimal morphological configuration, leading to the overprinting of otherwise dominant allocyclic processes by autocyclic behaviour. (ii) It is therefore required to extend the research focus to neighbouring and contemporaneous depositional systems in order to fully understand the dynamic stratigraphic history of a basin alternatively dominated by auto- and allocyclic processes.

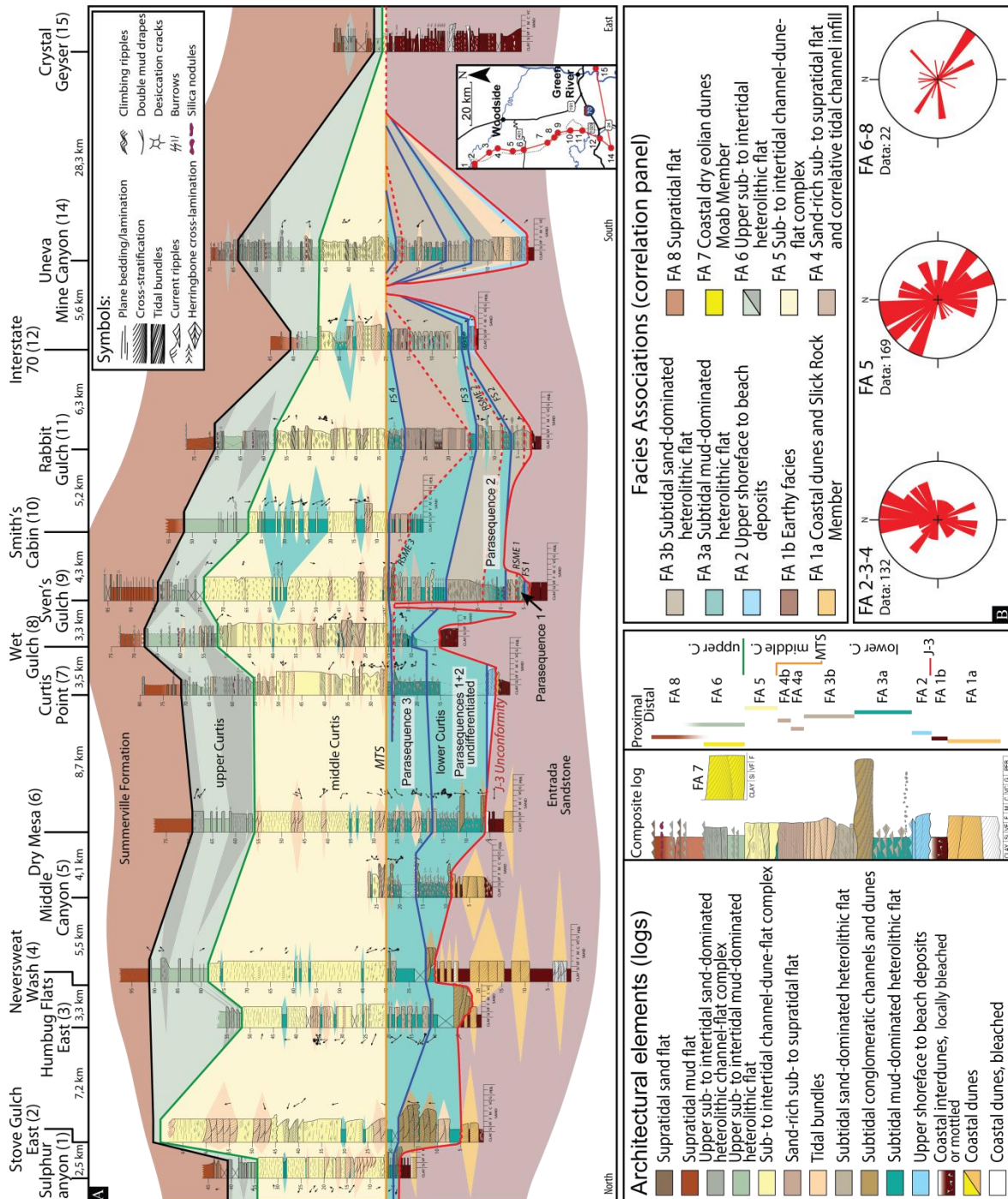


Fig. 9 (from Article III) – **A.** N-S-W oriented correlation panel along the NW margin of the San Rafael Swell, and the correlative spatial distribution of facies associations across the basin. The datum corresponds to the Major Transgressive Surface (MTS). **B.** Rose diagrams displaying the palaeocurrent measurements for the lower Curtis (FA 2, FA 3, and FA 4), the middle Curtis (FA 5), and the upper Curtis-Summerville Formation intervals (FA 6 and FA 8).

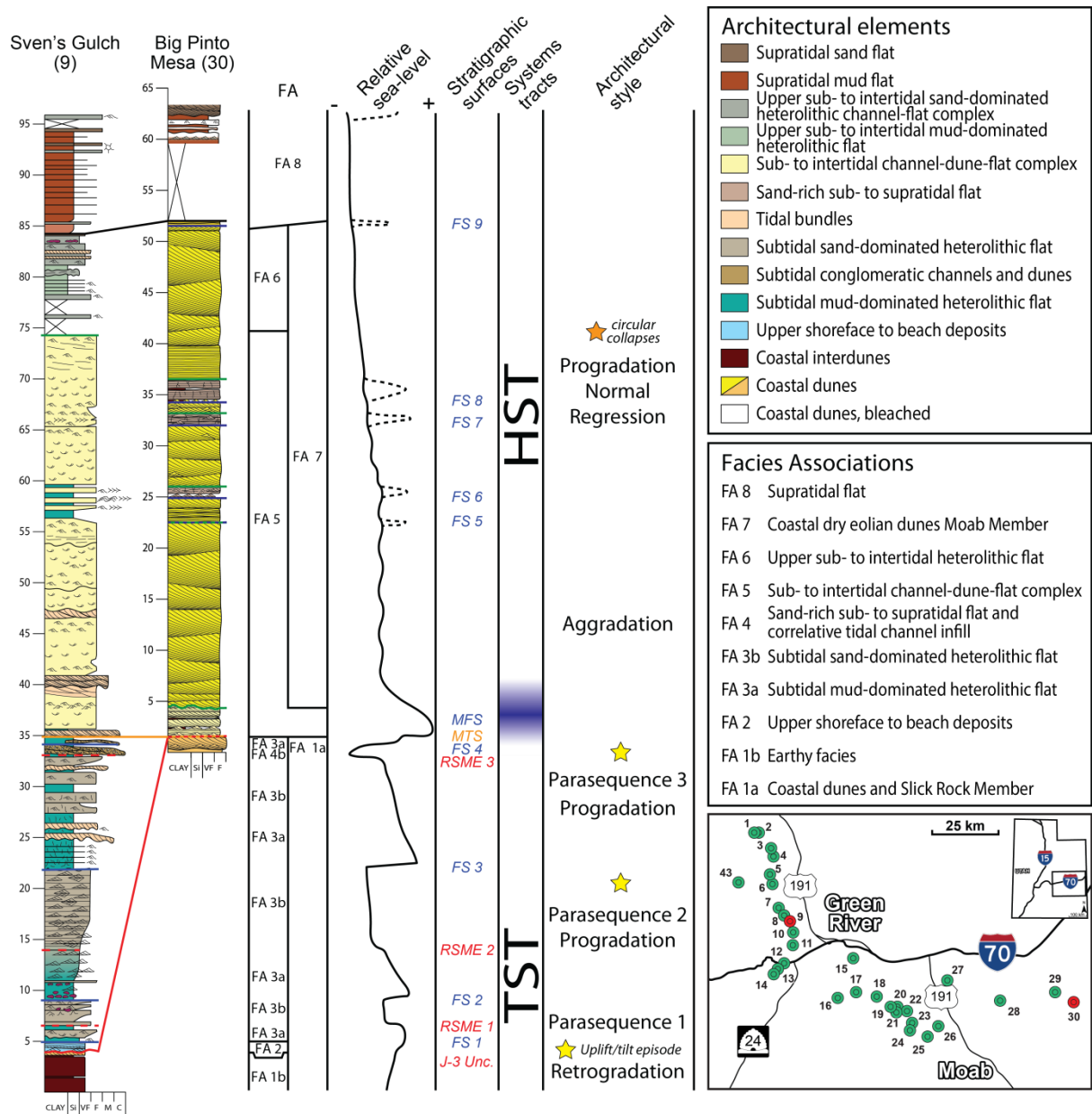


Fig. 10 (from Article III) – Comparison between the relative sea-level signal recorded by the marine part (Sven's Gulch, left red dot on the map) and the aeolian Moab Member of the Curtis Formation (Big Pinto Mesa, right red dot on the map), illustrating the overwriting of allocyclic signals by the tide-dominated system once it entered in resonance, accompanied by the deposition of the middle Curtis, whereas the contemporaneous continental deposits kept recording such allocyclicly-forced relative sea-level variations.

5. Discussion, application, and conclusive remarks

The potential for tide-dominated and/or tide-modulated deposits to bear hydrocarbons or to be considered for and CO₂ storage exists (Martinius *et al.*, 2005; Halland *et al.*, 2014). However, their intrinsic internal complexity (Kvale, 2012; Wang, 2012; Baas *et al.*, 2016) renders any attempt to accurately and faithfully implement these sub-seismic heterogeneities in a geological model extremely difficult. Consequently, it is necessary to balance these implementations and scaling challenges with a detailed and in-depth understanding of the system's dynamics and its development.

It is necessary to identify the different mechanisms involved in the deposition of these heterolithic sediments, which starts by conducting a detailed facies analysis of the studied strata, in the prospect of recognising the correct depositional environment and related facies association (FA; Article I). However, bedforms are non-unique (Burgess and Prince, 2015). This implies that a certain sedimentary structure, or lithofacies, can be formed by different processes, and that a specific process can lead to the deposition of various bedforms. In the pursuit of ascertaining the correct depositional setting(s), it is therefore required to search; (i) for evidences in under- and overlying sedimentary units, (ii) as well as other type of available evidences than the sole identification of sedimentary lithofacies, including, for instance, ichnofacies, and/or geochemical and petrophysical data.

The Curtis Formation is no stranger to Burgess and Prince's (2015) non-unique concept. Some of the bedforms occurring within the formation (see Fig. 5 in Article III) have been observed in mixed-energy environments, in which both fluvial and tidal forces interacted with one another (Martinius and Gowland, 2011; Baas *et al.*, 2016; Gugliotta *et al.*, 2016). However, the hypothesis of a mixed-energy system existing at the time the Curtis Formation was being deposited is difficult to support. Firstly, the earthy facies of the Entrada Sandstone is regarded as genetically related and contemporaneous to the lower Curtis, which is further enhanced by the preliminary and partially marine petrophysical signature of the earthy facies of the Entrada Sandstone (Article III), as well as the ravinement and time-transgressive nature of the J-3 Unconformity (Article II). Similarly, the supratidal sabkha deposits of the Summerville Formation co-existed with the middle- and upper Curtis (Article I, II, III). Therefore, if the Curtis Formation was deposited within a mixed-energy system, major fluvial systems are to be expected within these two sedimentary units neighbouring the Curtis Sea. Yet, such river systems, as well as significant wave current indicators, remain absent from the measured Entrada-Curtis-Summerville interval. This proof-by-absence, despite being potentially disputed by some, indicates a dominance of tidal forces within the shallow-marine Curtis Sea during the Oxfordian.

Once the main forces dominating the Curtis Sea are identified, it is possible to start reflecting on the dynamic development and causes behind the spatiotemporal energy variations recorded within the system and its neighbouring units. How is it possible to explain the differences between (i) the fine-grained, heterolithic deposits of the lower Curtis, in which sections can be correlated by the presence of traceable flooding and regressive surfaces, and (ii) the overlying, coarser-grained and cleaner sandstone of the middle Curtis, characterised by a complete lack of correlative surfaces? It is known that (i) tides played a significant role in the development of the Curtis Formation during the lower

Oxfordian (Article I, III), (ii) the Entrada Sandstone-to-middle Curtis interval represents an overall transgression punctuated by several short-lived regressive episodes (Article II, III), and (iii) the Curtis Sea's elongated dimensions approximated 800x150 km. It is therefore suggested that allocyclic processes were dominant during the deposition of the lower Curtis, leading to major facies belt shifts, accompanied by the development of traceable stratigraphic surfaces related to relative sea-level fluctuations. The basin subsequently entered into tidal resonance as the middle Curtis was deposited, which led to the dominance of autocyclic processes. Consequently, allocyclic processes' signatures within the sediments were overprinted by those of tidal currents. Yet, these cycles were recorded in neighbouring contemporaneous deposits outside of the shallow marine realm, highlighting the importance of including neighbouring sedimentary systems when studying a basin's dynamic history.

The concepts extracted from the Entrada-Curtis-Summerville updated and dynamic geological models, as well as the detailed development of the J-3 Unconformity, have two major applications. Despite the regional extent of the Curtis Basin, it provides an overview of the spatial energy distribution and temporal energy variations which can occur within a low-gradient, semi-enclosed tide-dominated basin, and their associated facies belts migration patterns. Understanding how the various depositional (sub-)systems react to both auto- and allocyclic forcing can help predict, for similar or resembling basin configurations, where reservoir-grade sandstones can be found, how connected they are, and what type of heterogeneities can be encountered, even with a limited amount of data available.

Further, as emphasised in Article II, the J-3 Unconformity is heterochronous, polygenetic and non-unique (*sensu* Burgess and Prince, 2015). This composite flooding-ravinement surface is time-transgressive, and, therefore, is not an unconformity *sensu* Mitchum *et al.* (1977), who defined unconformities as a "surface of erosion or nondeposition that separates younger strata from older rocks and represents a significant hiatus", thus acting as time barrier. Consequently, bounding surfaces within diverse sedimentary successions, including those recognised as unconformities *sensu stricto* in the literature, can record a non-negligible amount of information regarding the dynamic of their respective basin. Such an assessment of stratigraphic surfaces is even more important in the context of subsurface analysis, where only sparse data are available, and data resolution tends to be low, or lower than any outcropping analogue dataset, as exemplified by Fig. 11. This simplistic figure illustrates how different process and timing interpretations of the same dataset can have some significant impact on the geological model built from it. As a result, each of the constructed geological models will be characterised by different architectures and reservoir-grade sandstone interconnectivity, which can eventually lead to antipodal technical, business, and/or political decisions depending on the units' purpose(s) (hydrocarbon exploration reservoir, CO₂ storage reservoir, aquifer pumping, etc.).

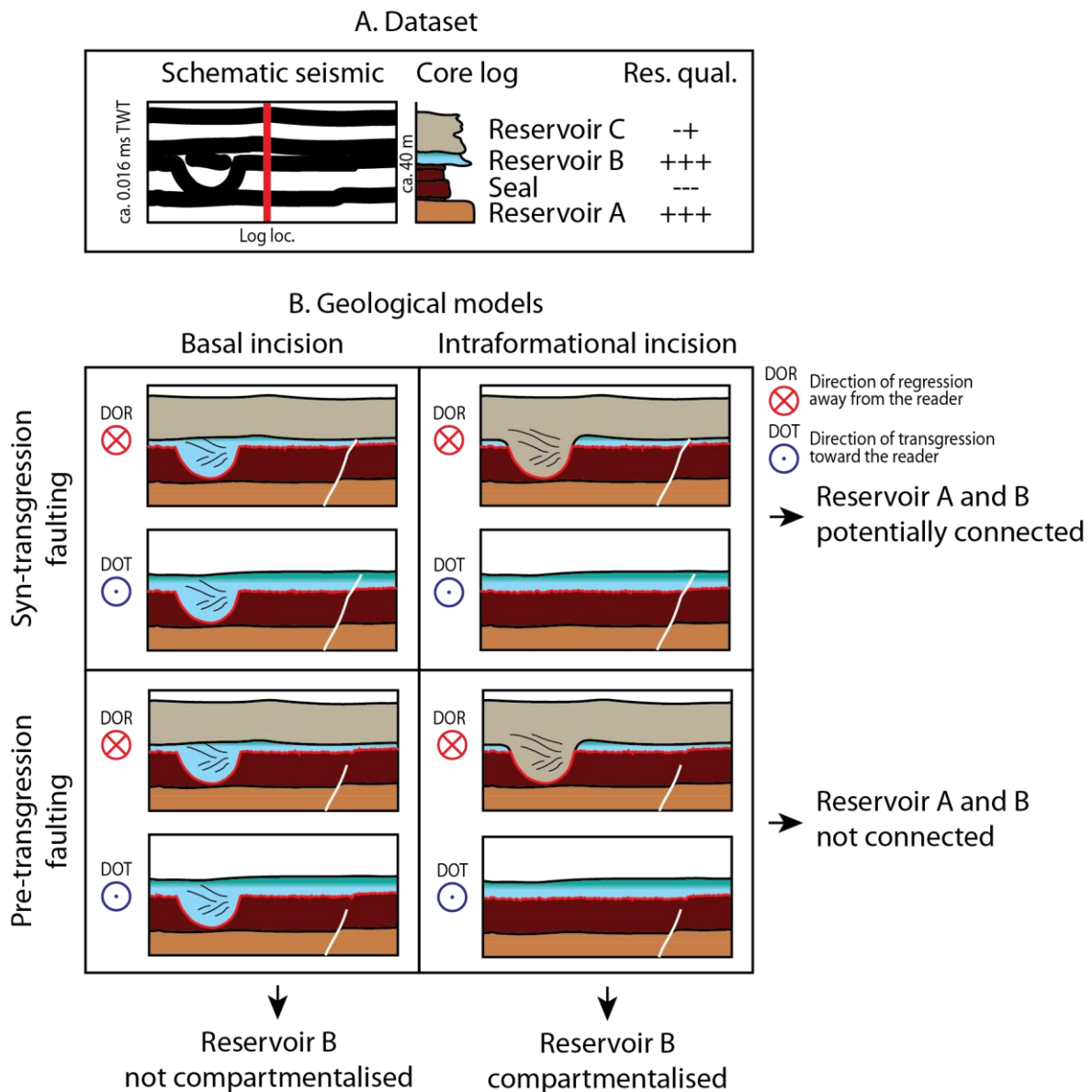


Fig. 11 (inspired by Article II) – Simplified example illustrating how, in the context of data-starved sub-surface analysis, various process and timing interpretations of the same dataset (A) can lead to different geological models (B) with completely different reservoir connectivity. Note that, in that hypothetical example, Reservoir B and C are not well connected due to Reservoir C's low porosity and permeability values. TWT approximation obtained using an average seismic velocity of 2500 m/s, after Bourbié et al.'s (1987) wet saturated sandstone seismic velocities values. The potential connectivity between reservoir A and B depends on whether the fault acts as a fluid conduct or not.

The work compiled in this doctoral thesis provides some detailed and key knowledge of the Entrada-Curtis-Summerville interval. It shows that bounding surfaces, similar to the J-3 Unconformity, can provide significant information related to the dynamic development of a sedimentary basin (Article II). This thesis also documented for the first time in the sedimentary record the onset of a tidal resonant system within a tide-dominated sedimentary basin, and recorded the impacts of such a transition onto the basin's dynamic (Article III). The concepts developed through the detailed analysis of the collected data are of value to the community, and can be applied to various contexts. Consequently, the

updated understanding of this sedimentary succession can further be built upon, and help decipher the secrets it still retains.

Further studies

This work, however, is not the panacea. The robustness of its conclusions will naturally require further testing. A first step is to assess whether similar or resembling tide-dominated basins exist in the sedimentary record. If so, could tidal resonant episodes be identified using criteria such as strong variations of grain- and bedform size, the disappearance of correlatable surfaces, and apparent contradictory sequence stratigraphic signals between neighbouring and contemporaneous depositional environments? In parallel, knowing the approximate dimension and water depth of the Curtis Sea, numerical modelling can test whether the laws of physics would have allowed for the Curtis Basin to enter a tidal resonant stage. Such numerical simulation requires the approximation of some input parameters, including basal shear stress values and the subaqueous morphology of the tidal system, using theoretical estimations and experimental results.

Additional studies will further improve the knowledge of the basin's dynamic history, and help developing the model for greater and more direct industry- and/or societal-related applications. Encouraged by promising preliminary results suggesting a continuous cyclicity across the Entrada-Curtis-Summerville interval (Article III), the systematic use of a hand-held gamma ray spectrometer across the complete sedimentary interval could help increase confidence in the resolution and correlation potential of these apparent cycles, across the study area. Data should be collected from the base of the Entrada Sandstone's earthy facies, through the Curtis and the Summerville formations, up to the J-5 Unconformity at the base of the Morrison Formation.

A thorough provenance analysis focusing particularly on the conglomeratic intervals within the lower Curtis would also be critical for a better understanding of the early stages of the Curtis Sea's transgression. A methodical diagenetic analysis of the interval would complement the dynamic depositional models developed in this thesis, by providing valuable post-depositional insights to the model. The study of silica nodules occurring, notably within the upper Curtis (Article I), could characterise the water chemistry, and potentially variations of thereof, at a time close to the deposition time as they precipitated shortly after the sediments had been deposited (Kile *et al.*, 2015).

The Entrada-Curtis-Summerville interval further requires a detailed reservoir and seal characterisation study in order to populate the geological model with the mechanical, physical and chemical properties of the rocks. Adequate fluid flow simulations can then be run, permitting, for instance, the assessment of similar strata in a context of CO₂ storage. Last but not least, the high-resolution, 8x2 km virtual outcrop model, collected at Last Chance Desert (38, 39), and displaying a superb along-strike and -dip succession across the Entrada-Curtis-Summerville interval can serve as geological analogue and open-air laboratory, such as seismic forward modelling, as well as high-resolution reservoir studies and associated fluid flow simulations.

6. References

- Anderson, T.H.** (2015). Jurassic (170–150 Ma) basins: The tracks of a continental-scale fault, the Mexico-Alaska megashear, from the Gulf of Mexico to Alaska. In: Anderson, T.H., Didenko, A.N., Johnson, C.L., Khanchuk, A.I., and MacDonald, J.H., (eds.), Late Jurassic Margin of Laurasia – A Record of Faulting Accommodating Plate Rotation. *Geological Society of America Special Papers*, **513**, 107-188.
- Anderson, O.J.** and **Lucas, S.G.** (1994). Middle Jurassic stratigraphy, sedimentation and paleogeography in the southern Colorado Plateau and southern High Plains. In: Caputo, M.V., Peterson, J.A. and Franczyk, K.J., (eds.), *Mesozoic Systems of the Rocky Mountain Region, USA*. The Rocky Mountain Section SEPM (Society for Sedimentary Geology), Denver, 299-314.
- Baas, J.H., Best, J.L., and Peakall, J.** (2016). Predicting bedforms and primary current stratification in cohesive mixtures of mud and sand. *Journal of the Geological Society*, **173(1)**, 12-45.
- Bjerrum, C.J.** and **Dorsey, R.J.** (1995) Tectonic controls on deposition of Middle Jurassic strata in a retroarc foreland basin, Utah - Idaho trough, western interior, United States. *Tectonics*, **14(4)**, 962-978.
- Bonaventura, X., Sima, A.A., Feixas, M., Buckley, S.J., Sbert, M., and Howell, J.A.** (2017). Information measures for terrain visualization. *Computers & Geosciences*, **99**, 9-18.
- Bourbié, T., Coussy, O., and Zinszner, B.** (1987). *Acoustics of porous media*. Editions Technip.
- Braathen, A., Bælum, K., Christiansen, H.H., Dahl, T., Eiken, O., Elvebakk, H., and Johnsen, H.** (2012). The Longyearbyen CO₂ Lab of Svalbard, Norway—initial assessment of the geological conditions for CO₂ sequestration. *Norwegian Journal of Geology/Norsk Geologisk Forening*, **92(4)**, 353-376.
- Brenner, R.L.** and **Peterson, J.A.** (1994). Jurassic sedimentary history of the northern portion of the Western Interior Seaway, USA. In: Caputo, M.V., Peterson, J.A. and Franczyk, K.J., (eds.), *Mesozoic Systems of the Rocky Mountain Region, USA*. The Rocky Mountain Section SEPM (Society for Sedimentary Geology), Denver, 233-272.
- Buckley, S., Ringdal, K., Dolva, B., Naumann, N., and Kurz, T.** (2017). LIME: 3D visualisation and interpretation of virtual geoscience models. *EGU General Assembly Conference Abstracts*, **19**, p. 15952.
- Burgess, P.M.** and **Prince, G.D.** (2015). Non-unique stratal geometries: implications for sequence stratigraphic interpretations. *Basin Research*, **27(3)**, 351-365.
- Bump, A.P.** and **Davis, G.H.** (2003). Late Cretaceous – early Tertiary Laramide deformation of the northern Colorado Plateau, Utah and Colorado. *Journal of Structural Geology*, **25(3)**, 421-440.
- Caputo, M.V.** and **Pryor, W.A.** (1991). Middle Jurassic tide- and wave-influenced coastal facies and paleogeography, upper San Rafael Group, east-central Utah. *Utah Geological Association*, **19**, 9-27.
- Catuneanu O.** (2006). *Principles of Sequence Stratigraphy*. Amsterdam, Elsevier, 1-375.
- Catuneanu, O., Abreu, V., Bhattacharya, J.P., Blum, M.D., Dalrymple, R.W., Eriksson, P.G., Fielding, C.R., Fisher, W.L., Galloway, W.E., Gibling, M.R., Giles, K.A., Holbrook, J.M., Jordan, R., Kendall, C.G.St.C, Macurda, B., Martinsen, O.J., Mial, A.D., Neal, J.E., Nummedal, D., Pomar, L., Posamentier, H.W., Pratt, B.R., Sarg, J.F., Shanley, K.W., Steel, R.J., Strasser, A., Tucker, M.E., and Winker, C.** (2009). Towards the standardization of sequence stratigraphy. *Earth-Science Reviews*, **92(1)**, 1-33.
- Carr-Crabaugh, M.** and **Kocurek, G.** (1998). Continental sequence stratigraphy of a wet eolian system: a key to relative sea-level change. *Society for Sedimentary Geology, Special Publication*, **59**, 213-228.
- Crabaugh, M., and Kocurek, G.** (1993). Entrada Sandstone—an example of a wet eolian system. In: Pye, K., (eds.), *The dynamics and environmental context of eolian sedimentary systems*. London Geological Society Special Publications, **72**, 103-126.
- Condon, S.M., and Huffman Jr, A.C.** (1988). Revisions in nomenclature of the middle Jurassic Wanakah Formation, northwestern New Mexico and northeastern Arizona. *U.S. Geological Survey Bulletin*, **1633-A**, A1-A12.
- Denchik, N., Pezard, P.A., Neyens, D., Lofi, J., Gal, F., Girard, J.F., and Levannier, A.** (2014). Near-surface CO₂ leak detection monitoring from downhole electrical resistivity at the CO₂ Field Laboratory, Svelvik Ridge (Norway). *International Journal of Greenhouse Gas Control*, **28**, 275-282.

- Dickinson, W.R., and Gehrels, G.E.** (2009). U-Pb ages of detrital zircons in Jurassic eolian and associated sandstones of the Colorado Plateau—evidence for transcontinental dispersal and intraregional recycling of sediment. *Geological Society of America Bulletin*, **121(3-4)**, 408-433.
- Dickinson, W.R., and Gehrels, G.E.** (2010). Insights into North American paleogeography and paleotectonics from U–Pb ages of detrital zircons in Mesozoic strata of the Colorado Plateau, USA. *International Journal of Earth Sciences*, **99(6)**, 1247-1265.
- Doelling, H.H.** (2001). *Geologic map of the Moab and eastern part of the San Rafael Desert 30' x 60' quadrangles, Grand and Emery Counties, Utah, and Mesa County, Colorado*. Utah Geological Survey Map 180, 3 plates, scale 1:100,000.
- Doelling, H.H., Kuehne, P.A., Willis, G.C., and Ehler, J.B.** (2015). *Geologic map of the San Rafael Desert 30' x 60' quadrangle, Emery and Grand Counties, Utah*. Utah Geological Survey, Map 267DM, scale 1:62,500.
- Eiken, O., Ringrose, P., Hermanrud, C., Nazarian, B., Torp, T.A., and Høier, L.** (2011). Lessons learned from 14 years of CCS operations: Sleipner, In Salah and Snøhvit. *Energy Procedia*, **4**, 5541-5548.
- Gilluly, J. and Reeside Jr., J.B.** (1928). Sedimentary rocks of the San Rafael Swell and some adjacent areas in eastern Utah. *U.S. Geological Survey, Professional Paper*, **150-D**, 61-110.
- Haq, B.U., Hardenbol, J., and Vail, P.R.** (1987). Chronology of fluctuating sea levels since the Triassic. *Science*, **235(4793)**, 1156-1167.
- Halland, E.K., Bjørnstad, A., Magnus, C., Riis, F., Meling, I.M., Tørneng Gjeldvik, I., Tappel, I.M., Mujezinović, J., Bjørheim M., Rød, R.S., and Pham, V.T.H.** (2014). *CO₂ storage atlas—Norwegian continental shelf*. Stavanger, Norway, Norwegian Petroleum Directorate.
- Heyman, O.G.** (1983). Distribution and structural geometry of faults and folds along the northwestern Uncompahgre uplift, western Colorado and eastern Utah. In: Averett, W. (ed), *Northern Paradox Basin-Uncompahgre uplift. Grand Junction Geological Society field trip*, 45-57.
- Hintze, L.F. and Kowallis, B.J.** (2009). *Geologic history of Utah*. Provo, Utah, Brigham Young University Studies. 225 pp.
- Imlay, R.W.** (1947). Marine Jurassic of Black Hills Area, South Dakota and Wyoming. *American Association of Petroleum Geologists Bulletin*, **31(2)**, 227-273.
- Imlay, R.W.** (1980). Jurassic paleobiogeography of the conterminous United States in its continental setting. *U.S. Geological Survey Professional Paper*, **1062**, 1-134.
- Kile, D.E., Dayvault, R.D., Hood, W.C., and Hatch, H.S.** (2015). Celestine-Bearing Geodes from Wayne and Emery Counties, Southeastern Utah: Genesis and Mineralogy. *Rocks & Minerals*, **90(4)**, 314-337
- Kocurek, G. and Havholm, K.G.** (1993). Eolian sequence stratigraphy: A conceptual framework. In: Weimer, P., & Posamentier, H.W., (eds.), *Siliciclastic Sequence Stratigraphy: Recent Developments and Applications*, American Association of Petroleum Geologists, Memoir, 58, 393–410.
- Kocurek, G. and Lancaster, N.** (1999). Aeolian system sediment state: theory and Mojave Desert Kelso dune field example. *Sedimentology*, **46(3)**, 505-515.
- Kocurek, G., Martindale, R.C., Day, M., Goudge, T.A., Kerans, C., Hassenruck - Gudipati, H.J., Mason, J., Cardenas, B.T., Petersen, E., Mohrig, D., Aylward, D.S., Hughes, C.M., and Nazworth, C.M.** (in press). Antecedent aeolian dune topographic control on carbonate and evaporite facies: Middle Jurassic Todilto Member, Wanakah Formation, Ghost Ranch, New Mexico, USA. *Sedimentology*.
- Kreisa, R.D. and Moiola, R.J.** (1986). Sigmoidal tidal bundles and other tide-generated sedimentary structures of the Curtis Formation, Utah. *Geological Society of America Bulletin*, **97(4)**, 381-387.
- Kvale, E.P.** (2012). Tidal constituents of modern and ancient tidal rhythmites: criteria for recognition and analyses. In: Davis, R.A., Jr., and Dalrymple, R.W., (eds.), *Principles of Tidal Sedimentology*. Springer Science and Business Media, Dordrecht, Netherlands, 1-17.
- Levander, A., Schmandt, B., Miller, M.S., Liu, K., Karlstrom, K.E., Crow, R.S., Lee, C.-T.A., and Humphreys, E.D.** (2011). Continuing Colorado plateau uplift by delamination-style convective lithospheric downwelling. *Nature*, **472(7344)**, 461-465.
- Lucas, S.G.** (2014). Lithostratigraphy of the Jurassic San Rafael Group from Bluff to the Abajo Mountains, southeastern Utah: Stratigraphic relationships of the Bluff Sandstone. *Volumina Jurassica*, **12**, 55-68.

- Mansfield, G.R. and Roundy, P.V.** (1916). Revision of the Beckwith and Bear River Formations of southeastern Idaho. *U.S. Geological Survey Professional Paper*, **98**, 75-84.
- Martinius, A.W., Ringrose, P.S., Brostrøm, C., Elfenbein, C., Næss, A., and Ringås, J.E.** (2005). Reservoir challenges of heterolithic tidal sandstone reservoirs in the Halten Terrace, mid-Norway. *Petroleum Geoscience*, **11(1)**, 3-16.
- McMullen, S.K., Holland, S.M., and O'Keefe, F.R.** (2014). The occurrence of vertebrate and invertebrate fossils in a sequence stratigraphic context: the Jurassic Sundance Formation, Bighorn Basin, Wyoming, USA. *Palaios*, **29(6)**, 277-294.
- Mitchum, R.J., Vail, P.R., and Thompson, S. III.** (1977) The depositional sequence as a basic unit for stratigraphic analysis. In: Payton, C.E., (ed.), *Seismic Stratigraphy: Applications to Hydrocarbon Exploration*, American Association of Petroleum Geologists Memoir, **26**, 205-212.
- Mountney, N.P.** (2006). Periodic accumulation and destruction of aeolian erg sequences in the Permian Cedar Mesa Sandstone, White Canyon, southern Utah, USA. *Sedimentology*, **53(4)**, 789-823.
- Mountney, N.P.** (2012). A stratigraphic model to account for complexity in aeolian dune and interdune successions. *Sedimentology*, **59(3)**, 964-989.
- Murray, K.E., Reiners, P.W., and Thomson, S.N.** (2016). Rapid Pliocene–Pleistocene erosion of the central Colorado Plateau documented by apatite thermochronology from the Henry Mountains. *Geology*, **44(6)**, 483-486.
- Nelson, S.T.** (1997). Reevaluation of the Central Colorado plateau laccoliths in the light of new age determination. *U.S. Geological Survey Bulletin*, **2158**, 37-9.
- Nuccio, V.F. and Condon, S.M.** (1996). Burial and thermal history of the Paradox Basin, Utah and Colorado, and petroleum potential of the Middle Pennsylvanian Paradox Formation. *U.S. Geological Survey Bulletin*, **41**, 57-76
- Ogg, J.G., Ogg, G., and Gradstein, F M.** (2016). *A Concise Geologic Time Scale: 2016*. Elsevier.
- Peterson, F.** (1994). Sand dunes, sabkhas, streams, and shallow seas: Jurassic paleogeography in the southern part of the Western Interior Basin. In: Caputo, M.V., Peterson, J.A. and Franczyk, K.J., (eds.), *Mesozoic Systems of the Rocky Mountain Region, USA*. The Rocky Mountain Section SEPM (Society for Sedimentary Geology), Denver, 233-272.
- Peterson, F. and Pippingos, G.N.** (1979). Stratigraphic relations of the Navajo Sandstone to Middle Jurassic formations, southern Utah and northern Arizona. *U.S. Geological Survey Professional Paper*, **1035-B**, 1-43.
- Petrie, E.S., Sundal, A., Gutierrez, M., and Braathen, A.** (2017). Deformation band formation and reactivation associated with a Laramide fault propagation fold (abs.). *Geological Society of America Abstract with Programs*, **49(6)**, 289-299.
- Pippingos, G.N. and O'Sullivan, R.B.** (1978). Principal unconformities in Triassic and Jurassic rocks, western interior United States: a preliminary survey. *U.S. Geological Survey, Professional Paper*, **1035-A**, 1-29.
- Pippingos, G.N. and Imlay, R.W.** (1979). Lithology and subdivisions of the Jurassic Stump Formation in southeastern Idaho and adjoining areas. *U.S. Geological Survey Professional Paper*, **1035-C**, 1-25.
- Sprinkel, D.A., Doelling, H.H., Kowallis, B.J., Waanders, G., and Kuehne, P.A.** (2011). Early results of a study of Middle Jurassic strata in the Sevier fold and thrust belt, Utah. In: Sprinkel, D.A., Yonkee, W.A., and Chidsey, T.C., Jr., (eds.), *Sevier Thrust Belt: Northern and Central Utah and Adjacent Areas*. Utah Geological Association, Publication, **40**, 151-172.
- Sullivan, K.R., Kowallis, B.J., and Mehnert, H.H.** (1991). Isotopic ages of igneous intrusions in southeastern Utah – Evidence for a mid-Cenozoic Reno–San Juan magmatic zone. *Brigham Young University Geology Studies*, **37**, 139-144.
- Sundal, A., Nystuen, J.P., Dypvik, H., Miri, R., and Aagaard, P.** (2013). Effects of geological heterogeneity on CO₂ distribution and migration-A case study from the Johansen Formation, Norway. *Energy Procedia*, **37**, 5046-5054.
- Sundal, A., Hellevang, H., Miri, R., Dypvik, H., Nystuen, J.P., and Aagaard, P.** (2014). Variations in mineralization potential for CO₂ related to sedimentary facies and burial depth—a comparative study from the North Sea. *Energy Procedia*, **63**, 5063-5070.
- Sundal, A., Miri, R., Ravn, T., and Aagaard, P.** (2015). Modelling CO₂ migration in aquifers; considering 3D seismic property data and the effect of site-typical depositional heterogeneities. *International Journal of Greenhouse Gas Control*, **39**, 349-365.

- Sundal, A., Nystuen, J.P., Rørvik, K. L., Dypvik, H., and Aagaard, P.** (2016). The Lower Jurassic Johansen Formation, northern North Sea—Depositional model and reservoir characterization for CO₂ storage. *Marine and Petroleum Geology*, **77**, 1376-1401.
- Thorman, C.H.** (2011). The Elko orogeny – A major tectonic event in eastern Nevada–western Utah. In: Sprinkel, D.A., Yonkee, W.A., and Chidsey, T.C., Jr., (eds.), *Sevier Thrust Belt: Northern and Central Utah and Adjacent Areas*. *Utah Geological Association Publication*, **40**, 117-129.
- Trudgill, B. D.** (2011). Evolution of salt structures in the northern Paradox Basin: Controls on evaporite deposition, salt wall growth and supra - salt stratigraphic architecture. *Basin Research*, **23(2)**, 208-238.
- Wang, P.** (2012). Principles of Sediment Transport Applicable in Tidal Environments. In: Davis, R.A., Jr., and Dalrymple, R.W., (eds.), *Principles of Tidal Sedimentology*, Springer Science and Business Media, Dordrecht, Netherlands, 19-34.
- Westoby, M.J., Brasington, J., Glasser, N.F., Hambrey, M.J., and Reynolds, J.M.** (2012). 'Structure-from-Motion' photogrammetry: A low-cost, effective tool for geoscience applications. *Geomorphology*, **179**, 300-314.
- Wilcox, W.T. and Currie, B.** (2008). Sequence Stratigraphy of the Jurassic Curtis, Summerville, and Stump Formations, Eastern Utah and Northwest Colorado. In: Longman, M.W. and Morgan, C.D., (eds.), *Hydrocarbon Systems and Production in the Uinta Basin, Utah*. *Rocky Mountain Association of Geologists and Utah Geological Association Publication*, **37**, 9-41.
- Witkind, I.J.** (1988). *Geologic map of the Huntington 30' X 60' quadrangle, Carbon, Emery, Grand, and Uintah Counties, Utah*. U.S. Geological Survey, Miscellaneous Investigations Series Map I-1764, scale 1:100,000.
- Yonkee, W.A. and Weil, A.B.** (2015). Tectonic evolution of the Sevier and Laramide belts within the North American Cordillera orogenic system. *Earth-Science Reviews*, **150**, 531-593.
- Yoshida, S., Johnson, H.D., Pye, K., and Dixon, R.J.** (2004). Transgressive changes from tidal estuarine to marine embayment depositional systems: The Lower Cretaceous Woburn Sands of southern England and comparison with Holocene analogs. *American Association of Petroleum Geologists Bulletin*, *88(10)*, 1433-1460.
- Zuchuat, V., Sleveland, A.R.N., Sprinkel, D.A., Rimkus, A., Braathen, A., and Midtkandal, I.** (2018). New insights on the impact of tidal currents on a low-gradient, semi-enclosed, epicontinental basin—the Curtis Formation, east-central Utah, USA. *Geology of the Intermountain West*, **5**, 131-165.
- Zuchuat, V., Midtkandal, I., Poyatos-Moré, M., da Costa, S., Halvorsen, K., Cote N., Sundal, A., and Braathen, A.** (submitted to *The Journal of Sedimentary Research*). Composite Unconformities in Low-Gradient Transitional Settings: the J-3 Unconformity and the Curtis Formation, East-Central Utah, USA.
- Zuchuat, V., Sleveland, A.R.N., Pettigrew, R.P., Dodd, T.J.H., Clarke, S.M., Rabbel, O., Braathen, A., and Midtkandal, I.** (submitted to *The Depositional Record*). Overprinted Allocyclic Processes by Tidal Resonance in an Epicontinental Basin: the Upper Jurassic Curtis Formation, East-Central Utah, USA.

7. Articles

7.1. Article I: New Insights on the Impact of Tidal Currents on a Low-gradient, Semi-enclosed, Epicontinental Basin – the Curtis Formation, East-central Utah, USA.

Zuchuat, V.¹, Sleveland, A.R.N.¹, Sprinkel, D.A.², Rimkus, A.¹, Braathen, A.¹, and Midtkandal, I.¹ (2018). New Insights on the Impact of Tidal Currents on a Low-gradient, Semi-enclosed, Epicontinental Basin – the Curtis Formation, East-central Utah, USA. *Geology of the Intermountain West*, 5, 131-165. DOI: <https://doi.org/10.31711/giw.v5i0.24>.

¹*Tectonostratigraphic Research Group, University of Oslo, Sem Sælands Vei 1, 0371 Oslo, Norway*

²*Utah Geological Survey, P.O. Box 146100, Salt Lake City, Utah 84114*



GEOLOGY OF THE INTERMOUNTAIN WEST

an open-access journal of the Utah Geological Association

ISSN 2380-7601

Volume 5

2018

NEW INSIGHTS ON THE IMPACT OF TIDAL CURRENTS ON A LOW-GRADIENT, SEMI-ENCLOSED, EPICONTINENTAL BASIN—THE CURTIS FORMATION, EAST-CENTRAL UTAH, USA

Valentin Zuchuat, Arve R.N. Sleveland, Douglas A. Sprinkel, Algirdas Rimkus,
Alvar Braathen, and Ivar Midtkandal



© 2018 Utah Geological Association. All rights reserved.

For permission to copy and distribute, see the following page or visit the UGA website at www.utahgeology.org for information.

Email inquiries to GIW@utahgeology.org.



GEOLOGY OF THE INTERMOUNTAIN WEST

an open-access journal of the Utah Geological Association

ISSN 2380-7601

Volume 5

2018

Editors

Douglas A. Sprinkel Utah Geological Survey 801.391.1977 GIW@utahgeology.org	Thomas C. Chidsey, Jr. Utah Geological Survey 801.537.3364 tomchidsey@utah.gov
--	---

Bart J. Kowallis Brigham Young University 801.422.2467 bkowallis@gmail.com	Steven Schamel GeoX Consulting, Inc. 801.583-1146 geox-slc@comcast.net
---	---

Production

Cover Design and Desktop Publishing
Douglas A. Sprinkel

Cover

View from the Lower South Desert Overlook, Capitol Reef National Park, displaying the earthy facies of the Callovian Entrada Sandstone (reddish-colored sandstone), overlain by the Oxfordian, tidally influenced Curtis Formation (light-colored sandstone). The two units are separated by the J-3 unconformity, which coincides here with the Major Transgressive Surface (MTS) at the base of the informal middle Curtis. Note the evidences of tidal ravinement at the base of the middle Curtis. The middle Curtis consists mainly very fine to fine-grained sandstone, and corresponds to a sub- to intertidal channel-dune-flat complex depositional setting. The middle Curtis gradually grades into the thinner-bedded, very fine-grained, sub- to intertidal heterolithic flat deposits of the upper Curtis, which is conformably overlain by the Summerville Formation. Note the geologist in the lower right quadrant of the photograph for scale.



This is an open-access article in which the Utah Geological Association permits unrestricted use, distribution, and reproduction of text and figures that are not noted as copyrighted, provided the original author and source are credited.

UGA Board

2018 President	Paul Inkenbrandt	paulinkenbrandt@utah.gov	801.537.3361
2018 President-Elect	Peter Nielsen	peternielsen@utah.gov	801.537.3359
2018 Program Chair	Emily McDermott	emcdermott@utah.gov	801.537.3389
2018 Treasurer	Zach Anderson	zanderson@utah.gov	801.538.4779
2018 Secretary	Christopher Kravits	ckravitsgeo@gmail.com	
2018 Past President	Bill Loughlin	bill@loughlinwater.com	435.649.4005

UGA Committees

Education/Scholarship	Loren Morton	lmorton@utah.gov	801.536.4262
Environmental Affairs	Craig Eaton	eaton@ihi-env.com	801.633.9396
Geologic Road Sign	Terry Massoth	twmassoth@hotmail.com	801.541.6258
Historian	Paul Anderson	paul@pbageo.com	801.364.6613
Membership	Rick Ford	rford@weber.edu	801.626.6942
Public Education	Paul Jewell	pwjewell@mines.utah.edu	801.581.6636
	Matt Affolter	gfl247@yahoo.com	
Publications	Roger Bon	rogerbon@xmission.com	801.942.0533
Publicity	Paul Inkenbrandt	paulinkenbrandt@utah.gov	801.537.3361
Social/Recreation	Roger Bon	rogerbon@xmission.com	801.942.0533

AAPG House of Delegates

2017–2020 Term	Tom Chidsey	tomchidsey@utah.gov	801.537.3364
----------------	-------------	---------------------	--------------

State Mapping Advisory Committee

UGA Representative	Jason Blake	blake-j@comcast.net	435.658.3423
--------------------	-------------	---------------------	--------------

Earthquake Safety Committee

Chair	Grant Willis	gwillis@utah.gov	801.537.3355
-------	--------------	------------------	--------------

UGA Website

www.utahgeology.org

Webmasters	Paul Inkenbrandt	paulinkenbrandt@utah.gov	801.537.3361
	Lance Weaver	lanceweaver@utah.gov	801.403.1636

UGA Newsletter

Newsletter Editor	Bill Lund	uga.newsletter@gmail.com	435.590.1338
-------------------	-----------	--------------------------	--------------

Become a member of the UGA to help support the work of the Association and receive notices for monthly meetings, annual field conferences, and new publications. Annual membership is \$20 and annual student membership is only \$5. Visit the UGA website at www.utahgeology.org for information and membership application.

The UGA board is elected annually by a voting process through UGA members. However, the UGA is a volunteer-driven organization, and we welcome your voluntary service. If you would like to participate please contact the current president or committee member corresponding with the area in which you would like to volunteer.

Utah Geological Association formed in 1970 from a merger of the Utah Geological Society, founded in 1946, and the Intermountain Association of Geologists, founded in 1949. Affiliated with the American Association of Petroleum Geologists.



New Insights on the Impact of Tidal Currents on a Low-gradient, Semi-enclosed, Epicontinental Basin—the Curtis Formation, East-central Utah, USA

Valentin Zuchuat¹, Arve R.N. Sleveland¹, Douglas A. Sprinkel², Algirdas Rimkus¹, Alvar Braathen¹, Ivar Midtkandal¹

¹ *University of Oslo, Department of Geosciences, Sem Sælands vei 1, 0371, Oslo, Norway; valentin.zuchuat@geo.uio.no*

² *Utah Geological Survey, PO Box 146100, Salt Lake City, Utah 84114; douglassprinkel@utah.gov*

ABSTRACT

Based on a methodic sedimentological analysis, the Late Jurassic (Oxfordian) Curtis Formation unravels the intricate facies variability which occurs in a tide-dominated, fluvially starved, low-gradient, semi-enclosed epicontinental basin. This unit crops out in east-central Utah, between the eolian deposits of the underlying Middle Jurassic (Callovian) Entrada Sandstone, from which it is separated by the J-3 unconformity, and the conformable overlying supratidal Summerville Formation of Oxfordian age. A high-resolution sedimentary analysis of the succession led to the recognition of eight facies associations (FA) with six sub-facies associations. Based on the specific three-dimensional arrangement of these eight facies associations, it is proposed to separate the Curtis Formation into three sub-units: the lower, middle and upper Curtis. The J-3 unconformity defines the base of the lower Curtis, which consists of upper shoreface to beach deposits (FA 2), mud-dominated (FA 3a) and sand-dominated heterolithic subtidal flat (FA 3b), sand-rich sub- to supratidal flat (FA 4a) and correlative tidal channel infill (FA 4c). It is capped by the middle Curtis, which coincides with the sub- to intertidal channel-dune-flat complex of FA 5, and its lower boundary corresponds to a transgressive surface of regional extent, identified as the Major Transgressive Surface (MTS). This surface suggests a potential correlation between the middle and the upper Curtis and the neighboring Todilto Member of the Wanakah Formation or Todilto Formation. The upper Curtis consists of the heterolithic upper sub- to intertidal flat (FA 6) and coastal dry eolian dunes belonging to the Moab Member of the Curtis Formation (FA 7), and it conformably overlies the middle Curtis.

The spatial distribution of these sub-units supports the distinction of three different sectors across the study area: sector 1 in the north, sector 2 in the south-southwest, and sector 3 in the east. In sector 1, the Curtis Formation is represented by its three sub-units, whereas sector 2 is dominated by the middle and upper Curtis, and sector 3 encompasses the extent of the Moab Member of the Curtis Formation.

This study also highlights the composite nature of the J-3 unconformity, which was impacted by various processes occurring before the Curtis Formation was deposited, as well as during the development of the lower and middle Curtis. Local collapse features within the lower and middle Curtis are linked to sand fluid overpressure within a remobilized sandy substratum, potentially triggered by seismic activity. Furthermore, the occurrence of a sub-regional angular relationship between the middle Curtis and substratum implies that the area of study was impacted by a regional deformational event during the Late Jurassic, before the deposition of the middle Curtis.

Citation for this article.

Zuchuat, V., Sleveland, A.R.N., Sprinkel, D.A., Rimkus, A., Braathen, A., and Midtkandal, I., 2018, *New insights on the impact of tidal currents on a low-gradient, semi-enclosed, epicontinental basin—the Curtis Formation, east-central Utah, USA: Geology of the Intermountain West*, v. 5, p. 131–165.

© 2018 Utah Geological Association. All rights reserved.

For permission to use, copy, or distribute see the preceding page or the UGA website, www.utahgeology.org, for information. Email inquiries to GIW@utahgeology.org.

INTRODUCTION

The complex aspect of tide-dominated environments was reported as early as first century AD, when Pliny the Elder, in his *Historia Naturalis*, wondered whether such areas “invaded twice each day and night by the overflowing waves of the ocean...are to be looked upon as belonging to the land, or whether as forming portion of the sea?” (translation from Bostock and Riley, 1855). Since then, it has been shown that the essence of tidal deposits resides within their typical three-dimensional intricate assemblage of heterolithic facies, which distribution is dictated by a fine equilibrium of sediment input, basinal hydrodynamic forces, as well as avulsing and migrating channels (Davis and Dalrymple, 2012; references therein). This complexity is further enhanced by temporal and cyclical variations of tidal currents in a basin, which unevenly impact the erosion-transport-deposition mechanisms of the different grain classes within the system (Kvale, 2012; Wang, 2012; references therein). Adding to the intrinsically dynamic system, the effects of fluctuating rates in relative sea-level variation are amplified by a low-gradient shelf through shifting facies belts over great distances (Midtkandal and Nystuen, 2009). Poor time constraints, limited but changing accommodation, and pre-existing basin floor relief further complicate the accurate interpretation and correlation of such deposits. Despite highly complex depositional scenarios, these conditions may produce substantial volumes of reservoir-grade sandstone, and represent potentially viable aquifers, CO₂-injection targets, or petroleum reservoirs (Martinius and others, 2005; Halland and others, 2014).

Research focusing on siliciclastic tide-dominated environments recognizes four main categories: (1) the upward fining, transgressive estuarine, (2) the (semi-)protected lagoonal systems, (3) the prograding tide-dominated deltas, as well as (4) the open-coast tidal flats (e.g., Boyd and others, 1992; Dalrymple and others, 1992; Fan, 2012). Whereas modern analogs can help scientists identifying such depositional systems in the rock record, Tape and others (2003) highlighted the fact that some tidally influenced sedimentary units do not belong to any of the above-mentioned classes and cannot be illustrated by modern equivalent

environments either, as they were deposited on broad and shallow epicontinental shelves. The outstanding outcrop quality and the significant internal variability of the Middle Jurassic Entrada Sandstone and Late Jurassic Curtis-Summerville Formations of east-central Utah allow a detailed investigation of gradual, subtle, and intricate interactions within such a low-gradient, continental to subtidal epeiric system, characterized by a starvation of major fluvial input (Kreisa and Moiola, 1986; Caputo and Pryor, 1991; Wilcox and Currie, 2008). The main objective of this study is to develop a detailed data-driven classification of heterolithic facies and facies associations present on a tidally influenced siliciclastic-dominated shelf of regional extent, represented by the Curtis Formation of Early Oxfordian age (about 161–159 Ma) (Kreisa and Moiola, 1986; Caputo and Pryor, 1991; Wilcox and Currie, 2008; Ogg and others, 2016). This work establishes the sedimentary basis for deconstructing the growth and infill dynamic of such a tide-dominated basin, which will be analyzed in a separate study. The overarching goal of this venture is to generate a multi-disciplinary predictive protocol to assess the combined seal-reservoir properties of such heterolithic deposits, notably for carbon capture and storage purposes.

GEOLOGICAL SETTING

Basinal Setting

Since the Mesozoic, Utah’s geological history has been profoundly influenced by several tectonic events, markedly by the development of the North American Cordillera and its cascade of orogenies; key orogenies, partly overlapping in time and space (Bump and Davis, 2003; Hintze and Kowallis, 2009; Thorman, 2011; Anderson, 2015; Yonkee and Weil, 2015; and references therein), are (1) the Middle Jurassic-Early Cretaceous Nevadan orogeny, whose remains notably consist of small granitic batholiths at today’s Utah-Nevada border, (2) the Middle Jurassic Elko orogeny, which differs from the other orogenies by alternating extensional and contractional tectonic events, (3) the Early Cretaceous to Paleogene Sevier orogeny, with its resultant thin-skinned contractional structures associated with a fore-

land basin development, and (4) the Late Cretaceous to Paleogene Laramide orogeny seen as basement-rooted monoclines, from which the San Rafael Swell and other large uplifts emerged. Additionally, rocks from east-central to southeastern Utah were also affected by movements of the Paradox Basin salt deposits (Trudgill, 2011), regional uplifts of the Colorado Plateau, and related extensional events (Levander and others, 2011; Murray and others, 2016). There were also intrusive and extrusive magmatic episodes during the Middle to Late Oligocene; the latter are expressed by the Henry, La Sal, and Abajo Mountains igneous complexes (Sullivan and others, 1991; Nelson, 1997). Burial history data compiled by Nuccio and Condon (1996) and Petrie and others (2017) suggest that the Curtis Formation was buried to depths of 2.45 km and 2.86 km near the San Rafael Swell.

Stratigraphy

The westward-thickening sedimentary succession of the San Rafael Group was deposited in neighboring areas of the Utah-Idaho trough, a north-northeast to south-southwest-trending distal retroarc foreland basin parallel to the Elko highlands (figure 1) (Anderson and Lucas, 1994; Brenner and Peterson, 1994; Peterson, 1994; Bjerrum and Dorsey, 1995; Thorman, 2011). This basin recorded multiple transgressive-regressive marine cycles (Anderson and Lucas, 1994). The marine and intertonguing eolian sediments of the coastal paleo-erg of the Middle Jurassic (Aalenian to Bajocian) Temple Cap Formation in southwestern and central Utah unconformably overlies the eolian Navajo Sandstone of Early Jurassic age on the J-1 unconformity (Pipiringos and O'Sullivan, 1978; Peterson and Pipiringos, 1979; Sprinkel and others, 2011). Paleowind indicators for the Navajo Sandstone suggest a north-northwest to south-southeast wind direction, whereas paleowind indicators for the Temple Cap Formation suggest a northeast to southwest wind direction (Parrish and Peterson, 1988; Peterson, 1988; Hartwick, 2010). To the east in south-central Utah, the former basal Harris Wash Member of the Page Sandstone unconformably overlies the Navajo Sandstone, above the J-2 unconformity of Pipiringos and O'Sullivan (1978) and Peterson and Pipirin-

gos (1979). Isotopic ages obtained from ash beds in the Harris Wash Member indicated they were time equivalent to the Temple Cap Formation and hence pre-dated the basal Carmel Formation (Kowallis and others, 2001; Dickinson and others, 2010; Sprinkel and others, 2011). This stratigraphic relationship brought into question the validity of the J-2 unconformity and led to the recommendation to re-assign the beds representing the Harris Wash Member of the Page Sandstone to the Temple Cap Formation (Sprinkel and others, 2011; Doelling and others, 2013). The shallow marine Middle Jurassic Carmel Formation (Gilluly and Reeside, 1928) conformably overlies the Temple Cap Formation, reflecting marine incursions from the northern Sundance seaway from Bajocian to early Callovian time (Anderson and Lucas, 1994; Brenner and Peterson, 1994; Peterson, 1994; Hintze and Kowallis, 2009; Sprinkel and others, 2011). However, the Carmel Formation does unconformably overlie the Navajo Sandstone in places where the Temple Cap Formation is missing because of irregular deposition of the Temple Cap on a pre-existing paleotopography and its depositional pinch-out in eastern Utah (Sprinkel and others, 2011; Doelling and others, 2013).

Continental conditions returned with the deposition of the Middle Jurassic (Callovian) Entrada Sandstone (Peterson, 1994; Hintze and Kowallis, 2009), formally defined by Gilluly and Reeside (1928). This sedimentary formation is divided into two units: (1) the basal Slick Rock Member, which consists of alternating eolian dune and interdune intervals, and (2) the overlying informal, intermittently vegetated, earthy facies, which was deposited in a marginal marine setting (Witkind, 1988; Crabaugh and Kocurek, 1993; Carr-Crabaugh and Kocurek, 1998; Mountney, 2012; Doelling and others, 2015). The Entrada Sandstone and correlative formations (Twist Gulch and Preuss Formations) thicken westward towards the Utah-Idaho trough and northwards towards the Sundance Seaway (Imlay, 1980; Kocurek and Dott, 1983). Dickinson and Gehrels (2009, 2010) showed that the siliciclastic grains of the Entrada Sandstone were mostly recycled from river systems sourced from the Appalachian Mountains, on the eastern side of the continent.

The Entrada Sandstone recorded four erg con-

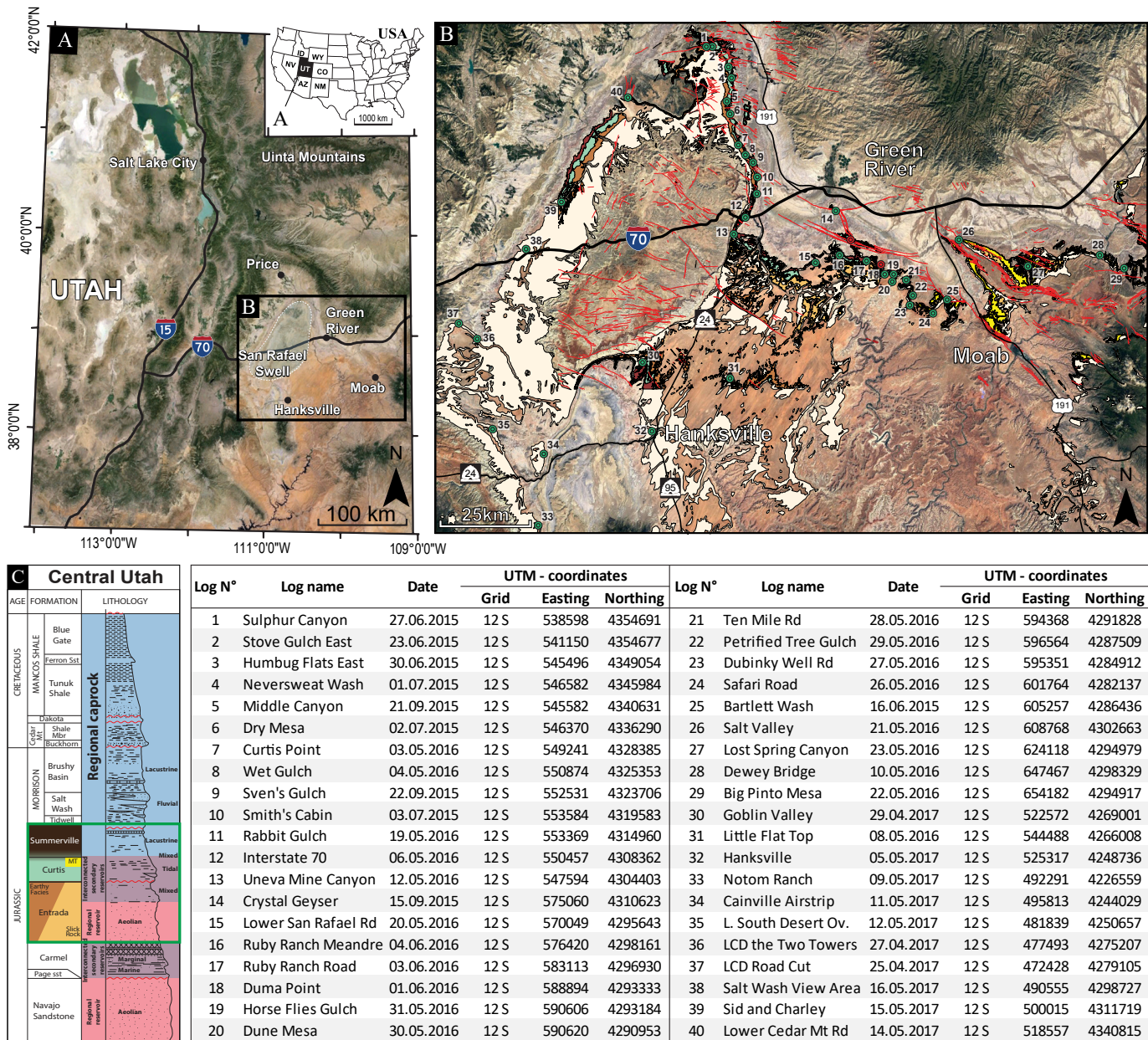


Figure 1. (A) Maps of the study area. (B) Green dots represent visited localities where the Curtis Formation crops out, whereas red dots (not numbered) illustrate its absence. Each dot number on the map refers to a specific locality in the attached table (geological units after Hintze, 1980; Witkind, 1988; Doelling, 2001; and Doelling and others, 2015). (C) Schematic stratigraphic column of the area (modified from Ogata and others, 2014).

struction-destruction cycles (sensu Mountney, 2006), dictated by regional variations of the paleo-water table, themselves related to relative sea level fluctuations (Carr-Crabaugh and Kocurek, 1998; Mountney, 2012). The entire system is truncated along its top by the regional J-3 unconformity (Pipiringos and O'Sullivan,

1978; Hintze and Kowallis, 2009), with local relief of up to about 23 m. In areas of south-central Utah, the J-3 unconformity truncates subtle, large-amplitude folds developed in the Entrada Sandstone and underlying formations, exhibiting distinctive angular relationships along the unconformity (see figure 7 of Wheatley and

others, 2016). Depending on location, this boundary can be characterized as a conformable contact, a paraconformity, a disconformity, or an angular unconformity. It is important to note that the precise time encapsulated in the composite J-3 unconformity remains unknown. Since the definition of an unconformity implies a “lacuna of substantial duration” (sensu Holbrook and Bhattacharya, 2012), the nature of the J-3 unconformity remains a point of discussion. Peterson (1994) argued that a regional tectonic uplift in the west played the major role in the development of this unconformity, whereas Caputo and Pryor (1991) as well as Eschner and Kocurek (1988), respectively, advocated that (unidentified) marine or tidal currents during the earliest stage of the Curtis transgression reworked the substratum.

The overlying tidally influenced Curtis Formation of Early Oxfordian age (Kreisa and Moiola, 1986; Caputo and Pryor, 1991; Wilcox and Currie, 2008; Ogg and others, 2016) was first formally defined by Gilluly and Reeside (1928), and its type section of Curtis Point is located about 5.3 km south of Dry Mesa, along the northeastern margin of the San Rafael Swell (UTM coordinates: 12S 547430/4331169). The formation is characterized by its greenish-whitish color due to the presence of glauconite or chlorite (Gilluly and Reeside, 1928; Caputo and Pryor, 1991; Peterson, 1994). Its striking color contrast to the underlying earthy red Entrada Sandstone is readily identifiable in outcrops. The typical thickness ranges between 30 and 80 m around the San Rafael Swell (Caputo and Pryor, 1991). Nevertheless, as it was deposited in the foredeep basin of the Elko orogeny (Thorman, 2011; Anderson, 2015), the formation pinches out southwards towards Tergeson Flats, about 38 km southwest of Hanksville, as well as eastwards in the vicinity of Duma Point, about 28 km south-southeast of Green River (figure 1) (Gilluly and Reeside, 1928; Caputo and Pryor, 1991; Peterson, 1994). As a note, the coastal paleo-erg of the Moab Member of the Curtis Formation is the lateral equivalent to the marine beds of the Curtis towards the east of the study area (Wright and others, 1962; Caputo and Pryor, 1991; Peterson, 1994; Doelling, 2001).

The Summerville Formation conformably overlies the Curtis Formation in the San Rafael Swell

and Henry Mountains basin and is characterized by dark-red and chocolate-brown hypersaline sabkha deposits, including evaporative ponds, which resulted in precipitation of gypsum and anhydrite (Gilluly and Reeside, 1928; Caputo and Pryor, 1991; Peterson, 1994; Lucas, 2014). Peterson (1994) described the marine Curtis Formation and the conformably overlying supra-tidal and sabkha deposits of the Summerville Formation as representing the fifth transgressive-regressive cycle within the Jurassic System of the Western Interior basin. This cycle potentially corresponds to Haq and others (1987) LZA-2.3 third-order transgressive-regressive interval, after calibrating their curve onto Wilcox and Currie (2008) age and Ogg and others (2016) time scale. The Curtis-Summerville interval correlates to the Redwater Shale Member of the Sundance Formation (Imlay 1947, 1980) in Wyoming, the Stump Formation around the Wyoming-Idaho border (Mansfield and Roundy, 1916; Pippingos and Imlay, 1979; Imlay, 1980), and the Stump Formation in the Uinta Mountains of northeastern Utah (Pippingos and Imlay, 1979; Imlay, 1980; Wilcox and Currie, 2008), reflecting the same transgressive-regressive period of the Sundance Sea (Pippingos and O’Sullivan, 1978; McMullen and others, 2014). In the Four Corners area, the Curtis Formation has been correlated to the Todilto Member of the Wanakah Formation, whereas the Summerville Formation is replaced by the Belclabito Member of the Wanakah Formation (Condon and Huffman, 1988). Note that Anderson and Lucas (1994) used a different nomenclature for the same interval; they regarded the Todilto as a formation rather than a member, whereas the Summerville Formation extends into the Four Corners area. The Summerville Formation is capped by the J-5 unconformity (Pippingos and O’Sullivan, 1978), which resulted from the fall of the regional base level (Caputo and Pryor, 1991; Peterson, 1994), generating a relief of at least 20 m, before being overlain by the fluvial sediments of the Tidwell Member, the lowermost unit of the continental Morrison Formation south of the Uinta Mountains (Waldschmidt and LeRoy, 1944; Peterson, 1988; Turner and Peterson, 1999). Figure 1C displays a summary stratigraphic column of the study area.

METHODS AND DATA

In order to understand the genesis of the Curtis Formation in the study area, fieldwork campaigns were conducted in 2015, 2016, and 2017. The data included in this paper comprise (1) 40 detailed sedimentary logs (figure 1), which locations were chosen based on outcrop exposure quality, accessibility, and regular distance between each measured section; (2) pictures taken at and between log-sites by all members of the research group involved in the project, as well as Unmanned Aerial Vehicles (UAVs), aerial photographs, satellite images, and open-source imagery available from Google and Microsoft Bing databases; and (3) recordings of paleocurrent directions and other structural data. Three-dimensional (3D) virtual outcrops were generated for selected localities following Westoby and others (2012) structure-from-motion photogrammetry principles, in order to assess the architecture of the sedimentary succession. UAV data were processed using PhotoScan Pro by Agisoft (Agisoft LLC, St. Petersburg, Russia), whereas the 3D-generated models were subsequently analyzed and interpreted in Lime (developed by the Virtual Outcrop Geology (VOG) Group from the Universities of Bergen and Aberdeen). Traditional sedimentologic methods were applied, such as identification of depositional sub-environments and correlation across short and long distances in order to reconstruct the spatial and temporal distribution of sub-units of the target strata. The resultant assimilation of data allows the construction of an improved depositional model for the Curtis Formation, and sheds light on how sediments are dispersed across a shallow shelf in general.

RESULTS

Twenty-four sedimentary facies were recognized and summarized in table 1. Rock fabric, composition, and structure(s) are the key to interpreting the processes and conditions under which these sediments were deposited. As a result, these facies have been organized in eight main facies associations (FA 1 to FA 8) with six sub-facies associations (FA 1a, FA 1b, FA 3a, FA 3b, FA 4a, and FA 4b), which are summarized in table 2 and carefully described below.

These facies associations are not homogeneously distributed across the study area (figures 2 and 3). It is important to mention that the datum on which the measured sections are aligned on figure 3 corresponds to the J-3 unconformity. To increase the visibility of the correlation, 19 out of 41 visited localities were selected based on spatial distribution and completeness of the sedimentary succession. Pie charts reflect the ratio between the different facies associations present in the Curtis Formation, whereas the Entrada Sandstone and the Summerville Formation are neglected. Based on the spatial distribution of these various facies associations, it is possible to divide the study area into sectors 1, 2 and 3 (figure 3), which are discussed further below.

FA 1 – Coastal Wet Eolian Deposits

Description

This unit corresponds to the cross-stratified eolian dunes and sandy interdunes (Facies A in table 1) of the Slick Rock Member (Entrada Sandstone, FA 1a), which crops out in the eastern and southeastern part of the study area (figure 1). Towards the west, FA 1 coincides with the parallel-laminated to mottled deposits (Facies B) dominating the earthy facies (FA 1b) of the Entrada Sandstone, with interfingering trough cross-stratified sandstone (Facies C), rippled cross-stratified sandstone (Facies U), and isolated coastal eolian dunes (Facies A). The hoodoos of Goblin Valley State Park mainly consist of structureless sandstone (Facies D). This sedimentary package thickens westward. Only at Safari Road (figure 1), FA 1 is capped by a rusty-red, calcite-cemented, thoroughly bioturbated, fine-grained sandstone (Facies E). Facies C (trough cross-stratified sandstone) occurs sporadically within FA 1, reaching a maximum thickness of about 1 m and is located 13 m below the base of the Curtis Formation at the Crystal Geyser section (figure 1). Here, the well-sorted foresets alternate between coarse and fine-grained sand with potential double mud drapes. Facies A, Facies B, Facies C, and Facies T are characterized by a sharp contact at their base, which can also be erosive, especially for Facies A, C, and T. Facies T usually appears both at the base and at the top of eolian dune packages (Facies A) but can also crop out

Table 1. Facies description for the Entrada Sandstone, Curtis Formation, and Summerville Formation (continued on following page).

Facies	Description	Structures	Grain Size*	Interpretation	Formation
A	Cross-stratified sandstone	Unidirectional tangential cross-bedded very fine to fine-grained sandstone, alternating grain flow and grain fall deposits, sharp base, rusty red or white, locally bleached, local occurrence of rhizoliths, varying bedform/bedform sets size, maximum individual dune thickness 15 m. Potential occurrence of counter-ripples at the toe of the foresets	VF - F	Eolian dune deposits, locally influenced by a dynamic and migrating water table/saturated level	Entrada Ss. Moab Mbr.
B	Plane parallel-laminated to mottled mudstone with localized evaporites	Dark red silty mudstone with pale yellow to white very fine to fine-grained sand lenses, plane parallel-laminated to -stratified or mottled, potential bleached patches around rhizoliths, localized evaporite-rich horizons, maximum individual horizon 1 cm	Si - Cl	Eolian interdune deposits showing occasional flooding with development of sabkha-type deposits and/or superficial vegetation	Entrada Ss. Summerville Fm.
C	Trough cross-stratified sandstone	Trough cross-stratified very fine to medium-grained sandstone, potential mud drapes and rip-up mud clasts, eventual desiccation cracks and/or evaporite-rich horizons. Thickness ranging between dm- to m values	VF - M	Tidally influenced migrating 3D-dunes	Entrada Fm. Curtis Fm. Summerville Fm.
D	Structureless fluidized sandstone	Deformed to structureless fluidized of green to pink silt to fine-grained sandstone, local fluid-escape and loading structures still visible, sometimes visually expressed as well rounded sandstone boulders with injected mudstone, maximum boulder diameter (Ø) 25 cm, maximum bed thickness 2 m	Si-F	Destruction of original sedimentary structures due to fluids flowing through the sandstone bed or through liquefaction of water-saturated horizons	Entrada Ss. Curtis Fm.
E	Thoroughly bioturbated condensed sandstone	Rusty-red condensed, cemented, fine-grained sandstone, thoroughly bioturbated, maximum thickness 25 cm	F	Sediment starvation in a semi-arid coastal plain setting	Entrada Ss.
F	Matrix-supported basal conglomerate	Rounded to well-rounded, matrix-supported basal conglomerate, no preferred clast orientation but their long axis tend to be parallel to the bedding plane, matrix consists of fine- to medium-grained sandstone, maximum clast Ø 8 cm, maximum bed thickness 20 cm	F-Pb	Flash flood deposits	Curtis Fm. ?
G	Planar- to low angle cross-stratified sandstone	Plane-parallel to low-angle cross-stratified, very fine to fine-grained, gray to green to white sandstone, potential herringbone cross-lamination, current and oscillation ripple-lamination, as well as dm-scale soft-sediment deformation, maximum individual bed thickness 60 cm	VF - F	Upper shoreface to beach deposits with tidal influence	Curtis Fm.
H	Tangential cross-stratified gravely sandstone	Matrix-supported conglomeratic dune, hm-scale lateral extent, sub-horizontal erosive base, rip-up mud clasts, extra-basinal sub- to rounded clasts, maximum clast Ø 2.5 cm, unidirectional current trough cross-stratification, maximum individual dune thickness 2.5 m	M - Gr	High energy, asymmetric tidal flow pattern within a laterally restricted embayment	Curtis Fm.
I	Tidally influenced cross-stratified conglomeratic sandstone	Matrix- to clast-supported lense-shaped intraformational conglomerate of restricted lateral extent, locally developed and amalgamated in tidal bundles; rip-up mud clasts, extra-basinal sub- to rounded clasts, maximum clast Ø 2.5 cm, bidirectional cross-stratification with superimposed current ripples, maximum bed thickness 60 cm	F - Gr	High-energy tidal channels-inlets	Curtis Fm.
J	Planar cross-stratified sandy conglomerate	Clast- to matrix-supported conglomerate, hm-scale lateral extent, convex-down erosive base, flat top, extra-basinal sub- to rounded clasts, maximum clast Ø 2.5 cm, planar cross-stratification, maximum individual thickness 3.0 m	M - Gr	Point bar lateral accretion within a migrating tidal channel	Curtis Fm.
K	Plane parallel-laminated mud- to siltstone	Plane parallel-laminated mud to siltstone, scattered bidirectional current ripple cross-stratifications, gray to green, occasional desiccation cracks, sporadic bioturbations both parallel and normal to the bedding planes	Si - Cl	Gentle flow activity with tidally related current reversals	Curtis Fm.

*Cl=clay, Si=silt, VF=very fine, F=fine, M=medium, Gr=gravel, Pb=pebble; Grain size in parentheses denotes rarely present and bracketed denotes at the boundary between VF and F

Table 1 (continued from previous page). Facies description for the Entrada Sandstone, Curtis Formation, and Summerville Formation.

Facies	Description	Structures	Grain Size*	Interpretation	Formation
L	Heterolithic silt- and sandstone with lenticular bedding	Rippled very fine to fine-grained sandstone, grayish lenses containing herringbone and current ripple cross-stratifications within a matrix of laminated gray to green mud- to siltstones, occasional desiccation cracks, sporadic bioturbations both parallel and normal to the bedding planes	Si - F	Current reversals in lower subtidal zone	Curtis Fm.
M	Heterolithic silt- and sandstone with wavy bedding	Ripple cross-stratified very fine to fine-grained grayish sand layers, with bi-directional current indicators and interbedded with laminated gray to green siltstone, occasional desiccation cracks, sporadic bioturbations both parallel and normal to the bedding planes. Varying amount of organic matter	Si - F	Current reversals in subtidal zone (shallower than Facies L)	Curtis Fm. Moab Mbr.
N	Heterolithic sandstone with flaser bedding	Ripple and herringbone cross-stratified very fine to fine-grained gray to green to white sandstone, scattered mud lenses, as well as single and double mud drapes, varying amount of organic matter	VF - F	Upper sub- to lower intertidal sandy flat	Curtis Fm.
O	Sandstone with climbing ripples	Climbing ripple cross-stratified very fine to fine-grained sandstone, gray to green	VF - F	Tidal channel overbank spill on tidal flat, Upper sub- to lower intertidal sandy flat	Curtis Fm.
P	Cross-stratified sandstone arranged in well-defined rhythmic tidal bundles	Very fine to fine-grained (medium-grained rarely present) gray to green to white sandstone, arranged in tidal bundles, with occasional anti-ripples documented from their toesets. Varying amount of organic matter	VF - F (M)	Tidal inlets, lower energy than Facies I	Curtis Fm.
Q	Structureless sandstone	Very fine to fine-grained gray to green to white sandstone, massive, with potential scattered single and/or double mud drapes. Usually rounded and smoothly weathered	VF - F	The nature of the lack of structure might only be due to intensive surface weathering. Presence of mud drapes indicate sub- or intertidal environment	Curtis Fm.
R	Thoroughly bi-directional rippled cross-stratified sandstone	Thoroughly rippled silt to very fine grained sandstone, dominated by herringbone cross-stratifications	S - VF	Deep subtidal environment with near equal flood and ebb tidal current conditions. Note that the weathering can in some cases erase most of the sedimentary structures	Curtis Fm. Moab Mbr.
S	Plane parallel-stratified sandstone	Plane parallel-stratified very fine to fine-grained sandstone with scattered current ripple lamination, white, pink or green. Note that the weathering expression of this facies varies between the different units of the Curtis Fm. Potential mud cracks and soft-sediment deformation	(Si-) VF - F	Sandy tidal flat, upper flow regime (to lower antidune-regime?). Documented mud cracks indicate short-lived subaerial exposure	Curtis Fm. Moab Mbr.
T	Condensed sandstone	Thin, yellow structureless sandstone, occasionally displaying low-amplitude undulations, exclusively observed capping the Moab Member of the Curtis Fm. Maximum bed thickness 10 cm	[VF-F] F	Condensed horizon	Moab Mbr.
U	Rippled cross-stratified sandstone	Undulated to rippled cross-stratified, very fine to fine-grained, gray to brown sandstone, with 3D current ripples, possible interference ripples, potential mud cracks and soft-sediment deformation	VF - F	3D migrating ripples under unidirectional current conditions	Entrada Ss. Curtis Fm. Moab Mbr. Summerville Fm.
V	Plane parallel-laminated siltstone	Dark red soft slope-forming siltstone, most probably plane parallel-laminated, scattered pale white bleached lenses and evaporites	Si	Supratidal plain	Summerville Fm.
W	Iron rich ripple- and parallel-laminated sandstone	Dark red to brown cemented very fine to fine-grained sandstone, gentle ripple cross-stratification, potential desiccation cracks	VF - F	Fluvial overbank flooding deposits	Summerville Fm.
X	Paleosol	Dark purple mud or silt	Cl-Si	Sub-aerially exposed surface with superficial soil development	Entrada Ss. Curtis Fm. Moab Mbr. Summerville Fm.

*Cl=clay, Si=silt, VF=very fine, F=fine, M=medium, Gr=gravel, Pb=pebble; Grain size in parentheses denotes rarely present and bracketed denotes at the boundary between VF and F

Table 2. Facies associations for the Entrada Sandstone, Curtis Formation, and Summerville Formation.

Facies Association	Depositional Environment	Facies Included	Formation
FA 1a	Coastal wet eolian dune system (Kocurek and Havholm, 1993; Mountney, 2012), with episodic (marine) partial flooding of interdunes deposits and superficial development of soil- and vegetated horizons	A, C, X	Entrada Ss. Slick Rock Mbr.
FA 1b	Coastal wet eolian interdune system (Kocurek and Havholm, 1993; Mountney, 2012), with episodic (marine) partial flooding of interdune deposits and superficial development of soil and vegetated horizons	B, C, D, X	Entrada Ss. earthy facies
FA 2	Beach deposits to upper shoreface deposits, with potential associated tidal channel cut-and-fill	C, G, S, U	Curtis Fm.
FA 3a	Subtidal heterolithic mud, silt, and very fine grained sandstone, generally coarsening up from laminated mudstone, wavy bedding, scarcely bioturbated	H, I, J, K, L, M	Curtis Fm.
FA 3b	Subtidal heterolithic vf- to f-grained sandstone generally coarsening up from wavy bedding to flaser bedding, scarcely bioturbated	H, I, M, N	Curtis Fm.
FA 4a	Sandy tidal flat with correlative major tidal channels, having potential subaerial exposures	S, U, X	Curtis Fm.
FA 4b	Tidal channel infills and splays, distal correlative of FA 4a in the northern areas	C, H, I, L, M, N, S, U	Curtis Fm.
FA 5	High energy, sub- to intertidal sand -dominated environments, encompassing tidal flats, tidal channels, and beaches	C, G, (K, L, M,) N, O, P, Q, R, S(, X)	Curtis Fm.
FA 6	Upper intertidal heterolithic channels and flats complex, fining up, with intermittent prolonged subaerial exposures and rare bioturbation, indicator of a more stressed environment than FA 3	K, L, M, N, Q, S, U, X	Curtis Fm.
FA 7	Coastal dry eolian dune field (Mountney, 2012), arranged in four to five sequences separated by supersurfaces, upon which transgressive water-carried sediments and/or paleosol can be observed	A, N, Q, S, T, U, X	Curtis Fm. Moab Mbr.
FA 8	Supratidal lower coastal plain, with episodic marine flooding	U, V, W, X	Summerville Fm.

as individual beds within a mottled interval (Facies B). Note that Facies B can locally grade up-section into paleosols (Facies X). Bleached patches of rock commonly underlie and overlie paleosols or are found in the direct

vicinity of such horizons, contributing to the mottled expression (Blodgett, 1988). The top of FA 1 is capped by regional J-3 unconformity of Pipingos and O’Sullivan (1978).

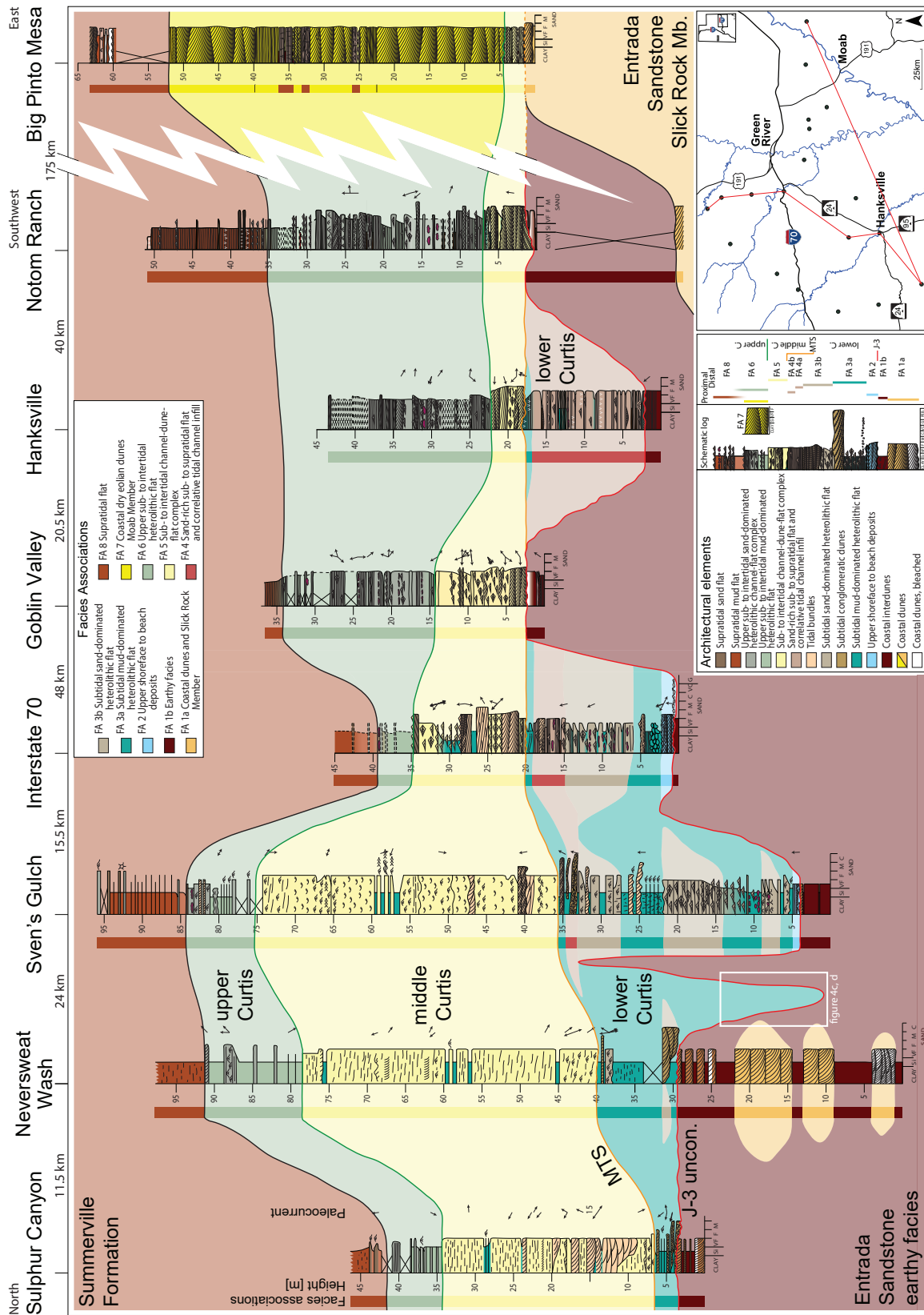


Figure 2. North-southwest-east cross section across the study area showing the spatial distribution of the main facies associations identified within the uppermost strata of the Entrada Sandstone, the Curtis Formation and the lowermost strata of the Summerville Formation along the western margin of the San Rafael Swell and south to the Henry Mountains. The Big Pinto Mesa measured section represents the typical expression of the Moab Member of the Curtis Formation. Detailed sedimentary information on the various architectural elements present at the selected localities is displayed on the measured sections, whereas facies associations are color-coded in each summary column next to their respective measured section.

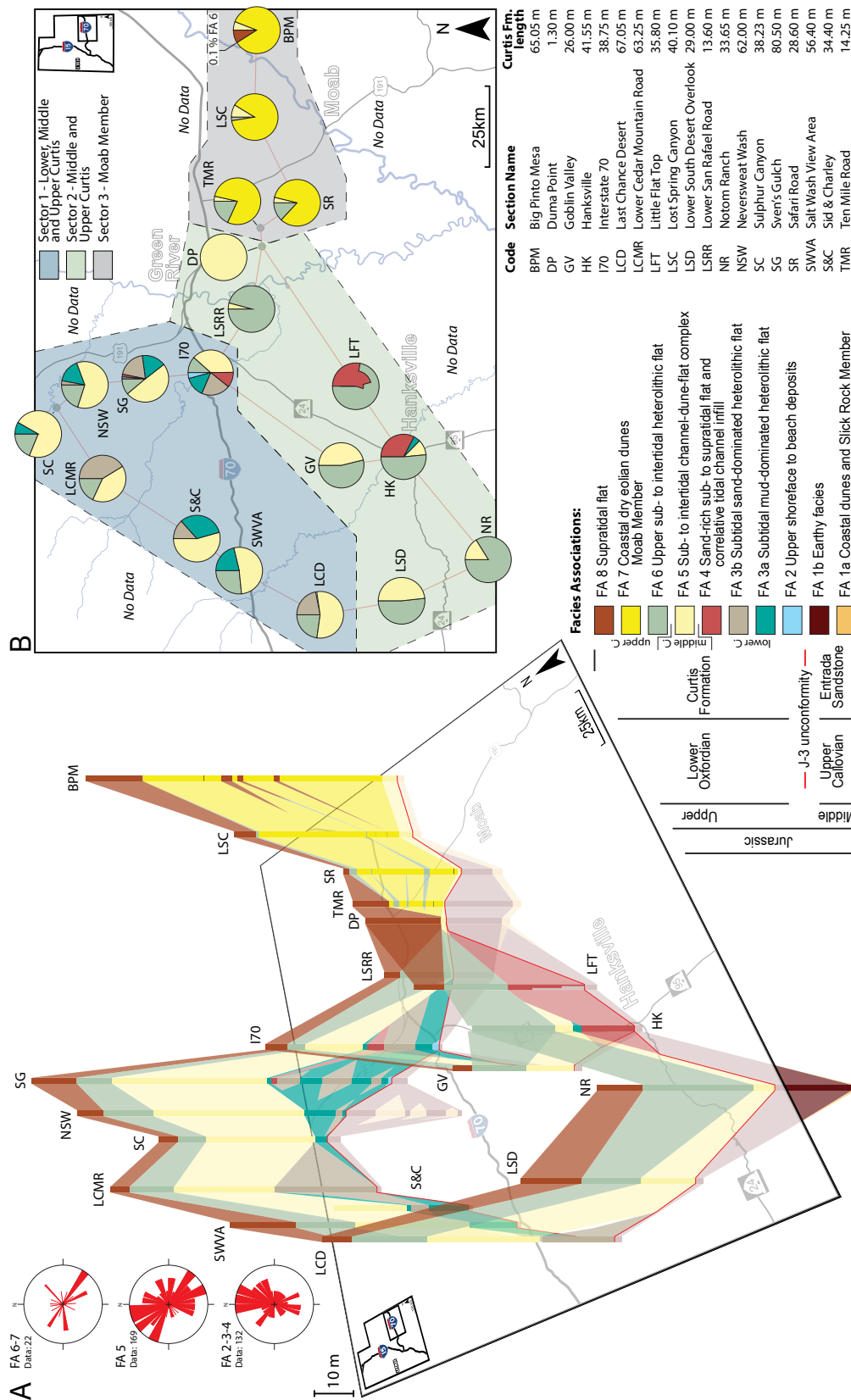


Figure 3. (A) 3D correlation between selected localities. As the sedimentary sections are aligned on the J-3 unconformity (red line), the Entrada Sandstone appears below the map, whereas the Curtis Formation remains above it. Paleocurrent measurements are arranged stratigraphically from bottom to top. (B) Pie charts representing the ratio between the different facies associations belonging to the Curtis Formation at each locality. See text for discussion of unusual pattern in Little Flat Top (LFT).

On a structural geology note, numerous conjugated extensional faults, associated fractures, and remobilized, injected and disintegrated sand (Facies D), as well as hydroplastic deformation occur in the upper Entrada Sandstone in the Humbug Flats area, at Smith's Cabin in the north, farther south between Interstate 70 and Uneva Mine Canyon, and north of Hanksville Airport (figure 1). Fractures typically feature a bleached front in their direct vicinity (figure 4A). Fault planes are mostly planar; however, growth-fault geometry on south-facing faults is found near Smith's Cabin. Faults show meter-scale offset in the earthy facies of the Entrada Sandstone, whereas most of them are concealed by the base of the Curtis Formation, which remains undisturbed. Faults strike east-west around the Humbug Flats-Smith's Cabin area in the north; whereas south of Interstate 70 they strike north-south. Note that bleaching is common along fractures and faults within FA 1 (figure 4a). However, 2.1 km north of Hanksville Airport, the earthy facies (FA 1b), was impacted by syn- to post-depositional localized extensional and contractional faults, as well as synchronous erosion, generating a 2 to 3 m relief at the top of the Entrada Sandstone (figure 4F). These fault clusters display a semi-circular surface expression. The heterolithic deposits of lower Curtis (FA 3-4) passively filled the preexisting topography, before being rapidly overlain by the middle Curtis sediments (FA 5), which abruptly collapsed by faulting while or shortly after being deposited. It remains unclear how precisely and when these processes jolted the deposits of the middle Curtis.

Interpretation

Interbedding of eolian dune, interdune, sabkha, and tidal deposits are typical features for coastal wet eolian desert environments, as interpreted and described by several authors (Crabaugh and Kocurek, 1993; Kocurek and Havholm, 1993; Mountney, 2012). Occurrence of marginal marine sandstones, gypsum-rich beds, and paleosols horizons within an interval dominated by Facies B are related to partial marine flooding and/or relative water table rises within the sediments (Carr-Crabaugh and Kocurek, 1998; Mountney, 2006). On the contrary, intervals dominated by eolian dunes reflect short-lived

relative base level falls (Mountney, 2006, 2012). Mottling is ascribed to forced disturbance from roots and has been enhanced by circulation of organic acids through the tight mudstones (Blodgett, 1988), most probably flowing along root burrows. Also, the development of the condensed and bioturbated sandstone bed (Facies E) at the top of FA 1 indicates an extended period of sediment starvation (Urash and Savrda, 2017) around the area known today as Safari Road (figure 1). Consequently, FA 1 is considered to represent a coastal eolian system, where marine processes and water table variations jointly and increasingly influenced the sedimentary development of the Entrada Sandstone. Bleached fronts observed along fractures in the earthy facies occurred as a consequence of post-depositional reducing fluid circulation within a naturally CO₂-charged system (Kampman and others, 2013; Ogata and others, 2014; Skurtveit and others, 2017; Sundal and others, 2017). As conjugated fault sets mostly offset the strata of the earthy facies, consequent extensional faulting appears to have occurred post-earthly facies deposition, but pre-Curtis sea transgression. The occurrence of disturbed earthy facies layers, as well as lower and middle Curtis strata 2.1 km north of Hanksville Airport implies that the lowermost Late Jurassic strata responded to episodes of sand mobility which impacted the surface morphology.

FA 2 – Beach to Upper Shoreface Deposits

Description

FA 2 is recorded at Curtis Point, Sven's Gulch, Interstate 70, and Uneva Mine Canyon measured sections (figure 1). It reaches a maximum thickness of about 1.70 m at Sven's Gulch. FA 2 shows a clear upward-fining trend, where the lowermost plane parallel-stratified sandstone of Facies S and planar to low-angle cross-stratified sandstone of Facies G are overlain by the trough cross-stratified sandstone of Facies C and/or ripple-laminated sandstone of Facies U. Mud drapes and rip-up clasts are also documented at Interstate 70 and Uneva Mine Canyon. FA 2 overlies FA 1, from which it is separated by the J-3 unconformity, locally displaying load structures (figure 5). The transition between FA 2 and the overlying FA 3 occurs either as a gradual and

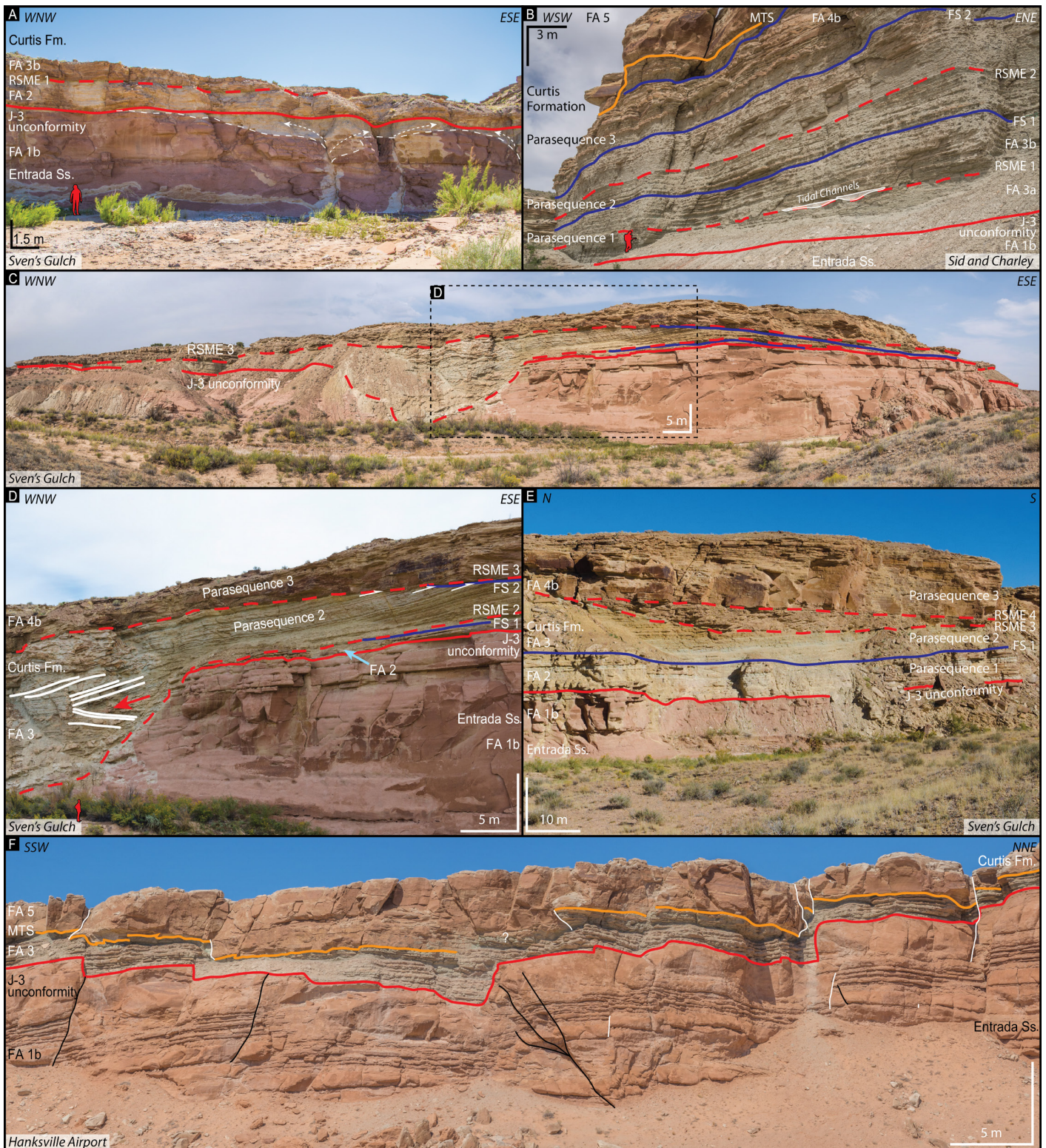


Figure 4. Caption on the following page.

Figure 4 (figure on the previous page). Overview of the lower Curtis in sector 1. See figure 3 for sectors, and figure 1 for photograph locations. (A) The beach to upper shoreface deposits of FA 2 overlie the earthy facies of Entrada Sandstone (FA 1b) at Sven's Gulch. FA 2 is truncated at its top by a Regressive Surface a Marine Erosion (RSME), corresponding to the base of FA 3b (Sand-Dominated Subtidal Heterolithic Flat). Note the plume geometry of the bleached zones below the J-3 unconformity, suggesting a trapping of the reducing fluids below the sand of FA 2 as they circulate along fractures within the Entrada Sandstone (white arrows; Skurtveit and others, 2017, Sundal and others, 2017). (B) The three parasequences occurring in the lower Curtis, as observed at the Sid and Charley sections on the western margin of the San Rafael Swell. Note the occurrence of two small tidal channels (white surfaces) at the base of RSME 1 (FS: Flooding Surface). The lower Curtis is capped the a Major Transgressive Surface (MTS), which can be traced across the study area. (C and D). Major tidal incision observed at Sven's Gulch, carved during a short-lived regressive phase within Parasequence 2. The red arrow points at a boulder of Entrada Sandstone within a matrix of Curtis Formation, indicating that the Entrada was poorly lithified when incised. The presence of this boulder, as well as FA 3 cannibalising its substratum, show that this depression was actually carved into the Entrada Sandstone by tidal currents, rather than being a pre-existing relief subsequently filled by the Curtis Formation. Note also the bi-truncation of Parasequence 2 during the early transgression of Parasequence 3, followed by the cannibalisation by FA 4b of its substratum during a short-lived regressive phase within Parasequence 3. (E) Display of two incision phases within the FA 4b deposits of Parasequence 3. (F) Collapse structure complex linked to sand mobility in the lower and middle Curtis cropping out 2.1 km north of Hanksville Airport. White lines indicate normal faults, whereas the black lines highlight contractional structures.

fining-upward changeover or corresponds to a sharp and erosive contact (figures 4a and 5). Note that the lateral extent of FA 2 reaches 200 to 500 m, and at the measured section Interstate 70, FA 2 is arranged in laterally accreting sandstone bodies, interbedded with FA 3 finer heterolithic material.

Interpretation

The high sand content of these rocks combined with the extremely low mud content indicate a high-energy marine environment. The deformation of the J-3 unconformity and the underlying FA 1b by loading suggests a poorly lithified Entrada Sandstone at the time of deposition (Owen and others, 2011). The occurrence of oscillation ripple lamination, as well as planar to low-angle cross-stratified sedimentary structures are clear indicators of upper shoreface to beach deposits. The occurrence of rip-up clasts and mud drapes testifies of secondary tidal action over the system. The overall fining-upward trend from FA 2 into FA 3 indicates a gradual transgression of the Curtis sea over the J-3 unconformity, whereas the restricted character of FA 2 suggests a direct influence of the pre-existing erosional relief over the distribution of these marginal marine deposits. They represent the onset of marine deposition into an erosional topography, and thus initially filled the available accommodation in the dips and furrows. FA 2

also displays the same deepening-upward development at Sven's Gulch. However, its base is characterized by a short-lived shallowing-upward event, as recorded by the basal oscillation ripple-laminated sandstone of Facies U (ripple-laminated sandstone). It is then overlain by the 3D migrating dunes of Facies C before grading into the high-energy deposits of Facies S (plane-parallel stratified sandstone) and G (planar to low-angle cross-stratified sandstone). It subsequently follows the same deepening-upward pattern as mentioned above. The fact that these marginal marine-beach deposits are only documented from the measured sections south of Curtis Point (figure 1) suggests a flooding of the southern areas from the northeast, before expanding towards the northern higher grounds.

FA 3 – Heterolithic Subtidal Flat and FA 4 – Sand-Rich Sub- to Supratidal Flat and Correlative Tidal Channel Infill

Description

FA 3 (figure 4) displays the lowermost sedimentary package, which represents the Gilluly and Reeside (1928) type section of the Curtis Formation and crops out mostly in sector 1, as well as Little Flat Top and Hanksville (figure 3). It is separated into a lower mud-dominated interval (FA 3a), which grades into an

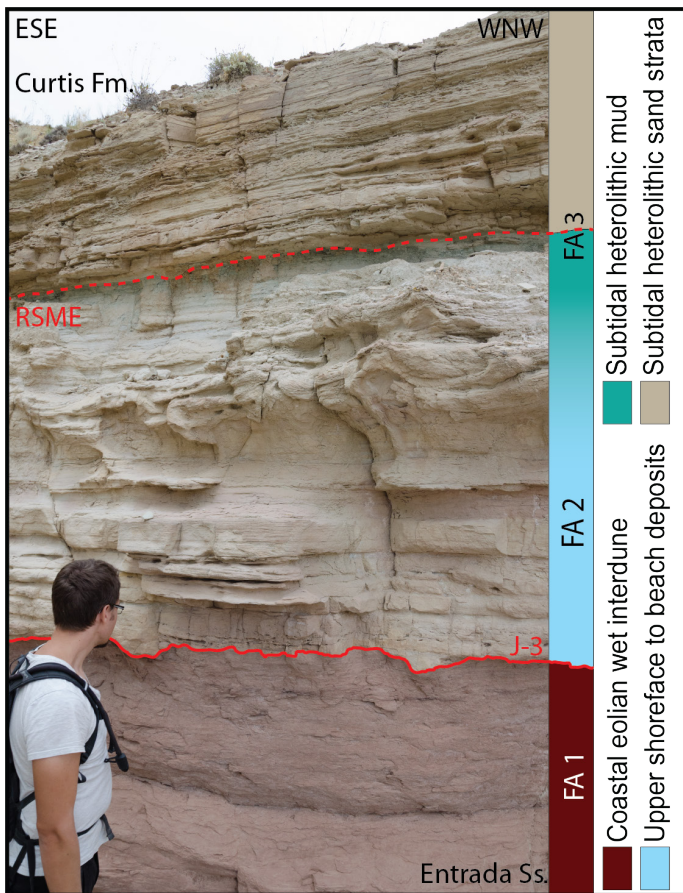


Figure 5. Transition from the Entrada Sandstone into the lower Curtis as observed at Sven's Gulch. FA 2 (beach to upper shoreface deposits) overlies the earthy facies of the Entrada Sandstone (FA 1b), from which it is separated by the J-3 unconformity. Note the presence of load casts at the base of FA 2 at some localities. FA 2 rapidly grades into FA 3a (mud-dominated heterolithic subtidal flat), which can be cannibalised by the sand-dominated subtidal deposits of FA 3b (RSME: Regressive Surface of Marine Erosion).

upper sand-dominated association (FA 3b) (table 2). FA 3a and FA 3b dark-green to gray color makes it readily identifiable in the field, where their combined thickness can vary significantly over a few hundred meters, ranging from less than a meter to about 30 m. FA 3 (dis)conformably overlies or onlaps the J-3 unconformity which caps FA 1 notably in the northern part of the study area (figure 1). It can also overlie FA 2 from which it fines upward or erodes into (figures 4 and 5). FA 3 displays at least two major coarsening-upward parasequences

(Parasequence 2 and Parasequence 3) (sensu Catuneanu and others, 2009). A third parasequence (Parasequence 1) has been observed at Sven's Gulch and the Sid and Charley section (figure 1). Both Parasequence 2 and Parasequence 3 comprise a suite of sedimentary facies commonly associated with tidal deposits: FA 3a includes laminated mudstone (Facies K), lenticular (Facies L), and wavy bedding (Facies M), whereas FA 3b comprises wavy bedding (Facies M) and flaser bedding (Facies N), with the presence of straight, sinuous-crested, and linguoid current ripples, as well as herringbone cross-lamination. Sub-vertical and sub-horizontal bioturbations are recorded in FA 3a and FA 3b; the degree of disturbance varies, but remains limited, and corresponds to Droser and Bottjer's (1986) ichnofabric index n°3. Furthermore, their diversity is circumscribed to only a few types, such as *Thalassinoides*, *Cruziana*, or *Gyrochorte comosa* ichnofossils, similarly reported from the Carmel Formation (De Gibert and Ekdale, 1999). FA 3 increases in grain size towards the south, with a generally higher sand-to-mud ratio on the western margin of the study area. Its upper boundary is truncated by FA 5, which can, however, be locally conformable.

A significant tidal incision can be observed at Sven's Gulch, carving about 15 m into its substratum (FA 1b and FA 2) and reaching a width of about 60 m (figures 4C and 4D). The infill of that incision shows an intricate architecture, which mostly consists of FA 3b material, as well as one boulder of earthy facies (FA 1b). Meter-scale, runnel-shaped gravelly bodies (Facies I) are also documented at all locations north of Sven's Gulch, displaying evidence of tidal reworking within a heterolithic environment. The area north of Middle Canyon (figure 1) is marked by the occurrence of laterally extensive gravel-rich compound dunes, displaying basinward-dipping, meter-thick tangential cross-stratification, with a non-erosive bedding-parallel base and a concave-up top surface (Facies H) (figure 6), and are usually found in the lowermost meters of the Curtis Formation. Conglomeratic dunes are not to be mistaken with the laterally accreting conglomeratic tidal channels, which are characterized by planar to tangential cross-stratification and a concave-down erosive base (Facies I and J). Also, at the measured section just south of Interstate 70, FA 2 is overlain by a 1-m-thick greenish-colored sandstone,



Figure 6. (A) Outline of a westward laterally migrating tidal channel observed in the cliffs of Cedar Mountain, filled by the conglomeratic sandstone of Facies I. The transition from a cross-stratified conglomerate into a more parallel-bedded conglomerate reflects a change in the channel orientation, as the cross-stratified deposits correspond to a transversal cross section of the channel, whereas the parallel-bedded part of the channel represents a longitudinal cross section through the same channel. (B) Transversal section across a north-westward migrating conglomeratic dune (Facies H, table 1) in the cliffs of Last Chance Desert. This dune was influenced by tidal processes, as illustrated by the bundle-like regular and rhythmic thickness variations observed between the foresets. The biggest discrepancy between the tidal channel and the tidal dune resides within their respective base. The tidal channel displays a concave-down erosive base and a flat upper surface, whereas the dune is characterised by a non-erosive and bedding-parallel base and a convex upper boundary.

completely disturbed by processes related to liquefaction and water escape (Facies D), which has not been observed anywhere else in the study area. The road cut section measured at Last Chance Desert (figure 1) also displays a unique feature which has not been documented anywhere else: a 20-cm-thick, matrix-supported basal conglomerate, with randomly oriented, rounded to well-rounded extra-basinal clasts that are about 8 cm in diameter (Facies F). The outcrop exposure of this conglomeratic bed limits the exact measurement of its lateral extent, but reaches a minimum of 70 m.

FA 4a conformably lies within and must interfinger with FA 3a and FA 3b within Parasequence 2. It represents 30% to 50% of the Curtis Formation in Hanksville and Little Flat Top, but it has not been observed at the locations north of Smith's Cabin nor on the western margin of the San Rafael Swell (figures 1, 2, 3, and 7). It is characterized by its dominant light-pink, plane parallel-stratified or structureless, very fine to fine-grained sandstone (Facies S) and subordinate unidirectional straight-crested 2D and 3D current ripple-dominated intervals (Facies U), as well as centimeter-thick marine mudstone. Episodes of subaerial exposure are recorded as dark-purple paleosol horizons (Facies X, figure 7) or desiccation cracks. Each individual bed measures as much as 1.50 m thick and can be laterally traced over several kilometers. Although appearing isopachous at outcrop scale, its thickness ranges from about 15 m at Rabbit Gulch to 2 m at Uneva Mine Canyon (figure 1), and it reaches a maximum of about 20 m thick at Little Flat Top (figure 1). About 250 m south of the Interstate 70 measured section, FA 4a forms a convex-down, flat-topped feature with sand-dominated heterolithic beds that thicken towards the center. It measures 6.25 m thick and about 45 m wide. At first glance, the architecture and shape resemble a channel infill succession, but it lacks any erosional scour at its base or internally. It only thickens in its central part due to differential loading (figure 7D). FA 4b has exclusively been documented in the Parasequence 3 interval at Sven's Gulch (figure 1), where the measured section traces a 15 m thick succession between two tidal channels that incise their FA 3 substratum by as much as about 10 m (figures 4C, 4D, and 4E). Note that at least two episodes of incision might have occurred during the deposition of FA 4b,

as visible in Sven's Gulch. The first incision carves the deepest into the FA 3a-3b deposits, whereas the second incision is shallower. The channel infills are dominated by Facies H, I, N, C, S, and U, with a very high sand-to-mud ratio. No evidence of subaerial exposure is recorded in FA 4b. The channel margins contain Facies H and Facies I, which interfinger with Facies E, F, M, P, and Q. Individual beds are >1 m thick. FA 2, FA 3, and FA 4 are dominated by a north to north-northeast paleocurrent direction, with some northeast flows and with a subordinate and opposing south-southwest component (figure 3). Note the strong underrepresentation of west-southwest to southwest flow indicators (figure 3).

Interpretation

The heterolithic nature of FA 3 indicates a fluctuating energy level within the system (Kvale, 2012). Straight-crested to linguoid ripple marks suggest different durations of flow events, as equilibrium linguoid morphology requires more time to form (Baas, 1999). The presence of Parasequence 0 exclusively at Sven's Gulch suggests that this area was the first part of the system to be flooded. The base of each parasequence is marked by a flooding surface and the development of FA 3a, followed by the coarsening-upward tidally influenced sediments of FA 3b. This is envisioned as a result of increased energy within the system due to shallower water and an increasingly proximal subtidal to tidal flat setting. The same increased energy trend is also indicated by the coarsening southward of FA 3, which suggests shallower water depth towards the present-day location of Hanksville. Whereas several flooding surfaces may be identified in outcrops, their exact correlation between the different measured sections is impossible due to the extreme dynamic nature of tidal environments, and because these flooding surfaces might stem from local variations in relative sea level such as avulsions, rather than regional signals.

When traced laterally, the infill of the steep and deep incision observed at Sven's Gulch (figures 4C and 4D) belongs to Parasequence 2. The occurrence of an Entrada Sandstone boulder within a matrix of Curtis Formation indicates that the Entrada Sandstone was

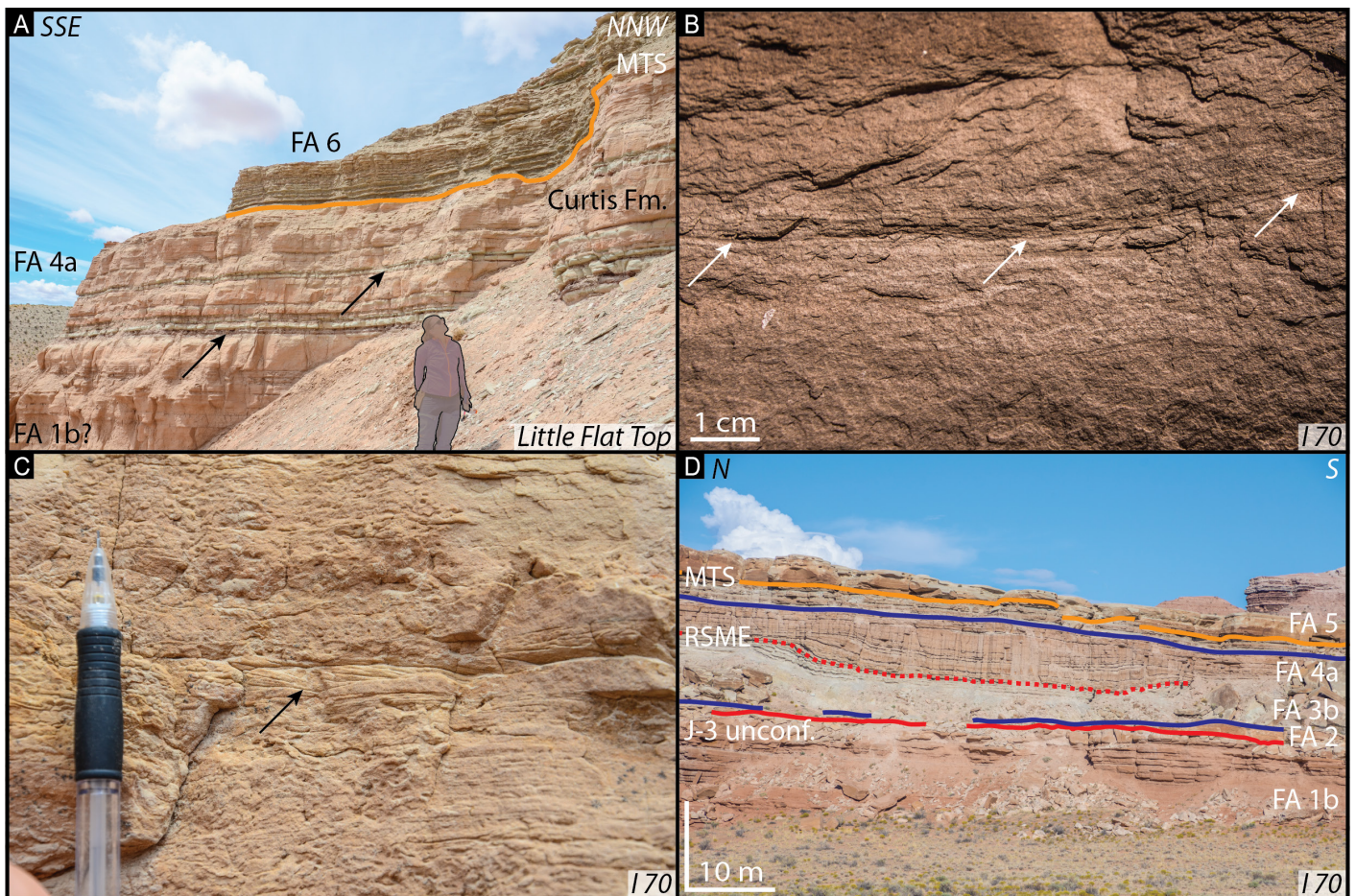


Figure 7. Overview of FA 4a. (A) Picture of Little Flat Top, where the light pink, isopachous sand-rich sub- to supratidal flat deposits of FA 4a overlie the earthy facies of the Entrada Sandstone (FA 1b). The exact location of the J-3 unconformity at that location remains uncertain due to the lack of an erosive, or flooding surface between these two facies associations, uncertainty reinforced by an unusual gradual color change between FA 1b and FA 4a. The black arrows indicate paleosol horizons which could potentially represent the lithostratigraphical boundary between the two formations. FA 4a is capped by the Major Transgressive Surface (MTS), and subsequently overlain by the sub- to intertidal deposits of FA 6, whereas the FA 5 is absent. (B) Double mud drape indicated by the white arrows, suggesting occasional subtidal depositional conditions. (C) Scattered unidirectional current ripple within a fine-grained sandstone dominated by upper-flow regime plane parallel-stratifications, which, together with the near-lack of clay material, suggest higher energy conditions in FA 4a with respect to FA 3. (D) Mini sag basin formed by the collapse of FA 3b deposits while being filled by the sandstone of FA 4a, just south of Interstate 70, near where the highway cuts through the eastern flank of the San Rafael Swell.

poorly lithified as the tidal currents funneled into it, highlighting the poly-nature of the J-3 unconformity. Both the presence of this boulder and a FA 3 cannibalizing its substratum show that this depression was actually carved into the Entrada Sandstone by tidal currents during a short-lived regressive phase within Parasequence 2, rather being a pre-existing negative relief sub-

sequently and passively filled by the Curtis Formation.

The limited bioturbation degree and diversity indicate stressed environmental conditions within a restricted, tidally influenced marginal-marine tidal flat setting, potentially indicating hypoxic conditions as well as salinity values superior to normal marine standards (Middleton, 1991; Nio and Yang, 1991; De Gibert and

Ekdale, 1999; Fan, 2012; Hughes, 2012; Daidu, 2013). The laterally extensive compound conglomeratic dunes of Facies H in the northern area require high energy within the system at time of deposition. This succession shows strong similarities with the modern submarine dune field in laterally restricted San Francisco Bay, especially regarding the protracted extent of these features and their unidirectional, basinward development, suggesting a dominant ebb tide and subordinate flood tide as advocated by Barnard and others (2006). These conglomeratic dunes coexist with laterally migrating tidal channels (Facies J). The occurrence of cross-stratified conglomeratic lenses with interfingering greenish-colored silt and mud implies significant variation and asymmetry in current velocities, at least locally. The dominant current will mobilize gravel and coarse sand, forming lens-shaped dunes, locally amalgamated within a tidal channel, whereas the subordinate current will cut the bedform, generating reactivation surfaces, and potentially develop counter ripples and small dunes.

The replacement of the greenish-colored tidally influenced deposits of FA 3 by the pinkish-colored relatively well-sorted plane parallel-stratified sediments of FA 4a suggests (1) higher energy and more stable current conditions within the system compared to FA 3, (2) a more oxygenated water column, oxidizing the iron present in the sediments, (3) a potential change in sediment sourcing, now originating from more homogeneous very fine to fine-grained sand-rich continental strata with a potential higher K-feldspar content, and (4) a short-lived relative sea-level drop with subaerial exposure. The channels of FA 4b are regarded as distal subtidal channels, due to the lack of intertidal indicators and the absence of any evidence of subaerial exposure, as well as the interfingering with the subtidal deposits of FA 3a and FA 3b. They are also regarded as the distal time correlative unit of the more proximal FA 4a. Also, the two incision events of FA 4b documented at Sven's Gulch (figure 4) might relate to the short lived relative sea-level fall and subsequent subaerial exposure episodes of FA 4a. The fact that the first incision carves deeper into the deposits of FA 3 implies a more important relative sea-level fall during the first episode of incision than during the second incision. FA 4 architecture and paleocurrent directions suggest a dominant basin-

ward ebb-flow direction and a subordinate flood-tide in the lower part of the Curtis Formation.

Interestingly, the basal conglomerate documented at Last Chance Desert (figure 1, Facies F) is interpreted as flash-flood deposits resting directly on Pipingos and O'Sullivan's (1978) J-3 unconformity, which implies that these deposits are older than the Curtis Formation as defined by Gilluly and Reeside (1928), yet younger than the Entrada Sandstone.

FA 5 – Sub- to Intertidal Channel-Dune-Flat Complex

Description

FA 5 is present in every locality in this study, with the notable exception of Little Flat Top (figures 1 and 3). In comparison with the underlying FA 3 and 4 deposits, the sand-dominated interval corresponding to FA 5 is relatively homogeneous (figure 8). FA 5 is easily identifiable in the field by its light green-white color, as well as its polished weathering appearance. It generally overlies FA 3 or FA 4, but between the measured sections Interstate 70 and Uneva Mine Canyon (figure 1), FA 5 caps FA 2 and FA 1 at a noticeable angle (figures 8F and 8G). FA 5 rests directly on FA 1 in sectors 2 and 3, with the exception of the Hanksville section, and is absent from Little Flat Top (figures 1, 2, and 3). The thickness and, to a lesser extent, the stacking architecture of this sedimentary unit strongly vary between studied sections, nevertheless displaying a southward-thinning trend, reaching more than 45 m thick at Stove Gulch, about 15 m thick at Interstate 70, and only 4.60 m thick at Hanksville (figures 1, 2, and 3). It also thins towards the east, measuring only about 1.30 m thick at Duma Point and about 0.8 m thick at Crystal Geyser, but never exceeding 3.80 m thick in sector 3 (figures 1 and 3). Its lower sharp contact is either conformable with the underlying strata, onlapping its substratum, or erosive in nature, and corresponds to the MTS. FA 5 is dominated by sand-rich facies, featuring sedimentary structures such as flaser bedding (Facies N), climbing ripples (Facies O), or thoroughly rippled intervals, dominated by herringbone cross-stratification (Facies R). Some bedding surfaces display interference ripple marks that are arranged in a nearly orthogonal pattern. Fine-grained

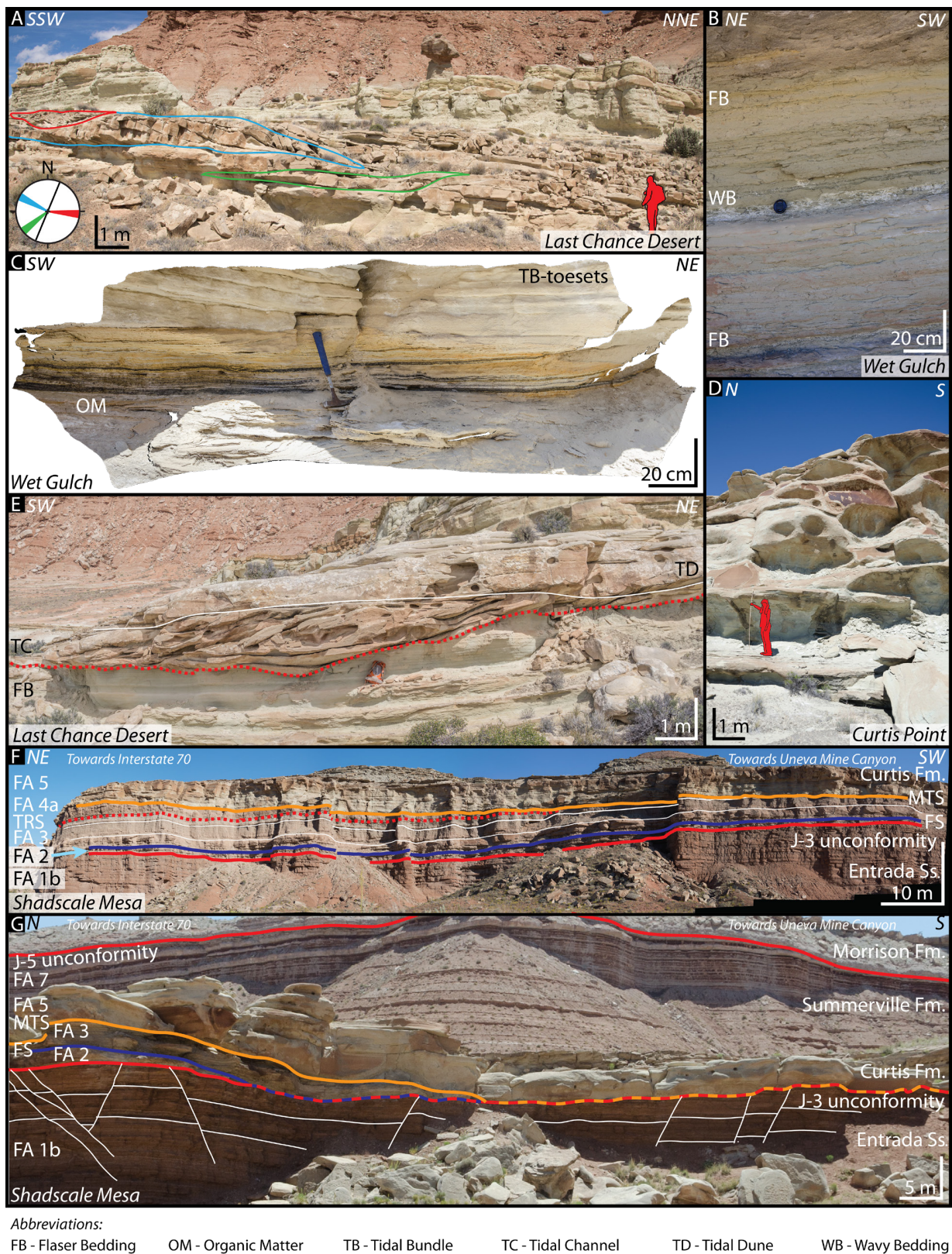


Figure 8. Caption on the following page.

Figure 8 (figure on the previous page). Overview of FA 5 (middle Curtis). (A) Bidirectional tidal inlets (red and blue contours), and a third south-westward laterally accreting tidal channel (green contour) within a sub- to intertidal flat surrounding environment. The respective migration direction of these three bedforms is color-coded on the rose-diagram, whereas the black line on the diagram illustrates the outcrop orientation. (B) Heterolithic sandstone with an alternation of flaser bedding (FB, Facies N) and wavy bedding (WB, Facies M). Lenses cap: 67 mm. (C) Enrichment of organic matter (OM) in the toesets of certain rhythmic tidal bundles (Facies P). (D) Weathered surface of a structureless sandstone. (E) South-westward laterally accreting tidal channel, incising into subtidal sandstone with flaser bedding (FB). The channel was subsequently overlain by 3D tidally influenced dunes (TD) migrating towards the northeast. (F and G) The two pictures are respectively taken 1.3 and 2.2 km south of the Interstate 70 measured section. They show the erosive and angular relationship between FA 5 and its substratum, as the Curtis Sea was transgressing its poorly consolidated and uplifted substratum. The MTS at the base of FA 5 can be traced over the entire study area.

material arranged in laminated mudstone to lenticular to wavy bedding is recorded at Smith's Cabin (Facies K, L, M, figure 1). Other sedimentary structures and type of architecture can be observed, such as (1) locally amalgamated cm- to m-scale tidal bundles with varying amount of organic matter captured within their toesets (Facies P), (2) 3D dunes cut by several reactivation surfaces on top of which counter ripples can sometimes be seen (Facies C), and (3) plane parallel-stratified intervals (Facies S). These facies interfinger with one another over about 5 to 40 m. Both single and double mud drapes as well as desiccation cracks occur within several horizons included in FA 5.

The fact that three shallow core-drilling attempts through these sandstone beds failed at providing any usable cored plugs suggests the unit is poorly consolidated, at least through its first 20 cm, but the degree of consolidation varies significantly over tens of meters. Weathering can obscure sedimentary structures, which results in a structureless appearance (Facies Q). The stacking pattern of these different facies is extremely intricate, and each locality has subtly unique architecture. Therefore, the internal complexities of FA 5, coupled with distance between each location, render the detailed correlation between the measured sections very challenging and incompletely constrained. Note that the thickness, size, and wavelength of tidal structures diminish up-section, whereas the lower half of FA 5 displays a relatively constant scale of sedimentary architecture. Towards the east, in sector 3, FA 5 is dominated by rippled cross-laminated to undulated beds, with scattered structureless intervals. Current data are shifted in comparison with the underlying units, from

a north-dominated to a more symmetrical northwest to southeast trend (figure 3). However, FA 5 shows similarities with the underlying facies associations, as recordings of a west-southwest to southwest flow direction are rare.

Interpretation

The overall high sand-to-mud ratio within FA 5 indicates an elevated energy level within the depositional environment, in comparison with the underlying units. However, this energy level fluctuated through space and time, as testified by the nature and the varying scale of the documented sedimentary structures, as well as by the intricate lateral and vertical interfingering and stacking pattern of the different facies. All of these features display the effect of individual and multiple tide cycles over a tidal flat (Facies C, L, M, N, O, and R), as well as neap-spring tidal cyclicity within a tidal channel (Facies P) (Kreisa and Moiola, 1986; Middleton, 1991; Nio and Yang, 1991; Fan, 2012; Hughes, 2012; Daidu, 2013). Ephemeral episodes of subaerial exposure occurred, as evident by desiccation cracks and, to a lesser extent, single intertidal mud drapes, typical for intertidal zones. Tidal channels are present, but never quite reach the size of the tidal channels observed in the underlying FA 3 as their lateral extent remains on the order of the decameter (dkm) with well-developed laterally accreting architecture (Facies I, figure 8E). The occurrence of other tidal channels is indicated by the presence of herringbone cross-stratification and sigmoidal tidal bundles (Kreisa and Moiola, 1986; Hughes, 2012). Considering this coastal setting, a highly various and undulating coastline is suggested, which Caputo and

Pryor (1991) and Wilcox and Currie (2008) bring forth and visualize by their paleoenvironment reconstruction models. As depositional energy conditions increase basinward, the clear change in grain size in comparison with the underlying finer grained deposits of FA 2, FA 3, and FA 4 and the extended erosive tidal ravinement surface at the base of FA 5 suggest an overall transgression within a context of limited available accommodation space, with the emplacement of high energy tidal channels and bars system, shielding the back barrier intertidal mix-flat in the southeast (FA 6) (see Dalrymple and others, 2012). The overall FA 5 interval corresponds to Flemming's (2012) bare tidal flat depositional system. The diminishing thickness, size, and wavelength of tidal structures up-section, as well as towards the east and the south, is interpreted to represent a decrease of tidal amplitude and influence over the study area as a result of the early stage of a prograding coastline within an asymmetrical, eastward-pinching foreland basin, which followed a period of architectural aggradation.

FA 6 – Upper Heterolithic Sub- to Intertidal Flat

Description

FA 6 (figure 9) represents the topmost overall fining-upward heterolithic interval of the Curtis Formation documented throughout the whole study area, but its occurrence is limited in sector 3 in comparison with the neighboring sectors 1 and 2. It conformably overlies the sand-dominated FA 5, whereas, at Little Flat Top, it directly overlies FA 3. Its thickness is fairly constant, gently varying between about 7 and 17 m. Internal structures include asymmetrical current- and wave-ripple lamination of Facies L, M, and N, interbedded with laminated mudstone, and structureless or planar parallel-stratified sandstone (Facies C, K, S). FA 6 is also marked by an increase of unidirectional current ripple lamination (Facies U), whereas bidirectional herringbone cross-laminations become increasingly sparse. Individual beds are as much as 10 to 40 cm thick. Dark-red paleosol horizons and scattered desiccation cracks, as well as scattered evaporite-rich levels are recorded throughout the successions. Reddish to orange-colored chert nodules often arranged along well-defined hori-

zons are also common within FA 6. Paleocurrent data must be regarded with caution due to the low number of measurements (figure 3). Further, FA 6 sees the return of bioturbation, exclusively consisting of root burrows. FA 6 is characterized by an extreme scarcity, and a dramatically reduced bioturbation size, which would correspond to Droser and Bottjer (1986) ichnofabric index n°2. Note that once again the Crystal Geysir section remains an outcast, as the 2 to 5 m of interpreted Curtis Formation displays only Facies S, U, and X.

Interpretation

The alternation of heterolithic deposits such as in FA 6 is closely related to systematic and periodic energy level fluctuations, typical of a tide-influenced environment (Kvale, 2012). In comparison with the underlying units, the amplitude of flow velocity change, as well as the available accommodation is reduced, as suggested by the limited thickness of each bed and the size of the bedforms populating them. The disappearance of relatively deep tidal channel-related herringbone cross-lamination and its gradual replacement by an increased frequency of unidirectional landward-oriented washover deposits directly reflects a reduced rate of relative sea level rise, which marks the onset of a normal regression (Highstand System Tract [HSST]). The development of FA 6 is accompanied by a weaker tidal and overall marine influence over the intertidal flat, which generates extremely stressed habitability conditions within the system (Jaglarz and Uchman, 2010) coupled with episodes of subaerial exposure, as supported by precipitation of gypsum, the desiccation cracks, and the development of superficially vegetated paleosol horizons. FA 6 represents a more restricted and more proximal depositional environment than its FA 5 basinward equivalent.

FA 7 – Coastal Dry Eolian Dune Field

Description

FA 7 corresponds to the eolian deposits of the Moab Member of the Curtis Formation, which crop out in the vicinity of Moab and Arches National Park, Utah (figure 1). The overall thickness of FA 7 is as much as 50 m

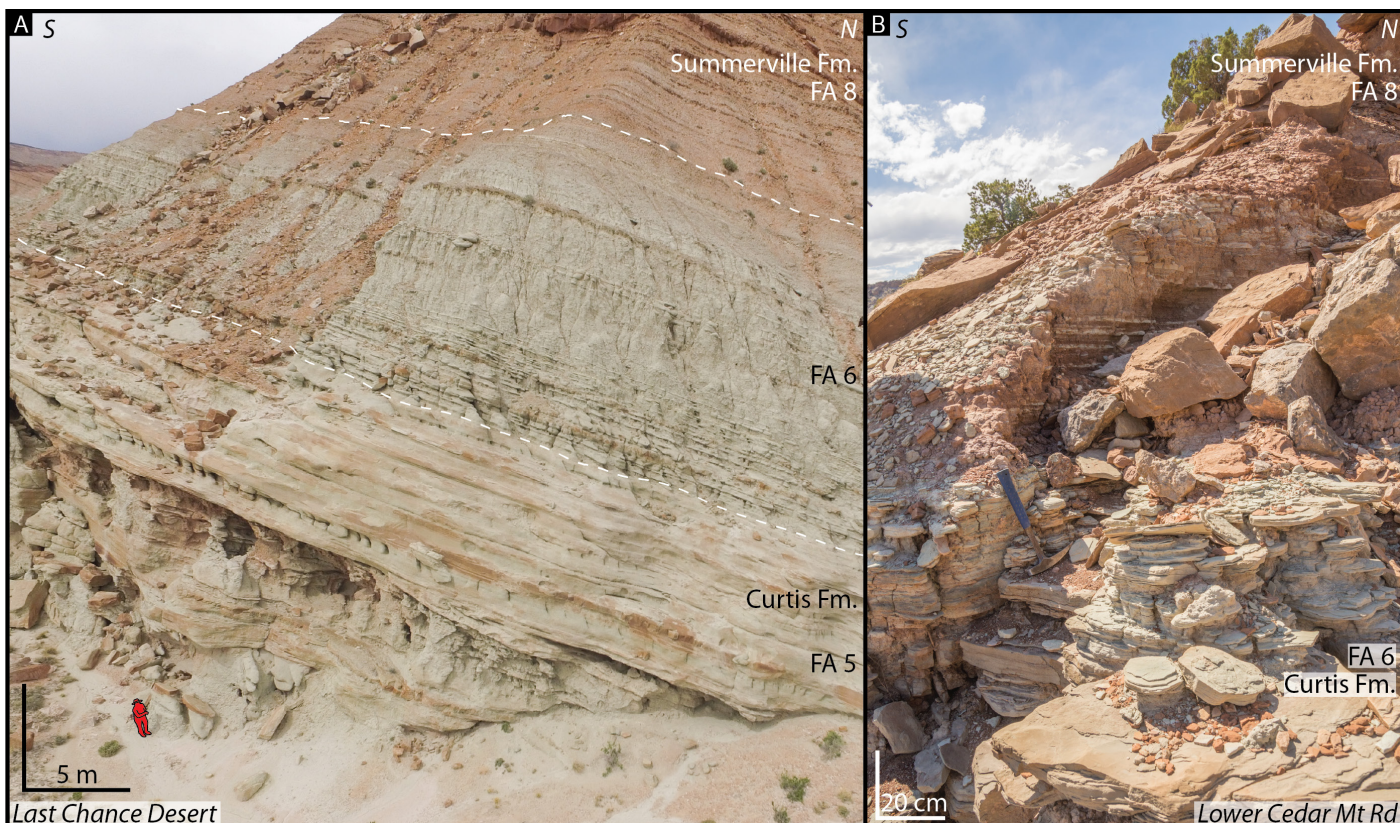


Figure 9. (A) Photo illustrating the conformable contact between the middle Curtis (FA 5), the upper Curtis (FA 6), and the Summerville Formation (FA 8), accompanied their upward-thinning and upward-finining of the beds. (B) Close up of the conformable contact between the upper Curtis and the Summerville Formation. The lithostratigraphic boundary lies at the top the hammer handle.

in the easternmost visited localities and pinches out a few 100 m east of Duma Point (figures 1 and 3). It rests directly on the Slick Rock Member of the Entrada Sandstone in the east and on the earthy facies towards Duma Point (figure 1). It is characterized at its base by a sedimentary package that mainly consists of light-green to white, structureless to ripple to trough cross-stratified, very fine to fine-grained sandstone (Facies Q and U), with greenish-colored silty sandstone intervals (Facies L), and superficial paleosols (Facies X). Facies Q and U are over-represented with respect to Facies X in the west, whereas this ratio inverts itself towards the east. Note that this facies has not been observed at Dewey Bridge section (figure 10). Soft-sediment deformation is common. This basal unit is overlain by a 1- to 3-m-thick, planar parallel-stratified, white fine-grained sandstone (Facies S), with locally occurring 0.3- to 0.5-m-thick tangential cross-stratified sandstone (Facies A) sets. The

rest of the succession consists of four to five packages of amalgamated, large-scale (>2 m) tangential cross-stratified, fine-grained white sandstone (Facies A). The maximum height of individual foreset reaches about 15 m. Each of these sedimentary packages is truncated at their top by a supersurface, upon which paleosols (Facies X) and/or fine-grained, undulating to rippled cross-stratified white sandstone (Facies U) that is as much as 1 m thick can be observed. Note that rhizoliths can be visible up to 2 m below these supersurfaces (figures 10C and 10D). FA 7 can be capped by a thin 10- to 20-cm-thick, fine-grained, structureless yellow sandstone (Facies T).

Interpretation

The thick, tangential cross-stratified sandstone beds are interpreted as migrating compound eolian dunes (Facies A), with alternating grain-fall and grain-

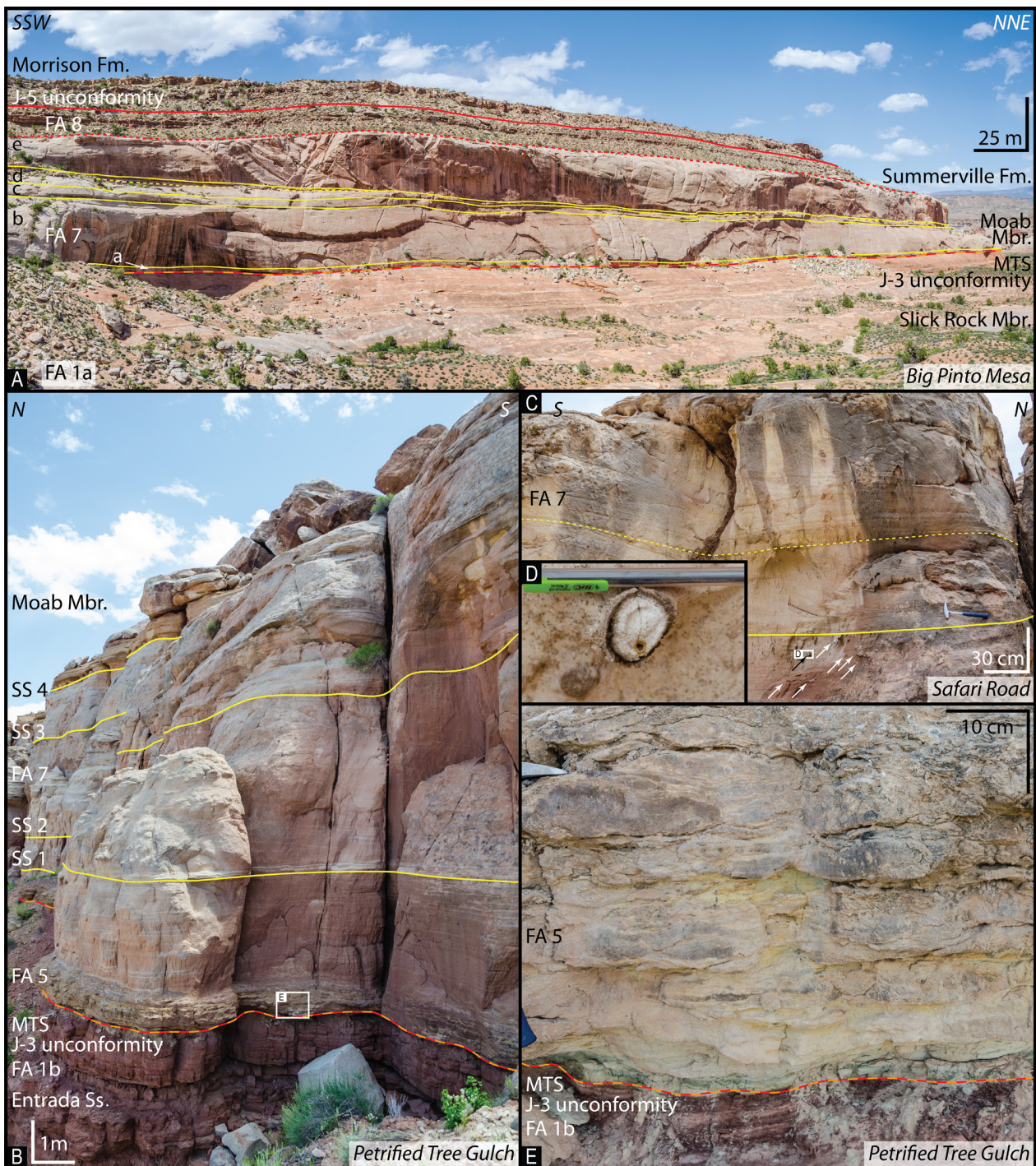


Figure 10. (A) Picture of the Moab Member (MTMb; FA 5 and FA 7) at Big Pinto Mesa, where a 50-m-thick section was measured through the eolian deposits of FA 7. It can be divided in five sequences (a-e). The MTMb crops out in sector 3 (see figure 3), and it overlies the earthy facies (FA 1b) in the western part of sector 3, whereas it rests directly on the Slick Rock Member (FA 1a) towards the east. (B, C, D, and E) Close-up photographs of the lowermost meters of FA 7, which conformably overlies water-carried sediments of FA 5. Each eolian sequence is capped by a supersurface (SS). Rhizoliths and their precipitation fronts (white arrows, and close-up D) can be present up to several decimeters below such a supersurface. They indicate that vegetation developed prior to the deposition of the following sequence.

flow deposits on the foresets of each dune. The westward-pinching geometry of FA 7 indicates that the main eolian depocenter was, at the time, located in the vicinity of Big Pinto Mesa (figure 1). The extent of the Moab Member (FA 7) suggests that the paleo-erg covered an area of at least 1800 km². However, this surface is certainly underestimated, due to the low preservation potential of eolian deposits (Rodríguez-López and others, 2014), as well as the limited area where the Moab Member has not yet been eroded.

The vertical stacking architecture of FA 7 makes it no stranger to the Kocurek (1988, 1999), Kocurek and Lancaster (1999), and Mountney (2006) cyclic depositional pattern: (1) construction, (2) accumulation, and (3) preservation phases of eolian deposits. The occurrence of the basal Facies Q, U, and L implies a marine incursion within a coastal plain domain, during a period of optimal climatic conditions allowing the development of (superficial) paleosols. Note that, when traced basinward, this basal tidally influenced marginal marine interval corresponds to the transgressive deposits of FA 5, which highlights the spatial extent of this major transgressive event, whereas the intervals characterized by Facies U represent short-lived marine transgression as FA 6 was being deposited farther to the west. The transition from a “wet” environment to a dry phase of eolian accumulation is accompanied by the deposition of sand sheets (Facies S) and small-scale eolian dunes (Facies A). The onset of this shift results from an increased amount of loose sediment available for wind transport, as a consequence of a lowering of the saturated level within the sedimentary column (Kocurek, 1988, 1999; Kocurek and Lancaster, 1999; Mountney, 2012). The replacement of small-scale bedforms by large-scale eolian dunes represents the major phase of accumulation, also indicative of peak aridity and highest loose sediment budget. Each eolian dune package (Facies A) is capped by laterally extensive deflation surfaces, which are referred to as supersurfaces (Brookfield, 1977; Talbot, 1985; Kocurek, 1988; Havholm and Kocurek, 1994), resulting from the cannibalization of the system down to the water saturated level, as the sand supply became exhausted. Similar to Mountney’s (2006) models from the Permian Cedar Mesa Sandstone, the observed supersurfaces are also characterized, at least

locally, by “abundant calcified rhizoliths and bioturbation and which represents the end product of a widespread deflation episode” (Mountney, 2006), and the potential development of superficial vegetation. The stacking of four to five of these eolian sequences suggests cyclic climatic alternations between humid and arid episodes (Mountney 2006, 2012). The near absence of interdune deposits, and the wedge-symmetry of the succession, assign FA 7 to a dry temporally and spatially dynamic eolian system (Kocurek and Havholm, 1993; Mountney, 2012).

FA 8 – Supratidal Flat

Description

FA 8 marks the stratigraphic top of this study and corresponds to the lowermost strata of the Summerville Formation, which is observed at each measured section (figure 9). FA 8 is characterized by a gradual yet short-lived transition from mostly greenish-colored tide-influenced strata (FA 6) into a succession dominated by dark-red laminated mudstone (Facies V), paleosols (Facies X), and evaporite-rich horizons. In the eastern part of the study area, FA 8 overlies FA 7, and the transition between the two units is abrupt, with no evidence of erosion. Centimeter- to decimeter-scale (cm- to dm-scale), light- to dark-green-colored, ripple-laminated strata (Facies U) and multi-dm-thick, trough cross-stratified sandstone beds (Facies I) occur repeatedly in FA 8. Facies U occurs ubiquitously within FA 8, whereas Facies I has been documented only in the eastern part of the study area. Both their number and thickness diminish up-section. Episodic but rare interbedded, fluvial-dominated strata (Facies W) occur within the succession. Note that both Facies U and Facies W locally display desiccation cracks.

Interpretation

Fine-dominated grain size, fairly well-sorted, small sedimentary structures, architecture, dark-red colors and evaporites suggest a quiet and arid coastal environment, with episodic seasonal fluvial floods as well as periodic short-lived marine incursions, marked by the thin greenish-colored ripple-laminated and thicker

trough cross-stratified beds. The fact that marine floods diminish up-section indicates a basinward-prograding coastline during a phase of normal regression (HSST).

DISCUSSION

Sector 1, Sector 2, and Sector 3

The study of these facies associations shows that the Curtis Formation, as defined by Gilluly and Reeside (1928) at their type section at Curtis Point (figure 1), can be divided in three lithostratigraphic sub-units easily identifiable in the field. These units are herein referred to as the lower, middle, and upper Curtis (informal nomenclature). The lateral equivalent Moab Member was originally defined by Wright and others (1962) as a member or a tongue of the Entrada Sandstone at the time. Doelling (2001) officially reassigned these eolian deposits as a member of the Curtis Formation. The spatial distribution of these three sub-units shows that the Curtis Formation displays three different expressions of itself over the study area, which are herein delimited as sectors 1, 2, and 3.

The complete sub-unit trilogy of the Curtis Formation are only found in sector 1 (figure 3), which extends north of Uneva Mine Canyon on the eastern limb of the San Rafael Swell monocline; however, the triptych character of the formation disappears south of Last Chance Desert on the western margin of the San Rafael Swell (figures 1 and 3). Sector 2 (figure 3) is dominated by the middle and upper Curtis, with the notable following exceptions: (1) Duma Point, where only the middle Curtis is exposed, (2) Little Flat Top, where the middle Curtis is absent, and (3) Hanksville, where the three sedimentary sub-units crops out again (figure 1). On figure 3B, Little Flat Top's pie chart displays a particular pattern in the sense that it reflects the uncertain location of the formation boundary between the Entrada Sandstone and the FA 4a of the Curtis Formation. At that specific locality, three lithological candidate boundaries remain, hence influencing the resulting ratio between the different facies associations present in the Curtis Formation. Sector 3 delineates the extent of the Moab Member of the Curtis Formation (figure 3).

Lower, Middle, and Upper Curtis

The lower Curtis crops out in sector 1, as well as at Little Flat Top and at Hanksville in sector 2 (figures 1, 2, and 3). Its base corresponds to the J-3 unconformity as defined by Pippingos and O'Sullivan (1978). As shown in figures 4C and 4D, figures 5 and 6, as well as figures 8F and 8G, the unconformity is characterized by various types of relief formed by different processes, such as eolian deflation, and fluvial or tidal currents, which impacted the unconformity at various times. However, defining the base of the lower Curtis by this polygenetic and composite surface notably implies that the basal flash-flood conglomerates at Last Chance Desert (figure 1, Facies F) also belong to the Curtis Formation, despite predating and being genetically unrelated to the formation. Instead, if it is decided to define the base of the formation using the multi-faceted transgressive surface while regrouping genetically related shallow marine deposits only, then this basal conglomerate at Last Chance Desert would become a-formational, as it would neither belong to the Entrada Sandstone nor the Curtis Formation. For lithostratigraphic convenience, it is suggested to use the highly diachronous J-3 unconformity of Pippingos and O'Sullivan (1978) as the boundary for the lower Curtis, and thus keep these basal conglomerate within this sub-unit.

The lower Curtis is dominated by FA 3a-b dark-green to gray subtidal heterolithic strata, whereas FA 2 and FA 4 are present locally in the eastern part of sector 1, notably at Neversweat Wash, Sven's Gulch, Rabbit Gulch, and Interstate 70 (figures 1, 2, and 3). The ratio between the mud-dominated (FA 3a) and the sand-dominated heterolithic succession (FA 3b) varies spatially. The highest concentration of coarser-grained material, including conglomeratic beds, occurs in the western part of sector 1 at Lower Cedar Mountain Road and Last Chance Desert, whereas, on the eastern margin of sector 1, Sven's Gulch and Rabbit Gulch show similar enriched sand-to-mud ratios (figures 1, 2, and 3). The exact provenance of the different conglomeratic facies occurring in the Curtis Formation remains indeterminate. It is certain, however, that these extra-basinal lithoclasts are sourced from terrane(s?) exposed beyond the extent of the underlying strata of the Entrada Sand-

stone, due to the presence of metamorphosed polycrystalline quartz within these gravels and pebbles. Skeletal carbonate fragments of unidentified bryozoan also exclude the Entrada Sandstone as a potential source for these conglomeratic beds, as opposed to the bulk of the Curtis Formation, which has a modal composition similar to the underlying Entrada Sandstone (Dickinson and Gehrels, 2009, 2010). Despite the lack of provenance data, we suggest that these conglomerate beds represent reworked material, potentially from flash flood deposits, sourced from the uplifted highlands west of the study area (Thorman, 2011; Anderson, 2015) or from the nearby Uncompahgre highlands to the east of Moab (Otto and Picard, 1976; Scott and others, 2001). The fact that most dune-forming and channel-filling conglomeratic facies are in the lowermost meters of the lower Curtis suggests that, as the overall Curtis transgression proceeded, their sediment supply was exhausted. It seems that another sediment entry point emerged in the south to southeast parts of the study area, draining a different basin, from which reworked material from the Entrada Sandstone could have been assimilated into the Curtis Formation. Indeed, towards the south to southeast, FA 4a consists of relatively similar texture with respect to the underlying earthy facies of the Entrada Sandstone; it becomes increasingly dominant within the lower Curtis, as the heterogeneity and complex architecture of FA 3 is replaced by the laterally extensive, light-pink beds of FA 4a. The fact that no bleached front along fractures has been observed in this unit suggests that, unlike bleached fractures and corridors in the Carmel Formation and in the Entrada Sandstone (Ogata and others, 2014), no reducing fluids have circulated within these rocks (Skurtveit and others, 2017; Sundal and others, 2017; figures 4a and 7).

The middle Curtis consists exclusively of FA 5 deposits (figure 3), and its lower boundary corresponds to the MTS, which can sometimes display an erosional relief of about 50 to 90 cm and is hence locally identified as a tidal ravinement surface. In sector 1, the middle Curtis overlies the lower Curtis in a possibly conformable to disconformable to angular way, whereas in sector 2 and 3, the MTS merges with and partially reworks the J-3 unconformity (figure 8G). The angular unconformity between the lower and middle Curtis, visible south of

Interstate 70 (figures 8F and 8G), suggests a sub-regional pre-middle Curtis uplift in the area which may signal regional yet unidentified tectonic activity over the area during the Late Jurassic, prior to the deposition of the middle Curtis. Further, local to sub-regional dome features, ascribed to sandy substratum mobility related to fluid overpressure and seismic activity (Jolly and Loneragan, 2002; Wheatley and others, 2016), are for instance visible 2.1 km north of Hanksville Airport, where the lower and middle Curtis display a fault system driven by an underlying, circular sand pillow (figure 4F). Just as for the J-3 unconformity, the terms unconformity and disconformity are to be taken with caution, as they imply, by definition, a significant time gap between the adjacent units (Van Wagoner and others, 1988; Holbrook and Bhattacharya, 2012), a temporal dimension, which, in the case of the Curtis Formation, cannot be assessed with great precision. The middle Curtis pinches out southward in sector 2 whereas it thins towards the east in sector 3. Due to the extreme low gradient present over the study area during the Jurassic (and through the Cretaceous) times (Heller and others, 1986; Fillmore, 1991; Lockley, 1991; Jones and Blakey, 1993), it is suggested that the time encapsulated in this transgression was short. This major and rapid transgression potentially reached far beyond the study area. Indeed, it may be linked to the deposition of the Todilto Formation and its calcareous saline sediments in southwestern Colorado and northwestern New Mexico (Lucas and Anderson, 1997), which were deposited after a blitz-flooding of the Entrada Sandstone by a marine incursion (Benan and others, 2000). It is important to note that other regional marine embayments co-existed with the Curtis sea in similar low-gradient conditions, such as the Ralston Creek Lobe of Anderson and Lucas (1994) in southeastern Colorado. Thus, the Todilto Formation is likely related to the MTS and to the base of the middle Curtis, which implies that the paleo-erg of the Entrada Sandstone existed in New Mexico until “instantaneous” transgression of Benan and others (2000), whereas it was cannibalized by the lower Curtis transgression in Utah.

The upper Curtis mainly consists of FA 6 deposits, with mud- and sand-dominated channel and tidal-flat complexes. It has been recorded at each visited locality

in sectors 1 and 2, with the notable exception of Duma Point (figure 3). Its lower boundary is gradational, as it conformably overlies the middle Curtis. The main differences between the middle and upper Curtis reside in the up-section's increased heterogeneity, as well as a more pronounced green color, and the gradual replacement of the multi-m-thick bedforms by smaller scale sedimentary structures and thinner strata. It implies that the rate of accommodation decreased in the basin, whereas the sediment supply remained either constant, or potentially increased. The upper Curtis corresponds to the laterally equivalent Moab Member, which crops out in sector 3. The Moab Member is characterized by the dominance of the eolian dunes of FA 7 arranged in four to five distinct sequences, representing at least 78% of the Curtis Formation in the eastern part of the study area. The remaining percentages are recorded as a thin basal middle Curtis interval, whereas marine incursions (FA 6) or superficial paleosols and supratidal deposits (FA 7) separate the different eolian sequences (figure 10). Note that the base of the Summerville Formation (FA 7), which stratigraphically overlies the Curtis Formation conformably in the study area despite their obvious lateral stratigraphic relationship on a more regional scale, suffers from the same gradual transition, from which no evident lithological boundary rises. It is therefore proposed to define the base of the Summerville Formation as the line where, over a meter of succession, more than 50% of the deposits belong to the supratidal FA 8.

SPATIAL DISTRIBUTION OF THE VARIOUS FACIES ASSOCIATIONS: ILLUSTRATION BY MODERN ANALOGS

No modern analogs exist to fully illustrate the overall Curtis Formation depositional evolution. Nevertheless, as shown in figure 11, the inner Gulf of California and the Wadden Sea are suggested to represent similarities to the aforementioned Curtis Formation subdivisions. Such comparisons have limitations, and mainly regard spatial extent of modern environments in comparison with the size of their respective Curtis Formation counterparts, as well as basinal geometry approximations. The modern analogs are not meant to

represent a similar tectonic setting to the Curtis Formation foreland basin conditions.

The lower Curtis is compared the fluviially starved, arid and unprotected tide-dominated bay of Las Lisas, Mexico (figure 11) (UTM coordinates: 12R 221191/3504767), on the northeastern margin of the Gulf of California. The bay offers a window on a probable convoluted facies belt arrangement which occurred during one of the lower Curtis short-lived regressive episodes. In the case of Las Lisas, such a regression is linked to rift flank uplift in the Neogene (Mark and others, 2014). As displayed on figure 11, the area close to the shoreline features sand-rich deposits similar to FA 4a interfingering with finer-grained, supratidal sediments of FA 8 and possibly conformably overlying pre-existing substratum (equivalent of FA 1a). Farther into the basin, the heterolithic subtidal flat deposits of FA 3 are interfingering with gravel-bearing tidal channels (FA 4b) and migrating dunes (Facies H).

The middle Curtis is paralleled with the Dutch part of the shielded and tide-dominated shallow Wadden Sea (figure 11; UTM coordinates: 31U 650032/5902807), where intricate and dynamic interplay of sub- to intertidal channels, tidal flats, and migrating tidal dunes and shoals (FA 5) has developed over an extensive and gently sloping area, behind barrier islands, as a result of a major and quick transgression (linked to Holocene glacio-eustatic sea-level rise in the Wadden Sea (Oost and de Boer, 1994)). It is important to point out that similar well-defined barrier islands are not recognized in the middle Curtis deposits (FA 5), although evidences for subaerial exposure episodes have been documented.

The selected paragon for the upper Curtis is the fluviially starved and arid, back-barrier bay of La Pinta, located 75 km to the southeast of Las Lisas (figure 11) (UTM coordinates: 12R 286227/3460602). Here, the sub- to intertidal sediments (FA 6) deposited in this protected environment are being progressively overlain by supratidal deposits (FA 8), as the underfilled depocenter morphs into an overfilled basin. It is accompanied by a seaward migration of the coastline, leading to the potential development of an eolian dune system (FA 7) in the neighboring area as sediments become subsequently available for transport (Carr-Crabaugh and Kocurek, 1998; Mountney, 2012).

A. Modern analogs of the Curtis Formation

Las Lisas, Mexico

Wadden Sea, the Netherlands

La Pinta, Mexico

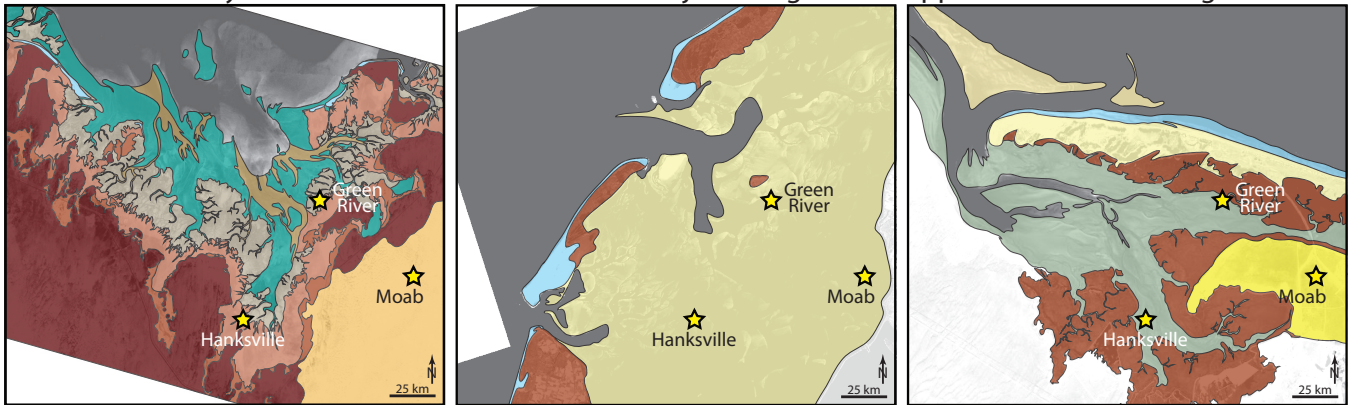


B. Modern analogs transposed to the Curtis Formation basinal setting

lower Curtis - TR cycles

middle Curtis - major transgression

upper Curtis - normal regression



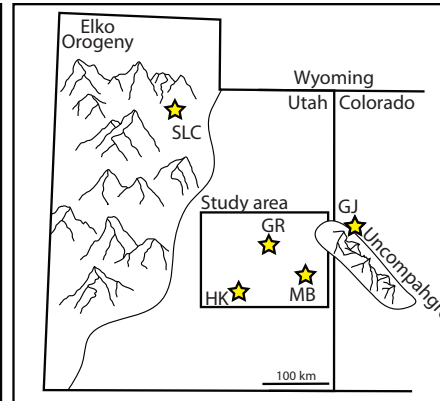
Legend

Facies Associations

- FA 8 Supratidal flat
- FA 7 Coastal dry eolian dunes, Moab Member
- FA 6 Upper sub- to intertidal heterolithic flat
- FA 5 Sub- to intertidal channel-dune-flat complex
- FA 4b Correlative tidal channel infill
- FA 4a Sand-rich sub- to supratidal flat
- FA 3b Subtidal sand-dominated heterolithic flat
- FA 3a Subtidal mud-dominated heterolithic flat
- FA 2 Upper shoreface to beach deposits
- FA 1b Earthy facies
- FA 1a Coastal dunes and Slick Rock Member

Tectonic setting

Oxfordian



SLC - Salt Lake City. GR - Green River. HK - Hanksville. MB - Moab. GJ - Grand Junction

Figure 11. (A) Modern analogs of the lower, middle, and upper Curtis Formation, respectively. Note that these pictures are not aligned to the true north, but are rotated in a way that allows them to fit the orientation of the Curtis basin (satellite images from Microsoft Bing Maps). (B) Modern analogs draped with the corresponding facies associations from the Curtis Formation. The change of scale between A and B illustrates how much bigger the Curtis basin setting is with respect to the three modern analogs. TR cycles – transgressive-regressive cycles. Tectonic setting after Heyman (1983) and Thorman (2011).

CONCLUSIONS

1. Eight main facies associations (FA), including six sub-facies associations, were identified based on lithology, internal sedimentary structures, architectural arrangements, and spatial relationships. These facies associations are regarded as diagnostic expressions resulting from tidal processes in a fluviially starved, low-gradient, semi-enclosed epicontinental basin.
2. It is proposed to divide the Curtis Formation into three sub-units: the lower, middle, and upper Curtis. The specific spatial distribution of these sub-units allows the distinction of three different sectors across the study area: sector 1 in the north, sector 2 in the south-southwest, and sector 3 in the east.
3. The lower Curtis consists of laterally restricted upper shoreface to beach deposits (FA 2) overlain by a subtidal mud-dominated heterolithic succession (FA 3a), which grades into a sand-dominated subtidal flat (FA 3b). FA 3a and FA 3b interfinger with the more proximal and shallower FA 4a sand-rich sub- to supratidal flat, as well as with its more distal FA 4b correlative tidal channel infill.
4. FA 5, which corresponds to the middle Curtis, is mainly composed of a characteristic light green to white, very fine to fine-grained sandstone, appearing as an intricate arrangement of tidal channels, dunes, and tidal flats. The base of the middle Curtis coincides with the MTS, which can be traced throughout the entire study area.
5. The upper Curtis conformably overlies the middle Curtis and is characterized by heterolithic subtidal to intertidal deposits of FA 6, as well as their lateral and contemporaneous continental eolian dunes of the Moab Member (FA 7). The transition from the upper Curtis into the Summerville Formation is also gradual, with a progressively increasing occurrence of supra-tidal deposits (FA 8) within the succession.
6. The lower, middle, and upper Curtis occur in sector 1, whereas only the middle and the upper Curtis crop out in sector 2 (with local exceptions). Sector 3 corresponds to the area where the Moab Member of the Curtis Formation was deposited.
7. It is possible to compare the lower Curtis to the Bay of Las Lisas in the Gulf of California, the middle Curtis to the Wadden Sea in the Netherlands, and the upper Curtis to the bay of La Pinta in the Gulf of California.
8. The Todilto Formation or Todilto Member of the Wanakah Formation, which crops out in southwestern Colorado and northwestern New Mexico, is likely related to the major transgression that defines the base of the middle Curtis and is considered its lateral contemporaneous equivalent. Hence, the upper Wanakah Formation is regarded as the lateral equivalent of the Summerville Formation.
9. The middle Curtis overlies its substratum with an angular relationship on a sub-regional scale, suggesting an underlying and more regional deformational event during the Late Jurassic. Further, with the occurrence of local- to sub-regional collapse features within the lower and middle Curtis, the Late Jurassic must have been impacted by episode(s) of sand mobility, which influenced the local surface morphology.
10. The J-3 unconformity exposed a composite nature, as it was impacted by various processes occurring before the Curtis Formation was deposited, as well as during the development of the lower and middle Curtis.

ACKNOWLEDGMENTS

The Norwegian Research Council is to be sincerely acknowledged, with their awarded grant COPASS 244049, which funded the first author and allowed the *ad hoc* conduct of the required field campaigns for this research. The authors would like to extend their gratitude to Dr. Anja Sundal, Anna van Yperen, Nathan “the Legend” Cote, Dr. Miquel Poyatos-Moré, Dr. Mark Mulrooney, Ole Rabbel, and Kristine Halvorsen for their assistance and helpful comments which elevated the standard of this work. Acknowledgments are to be extended to Grant C. Willis of the Utah Geological Survey (UGS) for his fruitful comments and review of an

early version of this manuscript. The authors also thank Kimm Harty (UGS) for her careful review and editing. Finally, we thank UGS technical editor Stephanie Carney, UGS Deputy Director Michael Hylland, and UGS Director Rick Allis for their reviews and support.

REFERENCES

- Anderson, T.H., 2015, Jurassic (170–150 Ma) basins—the tracks of a continental-scale fault, the Mexico-Alaska megashear, from the Gulf of Mexico to Alaska, *in* Anderson, T.H., Didenko, A.N., Johnson, C.L., Khanchuk, A.I., and MacDonald, J.H., editors, Late Jurassic margin of Laurasia—a record of faulting accommodating plate rotation: Geological Society of America Special Papers 513, p. 107–188.
- Anderson, O.J., and Lucas, S.G., 1994, Middle Jurassic stratigraphy, sedimentation and paleogeography in the southern Colorado Plateau and southern High Plains, *in* Caputo, M.V., Peterson, J.A., and Franczyk, K.J., editors, Mesozoic systems of the Rocky Mountain region, USA: Rocky Mountain Section SEPM (Society for Sedimentary Geology), p. 299–314.
- Baas, J.H., 1999, An empirical model for the development and equilibrium morphology of current ripples in fine sand: *Sedimentology*, v. 46, no. 1, p. 123–138.
- Barnard, P.L., Hanes, D.M., Rubin, D.M., and Kvitek, R.G., 2006, Giant sand waves at the mouth of San Francisco Bay: *EOS Transactions American Geophysical Union*, v. 87, no. 29, p. 285–289.
- Benan, A., Cheikh, A., and Kocurek, G., 2000, Catastrophic flooding of an eolian dune field—Jurassic Entrada and Todilto Formations, Ghost Ranch, New Mexico, USA: *Sedimentology*, v. 47, no. 6, p. 1069–1080.
- Bjerrum, C.J., and Dorsey, R.J., 1995, Tectonic controls on deposition of Middle Jurassic strata in a retroarc foreland basin, Utah-Idaho trough, Western Interior, United States: *Tectonics*, v. 14, no. 4, p. 962–978.
- Blodgett, R.H., 1988, Calcareous paleosols in the Triassic Dolores Formation, *in* Reinhardt, J., and Sigleo, W.R., editors, Paleosols and weathering through time—principles and applications: Geological Society of America Special Papers 216, p. 103–121.
- Bostock, J., and Riley, H.T., 1855, editors, Pliny the Elder, *The Natural History*: London Taylor and Francis, v. 2, book 16, chapter 1, unpaginated.
- Boyd, R., Dalrymple, R., and Zaitlin, B.A., 1992, Classification of clastic coastal depositional environments: *Sedimentary Geology*, v. 80, no. 3–4, p. 139–150.
- Brenner, R.L., and Peterson, J.A., 1994, Jurassic sedimentary history of the northern portion of the Western Interior Seaway, USA., *in* Caputo, M.V., Peterson, J.A. and Franczyk, K.J., editors, Mesozoic systems of the Rocky Mountain region, USA: Rocky Mountain Section SEPM (Society for Sedimentary Geology), p. 233–272.
- Brookfield, M.E., 1977, The origin of bounding surfaces in ancient eolian sandstones: *Sedimentology*, v. 24, no. 3, p. 303–332.
- Bump, A.P., and Davis, G.H., 2003, Late Cretaceous–early Tertiary Laramide deformation of the northern Colorado Plateau, Utah and Colorado: *Journal of Structural Geology*, v. 25, no. 3, p. 421–440.
- Caputo, M.V., and Pryor, W.A., 1991, Middle Jurassic tide- and wave-influenced coastal facies and paleogeography, upper San Rafael Group, east-central Utah, *in* Chidsey, T.C., Jr., *Geology of east-central Utah*: Utah Geological Association Publication 19, p. 9–27.
- Carr-Crabaugh, M., and Kocurek, G., 1998, Continental sequence stratigraphy of a wet eolian system—a key to relative sea-level change: *Society for Sedimentary Geology Special Publication* 59, p. 213–228.
- Catuneanu, O., Abreu, V., Bhattacharya, J.P., Blum, M.D., Dalrymple, R.W., Eriksson, P.G., Fielding, C.R., Fisher, W.L., Galloway, W.E., Gibling, M.R., Giles, K.A., Holbrook, J.M., Jordan, R., Kendall, C.G.St.C., Macurda, B., Martinsen, O.J., Mial, A.D., Neal, J.E., Nummedal, D., Pomar, L., Posamentier, H.W., Pratt, B.R., Sarg, J.F., Shanley, K.W., Steel, R.J., Strasser, A., Tucker, M.E., and Winker, C., 2009, Towards the standardization of sequence stratigraphy: *Earth-Science Reviews*, v. 92, no. 1, p. 1–33.
- Condon, S.M., and Huffman, A.C., Jr., 1988, Revisions in nomenclature of the middle Jurassic Wanakah Formation, northwestern New Mexico and northeastern Arizona: *U.S. Geological Survey Bulletin* 1633-A, p. A1–A12.
- Crabaugh, M., and Kocurek, G., 1993, Entrada Sandstone—an example of a wet eolian system, *in* Pye, K., editor, *The dynamics and environmental context of eolian sedimentary systems*: London, Geological Society Special Publications No. 72, p. 103–126.
- Daidu, F., 2013, Classifications, sedimentary features and facies associations of tidal flats: *Journal of Palaeogeography*, v. 2, no. 1, p. 66–80.
- Dalrymple, R.W., Zaitlin, B.A., and Boyd, R., 1992, Estuarine facies models—conceptual basis and stratigraphic implications: *Journal of Sedimentary Research*, v. 62, no. 6, p. 1130–1146.
- Dalrymple, R.W., Mackay, D.A., Ichaso, A.A., and Choi, K.S., 2012, Processes, morphodynamics, and facies of tide-dominated estuaries, *in* Davis, R.A., Jr., and Dalrymple, R.W., editors, *Principles of tidal sedimentology*: Dordrecht, Netherlands, Springer Science and Business Media, p. 79–107.
- Davis, R.A., Jr., and Dalrymple, R.W., editors, 2012, *Principles of tidal sedimentology*: Dordrecht, Netherlands, Springer Sci-

- ence and Business Media, 621 p.
- De Gibert, J.M., and Ekdale, A.A., 1999, Trace fossil assemblages reflecting stressed environments in the Middle Jurassic Carmel seaway of central Utah: *Journal of Paleontology*, v. 73, no. 4, p. 711–720.
- Dickinson, W.R., and Gehrels, G.E., 2009, U-Pb ages of detrital zircons in Jurassic eolian and associated sandstones of the Colorado Plateau—evidence for transcontinental dispersal and intraregional recycling of sediment: *Geological Society of America Bulletin*, v. 121, no. 3–4, p. 408–433.
- Dickinson, W.R., and Gehrels, G.E., 2010, Insights into North American paleogeography and paleotectonics from U–Pb ages of detrital zircons in Mesozoic strata of the Colorado Plateau, USA: *International Journal of Earth Sciences*, v. 99, no. 6, p. 1247–1265.
- Dickinson, W.R., Stair, K.N., Gehrels, G.E., Peters, L., Kowallis, B.J., Blakey, R.C., Amar, J.R., and Greenhalgh, B.W., 2010, U-Pb and ⁴⁰Ar/³⁹Ar ages for a tephra lens in the Middle Jurassic Page Sandstone—first direct isotopic dating of a Mesozoic eolianite on the Colorado Plateau: *The Journal of Geology*, v. 118, no. 3, p. 215–221.
- Doelling, H.H., 2001, Geologic map of the Moab and eastern part of the San Rafael Desert 30' x 60' quadrangles, Grand and Emery Counties, Utah, and Mesa County, Colorado: Utah Geological Survey Map 180, 3 plates, scale 1:100,000.
- Doelling, H.H., Kuehne, P.A., Willis, G.C., and Ehler, J.B., 2015, Geologic map of the San Rafael Desert 30' x 60' quadrangle, Emery and Grand Counties, Utah: Utah Geological Survey Map 267DM, 24 p., 2 plates, scale 1:62,500.
- Doelling, H.H., Sprinkel, D.A., Kowallis, B.J., and Kuehne, P.A., 2013, Temple Cap and Carmel Formations in the Henry Mountains basin, Wayne and Garfield Counties, Utah, in Morris, T.H., and Resselar, R., editors, *The San Rafael Swell and Henry Mountains Basin—geologic centerpiece of Utah*: Utah Geological Association Publication 42, p. 279–318.
- Droser, M.L., and Bottjer, D.J., 1986, A semiquantitative field classification of ichnofabric—research method paper: *Journal of Sedimentary Research*, v. 56, no. 4, p. 558–559.
- Eschner, T.B., and Kocurek, G., 1988, Origins of relief along contacts between eolian sandstones and overlying marine strata: *American Association of Petroleum Geologists Bulletin*, v. 72, no. 8, p. 932–943.
- Fan, D., 2012, Open-coast tidal flats, in Davis, R.A., Jr., and Dalrymple, R.W., editors, *Principles of tidal sedimentology*: Dordrecht, Netherlands, Springer Science and Business Media, p. 187–229.
- Fillmore, R.P., 1991, Tectonic influence on sedimentation in the southern Sevier foreland, Iron Springs Formation (Upper Cretaceous) southwestern, Utah: *Geological Society of America Special Papers* 260, p. 9–26.
- Flemming, B.W., 2012, Siliciclastic back-barrier tidal flats, in Davis, R.A., Jr., and Dalrymple, R.W., editors, *Principles of tidal sedimentology*: Dordrecht, Netherlands, Springer Science and Business Media, p. 231–267.
- Gilluly, J., and Reeside, J.B., Jr., 1928, Sedimentary rocks of the San Rafael Swell and some adjacent areas in eastern Utah: U.S. Geological Survey Professional Paper 150-D, p. 61–110.
- Halland, E.K., Bjørnstad, A., Magnus, C., Riis, F., Meling, I.M., Tørneng Gjeldvik, I., Tappel, I.M., Mujezinović, J., Bjørheim M., Rød, R.S., and Pham, V.T.H., 2014, CO₂ storage atlas—Norwegian continental shelf: Stavanger, Norway, Norwegian Petroleum Directorate, not paginated.
- Haq, B.U., Hardenbol, J., and Vail, P.R., 1987, Chronology of fluctuating sea levels since the Triassic: *Science*, v. 235, no. 4793, p. 1156–1167.
- Hartwick, E., 2010, Eolian architecture of sandstone reservoirs in the Covenant field, Sevier County, Utah [abs.]: *Geological Society of America, Abstracts with Programs*, v. 42, p. 52.
- Havholm, K.G., and Kocurek, G., 1994, Factors controlling eolian sequence stratigraphy—clues from super bounding surface features in the Middle Jurassic Page Sandstone: *Sedimentology*, v. 41, no. 5, p. 913–934.
- Heller, P.L., Bowdler, S.S., Chambers, H.P., Coogan, J.C., Hagen, E.S., Shuster, M.W., and Lawton, T.F., 1986, Time of initial thrusting in the Sevier orogenic belt, Idaho-Wyoming and Utah: *Geology*, v. 14, no. 5, p. 388–391.
- Heyman, O.G., 1983, Distribution and structural geometry of faults and folds along the northwestern Uncompahgre uplift, western Colorado and eastern Utah, in Averett, W., editor, *Northern Paradox Basin-Uncompahgre uplift, Grand Junction Geological Society field trip*, p. 45–57.
- Hintze, L.F., 1980, Geologic map of Utah: Utah Geological and Mineral Survey, scale 1:250,000, 2 sheets.
- Hintze, L.F., and Kowallis, B.J., 2009, Geologic history of Utah: *Brigham Young University Geology Studies Special Publication* 9, 225 p.
- Holbrook, J.M., and Bhattacharya, J.P., 2012, Reappraisal of the sequence boundary in time and space—case and considerations for an SU (subaerial unconformity) that is not a sediment bypass surface, a time barrier, or an unconformity: *Earth-Science Reviews*, v. 113, no. 3, p. 271–302.
- Hughes, Z.J., 2012, Tidal channels on tidal flats and marshes, in Davis, R.A., Jr., and Dalrymple, R.W., editors, *Principles of tidal sedimentology*: Dordrecht, Netherlands, Springer Science and Business Media, p. 269–300.
- Imlay, R.W., 1947, Marine Jurassic of Black Hills area, South Dakota and Wyoming: *American Association of Petroleum Geology*

- gists Bulletin, v. 31, no. 2, p. 227–273.
- Imlay, R.W., 1980, Jurassic paleobiogeography of the conterminous United States in its continental setting: U.S. Geological Survey Professional Paper 1062, 134 p.
- Jaglarz, P., and Uchman, A., 2010, A hypersaline ichnoassemblage from the Middle Triassic carbonate ramp of the Tatricum domain in the Tatra Mountains, southern Poland: *Palaeogeography, Palaeoclimatology, Palaeoecology*, v. 292, no. 1–2, p. 71–81.
- Jolly, R.J., and Lonergan, L., 2002, Mechanisms and controls on the formation of sand intrusions: *Journal of the Geological Society*, v. 159, no. 5, p. 605–617.
- Jones, L.S., and Blakey, R.C., 1993, Erosional remnants and adjacent unconformities along an eolian-marine boundary of the Page Sandstone and Carmel Formation, Middle Jurassic, south-central Utah: *Journal of Sedimentary Research*, v. 63, no. 5, p. 852–859.
- Kampman, N., Maskell, A., Bickle, M., Evans, J., Schaller, M., Purser, G., Zhou, Z., Gattacceca, J., Petrie, E., and Rochelle, C., 2013, Scientific drilling and downhole fluid sampling of a natural CO₂ reservoir, Green River, Utah: *Scientific Drilling*, v. 16, p. 33–43.
- Kocurek, G., 1988, First-order and super bounding surfaces in eolian sequences—bounding surfaces revisited: *Sedimentary Geology*, v. 56, no. 1–4, p. 193–206.
- Kocurek, G., 1999, The eolian rock record (Yes, Virginia, it exists, but it really is rather special to create one), *in* Goudie, A.S., Livingstone, I., and Stokes, S., editors, *Eolian environments, sediments and landforms*: New York, Wiley, p. 239–259.
- Kocurek, G., and Dott, R.H., Jr., 1983, Jurassic paleogeography and paleoclimate of the central and southern Rocky Mountains region, *in* Reynolds, M.W., and Dolly, E.D., editors, *Mesozoic paleogeography of west-central United States—Rocky Mountain paleogeography symposium 2: Rocky Mountain Section SEPM (Society for Sedimentary Geology)*, p. 101–116.
- Kocurek, G., and Havholm, K.G., 1993, Eolian sequence stratigraphy—a conceptual framework (chapter 16), *in* Weimer, P., and Posamentier, H., editors, *Siliciclastic sequence stratigraphy—recent developments and applications: American Association of Petroleum Geologists Memoir 58*, p. 393–409.
- Kocurek, G., and Lancaster, N., 1999, Eolian system sediment state—theory and Mojave Desert Kelso dune field example: *Sedimentology*, v. 46, no. 3, p. 505–515.
- Kowallis, B.J., Christiansen, E.H., Deino, A.L., Zhang, C., and Everett, B.H., 2001, The record of Middle Jurassic volcanism in the Carmel and Temple Cap Formations of southwestern Utah: *Geological Society of America Bulletin*, v. 113, no. 3, p. 373–387.
- Kreisa, R.D., and Moiola, R.J., 1986, Sigmoidal tidal bundles and other tide-generated sedimentary structures of the Curtis Formation, Utah: *Geological Society of America Bulletin*, v. 97, no. 4, p. 381–387.
- Kvale, E.P., 2012, Tidal constituents of modern and ancient tidal rhythmities—criteria for recognition and analyses, *in* Davis, R.A., Jr., and Dalrymple, R.W., editors, *Principles of tidal sedimentology*: Dordrecht, Netherlands, Springer Science and Business Media, p. 1–17.
- Levander, A., Schmandt, B., Miller, M.S., Liu, K., Karlstrom, K.E., Crow, R.S., Lee, C-T.A., and Humphreys, 2011, Continuing Colorado Plateau uplift by delamination-style convective lithospheric downwelling: *Nature*, v. 472, no. 7344, p. 461–465.
- Lockley, M.G., 1991, The Moab megatracksite—a preliminary description and discussion of millions of middle Jurassic tracks in eastern Utah, *in* Averett, W.R., editor, *Guidebook for dinosaur quarries and tracksites tour—western Colorado and eastern Utah*: Grand Junction Geological Society, p. 59–65.
- Lucas, S.G., 2014, Lithostratigraphy of the Jurassic San Rafael Group from Bluff to the Abajo Mountains, southeastern Utah: Stratigraphic relationships of the Bluff Sandstone. *Volumina Jurassica*, v. 12, p. 55–68.
- Lucas, S.G., and Anderson, O.J., 1997, The Jurassic San Rafael Group, Four Corners region, *in* Lucas, S.G., Anderson, O.J., and Kues, B.S., editors, *Mesozoic geology and paleontology of the Four Corners region: New Mexico Geological Society, 48th Annual Fall Field Conference Guidebook*, p. 115–132.
- Mansfield, G.R., and Roundy, P.V., 1916, Revision of the Beckwith and Bear River Formations of southeastern Idaho: U.S. Geological Survey Professional Paper 98, p. 75–84.
- Mark, C., Gupta, S., Carter, A., Mark, D.F., Gautheron, C., and Martín, A., 2014, Rift flank uplift at the Gulf of California—no requirement for asthenospheric upwelling: *Geology*, v. 42, no. 3, p. 259–262.
- Martinius, A.W., Ringrose, P.S., Brostrøm, C., Elfenbein, C., Næss, A., and Ringås, J.E., 2005, Reservoir challenges of heterolithic tidal sandstone reservoirs in the Halten Terrace, mid-Norway: *Petroleum Geoscience*, v. 11, no. 1, p. 3–16.
- McMullen, S.K., Holland, S.M., and O’Keefe, F.R., 2014, The occurrence of vertebrate and invertebrate fossils in a sequence stratigraphic context—the Jurassic Sundance Formation, Big-horn Basin, Wyoming, USA: *Palaios*, v. 29, no. 6, p. 277–294.
- Middleton, G.V., 1991, A short historical review of clastic tidal sedimentology, *in* Smith, D.G., Reinson, G.E., Zaitlin, B.A., and Rahmani, R.A., editors, *Clastic tidal sedimentology: Canadian Society of Petroleum Geologists Memoir 16*, p. ix–xv.
- Midtkandal, I., and Nystuen, J.P., 2009, Depositional architecture of a low-gradient ramp shelf in an epicontinental sea—the Lower Cretaceous of Svalbard: *Basin Research*, v. 21, no. 5, p. 655–675.

- Mountney, N.P., 2006, Periodic accumulation and destruction of eolian erg sequences in the Permian Cedar Mesa Sandstone, White Canyon, southern Utah, USA: *Sedimentology*, v. 53, no. 4, p. 789–823.
- Mountney, N.P., 2012, A stratigraphic model to account for complexity in eolian dune and interdune successions: *Sedimentology*, v. 59, no. 3, p. 964–989.
- Murray, K.E., Reiners, P.W., and Thomson, S.N., 2016, Rapid Pliocene–Pleistocene erosion of the central Colorado Plateau documented by apatite thermochronology from the Henry Mountains: *Geology*, v. 44, no. 6, p. 483–486.
- Nelson, S.T., 1997, Reevaluation of the central Colorado Plateau laccoliths in the light of new age determination: *U.S. Geological Survey Bulletin* 2158, p. 37–39.
- Nio, S.D., and Yang, C.S., 1991, Diagnostic attributes of clastic tidal deposits—a review, in Smith, D.G., Reinson, G.E., Zaitlin, B.A., and Rahmani, R.A., editors, *Clastic tidal sedimentology: Canadian Society of Petroleum Geologists Memoir* 16, p. 3–28.
- Nuccio, V.F., and Condon, S.M., 1996, Burial and thermal history of the Paradox Basin, Utah and Colorado, and petroleum potential of the Middle Pennsylvanian Paradox Formation: *U.S. Geological Survey Bulletin* 2000-O, p. 57–76.
- Ogata, K., Senger, K., Braathen, A., and Tveranger, J., 2014, Fracture corridors as seal-bypass systems in siliciclastic reservoir-cap rock successions—field-based insights from the Jurassic Entrada Formation (SE Utah, USA): *Journal of Structural Geology*, v. 66, p. 162–187.
- Ogg, J.G., Ogg, G., and Gradstein, F.M., 2016, *A concise geologic time scale*: Amsterdam, Netherlands, Elsevier, 240 p.
- Oost, A.P., and de Boer, P., 1994, *Sedimentology and development of barrier islands, ebb-tidal deltas, inlets and backbarrier areas of the Dutch Wadden Sea: Senckenbergiana Maritima*, v. 24, no. 1, p. 65–115.
- Otto, E.P., and Picard, M.D., 1976, Petrology of the Entrada Sandstone (Jurassic), northeastern Utah, in Hill, J.G., editor, *Geology of the Cordilleran hingeline: Rocky Mountain Association of Petroleum Geologists Guidebook*, p. 231–259.
- Owen, G., Moretti, M., and Alfaro, P., 2011, Recognising triggers for soft-sediment deformation—current understanding and future directions: *Sedimentary Geology*, v. 235, no. 3–4, p. 133–140.
- Parrish, J.T., and Peterson, F., 1988, Wind directions predicted from global circulation models and wind directions determined from eolian sandstones of the western United States—a compilation: *Sedimentary Geology*, v. 56, p. 261–282.
- Peterson, F., 1988, Pennsylvanian to Jurassic eolian transportation systems in the western United States: *Sedimentary Geology*, v. 56, p. 207–260.
- Peterson, F., 1994, Sand dunes, sabkhas, streams, and shallow seas—Jurassic paleogeography in the southern part of the Western Interior Basin, in Caputo, M.V., Peterson, J.A. and Franczyk, K.J., editors, *Mesozoic systems of the Rocky Mountain region, USA: Rocky Mountain Section SEPM (Society for Sedimentary Geology)*, p. 233–272.
- Peterson, F., and Pipiringos, G.N., 1979, Stratigraphic relations of the Navajo Sandstone to Middle Jurassic Formations, southern Utah and northern Arizona: *U.S. Geological Survey Professional Paper* 1035-B, 43 p.
- Petrie, E.S., Sandul, A., Gutierrez, M., and Bratthen, A., 2017, Deformation band formation and reactivation associated with a Laramide fault propagation fold [abs.]: *Geological Society of America Abstract with Programs*, v. 49, no. 6, p. 289–299.
- Pipiringos, G.N., and O’Sullivan, R.B., 1978, Principal unconformities in Triassic and Jurassic rocks, Western Interior United States—a preliminary survey: *U.S. Geological Survey Professional Paper*, 1035-A, 29, 1 plate, p. 1–29.
- Pipiringos, G.N., and Imlay, R.W., 1979, Lithology and subdivisions of the Jurassic Stump Formation in southeastern Idaho and adjoining areas: *U.S. Geological Survey Professional Paper* 1035-C, 25 p.
- Rodríguez-López, J.P., Clemmensen, L.B., Lancaster, N., Mountney, N.P., and Veiga, G.D., 2014, Archean to Recent aeolian sand systems and their sedimentary record—current understanding and future prospects: *Sedimentology*, v. 61, no. 6, p. 1487–1534.
- Scott, R.B., Harding, A.E., Hood, W.C., Cole, R.D., Livaccari, R.F., Johnson, J.B., Shroba, R.R., and Dickerson, R.P., 2001, *Geologic map of Colorado National Monument and adjacent areas, Mesa County, Colorado: U.S. Geological Map* I-2740, 40 p., 1 plate, scale 1:24,000.
- Sprinkel, D.A., Doelling, H.H., Kowallis, B.J., Waanders, G., and Kuehne, P.A., 2011, Early results of a study of Middle Jurassic strata in the Sevier fold and thrust belt, Utah, in Sprinkel, D.A., Yonkee, W.A., and Chidsey, T.C., Jr., editors, *Sevier thrust belt—northern and central Utah and adjacent areas: Utah Geological Association Publication* 40, p. 151–172.
- Skurtveit, E., Braathen, A., Larsen, E.B., Sauvin, G., Sundal, A., and Zuchuat, V., 2017, Pressure induced deformation and flow using CO₂ field analogues, Utah: *Energy Procedia*, v. 14, p. 3257–3266.
- Sullivan, K.R., Kowallis, B.J., and Mehnert, H.H., 1991, Isotopic ages of igneous intrusions in southeastern Utah—evidence for a mid-Cenozoic Reno–San Juan magmatic zone: *Brigham Young University Geology Studies*, v. 37, p. 139–144.
- Sundal, A., Miri, R., Hellevang, H., Tveranger, J., Midtkandal, I., Zuchuat, V., Aagaard, P., and Braathen, A., 2017, Movement of CO₂ charged fluids in low permeability rocks during deformation—migration patterns in the Carmel Formation, Utah: *En-*

- ergy Procedia, v. 114, p. 4537–4544.
- Talbot, M.R., 1985, Major bounding surfaces in eolian sandstones—a climatic model: *Sedimentology*, v. 32, no. 2, p. 257–265.
- Tape, C.H., Cowan, C.A., and Runkel, A.C., 2003, Tidal-bundle sequences in the Jordan Sandstone (Upper Cambrian), south-eastern Minnesota, USA—evidence for tides along inboard shorelines of the Sauk epicontinental sea: *Journal of Sedimentary Research*, v. 73, no. 3, p. 354–366.
- Thorman, C.H., 2011, The Elko orogeny—a major tectonic event in eastern Nevada–western Utah, in Sprinkel, D.A., Yankee, W.A., and Chidsey, T.C., Jr., editors, *Sevier thrust belt—northern and central Utah and adjacent areas*: Utah Geological Association Publication 40, p. 117–129.
- Trudgill, B.D., 2011, Evolution of salt structures in the northern Paradox Basin—controls on evaporite deposition, salt wall growth and supra-salt stratigraphic architecture: *Basin Research*, v. 23, no. 2, p. 208–238.
- Turner, C.E., and Peterson, F., 1999, Biostratigraphy of dinosaurs in the Upper Jurassic Morrison Formation of the Western Interior, U.S.A., in Gillette, D.D., editor, *Vertebrate paleontology in Utah*: Utah Geological Survey Miscellaneous Publication 99-1, p. 77–114.
- Urash, R.G., and Savrda, C.E., 2017, Ichnology of an Eocene shallow marine passive margin condensed section, eastern Gulf coastal plain, Alabama, USA: *Palaeogeography, Palaeoclimatology, Palaeoecology*, v. 471, p. 58–70.
- Van Wagoner, J.C., Posamentier, H.W., Mitchum, R.M.J., Vail, P.R., Sarg, J.F., Loutit, T.S., and Hardenbol, J., 1988, An overview of the fundamentals of sequence stratigraphy and key definitions: *Society of Economic Paleontologists and Mineralogists (SEPM) Special Publication No. 42*, p. 39–45.
- Waldschmidt, W.A., and LeRoy, L.W., 1944, Reconsideration of the Morrison Formation in the type area, Jefferson County, Colorado: *Geological Society of America Bulletin*, v. 55, no. 9, p. 1097–1114.
- Wang, P., 2012, Principles of sediment transport applicable in tidal environments, in Davis, R.A., Jr., and Dalrymple, R.W., editors, *Principles of tidal sedimentology*: Dordrecht, Netherlands, Springer Science and Business Media, p. 19–34.
- Westoby, M.J., Brasington, J., Glasser, N.F., Hambrey, M.J., and Reynolds, J.M., 2012, ‘Structure-from-Motion’ photogrammetry—a low-cost, effective tool for geoscience applications: *Geomorphology*, v. 179, p. 300–314.
- Wheatley, D.F., Chan, M.A., and Sprinkel, D.A., 2016, Clastic pipe characteristics and distributions throughout the Colorado Plateau—implications for paleoenvironments and paleoseismic controls: *Sedimentary Geology*, v. 344, p. 20–33.
- Wilcox, W.T., and Currie, B., 2008, Sequence stratigraphy of the Jurassic Curtis, Summerville, and Stump Formations, eastern Utah and northwest Colorado, in Longman, M.W., and Morgan, C.D., editors, *Hydrocarbon systems and production in the Uinta Basin, Utah*: Rocky Mountain Association of Geologists and Utah Geological Association Publication 37, p. 9–41.
- Witkind, I.J., 1988, Geologic map of the Huntington 30' x 60' quadrangle, Carbon, Emery, Grand, and Uintah Counties, Utah: U.S. Geological Survey, Miscellaneous Investigations Series Map I-1764, 1 plate, scale 1:100,000.
- Wright, J.C., Shawe, D.R., and Lohman, S.W., 1962, Definition of members of Jurassic Entrada Sandstone in east-central Utah and west-central Colorado: *American Association of Petroleum Geologists Bulletin*, v. 46, no. 11, p. 2057–2070.
- Yonkee, W.A., and Weil, A.B., 2015, Tectonic evolution of the Sevier and Laramide belts within the North American Cordillera orogenic system: *Earth-Science Reviews*, v. 150, p. 531–593.

7.2. Article II: Composite Unconformities in Low-Gradient, Transitional Settings: the J-3 Unconformity and the Curtis Formation, East-Central Utah, USA.

Zuchuat, V.¹, Midtkandal, I.¹, Poyatos-Moré, M.¹, Da Costa, S.¹, Halvorsen, K.¹, Cote, N.², Sundal, A.¹, and Braathen, A.¹ (in review). Composite Unconformities in Low-Gradient, Transitional Settings: the J-3 Unconformity and the Curtis Formation, East-Central Utah, USA. Submitted to *The Journal of Sedimentary Research*.

¹*Tectonostratigraphic Research Group, University of Oslo, Sem Sælands Vei 1, 0371 Oslo, Norway*

²*Natural and Environmental Sciences Department, Western State Colorado University, 600 North Adams Street, Gunnison, CO 81231*

COMPOSITE UNCONFORMITIES IN LOW-GRADIENT, TRANSITIONAL SETTINGS: THE J-3 UNCONFORMITY AND THE CURTIS FORMATION, EAST-CENTRAL UTAH, USA

VALENTIN ZUCHUAT¹, IVAR MIDTKANDAL¹, MIQUEL POYATOS-MORÉ¹, SIGRID DA COSTA¹, KRISTINE HALVORSEN¹, NATHAN COTE², ANJA SUNDAL¹, ALVAR BRAATHEN¹

¹*University of Oslo, Sem Sælands Vei 1, 0371 Oslo, Norway*

²*Natural and Environmental Sciences Department, Western State Colorado University, 600 North Adams Street, Gunnison, CO 81231*

Corresponding author: valentin.zuchuat@geo.uio.no

ABSTRACT

Unconformities, by definition, correspond to erosive- or nondepositional surfaces, which separate younger strata below, from younger rocks above, and they can encapsulate significant time gaps. However, recent studies have highlighted the composite nature of some unconformities, as well as their heterochronous character, which challenge the use of such a definition in a four-dimensional dynamic environment. The exhumed J-3 Unconformity, separating the Middle Jurassic Entrada Sandstone from the Upper Jurassic Curtis Formation (and laterally-equivalent units) in east-central Utah, displays eight different relief expressions. These include: (i) angular unconformity, (ii) paraconformity, (iii) steep incisions, (iv) undulating relief, (v) irregular relief, including fault-plane- and erosion-related relief irregularities, (vi) circular collapsed structures, (vii) hydroplastic sagging, and (viii) sedimentary loading. The first five types of relief were generated by erosion-related processes, such as aeolian deflation, and water-induced erosion, whereas the three remaining ones were driven by deformational processes. Thus, the J-3 Unconformity is a composite surface, with several processes that do not only interact and shape the unconformity on a differential three-dimensional space, but also in time. Results of this work therefore demonstrate the heterochronous and non-unique nature of this and potentially other surfaces interpreted as unconformities, where the same relief geometry can be produced by different processes, and one single process can generate different geometries. In this particular study, with coexisting aeolian and shallow-marine systems within a transgressed basin setting, the composite flooding-ravinement surface separating the two depositional systems is time-transgressive. Consequently, the regionally-extended, composite, and heterochronous J-3 Unconformity does not match with the classic unconformity definition, and should therefore not be considered as such. This outcrop example cautions against misunderstanding the subseismic complex character of these bounding surfaces, especially while conducting subsurface analyses, which may lead to inaccurate timing and sediment budget predictions, and ultimately have strong implications for basin evolution and reservoir models.

Key word: Unconformity, transitional basin, composite surface, ravinement, time-transgressive

INTRODUCTION

The contact nature and the relationship between two rock strata has been of interest for scientists and geologists for nearly three hundred and fifty years (Steno, 1669), and it has played an important role in understanding how the earth changes slowly but significantly over time. Hutton (1788) first described what then became his iconic Siccar Point angular unconformity, ca. 45 km east of Edinburgh (Scotland). Hutton also noted that the overlying Devonian Old Red Sandstone contained fragments of the underlying rocks at its base, implying that steeply inclined strata were eroded and reworked prior to the deposition of the overburden (Shanmugam, 1988). These reworked clasts occurring at the base of the Devonian sediments add an ontological dimension of (missing) time to these geological surfaces, that Blackwelder (1909) called unconformities. This time dimension is a key issue one is required to address, when deconstructing a basin dynamic history (Blackwelder, 1909; Barrell, 1917; Wheeler, 1958; Shanmugam, 1988; Miall, 2016, and references therein). Mitchum *et al.* (1977) defined unconformities as a “surface of erosion or nondeposition that separates younger strata from older rocks and represents a significant hiatus”, thus acting as time barrier, and using them as sequence boundary in the “Exxon School” of sequence stratigraphy.

Unconformities offer deeper insights into what processes are landscape-changing, and how they interact with one-another in a dynamic and evolving system (Kyrkjebø *et al.*, 2004; Holbrook and Bhattacharya, 2012; Miall, 2016; Gani, 2017, Zuchuat *et al.*, 2018). As a result, the definition of an unconformity has been recently challenged, notably by Holbrook and Bhattacharya (2012), and Blum *et al.* (2013), who showed that subaerial unconformities are not a singular bypass surface. Further, Gani (2017) argued, with reason, that Steno's law of superposition is only valid in one-dimensional system. Indeed, when looking at a regressive fluvio-deltaic system at regional scale, subaerial unconformities occur as composite, and multichronous fluvial scours and interfluvial exposure surfaces that do not separate older sediments below from younger sediments above them across a source-to-sink profile (Holbrook and Bhattacharya, 2012). Kyrkjebø *et al.* (2004) demonstrated the seismic-scale, polychronous nature of the regional “Base Cretaceous Unconformity” of the North Sea (Fig. 1). Instead of resulting from one singular erosive episode, as its name misleads, this unconformity actually displays an amalgamation of several local- to regional erosional surfaces, and “its substrate is not always overlain by Cretaceous sediments” (Kyrkjebø *et al.*, 2004). It should rather be referred to as the “North Sea Unconformity Complex” instead, which better reflects the complexity of the basin history (Kyrkjebø *et al.*, 2004). Further, both Miall (2016) and Gani (2017) highlighted the intricate multi-scale nature of the temporal dimension defining and impacting on any given unconformity, upon which, second- to millennia-lasting to Ma-scale processes interact with each other, such as ripples migration, orbitally-forced climatic and relative base-level oscillations, and plate tectonics, among others. Such complex processes interactions implies that the missing time unconformities record is highly heterogeneous (Miall, 2016; Gani, 2017), independently of the scale researchers work with.

Pipiringos and O'Sullivan (1978) defined ten regional unconformities within the Mesozoic Western Interior succession in North America, formally referred to as Tr-1 to Tr-4, J-0 to J-5, and K-0 Unconformities (Tr: Triassic, J: Jurassic, and K: Cretaceous). Blakey (1994, 2008), Bjerrum and

Dorsey (1995), and Miall (2016) discussed the major role that tectonics played in the development of these surfaces. These authors argued that most of them are angular unconformities which developed due to regional tectonic activity and eustatic sea level variations, and that the time gap encapsulated within each of these sedimentary breaks approaches 10^6 years. However, the impact of major climatic shifts on the development of unconformities must be also acknowledged, as illustrated notably by the Tr-3 Unconformity, which delimits the arid deposits and steep-sided canyons of the Moenkopi Formation from the overlying Chinle Formation humid environment and perennial drainage system (Blakey, 2008; Miall, 2016).

This study focuses on Pipiringos and O'Sullivan's (1978) J-3 Unconformity in east-central Utah (Fig. 2) in order to illustrate and understand the complex nature and intricate sub-seismic development of some unconformities. This unconformity separates the Middle Jurassic, continental Entrada Sandstone from the Upper Jurassic, shallow marine and tidally influenced Curtis Formation (Pipiringos and O'Sullivan's, 1978; Wilcox and Currie, 2008; Zuchuat *et al.* 2018). By documenting the J-3 sub-seismic relief expression, its spatial distribution, amplitude, and wavelength, this work identifies the various local and regional processes implicated in the making of this unconformity. Understanding these processes allows to deconstruct this bounding surface history, and to propose a relative involvement timing for each of these mechanisms and their relations to under- and overlying sedimentary facies. Understanding the development of such surfaces at a sub-seismic scale will ultimately improve the overall knowledge of a basin's dynamic at a regional scale, and will strengthen sub-surface interpretation by forcing geologists to assess their models with greater caution.

GEOLOGICAL SETTING

Basinal setting

Utah's geological record shows evidence of several major tectonic events occurring since the early Mesozoic and the development of the North American Cordillera (Hintze and Kowallis, 2009; Thorman, 2011; Anderson, 2015; Yonkee and Weil, 2015; references therein): (i) the Middle Jurassic - Lower Cretaceous Nevadan Orogeny, which left granitic intrusions at today's Utah-Nevada border, (ii) the Middle Jurassic Elko Orogeny, marked by an alternating extensional- and contractional stress regimes and the development of successive regional foreland basins, (iii) the Lower Cretaceous to Paleogene Sevier Orogeny, which resulted in thin-skinned contractional structures, and (iv) the Upper Cretaceous to Paleogene Laramide Orogeny, featuring notable basement-rooted monoclines, akin to the San Rafael Swell (Fig. 2) (Bump and Davis, 2003). Furthermore, the remobilisation and diapirism of the Paradox Basin evaporitic deposits affected rocks in east-central and south-eastern Utah (Trudgill, 2011). The Colorado Plateau uplift and its related extensional (sub-)regional phases also impacted on the stratigraphy of the studied area (Levander *et al.*, 2011; Murray *et al.*, 2016). Eventually, the sedimentary cover in central- and south-eastern Utah was affected by the Upper Oligocene igneous complexes of the Abajo, Henry and La Sal Mountains (Sullivan *et al.*, 1991;

Nelson, 1997). Nuccio and Condon (1996) and Petrie *et al.* (2017) showed that, in the San Rafael Swell vicinity, the Curtis Formation was buried to depth of 2.45 km and 2.86 km.

Stratigraphy

Both the Entrada Sandstone and the overlying Curtis Formation belong to the Middle- to Upper Jurassic San Rafael Group (Fig. 2C), together with the Temple Cap Formation, the Page Sandstone, the Carmel Formation, and the Summerville Formation (Gilluly and Reeside, 1928; Pipiringos and O'Sullivan, 1978; Peterson and Pipiringos, 1979; Anderson and Lucas, 1994; Sprinkel *et al.*, 2011). This sedimentary group recorded five stacked and eastward-wedging out of upward-thinning transgressive-regressive sequences, deposited within a retroarc foreland basin in the vicinity of the SSW-N-oriented Utah-Idaho Trough, parallel to the Elko Highlands (Fig. 2B; Anderson and Lucas, 1994; Brenner and Peterson, 1994; Peterson, 1994; Bjerrum and Dorsey, 1995; Thorman, 2011).

During the Callovian times, the retreating Sundance Sea was replaced by arid and continental conditions, with the deposition of the Entrada Sandstone (Fig. 2C; Gilluly and Reeside, 1928; Peterson, 1994; Hintze and Kowallis, 2009). The formation consists of two sedimentary units: (i) aeolian dunes interbedded with finer-grained interdune deposits of the Slick Rock Member, and (ii) overlying and spatially penecontemporaneous, recurrently yet superficially vegetated marginal marine sediments associated with the earthy facies (informal nomenclature) (Fig. 2). The formation thickens westwards to the Utah-Idaho Trough and northwards to the Sundance Seaway (Fig. 2B) (Witkind, 1988; Crabaugh and Kocurek, 1993; Carr-Crabaugh and Kocurek, 1998; Mountney, 2012; Doelling *et al.*, 2015). The Entrada Sandstone is mostly constituted of recycled fluvial sediments sourced from the Appalachian Mountains (Dickinson and Gehrels 2009, 2010). This coastal aeolian system comprises four construction-destruction sequences (*sensu* Mountney, 2006), related to regional fluctuations of the paleo-water table and/or sea level variations (Carr-Crabaugh and Kocurek, 1998; Mountney, 2012). The Entrada Sandstone is truncated at its top by Pipiringos and O'Sullivan's (1978) J-3 Unconformity, who described "an inferred relief of as much as 14 m in about 3 km" north of the San Rafael Swell. They did not discuss any of the erosive processes involved in the carving of this relief. Eschner and Kocurek (1988) differentiated between inherited mellow relief (up to 3 m) reflecting dune remains and steep and deep erosional relief (up to 7 m) sculpted by tidal currents and mass flow deposits. Caputo and Pryor (1991) reported a relief of 0.3 to 0.9 m, arguing that "marine currents reworked material along the J-3 Unconformity". Peterson (1994) wrote that "the surface appears to be a simple transgressive erosion surface that formed when Curtis seas advanced", arguing that the pre-Curtis denudation episode(s) was "related to local tectonics and was not related to eustatic processes".

The Lower Oxfordian Curtis Formation, consisting of shallow-marine, tidally-influenced deposits, overlies the Entrada Sandstone, and was defined by Gilluly and Reeside (1928) along the NE-margin of the San Rafael Swell (Fig. 2) (Kreisa and Moiola, 1986; Caputo and Pryor, 1991; Wilcox and Currie, 2008; Ogg *et al.*, 2016; Zuchuat *et al.*, 2018). These glauconitic and chlorite-rich sedimentary rocks are characterised by a green to white colour, which strongly contrasts with the underlying rusty red Entrada Sandstone (Gilluly and Reeside, 1928; Caputo and Pryor, 1991; Peterson, 1994). As the Elko Orogeny foredeep accommodation decreased at the end of the Middle Jurassic (Thorman,

2011), the Curtis Sea covered a gently dipping, shallow epicontinental basin (Zuchuat *et al.*, 2018). Due notably to the enclosed, and fluvially-starved nature of the basin (Zuchuat *et al.* 2018), as well as the lack of source-to-sink study for this arid, continental, to shallow marine transitional system, the sediment supply to the system is unconstrained. Polycrystalline Quartz grains found in some conglomeratic deposits within the Curtis Formation require, however, an extra-basinal source of sediment (Zuchuat *et al.*, 2018). The Curtis Formation as a whole displays an overall east- and southward pinching geometry, and its thickness varies between ca. 30 to 80 m in the San Rafael Swell area (Fig. 2) (Gilluly and Reeside, 1928; Caputo and Pryor, 1991; Peterson, 1994; Thorman, 2011; Anderson, 2015; see Fig. 2 and Fig. 3 in Zuchuat *et al.*, 2018). The formation can be divided in three readily identifiable yet informal sub-units: the lower, the middle and the upper Curtis (Zuchuat *et al.*, 2018). The lithostratigraphic lateral equivalent of the upper Curtis marginal marine deposits corresponds to the aeolian paleo-dunes of the Moab Member (of the Curtis Formation), cropping out in the vicinity of Moab (Fig. 2) (Caputo and Pryor, 1991; Peterson, 1994; Doelling, 2001; Zuchuat *et al.*, 2018).

The Summerville Formation dark brown and hypersaline sabkha deposits conformably overlie the Curtis Formation in the study area (Fig. 2) (Gilluly and Reeside, 1928; Caputo and Pryor, 1991; Peterson, 1994; Lucas, 2014). It is however highly probable that the Summerville Formation deposits co-existed with the Curtis Formation strata as a proximally placed coastal plain unit in neighbouring regions (Zuchuat *et al.*, 2018). The Curtis and the Summerville Formations have been respectively correlated to the Todilto Member and the Beclabito Member of the Wanakah Formation in the Four Corners area (Utah/Arizona/New Mexico/Colorado) (Fig. 2), (Condon and Huffman, 1988, Zuchuat *et al.*, 2018, Kocurek *et al.*, in press).

DATA AND METHODS

The datasets compiled to investigate the J-3 Unconformity were collected over three field seasons in 2015, 2016 and 2017, and comprise: (i) traditional sedimentary and structural data acquired through detailed logging of forty-three localities (Fig. 2) selected upon outcrop exposure quality, and accessibility; (ii) photographs collected at and between the measured sections, including classic camera images, pictures taken with an Unmanned Aerial Vehicle (UAV - DJI[®] Phantom 4), as well as satellite and aerial images accessible on Google Earth[®] and Microsoft Bing Map[®] engines; (iii) palaeocurrent indicators and other relevant structural information, such as fault plane orientation, fault motion indicators, throw, heave, and offset values. In furtherance of appraising the multi-scale sedimentary architecture of the succession, Structure-from-Motion (SfM) photogrammetry methods (after Westoby and others, 2012) were used to generate three-dimensional (3D) virtual outcrops for selected localities. Photogrammetric data were processed and virtual outcrops were generated in PhotoScan Pro[®] (Agisoft LLC, St. Petersburg, Russia). Virtual outcrop visualization, analysis, and interpretation were pursued in Lime[®], a software developed by both Bergen and Aberdeen Universities and their Virtual Outcrop Geology VOG group (Bonaventura *et al.*, 2017; Buckley *et al.*, 2017). At each visited locality, the J-3 Unconformity was characterised in terms of relief amplitude,

wavelength, visual appearance and bounding sedimentary units. Combining these datasets allows for the unveiling of the various processes involved in the J-3 Unconformity genesis, and to discuss both their spatial- and temporal distribution throughout the study area.

Regarding the characterisation of the J-3 Unconformity, the authors describe relief and processes as being either *facies-dependent*, or *facies-independent*. A certain relief expression is branded facies-dependant if it is bounded by and restricted to a specific facies, whereas a facies-independent one occurs unrestrictedly of the lithology. Additionally, faults and fault planes are referred to as *pre-*, *syn-*, and *post-Curtis* features, indicating their respective development time, with respect to the deposition of the Curtis Formation: pre-Curtis fault planes were generated prior to the deposition of the Curtis Formation; syn-Curtis fault planes developed as the Curtis Formation was being deposited; post-Curtis faulting occurred after the Curtis Formation was deposited, impacting younger sedimentary strata as well.

RESULTS

Sedimentology

The detailed sedimentology analysis of the Curtis Formation is developed in Zuchuat *et al.* (2018), upon which this manuscript bases its facies association (FA) scheme (Table 1). The Entrada Sandstone corresponds to Zuchuat *et al.*'s (2018) FA 1, which is subdivided into two sub-units. FA 1a encompasses the Slick Rock Member of the Entrada Sandstone, while FA 1b incorporates the earthy facies sabkha, marginal marine sediments, as well as coastal aeolian dune, interdune, and loess deposits (Table 1) (Zuchuat *et al.*, 2018). The Curtis Formation youngest and laterally restricted deposits are interpreted as tidally influenced upper shoreface to beach deposits (FA 2, Table 1). FA 3 deposits represent subtidal flats, and are either mud-dominated (FA 3a), or sand-dominated (FA 3b, Table 1). Note the presence of conglomeratic, tidally-influenced, subaqueous dunes, of gravel-rich subtidal channel infills within FA 3. FA 4a corresponds to a sub- to supratidal sandflat, which is easily recognisable in the field due to its light-pink colour, strongly contrasting with the archetypical green colour of the Curtis Formation (Table 1). FA 4b is interpreted as correlative, distal, subtidal channels, occasionally containing extra-basinal, gravel-size clasts (Table 1). FA 2, FA 3, and FA 4 form the informal lower Curtis (Zuchuat *et al.*, 2018). Chaotically arranged conglomeratic flash flood deposits occur sporadically at the base of the lower Curtis. This informal member consists of three parasequences, and is overlain by the middle Curtis (Zuchuat *et al.*, 2018), which corresponds to FA 5 homogenous, very fine- to fine-grained, light green to white sandstone, representing a complex interfingering of sub- to intertidal channels, dunes, and sandflats (Table 1). The base of the middle Curtis is defined by the Major Transgressive Surface (MTS), which can be traced throughout and beyond the study area, as it also corresponds to the base of Moab Member of the Curtis Formation, as well as the Todilto Member of the Wanakah Formation in the Four Corners area (Fig. 2C) (Zuchuat *et al.*, 2018). The upper Curtis FA 6 sub- to supratidal deposits conformably overlie the middle Curtis, and are characterised by finer grained and smaller bedforms in comparison with FA 5 (Table 1), reflecting a lower energy level within the system, and more protected and restricted, shallow marine environmental conditions. Cropping out in the eastern part of the study area, the Moab Member of the

Curtis Formation and its aeolian dunes (FA 7) is the lateral equivalent of FA 6 (Table 1, Fig. 2C). The Summerville Formation supratidal sabkha deposits (FA 8) gradually succeed the Curtis Formation (Table 1), as well as the Todilto Member of the Wanakah Formation in the Four Corners area (Fig. 2) (Zuchuat *et al.*, 2018).

Characterisation of the J-3 Unconformity

Despite the polychronous nature of the J-3 Unconformity (Zuchuat *et al.*, 2018), its name, hereunder, refers to the present-day, final expression of this bounding surface, as defined by Pipiringos and O'Sullivan's (1978). The J-3 Unconformity relief is divided into eight categories, based on its expressed geometry and the processes involved in its crafting and evolution (Fig. 3, Fig. 4): (i) angular unconformity, (ii) paraconformity, (iii) steep incisions, (iv) undulating relief, (v) irregular relief, including fault-plane- and erosion-related relief irregularities, (vi) circular collapsed structures, (vii) hydroplastic sagging, and (viii) sedimentary loading. Categories i-v are express erosion-related relief, whereas categories vi-viii display a deformed J-3 unconformity relief.

Erosion-related relief – angular unconformity

The first type of exposed relationship between the Entrada Sandstone and the overlying Curtis Formation (and the lateral correlative Todilto Member of the Wanakah Formation) is a flat surface (Fig. 4A, B, C). However, this bounding surface corresponds either to an angular unconformity, as visible at Ruby Ranch Road, on the Green River's eastern bank (Fig. 2, Fig. 4A), or paraconformity (Fig. 4B, C). In the case of the flat angular unconformity, the J-3 bounds the earthy facies of the Entrada Sandstone (FA 1b) from a thin ledge (less than a metre thick) of middle Curtis (FA 5) and upper Curtis (FA 6, Fig. 4A). A similar flat angular unconformity between the two formations in the vicinity of Notom Ranch (Fig. 2, see Fig. 7 in Wheatley *et al.*, 2016), but there, the J-3 Unconformity separates the Slick Rock Member (FA 1a) from a thin middle Curtis ledge (FA 5). This illustrates that these angular unconformities are combined with Zuchuat *et al.*'s (2018) Major Transgressive Surface (MTS) at the base of the middle Curtis, which strongly eroded its substratum, as recorded at Shadscale Mesa (Fig. 2, Fig 4H, I, J). Due to the erosive power accompanying the Major Transgression, such angular unconformities are interpreted to represent a tidal ravinement surface.

Erosion-related relief – paraconformity

The J-3 as paraconformity is probably the most widespread expression of the bounding surface (Fig. 3). It is not facies-dependant, since it bounds the earthy facies of the Entrada sandstone (FA 1b) and the lower Curtis (Last Chance Desert, Fig. 2, Fig. 4B), but it can also bound the earthy facies and the middle Curtis, as observed 1.5 km NW of Caineville Airstrip (Fig. 2, Fig. 4C). The J-3 as a paraconformity separates the Slick Rock Member of the Entrada Sandstone from the Moab Member of the Curtis Formation in the eastern study area, where the earthy facies is absent (Fig. 2, see also Fig. 3 and Fig. 10a in Zuchuat *et al.*, 2018). At Echo Amphitheater, close to Ghost Ranch, New Mexico (Fig. 2), the Slick Rock Member is also capped by a bed-parallel J-3 Unconformity, which separates it from the overlying Todilto Member of the Wanakah Formation (Lucas *et al.*, 2005). Note that, locally the contact between the Slick Rock Member and the Todilto Member can be undulating, as a result of "antecedent dune topography" (Kocurek *et al.*, in press). The Entrada Sandstone

underwent a period of aeolian deflation before, and as the Curtis transgression occurred (Mountney, 2006), which might or might not have further reworked the substratum (Kocurek *et al.*, in press).

Erosion-related relief – undulating relief

The most enigmatic type of relief characterising the J-3 Unconformity was only recorded in the northernmost zone of the study area, at Stove Gulch (Fig. 2), where the bounding surface between the earthy facies of the Entrada Sandstone and the lower Curtis displays an unusual sinuously undulating geometry (Fig. 4D). The undulating relief has an amplitude of up to 2-3 m, and a sinusoidal wavelength of ca. 8-10 m. Mud-dominated heterolithic deposits of FA 3a passively onlap the pre-existing relief (Fig. 4D), demonstrating that the relief predated the deposition of the lower Curtis.

Erosion-related relief – steep incision

Steep-sided incisions of the Curtis Formation into the Entrada Sandstone notably occur at Sven's Gulch (Fig. 4E), Uneva Mine Canyon, in the eastern cliffs of Cedar Mountain, and at Notom Ranch (Fig. 2). Geometrically, incisions range between 10 and 70 m in width (Notom Ranch and Uneva Mine Canyon, respectively), and they reach depths between 3 and 15 m. At Sven's Gulch, the incision is ca. 45 m wide, and carved ca. 10 m into the underlying earthy facies of the Entrada Sandstone (FA 1b, Fig. 4E). These narrow and localised features are facies-dependant, dissimilarly to the angular unconformity or the paraconformity, because all of the observed incisions cut into the earthy facies of the Entrada Sandstone. At Sven's Gulch (Fig. 2), the incision did not only erode the Entrada Sandstone, but it also carved into Curtis FA 2 shoreface and FA 3a subtidal deposits (Fig. 4E, see also Fig. 4C and 4D in Zuchuat *et al.*, 2018). Note that a boulder of Entrada material is contained within the incision infill (Fig. 4E). Such incisions are interpreted to be the product of channelised tidal currents, acting on a non- to semi-consolidated Entrada- and Curtis substratum. The cannibalisation of younger FA 2 and FA 3a deposits, as well as the presence of Entrada material within the channel infill imply that this incision didn't exist prior to the incision, but rather formed as a result of a short lived regressive episode, funnelling the tidal forces and carving into a poorly lithified substratum, encapsulating eroded material into the resultant infill strata in the process. Note that the Sven's Gulch incision belongs to the 2nd parasequence observed in the lower Curtis, entirely cannibalising its substratum (Zuchuat *et al.*, 2018), whereas the overlying sub-tidal channel deposits (FA 4b) belong to the lower Curtis 3rd parasequence.

Erosion-related relief – irregular relief

The J-3 Unconformity irregular relief, or disconformity, is the second most widespread bounding surface expression across the study area. Its wavelength ranges from 0.5 to 200 m, while its amplitude varies from 0.1 to 23 m, which corresponds to the highest relief value measured throughout the study area (Cedar Mountain, Fig. 4K). This type of irregular relief is partially facies-dependant, as it separates the earthy facies of the Entrada Sandstone (FA 1b) either (i) from lower Curtis deposits (Cedar Mountain, or Humbug Flat East (Fig. 2), where tidally-reworked, cross-stratified, basal flash flood conglomerates disconformably rest on earthy facies strata (Fig. 4G); or (ii) from the middle Curtis channel, dune and flat complex (FA 5), eroding into its substratum during the Major Transgression (Fig. 4J). Such irregular relief is therefore related to (i) sporadic flash floods gently

incising into the Entrada Sandstone before or during the Curtis Sea transgression; and to (ii) syn-transgression tidal ravinement (Zuchuat *et al.*, 2018).

Erosion-related relief – irregular relief: the impact of pre-existing faults

The impact of pre-Curtis fault planes on the J-3 relief can be regarded as (i) non-existent as they were eroded subsequently, yet the fault system did generate small (half-)graben structures (Humbug Flats East, Fig. 2, Fig. 4F); or (ii) limited, and marked by partial step-like subsequent reworking (Shadscale Mesa, Fig. 2, Fig. 4H, I). These faults are either planar, as visible at Shadscale Mesa (Fig. 4H, I), slightly curved-shape, or related to circular collapsed caldera-like structures in the earthy facies of the Entrada Sandstone (Hanksville Airport, Fig. 2, Fig. 4L, M). All pre-Curtis faults displaced the earthy facies of the Entrada Sandstone, whereas post-Curtis ones also cut through the underlying Slick Rock Member. Although the exact timing of these faulting episodes, as well as their precise triggering mechanism(s?) remain unknown, it seems that most of them are expression of local structural disturbances, rather than being associated with regional deep-rooted tectonic activity.

At Shadscale Mesa, the outcrop can be separated in three zones, each characterised by different fault-related J-3 Unconformity expressions (Fig. 4H). The NE-dipping normal faults displacing earthy facies strata (FA 1b) in the northern part of the outcrop have no impact of the geometry of the J-3 Unconformity, as their fault planes were entirely removed by subsequent erosion (Fig. 4H). It is suggested that the relief generated by these fault planes was primarily smoothed by a pre-Curtis and non-marine process, such as aeolian deflation, as the weak mechanical strength of saturated, marginal marine, loess deposits advocate against long-lasting, and unaltered, sub-aerially exposed fault planes (Yang *et al.*, 2016). Towards the central part of the outcrop, where the J-3 separates the earthy facies from the overlying middle Curtis, NE-dipping normal faults generated a step-like geometry of ca. 35-40 cm (Fig. 4H, 4I). Some of these pre-existing fault planes existing in the Entrada Sandstone did influence the subsequent marine erosion accompanying the middle Curtis Major Transgression and the deposition of FA 5a deposits (Fig. 4H, 4I) (Zuchuat *et al.*, 2018). Farther to the south of the outcrop, normal faults are dipping towards the SW (Fig. 4H). Contrastingly, these pre-existing SW-dipping fault planes had no impact on middle Curtis deposition. However, one south-dipping normal fault shows evidence of reactivation, as the throw reaches ca. 2 m in the earthy facies of the Entrada Sandstone, while the overlying middle Curtis only display a throw of ca. 60 cm (Fig. 4H, 4I). Looking at one laterally continuous paleosol horizon throughout the whole faulted cliff face, it appears that at least 3.2 m of earthy material eroded by aeolian deflation before the Curtis Sea transgressed the region (Fig. 4H, 4I, 4J). In the northern part of the outcrop, the unconformity was subsequently partially modified by strong currents accompanying the deposition of the lowermost FA 2 deposits. As the transgression progressed, and deposited FA 3 subtidal sediments, the erosive power of the currents diminished, as evidenced by a thicker remaining earthy facies of the Entrada Sandstone succession. Eventually, the tidal currents accompanying the major transgressive episode at the base of the middle Curtis further modified the unconformity, before the SW-dipping normal fault was reactivated, giving the J-3 Unconformity its final composite expression. The fact that these pre-existing faults dipping towards the NE did affect the Major Transgression and the deposition of the middle Curtis unit in the central part of the outcrop, whereas the northern part of the cliff was not

impacted by their occurrence, suggests a differential hardening of these fault planes, the ones flooded the latest being the most resistant.

Deformation-related relief – circular collapse

Approximately 2.1 km north of Hanksville Airport (Fig. 2, Fig. 4L, M), the J-3 Unconformity was strongly impacted by post-Curtis ring-faulting (Marti *et al.*, 1994; Gudmundsson, 2007). As the original J-3 Unconformity was sculpted by aeolian deflation and localised, meter-scale, water-induced incision, the earthy facies of the Entrada Sandstone (FA 1b) was jolted by sand-mobility-related gentle contractional folding, followed by a passive infill of the available accommodation by the lower Curtis deposits (FA 3, Fig. 4L). After the major Curtis Sea transgression, which led to the deposition of the middle Curtis (FA 5), a sudden 5.5 m, caldera-like collapse of the Entrada Sandstone occurred, forming a 60 m wide, steeply dipping ring-fault system, which displaced both formations (Fig. 4L, M). The maximum throw per individual fault reaches ca. 2.65 m. The ring-shaped surface expression of these faults, as well as several other similar circular collapsed structures, are observable from satellite and aerial images of the area (Fig. 4M). The capping Summerville Formation, when present, does not display any evidence of similar deformation. Note that these collapsed structures are more resistant to weathering than the unaltered, encasing deposits, leaving behind tubular and pillar-like structures.

Deformation-related relief – hydroplastic sagging

The only recorded example of hydroplastic sagging is visible on Cedar Mountain's cliff side, generating a 4 m deep and 20 m wide trough in the uppermost earthy facies of the Entrada Sandstone (FA 1b, Fig. 4N). The infilling marine deposits (FA 3a) overlapping relationship to the trough indicates that the uppermost earthy facies of the Entrada Sandstone, consisting of siltstone and very fine-grained sandstone strata, sagged prior to the deposition of the lower Curtis. Note that the Entrada Sandstone strata partially retained their physical integrity both on the mini-sag margins, and across the deformed zone, as individual hydroplastically deformed strata can be correlated through it. The triggering mechanism for such hydroplastic mini-sag basins remains open for discussion.

Deformation-related relief – loading

The J-3 Unconformity was also directly impacted by soft-sediment deformation processes, which include hydroplastic sagging of the earthy facies substratum (FA 1b, Fig. 4N), but also sedimentary loading of Curtis Formation beach to upper shoreface deposits (FA 2) onto the underlying earthy facies of the Entrada Sandstone (Fig. 4O), notably visible at Sven's Gulch (Fig. 2). Note that this location also displays cut-and-fill structures. The resulting J-3 Unconformity is irregular, with a dm-scale relief. Sedimentary loading requires a rapid deposition of liquidised sediments over a poorly consolidated substratum of contrasting density (e.g. Owen, 2003; Oliveira *et al.* 2011).

Spatio-temporal complexity of the J-3 Unconformity

The nature of the J-3 Unconformity relief is classified in two categories; erosion- and deformation-related relief. Angular unconformities, paraconformities, undulating surfaces, steep incisions, and irregular relief are interpreted to have been generated by erosive processes, such as aeolian

deflation, superficial incision linked to flash floods, tidal ravinement during transgression, and tidal currents funnelling as the sea regressed. Deformation-related processes are responsible for the development of ring-fault collapsed structures, hydroplastic mini-sags, and loading structures.

The spatial distribution of the J-3 Unconformity relief does not seem to reflect any specific or predictable pattern (Fig. 5A, B). Nevertheless, the northern part of the study area generally displays a greater vertical relief, with a maximum of *ca.* 23 m at Cedar Mountain (Fig. 4K), and diminishing southward. East of the study area, where the Entrada Sandstone's Slick Rock Member is directly overlain by the Curtis Formation, the J-3 Unconformity is, in its majority, an aeolian deflated paraconformity (*sensu* Mountney, 2012). However, the top of the earthy facies is characterised by a more variable relief, both in terms of geometry, and processes involved in the shaping of the unconformity, than the Slick Rock Member, as testified by the presence of steep tidal incisions, undulating relief, irregular relief impacted by tidal ravinement, sedimentary loading, hydroplastic sagging, and circular collapse, together with flat angular unconformities and paraconformities.

The fact that some of the deformation-related features in the J-3 Unconformity are only recorded at one specific locality, notably the hydroplastic mini-sag at Cedar Mountain, the loading structures at Sven's Gulch or the ring-fault collapsed cluster north of Hanksville Airport, makes it difficult to explain each of these singular behaviours by one single and exclusive factor. These would include uniform changes in mechanical properties of the earthy facies strata, or regional triggers such as earthquakes, among others. Since the earthy facies strata are laterally extensive and internally homogeneous, any overall change in their structural strength, for instance due to oscillating water saturation conditions (Assallay *et al.*, 1997; Li *et al.*, 2016), or any regional triggering mechanism, such as earthquakes linked to activity of large tectonic structures, are expected to impact the metastable sediments similarly at more than one location in both space and time, rather than generating location-specific deformation types. Thus, a more spatially restricted process to these localised structural deformations is required, which triggering factor(s) remain yet to be precisely identified. Furthermore, it seems that not only these three deformational events occurred at different locations, but also at different depths relatively to one-another. At Cedar Mountain, the infill of the hydroplastic mini-sag passively infilled the negative relief, which implies that the sagging geometry represented a paleo-ground, doline-like trough. The loading structures observed at Sven's Gulch developed at near-surface depth, once the lowermost Curtis Formation strata were deposited. The ring-fault collapsed system north of Hanksville Airport was generated at greater depth than the hydroplastic mini-sag and Sven's Gulch loading structures, as the overlying Curtis Formation in its entirety is distorted. However, since the capping Summerville Formation shows no evidence of deformation, these ring-fault collapsed structures must have developed at depth equalling the Curtis Formation thickness in the vicinity of Hanksville Airport. Despite these differences, each of these three geometric expressions of deformation-related unconformity relief requires a non- to poorly consolidated underlying earthy facies in order to develop.

The complexity of the unconformity increases as a temporal dimension is added to the correlation of all these different processes, as well as their respective duration (Fig. 5C, Fig. 6), not only at each specific locality, but at a more sub-regional to regional scale. Any regional correlation (Fig. 6), is limited by the lack of absolute dating, the absence of a regional marker bed in the Entrada Sandstone,

and the heterolithic nature of the Curtis Formation (Zuchuat *et al.*, 2018). Therefore, only a relative timing of different processes and events can be established (Fig. 5C, and Fig. 6). This timing shows that the different erosional and deformational processes involved in shaping the J-3 Unconformity overlapped both in time, and space, highlighting the composite nature of the surface. Fig. 5C and Fig. 6 illustrate the relative timing relationship between each of these processes affecting the J-3 Unconformity (i) before the Curtis Sea lower transgression, (ii) after the Curtis Sea lower transgression (t1, Fig. 5, Fig. 6), accompanied by the lower Curtis deposition, and (ii) after the Major Transgression occurred (t2, Fig. 5, Fig. 6) (Zuchuat *et al.*, 2018), marking the onset of the middle Curtis unit. For example, as aeolian deflation was shaping the unflooded J-3 Unconformity on a regional- to sub-regional scale (Fig. 6A, D, F, K, Q, R), flash floods reworked the J-3 locally (Fig. 6L) and punctually. Simultaneously, tidal ravinement (Fig. 6G), and loading (Fig. 6B) might have been impacting the J-3 Unconformity where the Curtis Sea had already flooded the Entrada Sandstone. As such, tidal reworking of the J-3 surface was a time-dependant process, as its impact varied whether the system was undergoing a transgression or a regression: localised, steep, and narrow incisions occurred during short-lived regressive phases as currents were funnelled (Fig. 6C), contrasting with the widespread irregular relief generated by transgressive tidal ravinement (Fig. 6H). Nevertheless, despite the limited impact of short-lived regressions cutting into the underlying semi-consolidated Entrada Sandstone's earthy facies substratum, subsequent relative base level falls were accompanied by significant reworking within the Curtis Formation, as notably visible at Sven's Gulch (Fig. 4E). Here, sub-tidal channels (FA 4b) extensively eroded more than 5 m into the underlying FA 3a, and FA 3b deposits (see Fig. 4C, D, E in Zuchuat *et al.* 2018).

Contrasting with the potential synchronicity of aeolian deflation and tidal ravinement, hydroplastic sagging and sedimentary loading correspond to a fixed point in time, pre-transgression and post-transgression, respectively. However, it is impossible to exclude the possibility of hydroplastic sagging developing in a post-transgression context. Also, similarities exist between the underlying tidally-influenced beach to upper shoreface deposits (FA 2) and the overlying subtidal channel-dune-flat complex (FA 5), notably in terms of grain size and rapid settling time. However, the spatio-temporal uniqueness of sedimentary loading below FA 2 and the lack of thereof at the base of FA 5 imply a relative hardening of the substratum between the deposition of the two units.

Not only can various processes occur at the same time, but also one process can have different impact on the J-3 Unconformity at the same time. The flat and extensive paraconformity(ies), capping both the earthy facies and the Slick Rock Member, is mostly associated with aeolian deflation (Fig. 4B, Fig. 5, Fig. 6, see also Fig. 10A in Zuchuat *et al.*, 2018). However, where pre-existing relief existed (Shadscale Mesa, Hanksville Airport, Fig. 2, Fig. 6E, F), aeolian deflation was only able to smoothen the relief, but never to flatten it entirely. This could be explained by an enhanced cohesion within the exposed sediments due to a high degree of saturation (Mountney, 2006; Mountney, 2012). On the other hand, as aeolian deflation could only smoothen but not flatten a pre-existing relief on its own, and since the transgression accompanying the middle Curtis deposition eroded the underlying uplifted lower Curtis at an angle (Zuchuat *et al.*, 2018) (t2, Fig. 6J). Thus, it is thought that flat angular unconformities separating the Entrada Sandstone from the middle Curtis were most likely created by

tidal ravinement forces during the Major Transgression, whereas aeolian deflation might have just played a minor role in the development of such a geometry prior to the transgression.

Nevertheless, the relief generated by the Major Transgression, which defines the base of the middle Curtis, is non-unique (*sensu* Burgess and Prince, 2015), as it corresponds to a flat angular unconformity (Fig. 7, see also Fig. 7 in Wheatley *et al.*, 2016), a paraconformity (Fig. 4A, 4C, Fig. 6, Fig. 7, see also Zuchuat *et al.*, 2018), or it displays an irregular erosive geometry (Fig. 4H, I, J, Fig. 7). The latter occurs only where the earthy facies crops out (Fig. 4H, I, J), whereas the flat angular unconformity and the paraconformity are facies-independent, as they cap both the earthy facies and the Slick Rock Member (Fig. 4C, Fig. 6, Fig. 7, see Fig. 7 in Wheatley *et al.*, 2016, and Fig. 10a in Zuchuat *et al.*, 2018). It is hard to explain why a uniform, and widespread earthy facies was impacted differently by a transgression which deposited an extensive, and relatively homogeneous sandstone (FA 5) in comparison with underlying sedimentary units, other than by invoking the intrinsically complex spatial energy distribution within a tide-dominated basin (Kvale, 2012; Wang, 2012; references therein). Such a random yet inherent spatial dispersion of erosive forces, as observed along the J-3 Unconformity, is, however, paradoxical with the homogeneous grain-size, and bedforms distribution which characterise FA 5 sandstone. The system's complexity rises even more when the Slick Rock Member is considered (Fig. 7), suggesting that the type of unconformity, the type of relief, as well as the processes accompanying the Major Transgression are all facies-independent.

As a summary, the composite nature of the J-3 Unconformity can be relatively easily described in terms of processes involved in the shaping of the bounding surface for each individual locality. The complexity rises when considering its spatial and temporal variability, and when attempting to correlate the same contact in multiple localities. This is notably due to the apparent randomness the spatio-temporal distribution of erosive forces and local deformational trigger mechanisms, and the limited chrono- and lithostratigraphic correlation constraints across the study area. The J-3 Unconformity is therefore not one single unconformity, but the amalgamation of several sub-seismic erosive and deformation surfaces.

This study demonstrates that a detailed work is required to adequately assess the true, heterochronous, and polygenetic nature of such bounding surfaces. Considering unconformities as the sole product of relative base level fall is reducing, and incomplete. Despite their unveiled intrinsic complexity and the potential correlation constraints they may carry, the high density and high value of information they recorded will improve a basin's dynamic history, in terms, notably, of the spatio-temporal distribution of different erosive and deformational processes, and the subsequent system's sedimentary response(s). Akin Rameil *et al.*'s (2012), who showed how short-lived transgressive-regressive cycles impacted on the development of "discontinuity surfaces" on a Cretaceous carbonate platform, the J-3 Unconformity exposes, notably, the intricate imprint that similar relative base level changes have on the development of such bounding surfaces. The study of the J-3 Unconformity highlights how the understanding of transitional zones and their correlative sedimentary basins can be improved by conducting such detailed research. This positive outcome brought by recognising the polygenetic, and amalgamated nature of unconformities is independent from the basinal setting in which, and the scale at which scientists are working. This was similarly illustrated by Sattler *et al.*

(2005), who demonstrated the spatio-temporal intricacy of processes involved in the shaping of “discontinuity surfaces” on carbonate platforms; by Al-Hinaai and Redfern (2014), who showed how the Knox Unconformity’s relief influenced that spatial distribution of “postunconformity carbonates” in a passive- to convergent-margin transition; or by Leszczyński and Nemeč (2014), who demonstrated how much information peripheral unconformities can record, and how valuable and complementary this information can be to the study of the sedimentary succession.

DISCUSSION

The J-3 Unconformity as a time barrier and a sequence boundary

The complexity of the J-3 Unconformity requires the results of this study to be placed in a broader conceptual context, in order to answer the following questions: (i) is such an intricate bounding surface an actual unconformity, and hence, a genuine time barrier, and (ii) can such a composite surface be applied as a sequence boundary?

The definition of an unconformity requires the surface considered to be erosive or non-depositional, separating younger strata above from older deposits below, thus representing a “significant hiatus” (Mitchum *et al.*, 1977). It is consequently regarded as effective time barriers. However, when studying depositional systems in their entirety, it becomes clear that regional surfaces often categorized as unconformities are not the result of one single bypass or erosive event, but the result of a very intricate amalgamation of spatially heterogeneous episodes of erosion-transport-deposition (Holbrook and Bhattacharya, 2012; Blum *et al.*, 2013; Hodgson *et al.*, 2016; Miall, 2016; Gani, 2017). The composite nature of such surfaces resides both in the variety of processes and time-dimensions involved in the intricate erosion-bypass-deposition history of these systems, and they are therefore time transgressive or diachronous, as they do not strictly separate the same older deposits below from younger deposits above everywhere (Holbrook and Bhattacharya, 2012; Blum *et al.*, 2013; Hodgson *et al.*, 2016; Gani, 2017). This work demonstrates that the J-3 Unconformity, developed within aeolian to shallow marine transitional setting, is a highly multichronous surface, as it was impacted by several processes acting at different times of its composite history. The J-3 Unconformity shows resemblances with other diachronous bounding surfaces, such as Holbrook and Bhattacharya’s (2012) Regional Composite Scour, which are the product of multiple episodes of incision-transport-deposition within a fluvio-deltaic system, or Hodgson *et al.*’s (2016) “diachronous lithological basal surface” in deep-water systems.

Fig. 8 considers a hypothetical, low-gradient, transitional depositional model, consisting of a tidally-influenced domain juxtaposing an active aeolian system. In order to assess the use of the unconformity’s definition (Mitchum *et al.*, 1977) in a context similar to the J-3 Unconformity environment, this basin is assumed to undergo a progressive climatic change towards a more humid period, a constant rate of relative sea level rise, and fed by a steady sediment supply. On a basin scale, these two systems coexist, and sediments are being eroded, transported and deposited in both of them simultaneously. As climatic conditions change and relative base level rises, the sediment

budget diminishes, forcing the aeolian system to adapt to the new conditions, by decreasing its bedform size, sometimes cannibalising itself as it migrates towards a more suitable depocentre (Kocurek, 1988; Crabaugh and Kocurek, 1993; Carr-Crabaugh and Kocurek, 1998; Mountney, 2012; Mountney, 2006; Rodríguez-López *et al.*, 2013). When considering a relatively local area in comparison to the entire basin, this adaptation can be translated into the aeolian system being locally terminated, potentially truncated by a deflation and/or ravinement surface, and unconformably overlain by tide-dominated deposits. However, as discussed by Gani (2017), when the entire basin is taken into account, a particular depositional system can migrate, morph, and adapt to the new climato-sedimentary conditions, concurrently to the other(s) system(s) development. This indicates that two evolving and developing depositional systems, marine (tidally-influenced) and terrestrial (aeolian), can coexist during a relative sea level rise, and be separated by a transgressive and/or a ravinement surface, which does not necessarily act as a time barrier (Fig. 8). These conditions are similar to what has been observed on continental shelves by Nummedal *et al.* (1987), Martinsen & Helland-Hansen (1995), and Helland-Hansen and Martinsen (1996). Such a simplistic two-dimensional model does not, however, account for the real three-dimensional and temporal variations of the rate of relative sea level rise, sediment supply, orbital forcing, and differential regression, among other factors. These cannot only impact the system at different places at different time, but also at different scales (Miall, 2016; Gani, 2017). Nevertheless, if the time-transgressive nature of such bounding surfaces can be shown on a simplistic 2D model, this property will only be enhanced when the system is studied in 3D (Martinsen and Helland-Hansen, 1995), and 4D (Burgess and Prince, 2015; Madof *et al.*, 2016; Miall, 2016; Gani, 2017).

This work demonstrates that most regional composite bounding surfaces are not unconformities *sensu stricto*. Despite the lack of a precise and well-defined nomenclature, such composite surfaces still encapsulate meaningful information regarding basin development, especially in terms of process identifications and interactions. Therefore, and because revisited definitions would never be able to encompass the entire complexity of any depositional system, authors do not appeal for such a renewed definition, but insist on the careful consideration of similar composite surfaces when studying a sedimentary basin history, while being aware of the limitations of such a scientific approach.

Implications of heterochronous and polygenetic unconformities

Subsurface analyses suffer a relative scarcity of available data, as well as a resolution limitation, in comparison with field-based studies. However, such constraints can be partially counteracted if unconformities are not regarded as monogenetic and isochronous surfaces anymore, but rather considered as sub-seismic (i) non-unique, (ii) polygenetic, and (iii) heterochronous features.

Burgess and Prince (2015) discussed in great detail the significance of non-unique stratal geometries, as well as the importance of considering several models to assess their stratigraphic signature, instead of using a singular sequence stratigraphic framework. A certain geometry and/or relief can be generated by different processes. For example, the J-3 as paraconformity was impacted partially by both aeolian deflation, and tidal ravinement; the concave-up J-3 surface could have been generated by hydroplastic sagging, or tidal incision. Further, Burgess and Prince's (2015) non-uniqueness

concept can be extended to encompass the various impacts that a single process can make on a given system. For instance, as the Major Transgression at the base of the middle Curtis occurred, tidal ravinement forces generated a range of reliefs as it merged with the J-3 Unconformity, which can be classified as angular unconformity, paraconformity, and a disconformity (Fig. 7). Hence, as a certain type of geometry can be attributed to several processes, and as one single process can generate multiple types of relief. Future works on regional unconformities are therefore required to carefully consider this before proposing unique interpretations, especially when analysing strata contacts based solely on geometrical attributes at one single location.

However, the non-unique character of several surfaces can sometimes lead to chronostratigraphic challenges. This is because some of the resulting unconformity geometries could have been equally generated by singular and time-dependant processes, such as syn-regression steep and narrow tidal incision, product of tidal currents being funnelled and erosive as available accommodation diminished. In the case of the J-3 Unconformity, however, this resulting concave-up geometry could have been potentially confounded with pre-transgressional hydroplastic mini-sags, leading to a significantly different basin dynamic history interpretation. Furthermore, even if the correct process was assumed (here, a syn-regression steep and narrow tidal incision), this might still not necessarily imply that the correct time-frame is considered. Due to the low-gradient basinal setting, minor changes in available accommodation would have been amplified, and significantly moved the facies and processes belt in a 3D space (Midtkandal and Nystuen, 2009; Zuchuat *et al.*, 2018). Therefore, it is imperative to assess whether such an incision was a “basal” incision, or if it also cannibalised its intraformational substratum. Indeed, if the geometry was caused by a “basal” incision, then the depression’s sedimentary (sealing or permeable) infill was laterally extended, and connected to the adjacent sedimentary bodies. If the incision also cannibalised its intraformational substratum, then the underlying sedimentary bodies will be disconnected from each other. The positive or negative impact of connected and laterally extensive-, or compartmented sedimentary bodies on the system depends (i) on the (sealing or permeable) nature of the infill and the underlying substratum, as well as (ii) the purpose(s) the system is considered for. The timing of these two *scenarii*, and the timespan existing between them, could also imply a differential diagenetic imprint over the system. As a result, before attributing any chronostratigraphic character to the resulting bounding surface, it must be correctly deconstructed, both regarding its polygenetic nature, as well as its heterochronous history.

However, even though this work demonstrates the intrinsic composite and time-transgressive nature of bounding surfaces, which isn’t conform to the definition of an unconformity, the scale at, and the purpose for which a system is studied dictate whether the polygenetic and heterochronous nature of considered boundaries is playing a potential important role, or if it can consciously be disregarded without major implications for the proposed basin model, and thus, independently of the amount of available data. For example, surfaces such as Kyrkjebø *et al.*’s (2004) North Sea Unconformity Complex (Fig. 1) are to be rigorously considered and assessed by scientists studying the high-resolution dynamic history of a regional basin, or by geologists appraising reservoir quality and seal integrity of petroleum/CO₂ plays occurring directly underneath it, or in its close vicinity. On the contrary, targets located at shallower depth than such a composite bounding surface (or potentially deep below it), can, most probably, disregard the complexity of it for their reservoir models. If stratal

bounding surfaces are overlooked and/or misinterpreted, especially in low-gradient, transitional settings, this might lead to over- or underestimation of sediment delivery/storage in the system, as well as erroneous basin dynamic models and reservoir predictions.

CONCLUSION

- Eight types of relief occur along the J-3 Unconformity, separating the Entrada Sandstone from the Curtis Formation in east-central Utah: (i) angular unconformity, (ii) paraconformity, (iii) steep incisions, (iv) undulating relief, (v) irregular relief, including fault-plane- and erosion-related relief irregularities, (vi) circular collapsed structures, (vii) sedimentary loading, and (viii) hydroplastic sagging.
- Angular unconformities, paraconformities, undulating surfaces, steep incisions, and irregular relief are the product of erosive processes, which includes aeolian deflation, superficial incision linked to flash floods, tidal ravinement during transgressive phases, and funnelling of the tidal forces as the sea regressed. Deformation-related processes are responsible for the development of ring-fault collapsed structures, hydroplastic mini-sags, as well as loading structures.
- The development of the J-3 Unconformity has to be considered within a four-dimensional frame, in which each individual parameter interacted with the bounding surface both through space and time. The impact of a single process in the J-3 Unconformity is spatio-temporally non-unique. Therefore, the composite and highly polychronous nature of such a surface implies it cannot be regarded as a genuine time barrier, and thus, as an unconformity *sensu stricto*.
- The concept of diachronous ravinement surface can be extended from the shelf into a transitional basinal setting between continental aeolian and shallow marine deposits. Future studies of these transitional settings, both outcrop and subsurface, should therefore be aware of the composite nature of such bounding surfaces, and be careful when giving them a clear chronostratigraphic character.
- However, even though this work demonstrates that several contacts described as unconformities might be in fact composite and time-transgressive surfaces, their use in basin reconstructions might still work depending on the research focus and the scale of the studies. In these cases, accurate dating would dictate whether the heterochronous nature of the considered boundary can be consciously disregarded without major implications for both timing and prediction of sediment delivery and storage in basin evolution models.

Acknowledgements

The authors of this paper would like to thank the Norwegian Research Council for their awarded COPASS grant 244049. Acknowledgements are to be extended to Dr Mark Mulrooney, Anna v. Yperen, Arve Sleveland, and Ole Rabbel for their assistance and fruitful comments, which enhanced the quality of this work. Reviewers 1 and 2 are to be sincerely acknowledged for their constructive observations and remarks.

REFERENCES

- Al-Hinaai, J., and Redfern, J. (2014). The late Carboniferous basal Grant Group unconformity, Canning Basin, Australia: a complex surface recording glacial tectonic and halotectonic processes. *Australian Journal of Earth Sciences*, 61(5), 703-717.
- Anderson, T.H. (2015). Jurassic (170–150 Ma) basins: The tracks of a continental-scale fault, the Mexico-Alaska megashear, from the Gulf of Mexico to Alaska. *In: Anderson, T.H., Didenko, A.N., Johnson, C.L., Khanchuk, A.I., and MacDonald, J.H., (eds.), Late Jurassic Margin of Laurasia – A Record of Faulting Accommodating Plate Rotation: Geological Society of America Special Papers*, 513, 107-188.
- Anderson, O.J. and Lucas, S.G. (1994). Middle Jurassic stratigraphy, sedimentation and paleogeography in the southern Colorado Plateau and southern High Plains. *In: Caputo, M.V., Peterson, J.A. and Franczyk, K.J., (eds.), Mesozoic Systems of the Rocky Mountain Region, USA. The Rocky Mountain Section SEPM (Society for Sedimentary Geology)*, Denver, 299-314.
- Assallay, A.M., Rogers, C.D.F., and Smalley, I.J. (1997). Formation and collapse of metastable particle packings and open structures in loess deposits. *Engineering Geology*, 48(1-2), 101-115.
- Bjerrum, C.J. and Dorsey, R.J. (1995) Tectonic controls on deposition of Middle Jurassic strata in a retroarc foreland basin, Utah-Idaho trough, western interior, United States. *Tectonics*, 14(4), 962-978.
- Blakey, R.C. (1994). Paleogeographic and tectonic controls on some Lower and Middle Jurassic erg deposits, Colorado Plateau. *In: Caputo, M.V., Peterson, J.A. and Franczyk, K.J., (eds.), Mesozoic Systems of the Rocky Mountain Region, USA. The Rocky Mountain Section SEPM (Society for Sedimentary Geology)*, Denver, 273-298.
- Blakey, R.C. (2008). Pennsylvanian–Jurassic sedimentary basins of the Colorado Plateau and southern Rocky Mountains. *Sedimentary Basins of the World*, 5, 245-296.
- Blum, M., Martin, J., Milliken, K., and Garvin, M. (2013). Paleovalley systems: insights from Quaternary analogs and experiments. *Earth-Science Reviews*, 116, 128-169.
- Bonaventura, X., Sima, A.A., Feixas, M., Buckley, S.J., Sbert, M., and Howell, J.A. (2017). Information measures for terrain visualization. *Computers & Geosciences*, 99, 9-18.
- Brenner, R.L. and Peterson, J.A. (1994). Jurassic sedimentary history of the northern portion of the Western Interior Seaway, USA. *In: Caputo, M.V., Peterson, J.A. and Franczyk, K.J., (eds.), Mesozoic Systems of the Rocky Mountain Region, USA. The Rocky Mountain Section SEPM (Society for Sedimentary Geology)*, Denver, 233-272.
- Buckley, S., Ringdal, K., Dolva, B., Naumann, N., and Kurz, T. (2017). LIME: 3D visualisation and interpretation of virtual geoscience models. *EGU General Assembly Conference Abstracts*, 19, p. 15952.
- Bump, A.P. and Davis, G.H. (2003). Late Cretaceous – early Tertiary Laramide deformation of the northern Colorado Plateau, Utah and Colorado. *Journal of Structural Geology*, 25(3), 421-440.
- Burgess, P.M. and Prince, G.D. (2015). Non-unique stratal geometries: implications for sequence stratigraphic interpretations. *Basin Research*, 27(3), 351-365.

- Campbell, M.R., Butts, C., Arnold, R., Fenneman, N.M., Gale, H.S., Lee, W.T., Schrader, F.C., Phalen, W.C., Ashley, G.H., Peck, F.B., Richardson, G.B., Taff, J.A., Darton, N.H., Fisher, C.A., Leonard, A.G., and Veatch, A.C. (1906). Contributions to economic geology, 1905: Coal, Lignite, and Peat, *U.S. Geological Survey, Bulletin*, 285-F, 203-356.
- Caputo, M.V. and Pryor, W.A. (1991). Middle Jurassic tide- and wave-influenced coastal facies and paleogeography, upper San Rafael Group, east-central Utah. *Utah Geological Association*, 19, 9-27.
- Carr-Crabaugh, M. and Kocurek, G. (1998). Continental sequence stratigraphy of a wet eolian system: a key to relative sea-level change. *Society for Sedimentary Geology, Special Publication*, 59, 213-228.
- Davis Jr, R.A. and Dalrymple, R.W., (eds.), (2011). *Principles of tidal sedimentology*. Springer Science & Business Media
- Demko, T.M., Currie, B.S., and Nicoll, K.A. (2004). Regional paleoclimatic and stratigraphic implications of paleosols and fluvial/overbank architecture in the Morrison Formation (Upper Jurassic), Western Interior, USA. *Sedimentary Geology*, 167(3), 115-135.
- Doelling, H.H. (2001). *Geologic map of the Moab and eastern part of the San Rafael Desert 30' x 60' quadrangles, Grand and Emery Counties, Utah, and Mesa County, Colorado*. Utah Geological Survey Map 180, 3 plates, scale 1:100,000.
- Doelling, H.H., Kuehne, P.A., Willis, G.C., and Ehler, J.B. (2015). *Geologic map of the San Rafael Desert 30' x 60' quadrangle, Emery and Grand Counties, Utah*. Utah Geological Survey, Map 267DM, scale 1:62,500.
- Emmons, S.F., Cross, W., and Eldridge, G.H. (1896). Geology of the Denver basin in Colorado. *U.S. Geological Survey, Monographs*, 27, 1-660.
- Eschner, T.B. and Kocurek, G. (1988). Origins of relief along contacts between eolian sandstones and overlying marine strata. *AAPG Bulletin*, 72(8), 932-943.
- Gilluly, J. and Reeside Jr., J.B. (1928). Sedimentary rocks of the San Rafael Swell and some adjacent areas in eastern Utah. *U.S. Geological Survey, Professional Paper*, 150-D, 61-110.
- Gudmundsson, A. (2007). Conceptual and numerical models of ring-fault formation. *Journal of Volcanology and Geothermal Research*, 164(3), 142-160.
- Helland-Hansen, W. and Martinsen, O.J. (1996). Shoreline trajectories and sequences; description of variable depositional-dip scenarios. *Journal of Sedimentary Research*, 66(4), 670-688.
- Heyman, O., (1983). Distribution and structural geometry of faults and folds along the northwestern Uncompahgre Uplift, western Colorado and eastern Utah. In: Averett, W., (eds.), *Northern Paradox Basin-Uncompahgre Uplift*. Grand Junction Geological Society, Grand Junction, Colorado, 45-57.
- Hintze, L.F. (1980). *Geologic map of Utah*. Utah Geological and Mineral Survey, scale 1:250,000, 2 sheets.
- Hintze, L.F. and Kowallis, B.J. (2009). *Geologic history of Utah*. Provo, Utah, Brigham Young University Studies. 225 pp.
- Hodgson, D.M., Kane, I.A., Flint, S.S., Brunt, R.L., and Ortiz-Karpf, A. (2016). Time-transgressive confinement on the slope and the progradation of basin-floor fans: Implications for the sequence stratigraphy of deep-water deposits. *Journal of Sedimentary Research*, 86(1), 73-86.

- Holbrook, J.M. and Bhattacharya, J.P. (2012). Reappraisal of the sequence boundary in time and space: case and considerations for an SU (subaerial unconformity) that is not a sediment bypass surface, a time barrier, or an unconformity. *Earth-Science Reviews*, 113(3-4), 271-302.
- Hutton, J. (1788). Theory of the Earth; or an Investigation of the Laws observable in the Composition, Dissolution, and Restoration of Land upon the Globe. *Earth and Environmental Science Transactions of The Royal Society of Edinburgh*, 1(2), 209-304.
- Kocurek, G. (1988). First-order and super bounding surfaces in eolian sequences—bounding surfaces revisited. *Sedimentary Geology*, 56(1-4), 193-206.
- Kocurek, G., Martindale, R.C., Day, M., Goudge, T.A., Kerans, C., Hassenruck-Gudipati, H.J., Mason, J., Cardenas, B.T., Petersen, E., Mohrig, D., Aylward, D.S., Hughes, C.M., and Nazworth, C.M. (in press). Antecedent aeolian dune topographic control on carbonate and evaporite facies: Middle Jurassic Todilto Member, Wanakah Formation, Ghost Ranch, New Mexico, USA. *Sedimentology*.
- Kreisa, R.D. and Moiola, R.J. (1986). Sigmoidal tidal bundles and other tide-generated sedimentary structures of the Curtis Formation, Utah. *Geological Society of America Bulletin*, 97(4), 381-387.
- Kvale, E.P. (2012). Tidal constituents of modern and ancient tidal rhythmites: criteria for recognition and analyses. In: Davis, R.A., Jr., and Dalrymple, R.W., (eds.), *Principles of Tidal Sedimentology*. Springer Science and Business Media, Dordrecht, Netherlands, 1-17.
- Kyrkjebø, R., Gabrielsen, R.H. and Faleide, J.I. (2004). Unconformities related to the Jurassic–Cretaceous synrift–post-rift transition of the northern North Sea. *Journal of the Geological Society*, 161(1), 1-17.
- Leszczyński, S., and Nemeč, W. (2015). Dynamic stratigraphy of composite peripheral unconformity in a foredeep basin. *Sedimentology*, 62(3), 645-680.
- Levander, A., Schmandt, B., Miller, M.S., Liu, K., Karlstrom, K.E., Crow, R.S., Lee, C.-T.A., and Humphreys, E.D. (2011). Continuing Colorado plateau uplift by delamination-style convective lithospheric downwelling. *Nature*, 472(7344), 461-465.
- Li, P., Vanapalli, S., and Li, T. (2016). Review of collapse triggering mechanism of collapsible soils due to wetting. *Journal of Rock Mechanics and Geotechnical Engineering*, 8(2), 256-274.
- Lucas, S.G., Hunt, A.P., and Spielmann, J. (2005). Jurassic stratigraphy in the Chama Basin, northern New Mexico: New Mexico Geological Society. *Guidebook*, 56, 182-192.
- Madof, A.S., Harris, A.D., and Connell, S.D. (2016). Nearshore along-strike variability: Is the concept of the systems tract unhinged?. *Geology*, 44(4), 315-318.
- Marti, J., Ablay, G.J., Redshaw, L.T., and Sparks, R.S.J. (1994). Experimental studies of collapse calderas. *Journal of the Geological Society*, 151(6), 919-929.
- Martinsen, O.J. and Helland-Hansen, W. (1995). Strike variability of clastic depositional systems: Does it matter for sequence-stratigraphic analysis?. *Geology*, 23(5), 439-442.
- Midtkandal, I., and Nystuen, J.P. (2009). Depositional architecture of a low-gradient ramp shelf in an epicontinental sea: the lower Cretaceous of Svalbard. *Basin Research*, 21(5), 655-675.
- Mountney, N.P. (2006). Periodic accumulation and destruction of aeolian erg sequences in the Permian Cedar Mesa Sandstone, White Canyon, southern Utah, USA. *Sedimentology*, 53(4), 789-823.

- Mountney, N.P. (2012). A stratigraphic model to account for complexity in aeolian dune and interdune successions. *Sedimentology*, 59(3), 964-989.
- Murray, K.E., Reiners, P.W., and Thomson, S.N. (2016). Rapid Pliocene–Pleistocene erosion of the central Colorado Plateau documented by apatite thermochronology from the Henry Mountains. *Geology*, 44(6), 483-486.
- Nelson, S.T. (1997). Reevaluation of the Central Colorado plateau laccoliths in the light of new age determination. *U.S. Geological Survey Bulletin*, 2158, 37-9.
- Nummedal, D. and Swift, D.J.P. (1987). Transgressive stratigraphy at sequence-bounding unconformities: Some principles derived from Holocene and Cretaceous examples *In: Nummedal, D., Pilkey, O.H., and Howard, J.D., (eds.), Sea-Level Fluctuation and Coastal Evolution*. SEPM Special Publication, 41, 241-260.
- Ogg, J.G., Ogg, G., and Gradstein, F M. (2016). *A Concise Geologic Time Scale: 2016*. Elsevier.
- Oliveira, C.M., Hodgson, D.M., and Flint, S.S. (2011). Distribution of soft-sediment deformation structures in clinoform successions of the Permian Ecca Group, Karoo Basin, South Africa. *Sedimentary Geology*, 235(3-4), 314-330.
- Owen, G. (2003). Load structures: gravity-driven sediment mobilization in the shallow subsurface. *Geological Society, London, Special Publications*, 216(1), 21-34.
- Peterson, F. (1994). Sand dunes, sabkhas, streams, and shallow seas: Jurassic paleogeography in the southern part of the Western Interior Basin. *In: Caputo, M.V., Peterson, J.A. and Franczyk, K.J., (eds.), Mesozoic Systems of the Rocky Mountain Region, USA*. The Rocky Mountain Section SEPM (Society for Sedimentary Geology), Denver, 233-272.
- Peterson, F. and Piringos, G.N. (1979). Stratigraphic relations of the Navajo Sandstone to Middle Jurassic formations, southern Utah and northern Arizona. *U.S. Geological Survey Professional Paper* 1035-B, 1-43.
- Piringos, G.N. and O'Sullivan, R.B. (1978). Principal unconformities in Triassic and Jurassic rocks, western interior United States: a preliminary survey. *U.S. Geological Survey, Professional Paper*, 1035-A, 1-29.
- Rameil, N., Immenhauser, A., Csoma, A.E., and Warrlich, G. (2012). Surfaces with a long history: the Aptian top Shu'aiba Formation unconformity, Sultanate of Oman. *Sedimentology*, 59(1), 212-248.
- Rodríguez-López, J.P., Meléndez, N., de Boer, P.L., Soria, A.R., and Liesa, C.L. (2013). Spatial variability of multi-controlled aeolian supersurfaces in central-erg and marine-erg-margin systems. *Aeolian Research*, 11, 141-154.
- Sattler, U., Immenhauser, A., Hillgärtner, H., and Esteban, M. (2005). Characterization, lateral variability and lateral extent of discontinuity surfaces on a carbonate platform (Barremian to Lower Aptian, Oman). *Sedimentology*, 52(2), 339-361.
- Shanmugam, G. (1988). Origin, recognition, and importance of erosional unconformities in sedimentary basins. *In: Kleinspehn, K.L. and Paola, C., (eds.), New perspectives in basin analysis*, Frontiers in Sedimentary Geology, Springer, New York, Springer, New York, 83-108.

- Skurtveit, E., Braathen, A., Larsen, E.B., Sauvin, G., Sundal, A., and Zuchuat, V. (2017). Pressure induced deformation and flow using CO₂ field analogues, Utah. *Energy Procedia*, 114, 3257-3266.
- Solum, J.G., Davatzes, N.C., and Lockner, D.A. (2010). Fault-related clay authigenesis along the Moab Fault: Implications for calculations of fault rock composition and mechanical and hydrologic fault zone properties. *Journal of Structural Geology*, 32(12), 1899-1911.
- Spieker, E.M. and Reeside, J.B. (1925). Cretaceous and tertiary formations of the Wasatch Plateau, Utah. *Geological Society of America Bulletin*, 36(3), 435-454.
- Sprinkel, D.A., Doelling, H.H., Kowallis, B.J., Waanders, G., and Kuehne, P.A. (2011). Early results of a study of Middle Jurassic strata in the Sevier fold and thrust belt, Utah. *In: Sprinkel, D.A., Yonkee, W.A., and Chidsey, T.C., Jr., (eds.), Sevier Thrust Belt: Northern and Central Utah and Adjacent Areas: Utah Geological Association, Publication*, 40, 151-172.
- Steno, N (1669). De solido intra solidum naturaliter contento dissertationis prodromus.
- Sullivan, K.R., Kowallis, B.J., and Mehnert, H.H. (1991). Isotopic ages of igneous intrusions in southeastern Utah – Evidence for a mid-Cenozoic Reno–San Juan magmatic zone. *Brigham Young University Geology Studies*, 37, 139-144.
- Thorman, C.H. (2011). The Elko orogeny – A major tectonic event in eastern Nevada–western Utah. *In: Sprinkel, D.A., Yonkee, W.A., and Chidsey, T.C., Jr., (eds.), Sevier Thrust Belt: Northern and Central Utah and Adjacent Areas: Utah Geological Association Publication*, 40, 117-129.
- Turner, C.E. and Peterson, F. (2004). Reconstruction of the Upper Jurassic Morrison Formation extinct ecosystem—a synthesis. *Sedimentary Geology*, 167(3), 309-355.
- Trudgill, B.D. (2011). Evolution of salt structures in the northern Paradox Basin: Controls on evaporite deposition, salt wall growth and supra-salt stratigraphic architecture. *Basin Research*, 23(2), 208-238.
- Van Wagoner, J.C. (1995). Sequence stratigraphy and marine to nonmarine facies architecture of foreland basin strata, Book Cliffs, Utah, USA. *In: Van Wagoner, J.C., Bertram, G.T., (eds.), Sequence Stratigraphy of Foreland Basin Deposits. American Association Petroleum Geologists Memoir*, 64, 137-223.
- Wang, P. (2012). Principles of Sediment Transport Applicable in Tidal Environments. *In: Davis, R.A., Jr., and Dalrymple, R.W., (eds.), Principles of Tidal Sedimentology*, Springer Science and Business Media, Dordrecht, Netherlands, 19-34.
- Westoby, M.J., Brasington, J., Glasser, N.F., Hambrey, M.J., and Reynolds, J.M. (2012). 'Structure-from-Motion' photogrammetry: A low-cost, effective tool for geoscience applications. *Geomorphology*, 179, 300-314.
- Wheatley, D.F., Chan, M.A., and Sprinkel, D.A. (2016). Clastic pipe characteristics and distributions throughout the Colorado Plateau: Implications for paleoenvironment and paleoseismic controls. *Sedimentary Geology*, 344, 20-33.
- Wilcox, W.T. and Currie, B. (2008). Sequence Stratigraphy of the Jurassic Curtis, Summerville, and Stump Formations, Eastern Utah and Northwest Colorado. *In: Longman, M.W. and Morgan, C.D., (eds.), Hydrocarbon Systems and Production in the Uinta Basin, Utah. Rocky Mountain Association of Geologists and Utah Geological Association Publication*, 37, 9-41.

Witkind, I.J. (1988). *Geologic map of the Huntington 30' X 60' quadrangle, Carbon, Emery, Grand, and Uintah Counties, Utah*. U.S. Geological Survey, Miscellaneous Investigations Series Map I-1764, scale 1:100,000.

Yang, Y.C., Zhou, J.W., Xu, F.G., and Xing, H.G. (2016). An experimental study on the water-induced strength reduction in Zigong argillaceous siltstone with different degree of weathering. *Advances in Materials Science and Engineering*, 1-12.

Yonkee, W.A. and Weil, A.B. (2015). Tectonic evolution of the Sevier and Laramide belts within the North American Cordillera orogenic system. *Earth-Science Reviews*, 150, 531-593.

Young, R.G. (1955). Sedimentary facies and intertonguing in the Upper Cretaceous of the Book Cliffs, Utah-Colorado. *Geological Society of America Bulletin*, 66(2), 177-202.

Zuchuat, V., Sleveland, A.R.N., Sprinkel, D.A., Rimkus, A., Braathen, A., and Midtkandal, I. (2018). New insights on the impact of tidal currents on a low-gradient, semi-enclosed, epicontinental basin—the Curtis Formation, east-central Utah, USA. *Geology of the Intermountain West*, 5, 131-165.

FIGURES

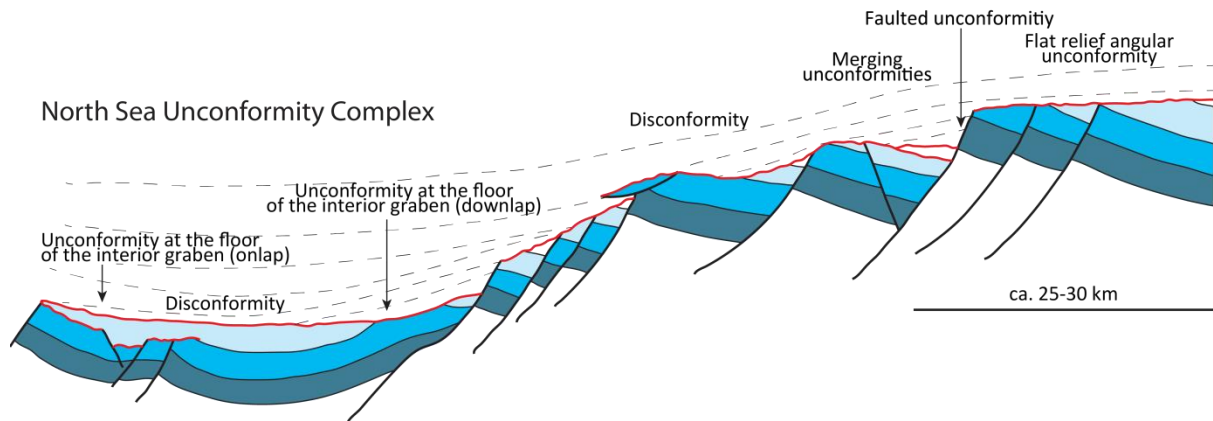


Fig. 1 – Scheme of the North Sea Unconformity Complex, illustrating the concept of regional composite unconformity (modified from Kyrkjebø *et al.*, 2004).

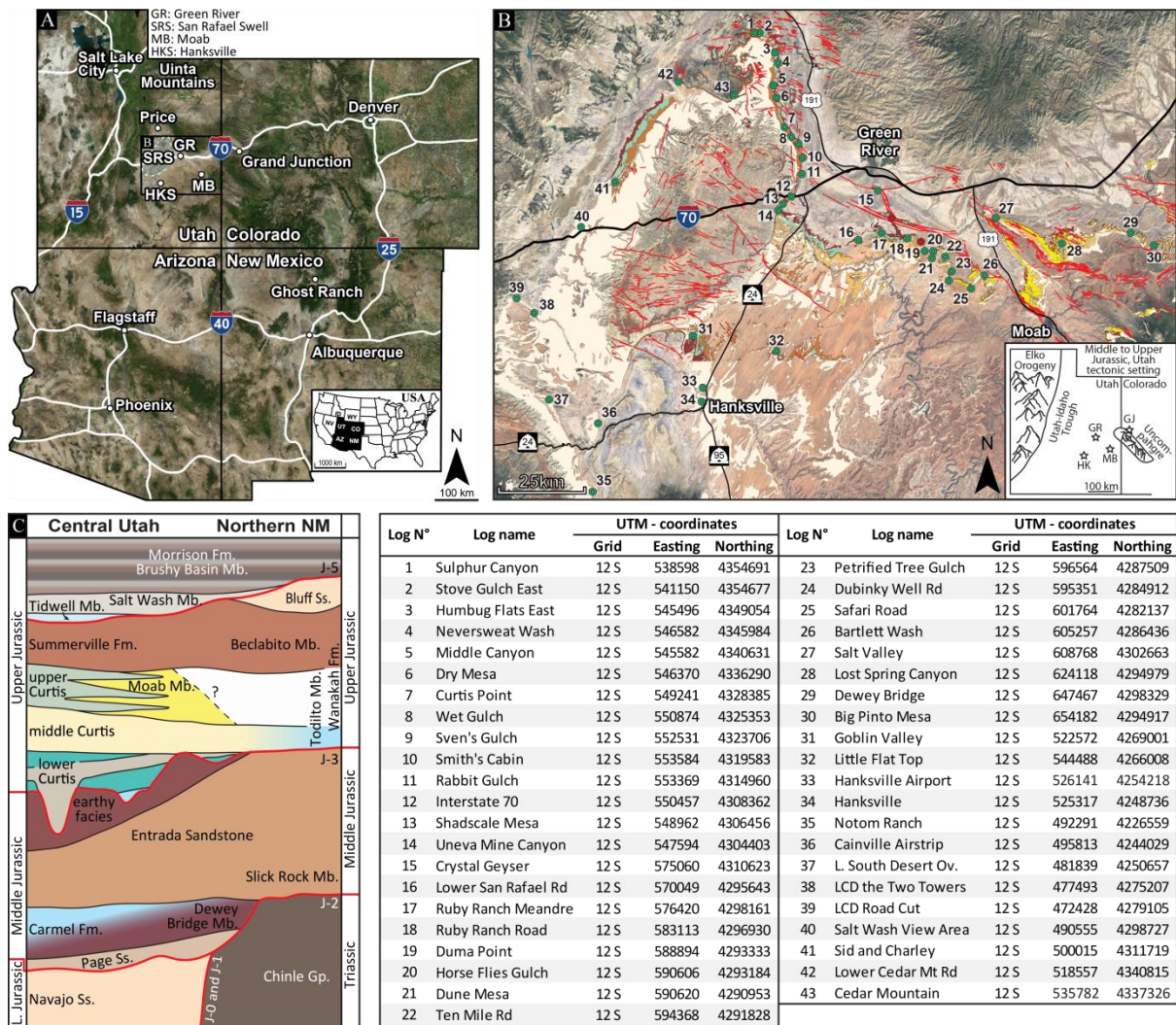


Fig. 2 – **A, B.** Maps of the study area. Green dots represent visited localities where the Curtis Formation crops out, while the red dots illustrate its absence. Each code number on the map refers to a specific locality in the attached table (Geological units after Hintze, 1980; Witkind, 1988; Doelling, 2001; and Doelling *et al.*, 2015) (Tectonic setting after Heyman, 1983; Thorman, 2011). **C.** Schematic stratigraphic column showing a correlation between the San Rafael Swell area, east-central Utah, and Ghost Ranch, in northern New Mexico (Doelling, 2001; Doelling *et al.*, 2015; Zuchuat *et al.*, 2018; Kocurek *et al.*, in press).

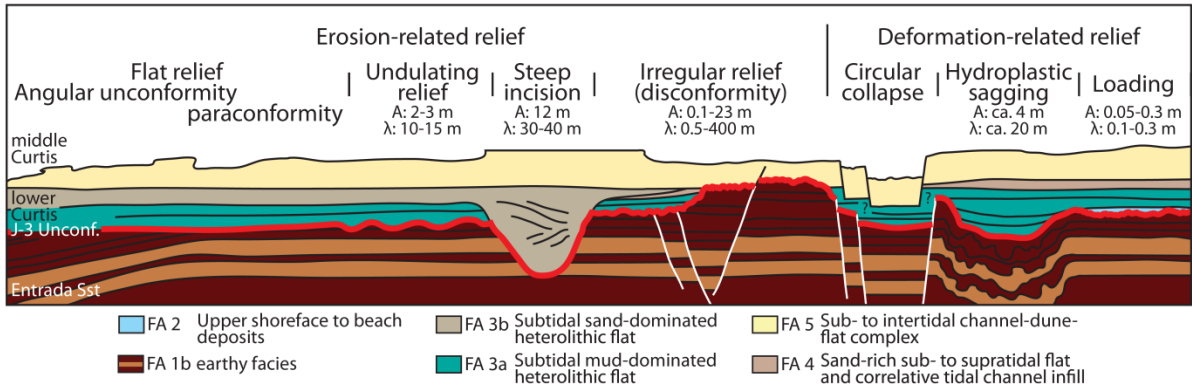


Fig. 3 – Diagram illustrating the five erosion-related, and the three deformation-related types of relief documented throughout the study area. The vertical- and horizontal scales are not representative of the reality.

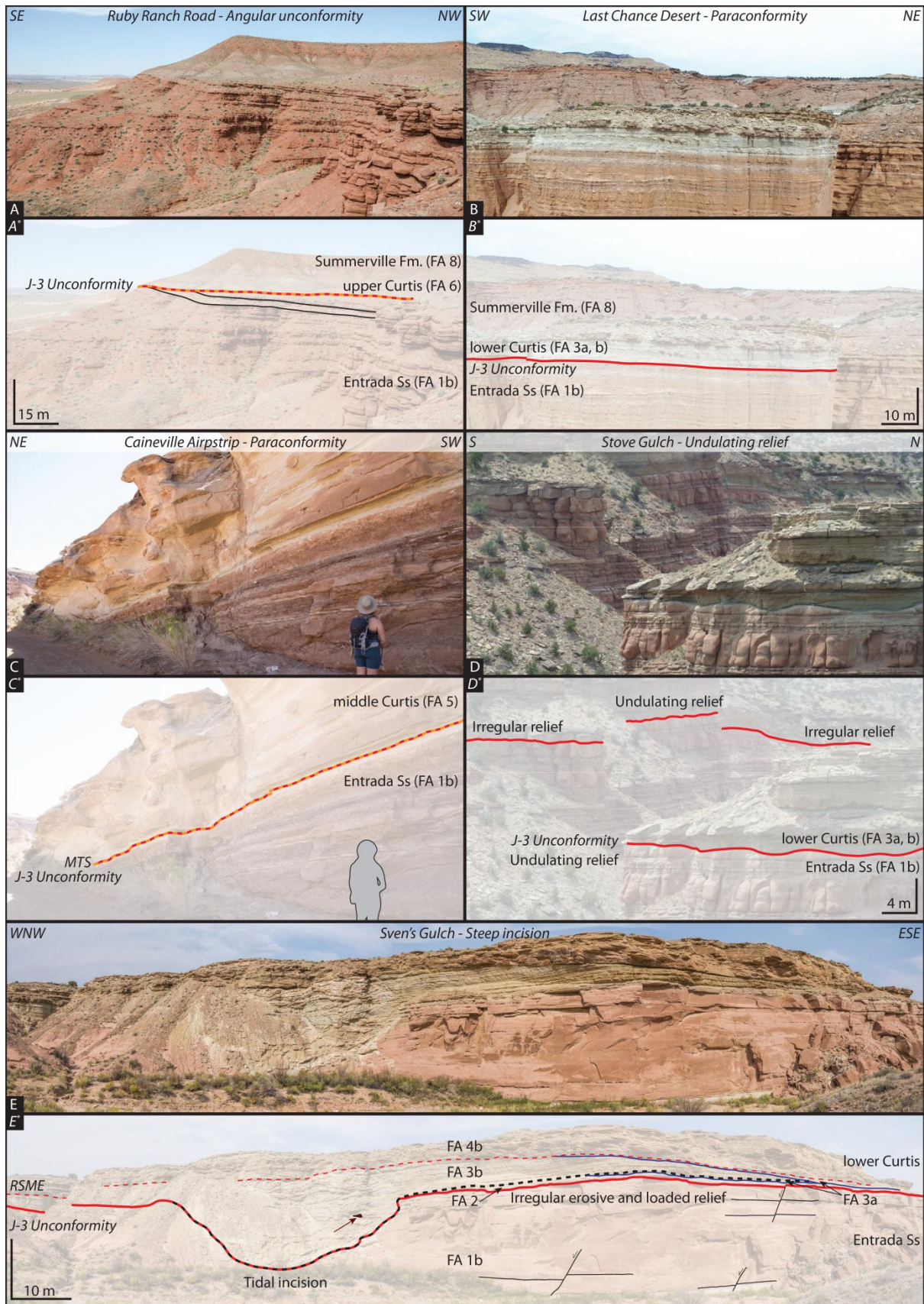


Fig. 4 – See legend on page 107.

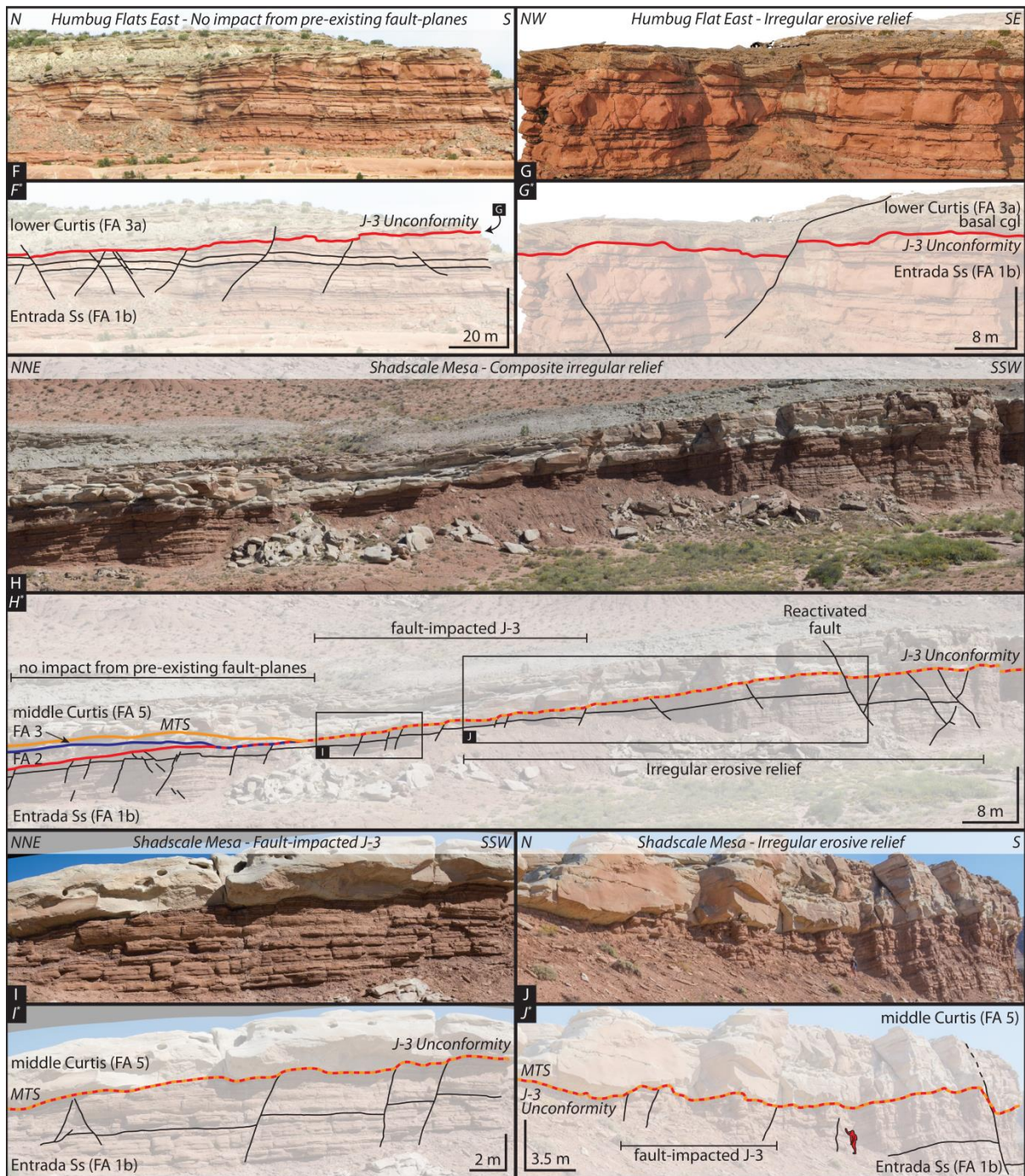


Fig. 4 (follow) – See legend on page 107.

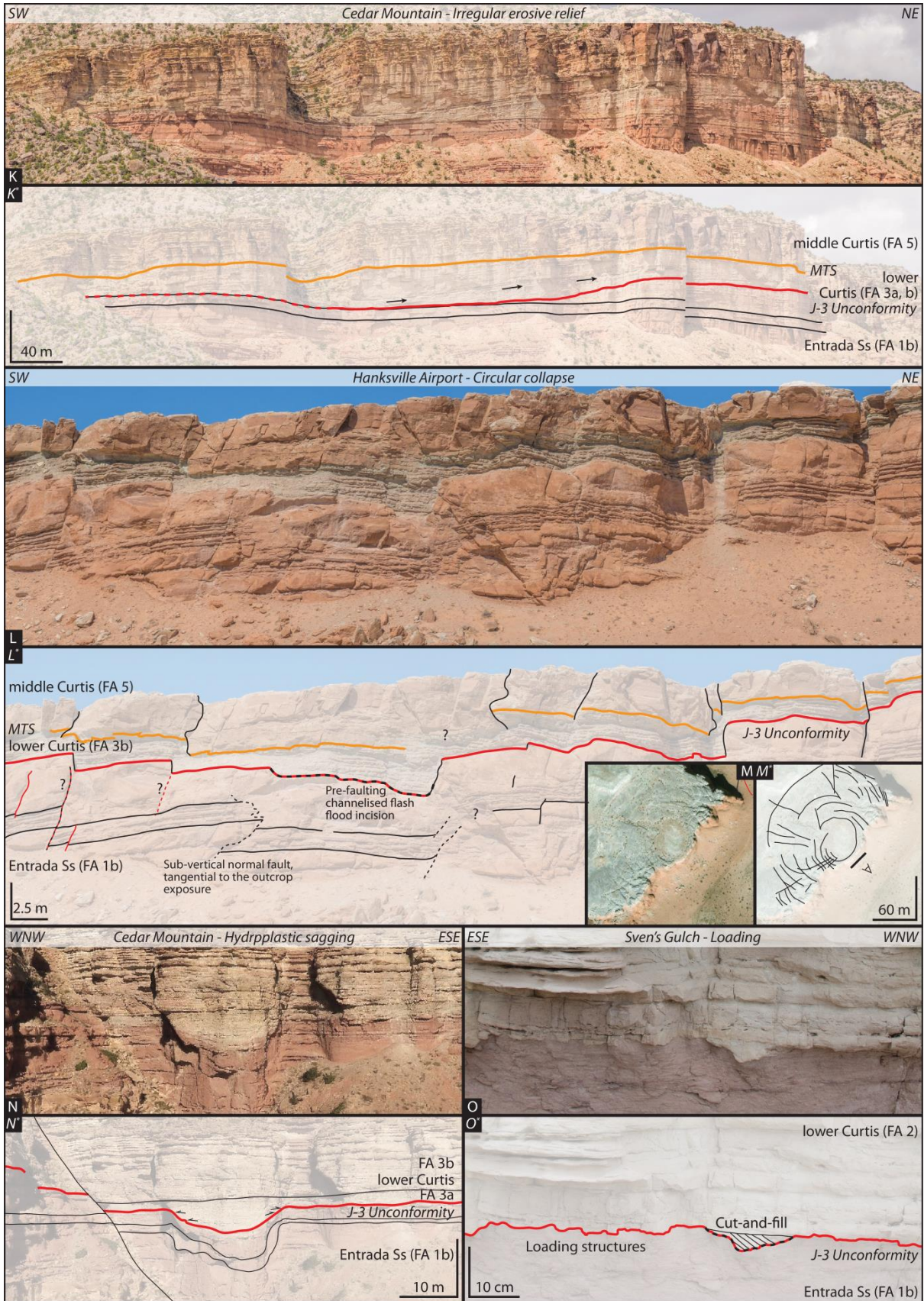


Fig. 4 (follow) – See legend on page 107.

Fig. 4 – Overview of the different types of relief, as they appear in the field. **A.** Example of an angular unconformity between the earthy facies of the Entrada Sandstone, and the middle Curtis (barely visible on the photo, less than a metre thick), conformably overlain by the upper Curtis, which then grades into the Summerville Formation. **B.** Paraconformable contact between the earth facies of the Entrada Sandstone, and the lower Curtis. **C.** Paraconformable contact between the earthy facies of the Entrada Sandstone, and the middle Curtis. Note that the J-3 Unconformity has merged with the Major Transgressive Surface, defining the base of the middle Curtis (Zuchuat *et al.*, 2018). Geologist for scale. **D.** Enigmatic occurrence of an undulating relief, observed only in the northern part of the study area, at Stove Gulch, separating the earth facies of the Entrada Sandstone from the lower Curtis. **E.** Example of a steep tidal incision at Sven's Gulch. The black, dashed line contours the base of this incision, which eroded first into its intraformational substratum (FA 2 (black arrow), FA 3a), before cutting into the underlying earthy facies of the Entrada Sandstone. The incision was filled in by FA 3b deposits, in which a boulder of Entrada Sandstone can be observed (brown arrow). Note how the overlying subtidal channel (FA 4b) also truncates its substratum, but does not reach the J-3 Unconformity.

Fig. 4 (follow) – F. Example of an irregular, erosion-related relief at the base of the lower Curtis, which was not impacted by pre-existing normal faults occurring in the earthy facies of the Entrada Sandstone. **G.** Close up on this irregular erosive contact, as the lower Curtis deposits carved into their Entrada Sandstone's substratum. Note that the whole succession was subsequently faulted. **H, I, J.** See text for detail explanations. Shadscale Mesa outcrop, where the middle Curtis completely truncated its lower Curtis Substratum, before starting to erode into the earthy facies of the Entrada Sandstone. Note that the transgression accompanying the lower Curtis' deposition was not impacted by pre-existing normal fault planes occurring in the earthy facies of the Entrada Sandstone, whereas the Major Transgression and associated the middle Curtis were impacted by these pre-existing normal fault planes, forming 30-50 cm escarpments, which suggests a differential hardening of these fault planes between the lower- and the middle Curtis' deposition.

Fig. 4 (follow) – K. Irregular erosive relief of ca. 23 m, visible at Cedar Mountain. The J-3 Unconformity separates the earthy facies of the Entrada Sandstone from the lower Curtis. The stratal arrangement within the lower Curtis might have required some local syn-depositional tilting, to account for the thickness variations and the sedimentary architecture of the unit. The three black arrows indicate the lateral accretion direction of cross-stratified channelised sandstone bodies. **L, M.** Cross-section across, and map view of one of the circular collapse structure present in the vicinity of Hanksville Airport. Black lines indicate normal faults, and red ones correspond to local thrusts. The dashed lines indicate uncertainties within the interpretation **N.** Hydroplastic sagging at the top of the Entrada Sandstone. The depression was passively infilled by the subtidal deposits of the lower Curtis. Note the post-depositional faulting of the entire succession. **O.** Loading structures occurring at the interface between the lower Curtis beach- to upper shoreface deposits (FA 2), and the underlying earthy facies of the Entrada Sandstone.

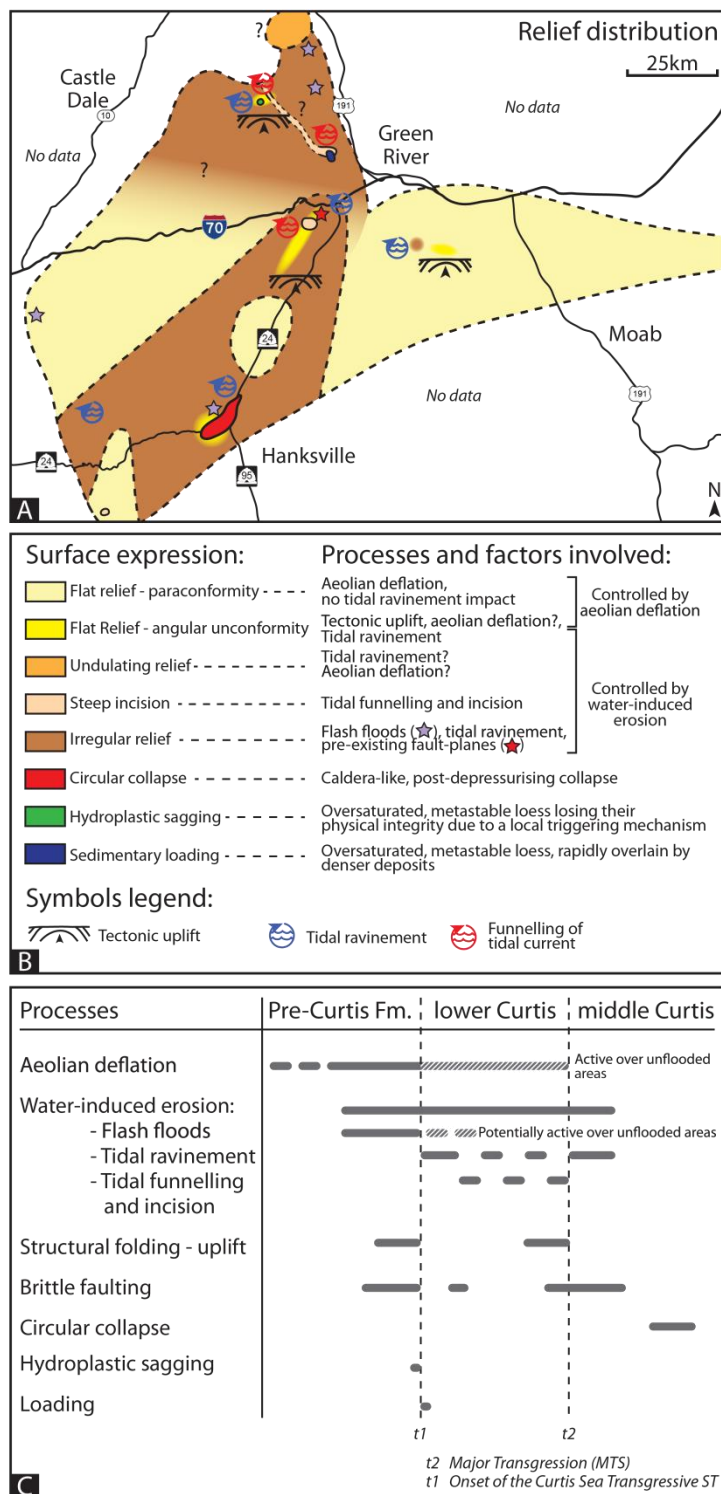
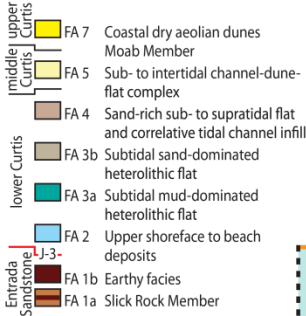


Fig. 5 – A. Map displaying how the various types of relief are distributed throughout the study area. **B.** Legend linking the different types of relief to the various processes involved in the making of the J-3 Unconformity. **C.** Diagram showing the relative timing of all the identified processes involved in the shaping of the unconformity. Three time periods are identified here: the Pre-Curtis Formation period corresponds to the period predating the start of the Curtis Sea transgression over the study area (t1), the second period corresponds to the time during which the lower Curtis was being deposited, and the third period corresponds to the processes involved in the shaping of the unconformity postdating the Major Transgression, and accompanying the deposition of the middle Curtis (t2).

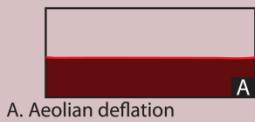
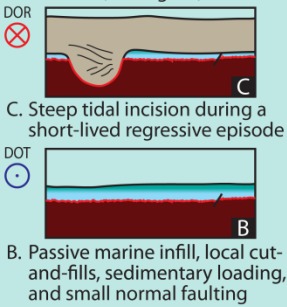
Composite J-3 Unconformity



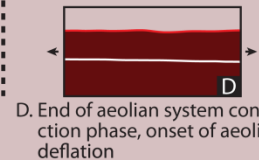
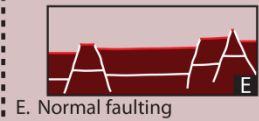
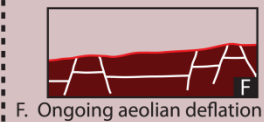
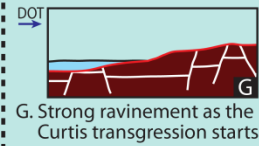
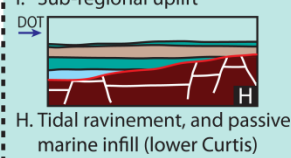
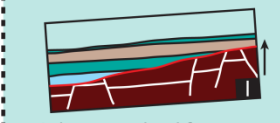
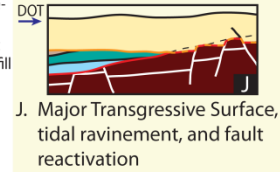
- t3 Onset of the High Stand ST (HST)
- t2 Major Transgression (MTS)
- t1 The Curtis Sea starts to transgress the study area (TST)



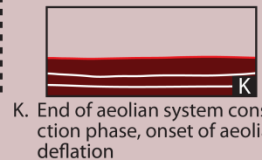
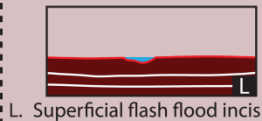
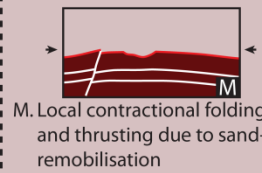
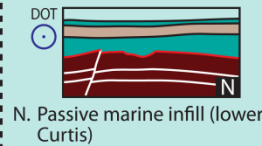
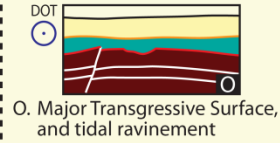
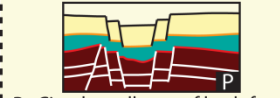
Sven's Gulch (SG) (See Fig. 4E)



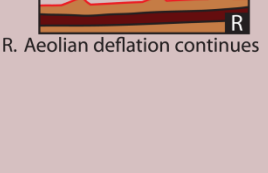
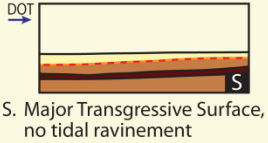
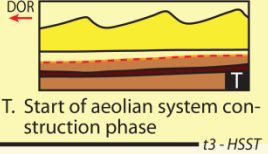
Shadscale Mesa (SM) (See Fig. 4H)



Hanksville Airport (HKA) (See Fig. 4L)



Big Pinto Mesa (BPM)



Coeval aeolian deflation over unflooded areas

Fig. 6 – Diagrams showing when the various processes impacted on the J-3 Unconformity at four selected localities. Note that the spacing between t1 (onset of the Curtis Sea Transgression), t2 (Major Transgression), and t3 (onset of the High Stand Systems Tract) do not hold any absolute time information, but these three lines themselves do represent fixed points in time.

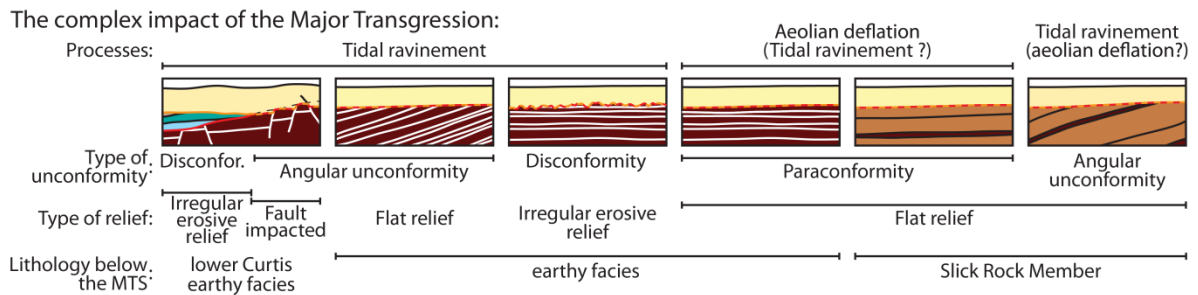


Fig. 7 – Diagram illustrating the non-uniqueness of the relief generated by the Major Transgression, highlighting the complexity existing in the system, between the processes involved, the types of unconformity and the types of relief they generated, as well as the underlying reworked lithology.

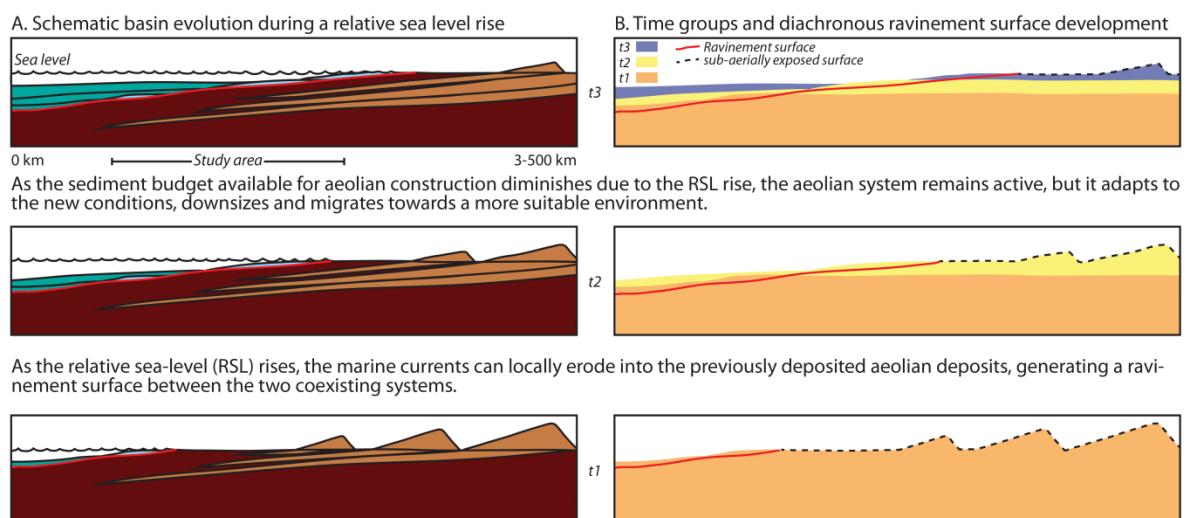


Fig. 8 – (A) Model showing the evolution, over time, of an aeolian system, adjacent and coexisting with a subaqueous domain. The whole composite system undergoes a progressive climatic change towards a more humid period, a constant relative sea-level rise (RSL) and is fed by a steady sediment supply. (B) The coexisting aeolian and subaqueous deposits are grouped according to their age, illustrating the time-transgressive nature of such a composite ravinement-flooding surface, across a transitional, continental to marine-setting. The nature of RSL rise is irrelevant to the model, and the vertical scale is not representative of the reality.

7.3. Article III: Overprinted Allocyclic Processes by Tidal Resonance in an Epicontinental Basin: the Upper Jurassic Curtis Formation, East-Central Utah, USA.

Zuchuat, V.¹, Sleveland, A.R.N.¹, Pettigrew, R.P.², Dodd, T.J.H.², Clarke, S.M.², Rabbel, O.¹, Braathen, A.¹, and Midtkandal, I.¹ (in review). Overprinted Allocyclic Processes by Tidal Resonance in an Epicontinental Basin: the Upper Jurassic Curtis Formation, East-Central Utah, USA. Submitted to *The Depositional Record*.

¹*Tectonostratigraphic Research Group, University of Oslo, Sem Sælands Vei 1, 0371 Oslo, Norway*

²*Basin Dynamics Research Group, Keele University, ST5 5BG, Keele, Staffordshire, United Kingdom*

OVERPRINTED ALLOCYCLIC PROCESSES BY TIDAL RESONANCE IN AN EPICONTINENTAL BASIN: THE UPPER JURASSIC CURTIS FORMATION, EAST-CENTRAL UTAH, USA

VALENTIN ZUCHUAT¹, ARVE R.N. SLEVELAND¹, ROSS PETTIGREW², THOMAS J.H. DODD², STUART M. CLARKE², OLE RABELL¹, ALVAR BRAATHEN¹, IVAR MIDTKANDAL¹

¹*Tectonostratigraphic Research Group, University of Oslo, Sem Sælands Vei 1, 0371 Oslo, Norway*

²*Basin Dynamics Research Group, Keele University, Keele, Staffordshire, ST5 5BG, United Kingdom*

Corresponding author: valentin.zuchuat@geo.uio.no

ABSTRACT

Modern, tide-dominated and/or tide-influenced coastlines correspond to deltas, estuaries, and lagoons. However, some tide-dominated basins and related sedimentary units in the rock record, such as the semi-enclosed, shallow, Utah-Idaho Trough foreland basin of the Jurassic Curtis Sea, do not correspond to any of these modern systems. Persistent aridity caused the characteristic severe starvation of perennial fluvial input throughout this basin, in which the informal lower, middle, and upper Curtis, as well as the Summerville Formation were deposited. Wave energy was efficiently dissipated by the shallow basin's elongated morphology (approximately 800x150 km), as well as its protected nature. Consequently, the semi-enclosed, shallow marine system was dominated by amplified tidal forces, resulting in a complex distribution of heterolithic deposits.

In the early stage of the transgression, as the lower Curtis was deposited, allocyclic forcing was strongly impacting upon the system's intrinsic autocyclic processes. Short-lived relative sea-level variations, as well as uplift and deformation episodes, resulted in three parasequences, separated by traceable flooding and ravinement surfaces. The subsequent transgression, which defines the base of the middle Curtis, allowed for the shallow-marine part of the system to enter into tidal resonance because the basin reached the optimal length-to-width configuration. This resonant system overprinted any evidence of allocyclic forcing and related traceable stratigraphic surfaces. However, the contemporaneous and neighbouring Moab Member's coastal aeolian dune field characterised by five stacked aeolian sequences, as well as the Summerville Formation's supratidal deposits, lingered to record allocyclic signals, as the Curtis Sea regressed.

This study shows that (i) a tide-dominated basin can enter into tidal resonance as it reaches its optimal morphological configuration, leading to the overprinting of otherwise dominant allocyclic processes by autocyclic behaviour. (ii) It is therefore required to extend the research focus to neighbouring and contemporaneous depositional systems in order to fully understand the dynamic stratigraphic history of a basin alternatively dominated by auto- and allocyclic processes.

Key word: Tidal resonance, autocyclic processes, allocyclic processes, stratigraphic surfaces, aeolian sequences, Curtis Formation

INTRODUCTION

Oceanic tides and their spatio-temporal variability are complex and dynamic phenomena (Kvale, 2012). The environments they act upon have raised people's interest as early as first century AD, when Pliny the Elder described areas "invaded twice each day and night by the overflowing waves of the ocean", leaving wonder if they "are to be looked upon as belonging to the land, or whether as forming portion of the sea?" (translation from Bostock and Riley, 1855).

Sedimentary successions deposited within tide-dominated basins are characterised by a three-dimensional, complex and potentially cyclic assemblage of heterolithic lithologies, the distribution of which depends on a fine balance between (i) basin configuration and the dispersal of basinal hydrodynamic forces, (ii) autogenic basin processes, such as the avulsion of tidal channels, and (iii) sediment input (Kvale, 2012; Wang, 2012, and references therein). Spatio-temporal variations of tidal currents, which variably influence the system's erosion-transport-deposition chain, further complicate the arrangement of these deposits. (Kvale, 2012; Wang, 2012; Baas *et al.*, 2016). In addition, modern-day, semi-enclosed basins, such as the Gulf of California, the Adriatic Sea, the Persian Gulf, or the Bay of Fundy, demonstrate that basin geometry can further amplify tidal forces, allowing the system to enter a tidal resonant stage if the length of the basin approximates to an odd multiple of a quarter of the tidal wavelength (Sztanó and de Boer, 1995; Martinius and Gowland, 2011; Roos and Schuttelaars, 2011; Longhitano *et al.*, 2012; Reynaud and Dalrymple, 2012; Shaw *et al.*, 2014). This leads to augmented tidal ranges and stronger tidal currents closer to the shoreline than in open water (Godin, 1993; Sztanó and de Boer's, 1995; Yoshida *et al.*, 2007; Martinius and Gowland, 2011; Roos and Schuttelaars, 2011; Longhitano *et al.*, 2012; Reynaud and Dalrymple, 2012; Shaw *et al.*, 2014).

The impact of such autocyclic processes has been detected in sediments deposited in transgressive settings, as the system's resonance typically increases with a relative sea-level rise (Sztanó and de Boer's, 1995; Martinius and Gowland, 2011; Longhitano *et al.*, 2012; Reynaud and Dalrymple, 2012; references therein). However, the time required to trigger or abandon a tidal resonance is geologically instantaneous, and the time interval encapsulated by the deposited sediments can be short, compound, and spatially variable, as different parts of the basin become resonant at different times (Reynaud and Dalrymple, 2012). To complicate the interpretation of the deposits of a tide-dominated basin further, sediment deposition typically takes place upon a low gradient, shallow marine slope and facies belts are shifted over large horizontal distances by comparatively small variations in water depth (Midtkandal and Nystuen, 2009, Zuchuat *et al.*, 2018).

Despite a complicated and spatio-temporally compartmentalised sedimentary architecture, tidally dominated sedimentary successions typically host sandstone bodies of reservoir grade that are laterally and vertically sealed by associated sediments with low porosity and permeability. Consequently, the sandstone bodies can provide a significant reservoir volume for hydrocarbon exploration, or they can form targets for aquifers appraisal, and CO₂ injection (Martinius *et al.*, 2005; Halland *et al.*, 2014).

Notwithstanding the inherent complexities of sediment character and distribution, most shallow-water, tide-dominated, coastal depositional systems can be classified as (i) transgressive, upward-fining estuaries, (ii) (semi-)protected lagoons, (iii) prograding, tide-dominated deltas, or (iv) open-coast tidal flat (Fig. 1) (e.g., Boyd *et al.*, 1992; Dalrymple *et al.*, 1992; Fan, 2012). However, not every sedimentary succession that displays strong evidence (or dominance) of tidal reworking corresponds to one of these four categories. Broad, shallow epicontinental basins (Tape *et al.*, 2003; Zuchuat *et al.*, 2018), and fluviially starved macro-embayments (Zuchuat *et al.*, 2018) may display strong evidence for tidal reworking of sediments within them, but a lack of modern day equivalents hampers interpretation of the sedimentary record, especially when three-dimensional continuous exposure is unavailable.

The continuous and 3D exposure of the middle to upper Jurassic succession of east-central Utah (Fig. 2) allows detailed investigations of a shallow marine to marginal aeolian environment that evolves into a semi-enclosed, fluviially starved and tidally influenced, epeiric setting through time.

This study provides a detailed analysis the Middle Jurassic Entrada Sandstone and the Upper Jurassic Curtis and Summerville formations (Wilcox and Currie, 2008) within the context of Zuchuat *et al.*'s (2018) lower, middle, and upper Curtis lithostratigraphic framework, and develops that framework further to reconstruct the kinematic history of the transition from aeolian to shallow marine basin. The study identifies key sequence stratigraphic surfaces that are the result of high-resolution systemic responses to varying climatic conditions (Boulila *et al.*, 2010; Alberti *et al.*, 2012; Boulila *et al.*, 2012; Strasser *et al.*, 2012; Pellenard *et al.*, 2014) and basinal reconfiguration during the Oxfordian Age. Identified traceable surfaces are likely the consequence of allocyclic forcing, but evidence for this within part of the succession is overprinted periodically by the sedimentary response to autocyclic processes, most notably when the tide-dominated embayment enters into a resonant stage. The study demonstrates that the understanding and interpretation of shallow marine sediments in settings where normally dominant allocyclic signatures are overprinted and obliterated by those of autogenic sediments requires an understanding of neighbouring and contemporaneous systems in order to fully assess the basin's history. Consequently, the study illustrates the value in identifying key sequence stratigraphic surfaces for correlating highly heterolithic, tidally influenced sedimentary packages.

GEOLOGICAL SETTING

Tectonic setting

Four major tectonic events impacted on Utah's geological development since the early Mesozoic, and the rise of the North American Cordillera (Hintze and Kowallis, 2009; Thorman, 2011; Anderson, 2015; Yonkee and Weil, 2015; and references therein): (i) the Nevadan Orogeny (Middle Jurassic-Lower Cretaceous), whose granitic intrusions can be observed at today's Utah-Nevada border, (ii) the Elko Orogeny (Middle Jurassic), characterised by alternating episodes of tectonic contraction and extensions, accompanied by the development of SSW-NNE-striking, stacked foreland basin development, (iii) the Sevier Orogeny (Lower Cretaceous to Paleogene), featuring thin-skinned contractional structures, and (iv) the Laramide Orogeny (Upper Cretaceous to Paleogene), associated

with the development of basement-rooted monoclines, such as the San Rafael Swell (Bump and Davis, 2003). The Stratigraphy of central-eastern Utah was also effected by diapirism and remobilisation of the Paradox Basin evaporitic strata (Trudgill, 2011), as well as by the Colorado Plateau uplift and its sub-regional to regional extensional episodes (Levander *et al.*, 2011; Murray *et al.*, 2016). The igneous intrusive complexes of the Abajo, Henry, and La Sal Mountains (Upper Oligocene) also impacted on the sedimentary strata in central-eastern Utah (Sullivan *et al.*, 1991; Nelson, 1997). The Upper Callovian to Lower Oxfordian Entrada-Curtis-Summerville lithostratigraphic sub-divisions were deposited within the Utah-Idaho Trough, a SSW-NNE-oriented retroarc foreland basin at the foot of the Elko Highlands (Thorman, 2011), which the Sundance Sea to the north flooded several times during its history (Hintze and Kowallis, 2009). In the San Rafael Swell area (Fig. 2), the Curtis Formation was buried by between 2.45 km and 2.86 km (Nuccio and Condon, 1996; Petrie *et al.*, 2017).

Stratigraphy

The Middle Jurassic Entrada Sandstone of southeastern Utah, and the overlying Upper Jurassic Curtis and Summerville formations, the coastal to shallow marine Temple Cap Formation, the aeolian Page Sandstone, and the shallow- to marginal-marine Carmel Formation comprise the San Rafael Group of the Colorado Plateau (Fig. 2; Gilluly and Reeside, 1928; Pippingos and O'Sullivan, 1978; Peterson and Pippingos, 1979; Anderson and Lucas, 1994; Sprinkel *et al.*, 2011). These sediments represent five upward-thinning, transgressive-regressive (TR) sequences with an eastward- and southward-wedging geometry that is a consequence of deposition within the Utah-Idaho Trough (Fig. 2B; Anderson and Lucas, 1994; Brenner and Peterson, 1994; Peterson, 1994; Bjerrum and Dorsey, 1995; Thorman, 2011).

As the early Jurassic shallow epeiric Sundance Sea, which covered North America at this time, regressed northward during the Callovian Age and warm arid conditions prevailed, sediments of the shallow- to marginal-marine Carmel Formation (Fig 2C) were overlain conformably by those of the marginal-marine to continental, rusty-red to light-orange, aeolian Entrada Sandstone (Fig. 2C; Gilluly and Reeside, 1928; Peterson, 1994; Hintze and Kowallis, 2009). The Entrada Sandstone is divided typically into (i) the Slick Rock Member that comprises aeolian dune and interdune sediments, and (ii) the overlying and partially contemporary informal unit of the 'earthy facies' (Imlay, 1952), characterised by repeated yet extraneously vegetated, mottled loess strata, interbedded with marginal-marine sabkha-like deposits (Witkind, 1988; Doelling *et al.*, 2015; and references therein). The Entrada Sandstone thickens westwards, in the direction of the Utah-Idaho Trough, and northwards, toward the Uinta Mountains (Fig. 2) Witkind, 1988; Crabaugh and Kocurek, 1993; Kocurek and Havholm, 1993; Carr-Crabaugh and Kocurek, 1998; Mountney, 2012; Doelling *et al.*, 2015). The earthy facies thins out to the south and east of the study area (Fig 2B), where the sediments of the Curtis Formation directly overlie the Slick Rock Member. Recycled fluvial sediments originating from the Appalachian Mountains are the main constituents of the Entrada Sandstone (Dickinson and Gehrels 2009, 2010). Four 'construction-destruction' sequences (*sensu* Mountney, 2006), related to regional base-level oscillations, are recognised within this coastal aeolian system (Carr-Crabaugh and Kocurek, 1998; Kocurek and Lancaster, 1999; Kocurek, 2003; Mountney, 2012),

and the Entrada Sandstone is capped at its top by the regional, polygenetic, and heterochronous J-3 Unconformity (Zuchuat *et al.*, 2018; submitted), first defined by Pippingos and O'Sullivan (1978). The unconformity displays relief with an amplitude ranging from 0.1 m to 23 m, and a wavelength varying from the decimetre to the hectometre scale (Zuchuat *et al.*, submitted). Relief was generated by both erosion-related and deformational processes, and surface types include flat angular unconformities, paraconformities, steep tidal incisions, sinuous undulations, irregular tidal ravinement surfaces, circular collapse structures, sedimentary loading, and hydroplastic sagging (Zuchuat *et al.*, submitted).

The Entrada Sandstone is overlain by the lower Oxfordian Curtis Formation, originally defined by Gilluly and Reeside (1928) from exposures along the northeast margin of the San Rafael Swell (Fig. 2). The Curtis sediments comprise complexly arranged, shallow-marine, tidally influenced heterolithic (Kreisa and Moiola, 1986; Caputo and Pryor, 1991; Wilcox and Currie, 2008; Ogg *et al.*, 2016; Zuchuat *et al.*, 2018) deposited as the Curtis Sea flooded a gently dipping, shallow, and fluviially starved, epicontinental basin that developed as the rate of creation of accommodation diminished at end of the Callovian Age (Thorman, 2011; Zuchuat *et al.*, 2018). The underrepresentation of wave-related structures within the Curtis Formation can be attributed to the protected nature of the Curtis Sea, as well as the elongate basin configuration, which facilitated dissipation of wave energy (Yoshida *et al.*, 2007). The Curtis Formation has a green to white colouration, which is due to the presence of shallow-marine glauconite and chlorite in the sediments, and it strongly contrasts with the underlying rusty-red Entrada Sandstone (Gilluly and Reeside, 1928; Caputo and Pryor, 1991; Peterson, 1994). The Curtis Sea basin reached approximately 800 km in length, and at least 150 km in width. As a result, the Curtis Formation is characterised by an east- and south-wedging geometry, with a maximum thickness of approximately 80 m at Sven's Gulch (9*), in the San Rafael Swell area (Gilluly and Reeside, 1928; Caputo and Pryor, 1991; Peterson, 1994; Thorman, 2011; Anderson, 2015; see also Fig. 2 and Fig. 3 in Zuchuat *et al.*, 2018). The Curtis Formation is separated into three informal units based on their outcrop character: the lower, middle, and upper Curtis (Fig. 2; Zuchuat *et al.*, 2018). The lower Curtis comprises laterally restricted upper shoreface to beach deposits, grading into thinly bedded, dark-green to grey, heterolithic subtidal flat deposits in which gravel-rich, subtidal channels and dunes occur (Zuchuat *et al.*, 2018). The overlying middle Curtis is characterised by a lighter coloured and better sorted sandstone by comparison to the underlying heterolithic lower Curtis (Zuchuat *et al.*, 2018). Its base corresponds to the regional Major Transgressive Surface (MTS), and consists of complex arrangements of subtidal channels, sub-to intertidal dune and flat deposits (Zuchuat *et al.*, 2018). The dark green, upper Curtis conformably overlies the middle Curtis, and comprises thinly bedded, sub- to intertidal deposits, which grade into the supratidal deposits of the Summerville Formation (Zuchuat *et al.*, 2018). Towards the Utah-Colorado border (Fig. 2), these deposits form lateral and contemporaneous equivalents to the aeolian deposits that form Moab Member of the Curtis Formation (Caputo and Pryor, 1991; Peterson, 1994; Doelling, 2001; Zuchuat *et al.*, 2018).

In the study area (Fig. 2), the Upper Curtis is overlain conformably by dark brown, sabkha deposits of the Summerville Formation (Gilluly and Reeside, 1928; Caputo and Pryor, 1991; Peterson, 1994;

* Numbers in parenthesis following the names of places refer to locality numbers on Fig. 2.

Lucas, 2014). However, in the unflooded neighbouring regions to the east and to the south, the Summerville Formation must have coexisted with the Curtis Formation as its coastal plain environment (Zuchuat *et al.*, 2018).

In the 'Four Corners' area, where the states of Utah, Colorado, Arizona and New Mexico meet (Fig. 2a), the Todilto Member of the Wanakah Formation is the lateral equivalent of the Curtis, while the Beclabito Member of the Wanakah Formation corresponds to the Summerville (Fig. 2c; Condon and Huffman, 1988, Zuchuat *et al.*, 2018, Kocurek *et al.*, in press). Further north in Uinta Mountains area (Fig. 2a), the Curtis-Summerville interval is the lateral equivalent of the Stump Formation (Pipiringos and Imlay, 1979; Imlay, 1980; Wilcox and Currie, 2008). More regionally, it is equivalent to the Redwater Shale Member of the Sundance Formation in Wyoming (Imlay, 1947, 1980), and the Stump Formation in the vicinity of the Wyoming-Idaho border (Mansfield and Roundy, 1916; Pipiringos and Imlay, 1979; Imlay, 1980).

The Curtis-Summerville interval corresponds to Peterson's (1994) fifth (TR) cycle within the Jurassic system of the Sundance Sea and the Western Interior Basin (Pipiringos and O'Sullivan, 1978; McMullen *et al.*, 2014), and likely corresponds to the LZA-2.3 third-order TR-interval of Haq *et al.* (1987), post calibration onto Wilcox and Currie's (2008) age and Ogg and others' (2016) timescale.

DATA AND METHODS

The data necessary for this study were gathered during three field campaigns between 2015 and 2017 and augmented with small-scale studies in 2018. The study area in central-eastern Utah (Fig. 2) extends from the Humbug Flats (1 to 5), north of the San Rafael Swell, southward to Notom Ranch (35), 44 km southwest of Hanksville, and from Last Chance Desert (38 and 39) on the western margin of the San Rafael Swell, eastward to Big Pinto Mesa (30) on the Utah-Colorado border. In order to cover the study area systematically along the exposure of the Entrada-Curtis-Summerville interval, forty-three localities were visited (Fig. 2). Forty-one sections were measured to collect sedimentary, palaeocurrent and structural information, and a total of 2291 m were logged across the Entrada-Curtis-Summerville stratigraphic interval. This dataset is complemented by aerial images, as well as photographic material collected at and between the visited localities using unmanned aerial vehicles (UAV) and terrestrial techniques. In order to document, illustrate and understand the complex three-dimensional (3D) sedimentary architecture of the interval of interest, 3D virtual outcrop models were produced from the collected photogrammetric material (after Westoby *et al.*, 2012). The models were generated using PhotoScan Pro[®] (Agisoft LLC, St. Petersburg, Russia), before being analysed and interpreted with Lime[®], a software developed by the Virtual Outcrop Geology VOG group of both Bergen and Aberdeen universities (Bonaventura *et al.*, 2017; Buckley *et al.*, 2017). To augment the sedimentary detail, 35 m of section covering the Entrada-Curtis-Summerville interval were logged using a hand-held gamma ray spectrometer in full assay mode at 20 cm intervals.

Standard facies and architectural analysis of sedimentary data permits interpretations of depositional settings. Merging sedimentary data with photogrammetric models and structural data sets provides a means of tracing key sequence stratigraphic surfaces, such as subaerial unconformities,

transgressive surfaces, regressive surfaces of marine erosion, flooding surfaces, and tidal ravinement surfaces (*sensu* Catuneanu, 2006; Catuneanu *et al.*, 2009) to provide a regional sequence stratigraphic framework and interpretation.

RESULTS

The facies (Table 1) and facies associations (FA; Table 2) schemes are developed in this work summarise Zuchuat *et al.*'s (2018) detailed sedimentological assessment of the Curtis Formation and its neighbouring units. They will be used to decipher the dynamic history of the basin, and to identify depositional environments and their spatiotemporal relationships.

The Entrada Sandstone at the base of the studied interval comprises two facies associations that are broadly comparable to the unit's lithostratigraphic subdivisions. **FA 1a** comprises deposits of aeolian dunes and interdunes of the Slick Rock Member, and **FA 1b** comprises the sediments of the overlying marginal-marine, rusty-red informal earthy facies, which include singular coastal dunes with sabkha and loess strata displaying a varying degree of mottling (Fig. 3a, 3b, Table 2). FA 1b thickens north-westwards, and pinches out southwards around Notom Ranch (35), and eastwards in the vicinity of Moab (Fig. 2). FA 1 is capped by the polygenetic, heterochronous, and diachronous (Zuchuat *et al.*, submitted) J-3 Unconformity of Pippingos and O'Sullivan (1978). Locally, erosive scours at the top of the FA 1b are occupied by matrix-supported, chaotically arranged conglomerates, comprising rounded to well-rounded extra-basinal pebbles and cobbles, up to 7 cm in diameter (Fig. 4a, 4b, 4c). These erosive scours are interpreted as the product of flash floods predating the transgression of the Curtis Sea, and the accompanied deposits settled as the flows decelerated. Except for these flash flood deposits and some episodic fluvial terminal splays (Valenza, 2016), evidence for major fluvial development is lacking within the Entrada Sandstone.

In the northern and western parts of the study area, notably at Sven's Gulch (9), Interstate 70 (12) and Shadscale Mesa (13), the dynamic surface of the J-3 Unconformity was locally modified as an approximately 2 m thick, laterally restricted (200-500 m), and tidally influenced upper shoreface succession was deposited (**FA 2**) (Fig. 3c, Table 2). These upper shoreface deposits represent the oldest deposits of the Curtis Formation (Zuchuat *et al.*, 2018). Sediments of **FA 3** overlay FA 2 (or the J-3 unconformity where FA 2 is not present) and are dominated by thinly bedded and laterally extensive, heterolithic subtidal heterolithic deposits, showing a varying sand-to-mud ratio, ranging from mud-dominated (**FA 3a**) to sand-dominated (**FA 3b**) (Fig. 3d, Table 2). FA 3 is characterised by abundant bidirectionally rippled, cross-stratified, lenticular- to flaser-bedded siltstone and sandstone strata (Fig. 5a, 5b, 5c). A bed typically reaches thicknesses of 3-10 cm. The base of FA 3a is either gradational, or it corresponds to an erosive ravinement surface. The base of FA 3b is either conformable, or it corresponds to a regressive surface of marine erosion, capable of cutting 45 m wide and 10 m deep incisions into its substrata (Fig. 3e). Despite their intraformational erosive power, FA 3a and FA 3b both passively onlap the J-3 Unconformity (Zuchuat *et al.*, submitted).

In the north of the study area, cross-stratified, heterolithic, subtidal channels, with concave up, erosive bases and flat upper surfaces (Fig. 4a, 4d) form part of FA3. Channel fills comprise rounded- to well-

rounded, gravel-size, extra-basinal clasts within a matrix of fine- to very coarse-grained sand, with green mud locally interbedded between the gravelly foresets (Fig. 5d). Heterolithic gravelly dunes arranged in thin-thick-thin cyclical bundles, with cm-thick mud drapes between foresets (Fig. 4a, 4e) are also present. These deposits are characterised by a sharp but non-erosive flat base, and concave down top surface, migrating on FA 3 substrata.

FA 4 is subdivided into **FA 4a** and **FA 4b**, representing proximal sub- to supratidal sandflat, and the correlative, more distal, gravel-rich, subtidal channels, respectively (Table 2). FA 4a comprises light-pink, very-fine- to fine grained deposits that extend over tens of kilometres on the eastern margin of the San Rafael Swell only, in the central part of the study area (Fig. 2, Fig. 3f). FA 4a is characterised by a southward thickening, 4 to 15 m thick succession of plane parallel-bedded to plane parallel-laminated strata, with double and single mud drapes, as well as scarce unidirectional current ripples and herringbone cross-stratification. FA 4b is restricted to the north-eastern margin of the San Rafael Swell, where it consists of a 1 to 10 m thick, multi-storey, coarse-grained, subtidal channel complex, with rounded to well rounded, gravel size extra-basinal clasts (Fig 3g).

Facies Associations 2, 3 and 4 together constitute the informally named lower Curtis, in which they stack to form three upwards shallowing (US) successions within which minor erosive and incision surfaces are present (Fig. 6a; Zuchuat *et al.*, 2018). The lowermost US succession, occurs only at Sven's Gulch (9), Cedar Mountain (43), and Sid and Charley (41) (Fig. 3D). It is characterised by steep tidal incisions (Fig. 3E). FA 4 occurs only within the uppermost succession. Some minor erosive and incision surfaces within the US successions are traceable between outcrops, while others are localised. Despite evidence of current reversals within the sediments (Fig. 5a, c), the lower Curtis is dominated by a basinward (northward) current direction (Fig. 6b).

The lower Curtis is overlain disconformably by **FA 5** (Fig. 3h, Fig. 6a, Table 2) which represents the informal middle Curtis unit (Zuchuat *et al.*, 2018). Its base corresponds to the Major Transgressive Surface (MTS; Zuchuat *et al.*, 2018): an erosive ravinement surface which can be traced throughout the study area, all the way to Ghost Ranch, northern New Mexico, where it marks the base of the Todilto Member of the Wanakah Formation (Fig. 2; Zuchuat *et al.*, 2018; Zuchuat *et al.*, submitted). The thickness of FA 5 varies from more than 45 m in the northern part of the study area, to approximately 1 m, as it thins south- and eastwards. These sediments comprise light green to white, very fine- to fine-grained well sorted sandstone, arranged in an intricate interdigitating of sub- to intertidal channels and associated tangential to sigmoidal cross-stratified sandstones arranged in tidal bundles, subaqueous dunes with associated abundant reactivation surfaces, and sandflats with a strong bidirectional current component (Fig. 5e, 5f, 5g, 5h, 5i). Individual bedforms in FA 5 reach a maximum height of 2 to 3 m, and the average bedform size is one to two orders of magnitude higher than that in the underlying lower Curtis deposits. Bedform thickness decreases up-section, as well as south- and eastwards, as FA 5 thins in these directions. Palaeocurrent measurements indicate a strong bi-modal distribution of current motion at the time of deposition, oriented NW-SE (Fig. 6b).

The middle Curtis FA 5 deposits are conformably overlain by **FA 6** that constitutes the informal upper Curtis (Zuchuat *et al.* 2018). FA 6 consists of sub- to supratidal strata (Fig. 3i, Table 2), and crops out

in the northern, central, and southern parts of the study area (Fig. 6, Fig. 7; Zuchuat *et al.*, 2018). By contrast to the underlying FA5 deposits, FA 6 thins northwards, from a maximum thickness of approximately 28 m near Hanksville (34) to a minimum of 5 m at Sulphur Canyon (1) (Fig. 6). FA 6 is characterised by green, silt- to fine-grained, laterally extensive, isopachous sandstone beds, distinguished by plane parallel stratification, unidirectional current ripple- and herringbone cross-stratification. Individual bed set thicknesses range from 3 to 40 cm, and beds become thinner up-section. Consequently, the deposits of FA 6 reflect lower energy environment with respect to those of the underlying FA 5.

Towards the eastern part of the study area, FA 6 is replaced by the aeolian dunes of **FA 7**, which corresponds to Doelling's (2001) Moab Member of the Curtis Formation (Fig. 3j, Fig. 7, Table 2). FA 7 reaches a maximum thickness of approximately 50 m close to the Utah-Colorado border, and pinches out between Duma Point (19) and Horse Flies Gulch (20). It is composed of five packages of aeolian dunes, reaching a maximum individual thickness of approximately 20 m at Lost Spring Canyon (28), on the eastern border of Arches National Park. Each package is capped by supersurfaces (*sensu* Kocurek, 1988), under which abundant rhizoliths can be observed (Zuchuat *et al.* 2018). These supersurfaces can be overlain by shallow marine, tidally influenced deposits, including herringbone cross-stratified sandstones and mud drapes arranged in flaser-bedded packages, or by inter- to supratidal strata, suggesting potential local microbial activity and the development of palaeosol horizons. Subaqueous deposits are less frequent towards the eastern border of the study area, as the supratidal deposits become more common. Note that the uppermost aeolian sequence is also overlain by a thin sandstone crust that is typically structureless, yet shows evidence of local subaqueous reworking, and potential sand stromatolite structures, similar to those described by Getty and Hagadorn (2009).

Whereas FA 7 is sharply overlain by the supratidal, rusty red to dark brown, evaporite-rich, sabkha deposits of **FA 8** (Summerville Formation), the transition from the upper Curtis FA 6 sub- to supratidal strata into FA 8 supratidal environment is gradual (Fig. 3i, k, Table 2). Despite a gradual transition, episodic and regular marine incursions can be observed within FA 8. However, their amplitude, diminishes up-section (Zuchuat *et al.*, 2018). It is also important to note that three 30-50 m wide, and 0.5-1 m deep channels were observed in FA 8, which suggest an extremely minor fluvial impact on this supratidal system and the contemporaneous and neighbouring marine system.

DEPOSITIONAL MODEL

Several authors have presented the Curtis and Summerville formations as an overall transgressive-regressive cycle (Caputo and Pryor 1991; Wilcox and Curie 2008; Peterson, 1994). This study supports their interpretation as a general conclusion, but the spatially and stratigraphically diverse body of data assembled here suggests that the detailed stratigraphic history of the interval is more intricate than that previously proposed (Fig. 8).

Importantly, in low-gradient systems like the Curtis basin the interpretation of stratigraphic detail is strongly influenced by the effects of relatively minor changes in sea-level upon the position of the shoreline and by consequence the facies distribution (e.g.: Midtkandal and Nystuen 2009).

Pre-Curtis Sea transgression

The J-3 Unconformity is intrinsically polygenetic, hetero-, and diachronous by nature (Zuchuat *et al.* 2018; submitted), comparable to the compound surface discussed by Ahokas *et al.* (2014), as the deposition of the Entrada Sandstone, the Curtis, and the Summerville formations, and the accompanying relative sea-level variations, all influenced the genesis of this bounding surface. Consequently, the J-3 Unconformity is not the product of a forced regression, as suggested by Mitchum *et al.*'s (1977) definition of unconformities, but was primarily developed as the Curtis Sea started to transgress from the north.

This interpretation of the J-3 Unconformity is supported by preliminary gamma-ray data obtained from the earthy facies of the Entrada Sandstone at Duma Point (19) (Fig. 7, Fig. 9). As these Thorium/Uranium ratios (Th/U) measurements fall generally below 7 at approximately 5, they suggest a more prominent marine origin for these sediments, rather than a fully continental provenance (Fertl *et al.*, 1982). However, interpretation of these data must be considered within the context of the sediment calibre: Th/U ratios as a discriminator of marine over continental provenance are reliable only in mud-dominated successions (Fertl *et al.*, 1982), yet they remain relevant for coarser-grained sediments (Svendsen and Hartley, 2001). However, interpretation of these data must be considered within the context of the sediment calibre: Th/U ratios as a discriminator of marine over continental provenance are reliable only in mud-dominated successions (Fertl *et al.*, 1982). However, U_{excess} calculations clearly identify cyclicity with distinctive peaks that indicate periods of marine flooding (Fig. 9). This interpretation is supported by total count gamma ray data and, to some degree, by the sedimentology, notably illustrated by the Major Transgression at the base of the Curtis Formation. Consequently, it is difficult to conclude anything other than a prominent and cyclical marine influence upon the sediment of these strata. These lines of evidence together support an interpretation of the earthy facies as partly influenced by marine flooding as the early Curtis Sea migrated southwards and into a coastal aeolian system in the south and eastern part of the study area (Fig. 8i, ii), accompanied by the development of the J-3 Unconformity as a ravinement surface (Zuchuat *et al.*, submitted), rather than an unconformity *sensu stricto*. Furthermore, recent studies of tephra layers within its uppermost strata of the Entrada Sandstone in southern Utah provide an Oxfordian depositional date of $160.8 \pm 0.2-0.4$ Ma (Dosset, 2014), rather than the earlier Callovian age suggested by previous workers (Peterson, 1994; Hintze and Kowallis, 2009).

Early Curtis Sea transgression

The oldest sediments of the Curtis Formation developed during the earliest flooding of the earthy facies, and correspond to FA 2 shoreface deposits. The fact that these sedimentary bodies are constrained to certain localities only (Curtis Point (7), Sven's Gulch (9), and Uneva Mine Canyon (14)) can be regarded as evidence for pre-existing relief on the J-3 Unconformity, as palaeo-highs within the Entrada Sandstone acted as interfluvial surfaces that remained unflooded until the subsequent

transgression (Fig. 8ii). The exact nature of these palaeo-highs remains equivocal. Nevertheless, as FA 2 typically overlies deposits of the earthy facies (FA 1b), a purely sedimentary explanation for the existence of palaeo-topography seems unlikely. They could however be linked to pre-transgression, sub-regional folding and tilting episodes, which generated low-amplitude and long wavelength relief.

The transgression continued, and reached areas around Hanksville, which represents the most proximal domain of the study area (Fig. 2, Fig. 8iii). As transgression progressed, the energy of the system diminished and sub-tidal heterolithic successions of FA 3 were deposited. The eastern part of the study area remained unaffected by the marine flooding. Sub-regional uplift episodes, coupled with the erosive nature of the MTS that accompanied deposition of the middle Curtis (Zuchuat *et al.*, 2018; submitted), mean that the western extent of the transgression remains unconstrained.

FA 3a mud-dominated deposits that are more common in the northern parts of the study area represent a tidally influenced distal domain of the Curtis sea, whereas FA 3b coarser grained, sand-dominated strata are concentrated towards the more proximal domain of tidal influence (Fig. 6; Zuchuat *et al.*, 2018). The proximal sediments (FA3b) are characterised by better-sorted and coarser grained deposits compared to the distal setting (FA 3a). While this observation is generally valid, it should be noted that sporadic localities within the more distal domain of the Curtis, such as Cedar Mountain (43), can display a succession dominated by FA 3b sand-dominated deposits. Textural trends such as these that show an increase in the degree of sorting and grain size with increasing proximity to the coastline are in direct contrast to the classical 'coarse- to fine-grained', trend observed within modern-day, tide-dominated environments (Fig. 1; Boyd *et al.*, 1992; Dalrymple *et al.*, 1992; Fan, 2012).

The exclusive occurrence of the gravel-rich dunes and conglomeratic sub-tidal channels at the localities north of Dry Mesa (6) and Last Chance Desert (38, 39) (Fig. 4), may be symptomatic of tidally influenced environments, in which higher energy tidal currents were in operation. Palaeo-current indicators from the lower Curtis (Fig. 6), as well as the generally basinward orientation of these dune foresets, suggest a strong basin-floor ebb-current over the area. The three major upward-shallowing successions (P1, P2, P3) that characterise the lower Curtis, represent parasequences bound by traceable flooding/ravinement surfaces that have resulted from short-lived falls in relative sea-level (Fig. 6, Fig. 10). Traceable erosive surfaces within the parasequence are interpreted as regressive surfaces of marine erosion that testify to rapid relative sea-level falls, accompanied by major basinward shifts of the facies belt across Curtis Basin. The steep tidal incisions (Fig. 3E) developed at the top of the lowermost parasequence (P1) are a consequence of a short-lived relative sea-level drop of decametre magnitude accompanying the second parasequence (P2) (Zuchuat *et al.*, 2018; submitted). The amplitudes of the relative sea-level variations increase up-section such that FA4a proximal, sub- to supratidal sandflat deposits (Fig. 3F), and correlative FA 4b gravel-rich, subtidal channels (Fig. 3G) prograded basinwards during the uppermost parasequence (P3), as a result of the most pronounced relative sea-level fall recorded within the lower Curtis (Fig. 6, Fig. 8iv, and Fig. 10). However, despite increases in the amplitudes of relative sea-level variations during Curtis times, some of the distal parts of the basin directly adjacent to Cedar Mountain (43) (Fig. 11)

were less influenced by relative sea-level variations during the development of Parasequence 3 than their more proximal counterparts, as FA 4b subtidal channels didn't reach these distal areas.

Major Transgression

The top of the lower Curtis is capped by the Major Transgressive Surface (MTS) as a consequence of an abrupt relative sea-level rise which completely flooded the study area (Fig. 8v), and the area as far south as the present day New Mexico border (Zuchuat *et al.*, 2018; submitted). This surface is a complex arrangement of paraconformities and disconformities (Zuchuat *et al.*, 2018; submitted). The area between Interstate 70 (12), Shadscale Mesa (13), and Uneva Mine Canyon (14), as well as Cedar Mountain (43) (Fig. 11), shows evidence of sub-regional, early Oxfordian uplift prior to the Major Transgression (Zuchuat *et al.*, 2018; submitted), as the MTS truncates lower Curtis strata with an angular relationship.

The sediments of FA 5, particularly subaqueous dunes with associated abundant reactivation surfaces, and sandflats with a strong bidirectional current component (Fig. 5e, 5f, 5g, 5h, 5i) are in stark contrast to the underlying lower Curtis strata and suggest a higher energy level within the marine system by middle Curtis times. Grain sizes generally fine toward the coastline and the middle Curtis thickens toward the distal basin (Zuchuat *et al.*, 2018), as is common in many modern-day, tide-dominated environments (Fig. 1; Boyd *et al.*, 1992; Dalrymple *et al.*, 1992; Fan, 2012). The partial flooding of the aeolian dunes of the Slick Rock Member resulted in the reworking of these sediments into the deposits of the Curtis Formation (Dickinson and Gehrels, 2009; 2010).

A distinctive characteristic of the middle Curtis sediments is the absence of traceable stratigraphic surfaces. Such a dramatic shift in sedimentology within an elongated, semi-enclosed basin of this size may be interpreted as the onset of tidal resonance within the Curtis Sea resulting in overprinting of any significant sedimentary response to allocyclic forcing by autocyclic processes (Godin, 1993; Sztanó and de Boer, 1995; Yoshida *et al.*, 2007). Because the system enters tidal resonance, and the signatures of autocyclic processes dominate the sediments, it is impossible to trace a maximum flooding surface (MFS) across localities. However, upward-thinning, and upward-finishing of FA 5 deposits, as well as the overall up-section progradation of the sediments, suggest that a MFS must be located within the lowermost few metres of the middle Curtis.

Curtis Sea Regression

As the Curtis Sea retreated rapidly from the eastern inundated coastal plains, the system saw the concomitant development of a dry aeolian dune system (FA7; Kocurek and Havholm, 1993; Kocurek and Lancaster, 1999; Kocurek, 2003), neighbored by an extensive supratidal flat (FA 8, Fig. 10). The calm and restricted setting for thin FA 6 strata suggests deposition in the proximal and protected zones of the contemporaneous marine system, and FA 5 sediments with metre-scale bedforms were deposited in the distal setting to the west and north (Fig. 7, Fig. 8vi, Fig. 12). The asymmetrical, eastward-pinching FA 5 and FA 6 deposits, overlain by FA 8 supratidal sediments, and the growth of the aeolian dune fields of FA 7 (Moab Member; Fig. 7, Fig. 8vii), suggest rapid coastline progradation, accompanied by increased sediment availability for aeolian transport. As a result, FA 7 thickens

eastwards, and its five distinct aeolian packages may be interpreted as sequences (*sensu* Kocurek 1988) separated by sub- to intertidal deposits in its western parts (Fig. 7, Fig. 10), and by correlative supratidal deposits, as well as by local development of vegetation, towards the present day Utah-Colorado border (Zuchuat *et al.*, 2018). The five sequences of the Moab Member likely reflect humid-arid climatic variations (Kocurek, 1998; Mountney, 2006; 2012) during which episodes of relative base-level fall promoted growth of the aeolian system, and transgressive phases partially inundated and terminated the aeolian dune field. The abrupt termination of dune fields of FA 7 (Fig. 8viii) contrasts with the gradual infill of the contemporaneous marine basin by FA 6 and FA 8, suggesting that a major climatic shift as an explanation for the termination of the dune fields cannot be justified. It is proposed that a final, short-lived marine transgression shut down the sediment supply to the aeolian system, preserved it in its final form, and deposited a thin interval (<1 m) of shallow marine deposits to supratidal deposits, with localised sand stromatolite structures.

The relative influence of autocyclic and allocyclic processes upon the system

Sedimentary and petrophysical data presented here indicate that the Entrada-Curtis-Summerville interval was influenced continuously by allocyclic processes, most notably by relative sea-level variations and climatic changes, but also by sub-regional uplift episodes (Fig. 7, Fig. 9, Fig. 10; Zuchuat *et al.*, submitted). The petrophysical data (Fig. 7) display cyclical patterns within the studied interval without abrupt breaks. The marine influence upon the sediments of the earthy facies, together with the ravinement nature of the J-3 Unconformity (Zuchuat *et al.*, submitted), suggest a near-continuous and “gapless” sedimentary development from the earthy facies of the Entrada Sandstone, through lower Curtis transgressive deposits, into the post-Major-Transgressive middle- and upper Curtis sediments, and associated strata of the Summerville Formation. Consequently, the succession may be used to interpret the relative dominance of allocyclic or autocyclic processes upon sediment dispersal and the preserved strata.

During deposition of the lower Curtis, the system was not in tidal resonance. Consequently the system’s responses to both auto- and allocyclic processes were recorded, as observed at Cedar Mountain (43) (Fig. 11). The heterogeneous energy distribution of the tidal system was responsive to minor changes in basin morphology, influencing the sediment dispersion and bedform development as part of a self-sustained feedback loop (Cecil, 2003; de Boer *et al.*, 2011). Minor current reorganisation was probably responsible for local incisions and/or continuous deposition within each of the three parasequences (Fig. 10), by contrast to regionally significant and regionally traceable stratigraphic surfaces.

The Major Transgression and the resulting Major Transgressive Surface (MTS), which defines the base of the middle Curtis, flooded locations beyond the extent of the present study area (Zuchuat *et al.*, 2018; submitted), and allowed the system to enter a tidally resonant stage. Traceable stratigraphic surfaces generated by allocyclic relative sea-level variations were not preserved, as autocyclic processes dominated the marine system (Figs 6, 7 and 10). However, retreat of the Curtis Sea was accompanied by the development of extensive supra-tidal flats of the Summerville Formation (FA 8), and coastal aeolian systems Moab Member of the Curtis Formation (FA 7). Contrary to the

dominance of autocyclic process acting upon the deposits of the contemporaneous and resonant tide-dominated system, autocyclic processes impacting on FA 7 and FA 8 were strongly influenced and modulated by allocyclic relative sea-level variations and associated climatic oscillations (Fig. 7, Fig. 10; Kocurek and Havholm, 1993; Kocurek, 2003; Mountney, 2006).

In addition to modulating the shape, size and type of bedforms occurring within the supratidal and coastal aeolian systems, allocyclic processes were responsible for the rate at which these sediments were deposited and the cyclic nature of those sediments' arrangement. This is visible in the vertical stacking of the aeolian sequences of the Moab Member, which are terminated by marine flooding in the areas close to the palaeo-coastline, whereas palaeosols and superficial vegetation often developed where the system remained unflooded by these short-lived marine transgressions.

DISCUSSION

The sequence stratigraphic model for the Entrada-Curtis-Summerville interval presented in the study interprets sediments of the Curtis formation to be deposited in a shallow marine to marginal-marine setting with variable tidal influence. The lower Curtis sediments (FA2 – 4) represent early marine transgression of the Curtis Sea in which three parasequences can be correlated over distance by the flooding surfaces that bound them. The sedimentary signature of tidal influence is present within the shallowing upwards successions but it is subordinate to the effects of allocyclic controls upon the sedimentology. The middle Curtis sediments (FA5) represent a significantly higher energy environment. They display evidence of tidal processes, but they lack both wave-related sedimentary structures and surfaces of sequence-stratigraphic significance. These observations are interpreted as the product of an overprinting of allocyclic sedimentary signatures by those of a dominant and localised tidal influence. Consequently, it is concluded that the basin was in a state of tidal resonance during middle Curtis times. The upper Curtis sediments (FA 6 – 8) display stratigraphically significant surfaces that represent marine regression, and the influence of tidal processes upon the sedimentology is subordinate.

It is important to note that similar bedforms to the ones observed in the Curtis Formation (Fig. 5) do occur in other depositional systems in which tidal currents act only as a modulating factor rather than a dominant control upon sedimentary character (Martinius and Gowland, 2011; Baas *et al.*, 2016; Gugliotta *et al.*, 2016). However, because of the lack of any major fluvial systems within the neighbouring and contemporaneous Entrada Sandstone and Summerville Formation, as well as the absence of wave current indicators, a hypothesis of a mixed-energy system for Curtis times is hard to support. The near-exclusively tidally influenced deposits of the Curtis Formation, coupled with a semi-enclosed, elongated basin configuration at the time, suggest that onset of tidal resonance can be regarded as a reasonable hypothesis for the major energy jump accompanying the deposition of the middle Curtis (Sztanó and de Boer's, 1995; Martinus and Gowland, 2011; Roos and Schuttelaars, 2011; Longhitano *et al.*, 2012; Reynaud and Dalrymple, 2012; Shaw *et al.*, 2014). This hypothesis explored further here.

Facies distribution, energy levels, basin geometry and tidal resonance

The sedimentology of the Curtis suggests that energy levels within the Curtis Sea during deposition of the lower Curtis sediments were generally lower than those present during deposition of the middle and upper Curtis sediments. However, the distal to proximal sedimentological trends displayed within the lower Curtis are counter those normally expected within tidally dominated systems (Boyd *et al.*, 1992; Dalrymple *et al.*, 1992; Fan, 2012). They imply a generally consistent average energy level towards the coast at the time of deposition, compared to a spatial and temporal partitioning of energy levels distally (Fig. 12) that promote development of conglomeratic channels and dunes within a finer-grained matrix. This may be explained by a tidal reworking within a confined basin of extra-basinally sourced flash flood deposits (Zuchuat *et al.*, 2018), that may have originated from the neighbouring Uncompahgre uplifted terraces to the east (Otto and Picard, 1976; Scott *et al.*, 2001), and/or from uplifted highlands to the west (Thorman, 2011; Anderson, 2015). Similar gravel- to pebble- to cobble sized conglomeratic bedforms are found in modern tidally influenced and confined basins, such as the Bay of Fundy (Li *et al.*, 2014; Shaw *et al.*, 2014; Todd *et al.*, 2014), the San Francisco Bay (Barnard *et al.*, 2006) or the bay of Brest (Gregoire *et al.*, 2016). Alternatively, conglomeritic channels and dunes may result from the influx of a coarser sediment as short-lived regressive pulses brought material from the proximal part of the basin into distal areas, and regressive pulses are notable during the development of the uppermost parasequence P3 (Zuchuat *et al.*, 2018).

The southwards positive energy gradient, and the presence of sandier and more homogeneous strata within the more proximal parts of the system, may be linked also to tidal amplification as a result of an optimal basin configuration (Godin, 1993; Sztanó and de Boer, 1995; Yoshida *et al.*, 2007) that developed towards the end of lower Curtis times. This may be the pre-cursor to the onset of tidal resonance in middle Curtis times. The physical dimensions of the basin at this time and the subdued nature of the pre-transgression relief by this time (Godin, 1993; Sztanó and de Boer, 1995; Yoshida *et al.*, 2007) may serve to promote resonance.

As the dimensions of the semi-enclosed, fluviially starved Curtis Sea reached approximately 800 km in length, and at least 150 km in width, it is possible to determine whether an amphidromic tidal system (Sztanó and de Boer, 1995) could have developed that may provide an explanation for the sedimentology observed.

The water depth (d) in tidal systems can be determined from the average bedform thickness (h) by (Allen 1968):

$$h = 0.086(d)^{1.19} \quad (1)$$

In the Curtis sediments, bedform thickness h can reach 3 to 4 m, which gives a minimum approximation for the deepest waters of the Curtis Sea in the study area of approximately 20-25 m. The Rossby Deformation Radius (R) for a given palaeo-latitude approximately indicates the required basin width for an amphidromic system to develop (Sztanó and de Boer, 1995):

$$R = \sqrt{g * d} / f \quad (2)$$

where g is the gravitational acceleration (9.81 m/s^2), d is the water depth, and f is the Coriolis coefficient ($8.3651 \times 10^{-5} \text{ rad/s}$ at 35° latitude (after Vallis' (2006) Coriolis coefficient equation; palaeolatitude after Hintze and Kowallis (2009)). The solution to equation (2) is approximately 167.5 km, which is close to the width the Curtis Sea. The calculations imply that an amphidromic system could have developed within the Curtis Sea basin, but the location of the rotational centre of the tidal wave remains unknown and impossible to constrain.

Tidal resonance can develop within a semi-enclosed basin, such as the Gulf of California, the Adriatic Sea, the Persian Gulf, or the Bay of Fundy (Sztanó and de Boer, 1995; Martinius and Gowland, 2011; Roos and Schuttelaars, 2011; Longhitano *et al.*, 2012; Reynaud and Dalrymple, 2012; Shaw *et al.*, 2014), if the length of the embayment approaches an odd multiple of a quarter of the tidal wavelength (Godin, 1993; Sztanó and de Boer's, 1995; Yoshida *et al.*, 2007):

$$L = T * \sqrt{g * d} \quad (3)$$

where L is the tidal wavelength, T is the period of the M2 tide (44712 seconds; Roos and Schuttelaars, 2011), g is the gravitational acceleration (9.81 m/s^2), and d is the water depth. However, such resonant behaviour depends also upon the basal shear stresses and the subaqueous morphology of the tidal system (Roos and Schuttelaars, 2011; Wang *et al.*, 2014).

For water depths d of approximately 20 m and 25 m (equation 1), the tidal wavelength L approaches approximately 625 km, or 700 km respectively, which gives a quarter wavelength of approximately 156 km or 175 km, respectively. As these values are approximately one fifth of the total length of the Curtis Sea, tidal resonance could have developed within the basin and may provide some explanation for the variation in sedimentology observed throughout Curtis times.

The phenomenon of resonance may have been triggered by the Major Transgression at the base of the middle Curtis, the regional extent and abrupt nature of which may be linked to an allocyclic, orbitally-forced, relative sea-level rise during the lower Oxfordian Age (Boulila *et al.*, 2010; Boulila *et al.*, 2012; Strasser *et al.*, 2012; Pellenard *et al.*, 2014). The resultant tidally resonant system, as the middle and upper Curtis were being deposited, was dominated by autocyclic interactions, which overprinted the stratigraphic signatures of most of Lower Oxfordian, allocyclic relative sea-level variations (Boulila *et al.*, 2010; Boulila *et al.*, 2012; Strasser *et al.*, 2012; Pellenard *et al.*, 2014).

Causes of cyclicity

A lack of precise dating constraints within the shallow marine, supratidal, and aeolian deposits of the studied area and their local equivalents prevents an analysis of cycle wavelength. However, 405 and 100 kyr, orbitally forced eccentricity cycles have been documented within the Tethyan Ocean during the Callovian and Oxfordian ages, within which $\delta^{18}\text{O}$ isotopic data indicate a cooling event during the Upper Callovian Age (Boulila *et al.*, 2010; Boulila *et al.*, 2012; Strasser *et al.*, 2012; Pellenard *et al.*, 2014). Such a cooling episode, accompanied by increased sediment available for wind transport, may explain the growth and demise of the Entrada aeolian system. Consequently, it may be suggested that sedimentary cycles recorded in the Entrada Sandstone, the lower Curtis, the Moab Member of

the Curtis Formation, and the Summerville Formation (Fig. 7 Fig. 10), may be related to one (or both) of these two Milankovitch cycles. However, the exact nature of relative sea-level variations remains uncertain.

Short-lived episodes of tectonic uplift have accompanied deposition of parts of the Entrada-Curtis-Summerville interval, which may have impacted upon relative sea-level within the basin (Zuchuat *et al.*, 2018; submitted). Furthermore, debate persists over whether the eccentricity cycles lead to small-scale, glacio-eustatic sea-level variations (Dromart *et al.*, 2003; Wierzbowski *et al.*, 2009; Donnadiou *et al.*, 2011; Alberti *et al.*, 2012; Chumakov *et al.*, 2014), or whether these sea-level variations are due to orbitally-forced cycles, of thermal water expansion and/or ground-water recharge (Schulz and Schäfer-Neth, 1997; Boulila *et al.*, 2012).

The amplitude of the relative sea-level variations also remains unconstrained. However, tidal incision at Sven's Gulch (9) (Fig. 3E), suggests relative sea-level variations of the order of one decametre. This magnitude matches estimations of the amplitudes of relative sea-level variations within a Mesozoic greenhouse period, driven by 100 or 405 kyr eccentricity cycles (Aurell and Bádenas, 2004; Boulila *et al.*, 2010; Boulila *et al.*, 2012; Strasser *et al.*, 2012; Pellenard *et al.*, 2014). Consequently, as nine relative sea-level cycles were recorded within the Curtis Formation (Fig. 10), it is possible to bracket the time encapsulated within the Curtis Formation to between approximately 0.9 and 3.6 Ma.

CONCLUSION

The sediments of the Upper Jurassic Curtis formation of the Colorado Plateau, Utah, USA, were deposited in a shallow-marine to marginal-marine, tidally dominated environment that responded to allocyclicly controlled fluctuations in relative sea level. Evidence of a strong tidal dominance on deposition includes bi-directional ripple cross-stratified silt- to sandstone strata, as well as cross-stratified and heterolithic sandstone with flaser bedding, both of which are often arranged in cyclical tidal bundles. Tidal dominance is emphasised by a lack of fluvial influence from contemporary and neighbouring systems, and a lack of wave influence within the elongate and protected basin.

The lower Curtis sediments represent early transgression of the Curtis Sea and are generally contemporaneous with the neighbouring wet interdune to coastal sabkha sediments of earthy facies of Entrada sandstone. The lower - middle Curtis boundary represents the onset of major transgression. The middle and upper Curtis units, along with the contemporaneous deposits of the Moab Member of the Curtis Formation and Summerville Formation, represent post-major transgression deposition.

Major stratigraphic surfaces (flooding surfaces, ravinement surfaces, and regressive surfaces of marine erosion) are traceable through sediments of the lower Curtis, sediments of the upper Curtis and sediments of their correlative continental equivalents. These surfaces are related to oscillations in relative sea level that may be connected to 100 and or 405 kyr Milankovitch cycles, although the exact causes remain equivocal. The surfaces divide the sedimentary succession into a number of packages that are governed by allo-control, but that display internal sedimentology dominated by tidal processes.

Sediments of the middle Curtis unit are characterised exclusively by tidal facies and a lack of correlatable stratigraphic surfaces. These sediments are interpreted as representing the onset of tidal amplification by resonance within the Curtis Sea. The signatures of allocyclic processes within the sediments are overprinted by those of tidal currents, despite their presence in neighbouring contemporaneous deposits outside of the shallow marine realm.

The study demonstrates that, given the right sedimentary basin geometry and conditions, the normally dominant allocyclic signatures within shallow marine sediments that are related to relative sea level oscillations may be overprinted and obscured by the usually subordinate localised autocyclic processes of the marine system, such as tides. As a consequence, the study highlights the importance of studying shallow marine strata in the context of the deposits of their neighbouring and contemporaneous environments, particularly in settings where the marine basin forms a small and protected embayment.

Acknowledgements

The authors of this paper would like to thank the Norwegian Research Council for their awarded COPASS grant 244049. Acknowledgements are to be extended to Dr Hannah L. Brooks, Dr Mark Mulrooney, and Anna v. Yperen for their assistance and fruitful comments, which enhanced the quality of this work. Reviewers 1 and 2 are to be sincerely acknowledged for their constructive observations and remarks.

REFERENCES

- Ahokas, J.M., Nystuen, J.P., and Martinius, A.W. (2014). Depositional dynamics and sequence development in a tide-influenced marginal marine basin: Early Jurassic Neill Klinter Group, Jameson Land Basin, East Greenland. *In: Martinius, A.W., Ravnas, R., Howell, J., Steel, R.J., & Wonham, J. (eds.), From depositional systems to sedimentary successions on the Norwegian continental margin. IAS Special Publication, 46, 291-338.*
- Alberti, M., Fürsich, F.T., and Pandey, D.K. (2012). The Oxfordian stable isotope record ($\delta^{18}\text{O}$, $\delta^{13}\text{C}$) of belemnites, brachiopods, and oysters from the Kachchh Basin (western India) and its potential for palaeoecologic, palaeoclimatic, and palaeogeographic reconstructions. *Palaeogeography, Palaeoclimatology, Palaeoecology, 344, 49-68.*
- Allen, J.R.L. (1968). The nature and origin of bed-form hierarchies. *Sedimentology, 10(3), 161-182.*
- Anderson, T.H. (2015). Jurassic (170–150 Ma) basins: The tracks of a continental-scale fault, the Mexico-Alaska megashear, from the Gulf of Mexico to Alaska. *In: Anderson, T.H., Didenko, A.N., Johnson, C.L., Khanchuk, A.I., and MacDonald, J.H., (eds.), Late Jurassic Margin of Laurasia – A Record of Faulting Accommodating Plate Rotation. Geological Society of America Special Papers, 513, 107-188.*
- Anderson, O.J. and Lucas, S.G. (1994). Middle Jurassic stratigraphy, sedimentation and paleogeography in the southern Colorado Plateau and southern High Plains. *In: Caputo, M.V., Peterson, J.A. and Franczyk, K.J., (eds.), Mesozoic Systems of the Rocky Mountain Region, USA. The Rocky Mountain Section SEPM (Society for Sedimentary Geology), Denver, 299-314.*
- Aurell, M., and Bádenas, B. (2004). Facies and depositional sequence evolution controlled by high-frequency sea-level changes in a shallow-water carbonate ramp (late Kimmeridgian, NE Spain). *Geological Magazine, 141(6), 717-733.*
- Barnard, P.L., Hanes, D.M., Rubin, D.M., and Kvittek, R.G. (2006). Giant sand waves at the mouth of San Francisco Bay. *Eos, Transactions American Geophysical Union, 87(29), 285-289.*
- Baas, J.H., Best, J.L., and Peakall, J. (2016). Predicting bedforms and primary current stratification in cohesive mixtures of mud and sand. *Journal of the Geological Society, 173(1), 12-45.*
- Bjerrum, C.J. and Dorsey, R.J. (1995) Tectonic controls on deposition of Middle Jurassic strata in a retroarc foreland basin, Utah-Idaho trough, western interior, United States. *Tectonics, 14(4), 962-978.*
- de Boer, W.P., Roos, P.C., Hulscher, S.J., and Stolk, A. (2011). An idealized model of tidal dynamics in semi-enclosed basins: The effects of a mega-scale sand extraction trench in the North Sea. *Coastal Engineering Proceedings, 1(32), 1-7.*
- Boyd, R., Dalrymple, R., and Zaitlin, B.A. (1992). Classification of clastic coastal depositional environments. *Sedimentary Geology, 80(3-4), 139-150.*

- Bostock, J., and Riley, H.T. (1855). Pliny the Elder. *The Natural History*, 16:1(2).
- Boulila, S., Galbrun, B., Hinnov, L.A., Collin, P.Y., Ogg, J.G., Fortwengler, D., and Marchand, D. (2010). Milankovitch and sub-Milankovitch forcing of the Oxfordian (Late Jurassic) terres noires formation (SE France) and global implications. *Basin Research*, 22(5), 717-732.
- Boulila, S., Galbrun, B., Miller, K.G., Pekar, S.F., Browning, J.V., Laskar, J., and Wright, J.D. (2011). On the origin of Cenozoic and Mesozoic “third-order” eustatic sequences. *Earth-Science Reviews*, 109(3-4), 94-112.
- Brenner, R.L. and Peterson, J.A. (1994). Jurassic sedimentary history of the northern portion of the Western Interior Seaway, USA. In: Caputo, M.V., Peterson, J.A. and Franczyk, K.J., (eds.), *Mesozoic Systems of the Rocky Mountain Region, USA*. The Rocky Mountain Section SEPM (Society for Sedimentary Geology), Denver, 233-272.
- Bonaventura, X., Sima, A.A., Feixas, M., Buckley, S.J., Sbert, M., and Howell, J.A. (2017). Information measures for terrain visualization. *Computers & Geosciences*, 99, 9-18.
- Buckley, S., Ringdal, K., Dolva, B., Naumann, N., and Kurz, T. (2017). LIME: 3D visualisation and interpretation of virtual geoscience models. *EGU General Assembly Conference Abstracts*, 19, p. 15952.
- Bump, A.P. and Davis, G.H. (2003). Late Cretaceous – early Tertiary Laramide deformation of the northern Colorado Plateau, Utah and Colorado. *Journal of Structural Geology*, 25(3), 421-440.
- Caputo, M.V. and Pryor, W.A. (1991). Middle Jurassic tide- and wave-influenced coastal facies and paleogeography, upper San Rafael Group, east-central Utah. *Utah Geological Association*, 19, 9-27.
- Catuneanu O. (2006). *Principles of Sequence Stratigraphy*. Amsterdam, Elsevier, 1-375.
- Catuneanu, O., Abreu, V., Bhattacharya, J.P., Blum, M.D., Dalrymple, R.W., Eriksson, P.G., Fielding, C.R., Fisher, W.L., Galloway, W.E., Gibling, M.R., Giles, K.A., Holbrook, J.M., Jordan, R., Kendall, C.G.St.C, Macurda, B., Martinsen, O.J., Mial, A.D., Neal, J.E., Nummedal, D., Pomar, L., Posamentier, H.W., Pratt, B.R., Sarg, J.F., Shanley, K.W., Steel, R.J., Strasser, A., Tucker, M.E., and Winker, C. (2009). Towards the standardization of sequence stratigraphy. *Earth-Science Reviews*, 92(1), 1-33.
- Carr-Crabaugh, M. and Kocurek, G. (1998). Continental sequence stratigraphy of a wet eolian system: a key to relative sea-level change. *Society for Sedimentary Geology, Special Publication*, 59, 213-228.
- Cecil, C.B. 2003. The concept of autocyclic and allocyclic controls on sedimentation and stratigraphy, emphasizing the climatic variable. In: Cecil, C.B., Edgar, N.T. (eds.), *Climate Controls on Stratigraphy, SEPM (Society for Sedimentary Geology) Special Publication*, 77, 13-20.
- Chumakov, N.M., Zakharov, V.A., and Rogov, M.A. (2014). Did an ice sheet exist in Northeast Asia at the Middle-Late Jurassic boundary? (Critical remarks on the article by Y. Donnadiou et al.(2011)“A

mechanism for brief glacial episodes in the Mesozoic greenhouse"). *Stratigraphy and Geological Correlation*, 22(6), 655-658.

Crabaugh, M., and Kocurek, G. (1993). Entrada Sandstone—an example of a wet eolian system. In: Pye, K., (eds.), *The dynamics and environmental context of eolian sedimentary systems*. London Geological Society Special Publications, 72, 103-126.

Condon, S.M., and Huffman Jr, A.C. (1988). Revisions in nomenclature of the middle Jurassic Wanakah Formation, northwestern New Mexico and northeastern Arizona. *U.S. Geological Survey Bulletin*, 1633-A, A1-A12.

Dalrymple, R.W., Zaitlin, B.A., and Boyd, R. (1992). Estuarine facies models: conceptual basis and stratigraphic implications: perspective. *Journal of Sedimentary Research*, 62(6), 1130-1146.

Dickinson, W.R., and Gehrels, G.E. (2009). U-Pb ages of detrital zircons in Jurassic eolian and associated sandstones of the Colorado Plateau—evidence for transcontinental dispersal and intraregional recycling of sediment. *Geological Society of America Bulletin*, 121(3-4), 408-433.

Dickinson, W.R., and Gehrels, G.E. (2010). Insights into North American paleogeography and paleotectonics from U–Pb ages of detrital zircons in Mesozoic strata of the Colorado Plateau, USA. *International Journal of Earth Sciences*, 99(6), 1247-1265.

Doelling, H.H. (2001). *Geologic map of the Moab and eastern part of the San Rafael Desert 30' x 60' quadrangles, Grand and Emery Counties, Utah, and Mesa County, Colorado*. Utah Geological Survey Map 180, 3 plates, scale 1:100,000.

Doelling, H.H., Kuehne, P.A., Willis, G.C., and Ehler, J.B. (2015). *Geologic map of the San Rafael Desert 30' x 60' quadrangle, Emery and Grand Counties, Utah*. Utah Geological Survey, Map 267DM, scale 1:62,500.

Donnadieu, Y., Dromart, G., Godd ris, Y., Puc at, E., Brigaud, B., Dera, G., Dumas, C., and Olivier, N. (2011). A mechanism for brief glacial episodes in the Mesozoic greenhouse. *Paleoceanography and Paleoclimatology*, 26(3), 1-10.

Dossett, T. S. (2014). *The first 40Ar/39Ar ages and tephrochronologic framework for the Jurassic Entrada Sandstone in central Utah*. Brigham Young University, Utah, master thesis, 1-46.

Dromart, G., Garcia, J.P., Picard, S., Atrops, F., L cuyer, C., and Sheppard, S.M.F. (2003). Ice age at the Middle–Late Jurassic transition?. *Earth and Planetary Science Letters*, 213(3-4), 205-220.

Fan, D. (2012). Open-coast tidal flats. In: Davis, R.A., Jr., and Dalrymple, R.W., (eds.), *Principles of tidal sedimentology*. Dordrecht, Netherlands, Springer Science and Business Media, 187–229.

Fertl, W.H., Chilingarian, G.V., and Yen, T.F. (1982). Use of natural gamma ray spectral logging in evaluation of clay minerals. *Energy Sources*, 6(4), 335-360.

- Getty, P.R., and Hagadorn, J.W. (2009). Palaeobiology of the *Climactichnites* tracemaker. *Palaeontology*, 52(4), 753-778.
- Gilluly, J. and Reeside Jr., J.B. (1928). Sedimentary rocks of the San Rafael Swell and some adjacent areas in eastern Utah. *U.S. Geological Survey, Professional Paper*, 150-D, 61-110.
- Godin, G. (1993). On tidal resonance. *Continental Shelf Research*, 13(1), 89-107.
- Gregoire, G., Ehrhold, A., Le Roy, P., Jouet, G., and Garlan, T. (2016). Modern morpho-sedimentological patterns in a tide-dominated estuary system: the Bay of Brest (west Brittany, France). *Journal of Maps*, 12(5), 1152-1159.
- Gugliotta, M., Flint, S.S., Hodgson, D.M., and Veiga, G.D. (2016). Recognition criteria, characteristics and implications of the fluvial to marine transition zone in ancient deltaic deposits (Lajas Formation, Argentina). *Sedimentology*, 63(7), 1971-2001.
- Halland, E.K., Bjørnstad, A., Magnus, C., Riis, F., Meling, I.M., Tørneng Gjeldvik, I., Tappel, I.M., Mujezinović, J., Bjørheim M., Rød, R.S., and Pham, V.T.H. (2014). *CO₂ storage atlas—Norwegian continental shelf*. Stavanger, Norway, Norwegian Petroleum Directorate.
- Haq, B.U., Hardenbol, J., and Vail, P.R. (1987). Chronology of fluctuating sea levels since the Triassic. *Science*, 235(4793), 1156-1167.
- Heyman, O.G. (1983). Distribution and structural geometry of faults and folds along the northwestern Uncompahgre uplift, western Colorado and eastern Utah. In: Averett, W. (ed), *Northern Paradox Basin-Uncompahgre uplift. Grand Junction Geological Society field trip*, 45-57.
- Hintze, L.F. and Kowallis, B.J. (2009). *Geologic history of Utah*. Provo, Utah, Brigham Young University Studies. 225 pp.
- Imlay, R.W. (1947). Marine Jurassic of Black Hills Area, South Dakota and Wyoming. *American Association of Petroleum Geologists Bulletin*, 31(2), 227-273.
- Imlay, R. W. (1952). Marine origin of Preuss sandstone of Idaho, Wyoming, and Utah. *American Association of Petroleum Geologists Bulletin*, 36(9), 1735-1753.
- Imlay, R.W. (1980). Jurassic paleobiogeography of the conterminous United States in its continental setting. *U.S. Geological Survey Professional Paper*, 1062, 1-134.
- Kocurek, G. (1988). First-order and super bounding surfaces in eolian sequences—bounding surfaces revisited. *Sedimentary Geology*, 56(1-4), 193-206.
- Kocurek, G. 2003. Limits on extreme eolian systems: Shara of Mauritania and Jurassic Navajo Sandstone examples. In: Chan, M.A., Archer, A.W. (eds.), *Extreme depositional environments: mega end members in geologic time. Geological Society of America Special Paper*, 370, 43-52.

Kocurek, G., and Havholm, K.G. (1993). Eolian sequence stratigraphy: A conceptual framework. *In: Weimer, P., & Posamentier, H.W., (eds.), Siliciclastic Sequence Stratigraphy: Recent Developments and Applications, American Association of Petroleum Geologists, Memoir, 58, 393–410.*

Kocurek, G., and Lancaster, N. (1999). Aeolian system sediment state: theory and Mojave Desert Kelso dune field example. *Sedimentology, 46(3), 505-515.*

Kocurek, G., Martindale, R.C., Day, M., Goudge, T.A., Kerans, C., Hassenruck-Gudipati, H.J., Mason, J., Cardenas, B.T., Petersen, E., Mohrig, D., Aylward, D.S., Hughes, C.M., and Nazworth, C.M. (in press). Antecedent aeolian dune topographic control on carbonate and evaporite facies: Middle Jurassic Todilto Member, Wanakah Formation, Ghost Ranch, New Mexico, USA. *Sedimentology.*

Kreisa, R.D. and Moiola, R.J. (1986). Sigmoidal tidal bundles and other tide-generated sedimentary structures of the Curtis Formation, Utah. *Geological Society of America Bulletin, 97(4), 381-387.*

Kvale, E.P. (2012). Tidal constituents of modern and ancient tidal rhythmites: criteria for recognition and analyses. *In: Davis, R.A., Jr., and Dalrymple, R.W., (eds.), Principles of Tidal Sedimentology.* Springer Science and Business Media, Dordrecht, Netherlands, 1-17.

Kyrkjebø, R., Gabrielsen, R.H. and Faleide, J.I. (2004). Unconformities related to the Jurassic–Cretaceous synrift–post-rift transition of the northern North Sea. *Journal of the Geological Society, 161(1), 1-17.*

Levander, A., Schmandt, B., Miller, M.S., Liu, K., Karlstrom, K.E., Crow, R.S., Lee, C.-T.A., and Humphreys, E.D. (2011). Continuing Colorado plateau uplift by delamination-style convective lithospheric downwelling. *Nature, 472(7344), 461-465.*

Li, M.Z., Shaw, J., Todd, B.J., Kostylev, V.E., and Wu, Y. (2014). Sediment transport and development of banner banks and sandwaves in an extreme tidal system: Upper Bay of Fundy, Canada. *Continental Shelf Research, 33, 86-107.*

Longhitano, S.G., Mellere, D., Steel, R.J., and Ainsworth, R.B. (2012). Tidal depositional systems in the rock record: a review and new insights. *Sedimentary Geology, 279, 2-22.*

Lucas, S.G. (2014). Lithostratigraphy of the Jurassic San Rafael Group from Bluff to the Abajo Mountains, southeastern Utah: Stratigraphic relationships of the Bluff Sandstone. *Volumina Jurassica, 12, 55-68.*

Mansfield, G.R., and Roundy, P.V. (1916). Revision of the Beckwith and Bear River Formations of southeastern Idaho. *U.S. Geological Survey Professional Paper, 98, 75-84.*

Martinius, A.W., and Gowland, S. (2011). Tide-influenced fluvial bedforms and tidal bore deposits (late Jurassic Lourinhã Formation, Lusitanian Basin, Western Portugal). *Sedimentology, 58(1), 285-324.*

- Martinius, A.W., Ringrose, P.S., Brostrøm, C., Elfenbein, C., Næss, A., and Ringås, J.E. (2005). Reservoir challenges of heterolithic tidal sandstone reservoirs in the Halten Terrace, mid-Norway. *Petroleum Geoscience*, 11(1), 3-16.
- McMullen, S.K., Holland, S.M., and O'Keefe, F.R. (2014). The occurrence of vertebrate and invertebrate fossils in a sequence stratigraphic context: the Jurassic Sundance Formation, Bighorn Basin, Wyoming, USA. *Palaios*, 29(6), 277-294.
- Midtkandal, I., and Nystuen, J.P. (2009). Depositional architecture of a low-gradient ramp shelf in an epicontinental sea: the lower Cretaceous of Svalbard. *Basin Research*, 21(5), 655-675.
- Mitchum, R.J., Vail, P.R., and Thompson, S. III. (1977) The depositional sequence as a basic unit for stratigraphic analysis. In: Payton, C.E., (ed.), *Seismic Stratigraphy: Applications to Hydrocarbon Exploration, American Association of Petroleum Geologists Memoir*, 26, 205-212.
- Mountney, N.P. (2006). Periodic accumulation and destruction of aeolian erg sequences in the Permian Cedar Mesa Sandstone, White Canyon, southern Utah, USA. *Sedimentology*, 53(4), 789-823.
- Mountney, N.P. (2012). A stratigraphic model to account for complexity in aeolian dune and interdune successions. *Sedimentology*, 59(3), 964-989.
- Murray, K.E., Reiners, P.W., and Thomson, S.N. (2016). Rapid Pliocene–Pleistocene erosion of the central Colorado Plateau documented by apatite thermochronology from the Henry Mountains. *Geology*, 44(6), 483-486.
- Nelson, S.T. (1997). Reevaluation of the Central Colorado plateau laccoliths in the light of new age determination. *U.S. Geological Survey Bulletin*, 2158, 37-9.
- Nuccio, V.F., and Condon, S.M. (1996). Burial and thermal history of the Paradox Basin, Utah and Colorado, and petroleum potential of the Middle Pennsylvanian Paradox Formation. *U.S. Geological Survey Bulletin*, 41, 57-76
- Ogg, J.G., Ogg, G., and Gradstein, F. M. (2016). *A Concise Geologic Time Scale: 2016*. Elsevier.
- Otto, E.P., and Picard, M.D. (1976). Petrology of the Entrada Sandstone (Jurassic), northeastern Utah. In: Hill, J.G., (ed), *Geology of the Cordilleran hingeline*. Rocky Mountain Association of Petroleum Geologists Guidebook, 231-259.
- Pellenard, P., Tramoy, R., Pucéat, E., Huret, E., Martinez, M., Bruneau, L., & Thierry, J. (2014). Carbon cycle and sea-water palaeotemperature evolution at the Middle–Late Jurassic transition, eastern Paris Basin (France). *Marine and Petroleum Geology*, 53, 30-43.
- Peterson, F. (1994). Sand dunes, sabkhas, streams, and shallow seas: Jurassic paleogeography in the southern part of the Western Interior Basin. In: Caputo, M.V., Peterson, J.A. and Franczyk, K.J., (eds.), *Mesozoic Systems of the Rocky Mountain Region, USA*. The Rocky Mountain Section SEPM (Society for Sedimentary Geology), Denver, 233-272.

- Peterson, F. and Pippingos, G.N. (1979). Stratigraphic relations of the Navajo Sandstone to Middle Jurassic formations, southern Utah and northern Arizona. *U.S. Geological Survey Professional Paper* 1035-B, 1-43.
- Petrie, E.S., Sundal, A., Gutierrez, M., and Braathen, A. (2017). Deformation band formation and reactivation associated with a Laramide fault propagation fold (abs.). *Geological Society of America Abstract with Programs*, 49(6), 289-299.
- Pippingos, G.N. and O'Sullivan, R.B. (1978). Principal unconformities in Triassic and Jurassic rocks, western interior United States: a preliminary survey. *U.S. Geological Survey, Professional Paper*, 1035-A, 1-29.
- Pippingos, G.N., and Imlay, R.W. (1979). Lithology and subdivisions of the Jurassic Stump Formation in southeastern Idaho and adjoining areas. *U.S. Geological Survey Professional Paper*, 1035-C, 1-25.
- Reynaud, J.Y., and Dalrymple, R.W. (2012). Shallow-marine tidal deposits. In: Davis, R.A., Jr., and Dalrymple, R.W., (eds.), *Principles of Tidal Sedimentology*. Springer Science and Business Media, Dordrecht, Netherlands, 335-369.
- Roos, P.C., and Schuttelaars, H.M. (2011). Influence of topography on tide propagation and amplification in semi-enclosed basins. *Ocean Dynamics*, 61(1), 21-38.
- Schulz, M., and Schäfer-Neth, C. (1997). Translating Milankovitch climate forcing into eustatic fluctuations via thermal deep water expansion: a conceptual link. *Terra Nova*, 9(5-6), 228-231.
- Scott, R.B., Harding, A.E., Hood, W.C., Cole, R.D., Livaccari, R.F., Johnson, J.B., Shroba, R.R., and Dickerson, R.P. (2001). *Geologic map of Colorado National Monument and adjacent areas, Mesa County, Colorado*. U.S. Geological Map I-2740, 40 p., 1 plate, scale 1:24,000.
- Shaw, J., Todd, B.J., and Li, M.Z. (2014). Geologic insights from multibeam bathymetry and seascape maps of the Bay of Fundy, Canada. *Continental Shelf Research*, 34, 53-63.
- Sprinkel, D.A., Doelling, H.H., Kowallis, B.J., Waanders, G., and Kuehne, P.A. (2011). Early results of a study of Middle Jurassic strata in the Sevier fold and thrust belt, Utah. In: Sprinkel, D.A., Yonkee, W.A., and Chidsey, T.C., Jr., (eds.), *Sevier Thrust Belt: Northern and Central Utah and Adjacent Areas*. *Utah Geological Association, Publication*, 40, 151-172.
- Strasser, A., Vedin, S., and Stienne, N. (2012). Rate and synchronicity of environmental changes on a shallow carbonate platform (Late Oxfordian, Swiss Jura Mountains). *Sedimentology*, 59(1), 185-211.
- Sullivan, K.R., Kowallis, B.J., and Mehnert, H.H. (1991). Isotopic ages of igneous intrusions in southeastern Utah – Evidence for a mid-Cenozoic Reno–San Juan magmatic zone. *Brigham Young University Geology Studies*, 37, 139-144.

Svendsen, J.B., and Hartley, N.R. (2001). Comparison between outcrop-spectral gamma ray logging and whole rock geochemistry: Implications for quantitative reservoir characterisation in continental sequences. *Marine and Petroleum Geology*, 18(6), 657-670.

Sztanó, O., and de Boer, P.L. (1995). Basin dimensions and morphology as controls on amplification of tidal motions (the Early Miocene North Hungarian Bay). *Sedimentology*, 42(4), 665-682.

Tape, C.H., Cowan, C.A., and Runkel, A.C. (2003). Tidal-bundle sequences in the Jordan Sandstone (Upper Cambrian), southeastern Minnesota, USA: evidence for tides along inboard shorelines of the Sauk epicontinental sea. *Journal of Sedimentary Research*, 73(3), 354-366.

Thorman, C.H. (2011). The Elko orogeny – A major tectonic event in eastern Nevada–western Utah. In: Sprinkel, D.A., Yonkee, W.A., and Chidsey, T.C., Jr., (eds.), *Sevier Thrust Belt: Northern and Central Utah and Adjacent Areas*. *Utah Geological Association Publication*, 40, 117-129.

Todd, B.J., Shaw, J., Li, M.Z., Kostylev, V.E., and Wu, Y. (2014). Distribution of subtidal sedimentary bedforms in a macrotidal setting: The Bay of Fundy, Atlantic Canada. *Continental Shelf Research*, 83, 64-85.

Trudgill, B. D. (2011). Evolution of salt structures in the northern Paradox Basin: Controls on evaporite deposition, salt wall growth and supra - salt stratigraphic architecture. *Basin Research*, 23(2), 208-238.

Valenza, J.M. (2016). Redbeds of the Upper Entrada Sandstone, Central Utah: Facies Analysis and Regional Implications of Interfingered Sabkha and Fluvial Terminal Splay Sediments. Brigham Young University, Utah, master thesis, 1-54.

Vallis, G.K. (2017). *Atmospheric and oceanic fluid dynamics*. Cambridge University Press. 745 pp.

Wang, P. (2012). Principles of Sediment Transport Applicable in Tidal Environments. In: Davis, R.A., Jr., and Dalrymple, R.W., (eds.), *Principles of Tidal Sedimentology*. Springer Science and Business Media, Dordrecht, Netherlands, 19-34.

Wang, D., Liu, Q., and Lv, X. (2014). A study on bottom friction coefficient in the Bohai, Yellow, and East China Sea. *Mathematical Problems in Engineering*, 2014, 1-7.

Westoby, M.J., Brasington, J., Glasser, N.F., Hambrey, M.J., and Reynolds, J.M. (2012). 'Structure-from-Motion' photogrammetry: A low-cost, effective tool for geoscience applications. *Geomorphology*, 179, 300-314.

Wilcox, W.T. and Currie, B. (2008). Sequence Stratigraphy of the Jurassic Curtis, Summerville, and Stump Formations, Eastern Utah and Northwest Colorado. In: Longman, M.W. and Morgan, C.D., (eds.), *Hydrocarbon Systems and Production in the Uinta Basin, Utah*. *Rocky Mountain Association of Geologists and Utah Geological Association Publication*, 37, 9-41.

Witkind, I.J. (1988). *Geologic map of the Huntington 30' X 60' quadrangle, Carbon, Emery, Grand, and Uintah Counties, Utah*. U.S. Geological Survey, Miscellaneous Investigations Series Map I-1764, scale 1:100,000.

Wierzbowski, H., Dembicz, K., and Praszker, T. (2009). Oxygen and carbon isotope composition of Callovian–Lower Oxfordian (Middle–Upper Jurassic) belemnite rostra from central Poland: A record of a Late Callovian global sea-level rise? *Palaeogeography, Palaeoclimatology, Palaeoecology*, 283(3-4), 182-194.

Yonkee, W.A. and Weil, A.B. (2015). Tectonic evolution of the Sevier and Laramide belts within the North American Cordillera orogenic system. *Earth-Science Reviews*, 150, 531-593.

Yoshida, S., Johnson, H.D., Pye, K., and Dixon, R.J. (2004). Transgressive changes from tidal estuarine to marine embayment depositional systems: The Lower Cretaceous Woburn Sands of southern England and comparison with Holocene analogs. *American Association of Petroleum Geologists Bulletin*, 88(10), 1433-1460.

Yoshida, S., Steel, R.J., and Dalrymple, R.W. (2007). Changes in depositional processes—an ingredient in a new generation of sequence-stratigraphic models. *Journal of Sedimentary Research*, 77(6), 447-460.

Zuchuat, V., Sleveland, A.R.N., Sprinkel, D.A., Rimkus, A., Braathen, A., and Midtkandal, I. (2018). New insights on the impact of tidal currents on a low-gradient, semi-enclosed, epicontinental basin—the Curtis Formation, east-central Utah, USA: *Geology of the Intermountain West*, 5, 131-165.

Zuchuat, V., Midtkandal, I., Poyatos-Moré, M., da Costa, S., Halvorsen, K., Cote N., Sundal, A., Braathen, A. (submitted to *The Journal of Sedimentary Research*). Composite Unconformities in Low-Gradient Transitional Settings: the J-3 Unconformity and the Curtis Formation, East-Central Utah, USA.

FIGURES

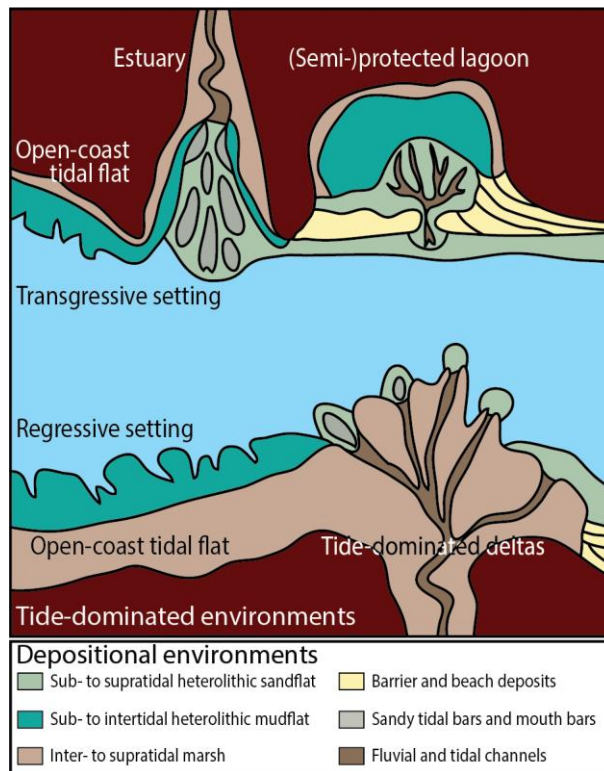


Fig. 1 – Modern day, tide-dominated coastline (modified from Fan, 2012).

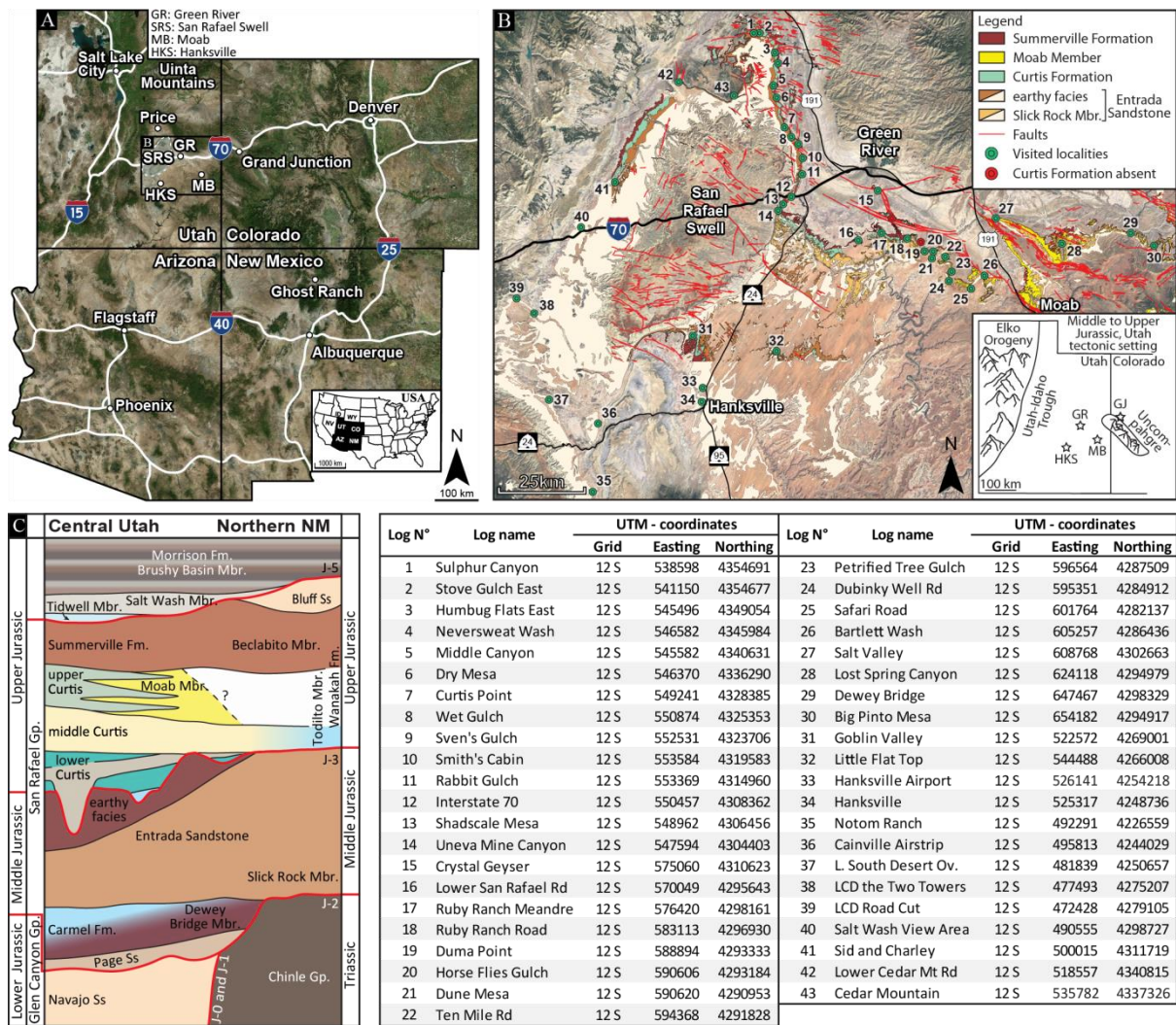


Fig. 2 – A-B. Maps of the study area. Green dots represent visited localities where the Curtis Formation crops out, while the red dots illustrate its absence. Each code number on the map refers to a specific locality in the attached table (Geological units after Hintze, 1980; Witkind, 1988; Doelling, 2001; and Doelling *et al.*, 2015; Tectonic setting after Heyman, 1983; Thorman, 2011). GJ: Grand Junction, GR: Green River, HKS: Hanksville, MB: Moab, SRS: San Rafael Swell. **C.** Schematic lithostratigraphic column showing a correlation between the San Rafael Swell area, east-central Utah, and Ghost Ranch, in northern New Mexico (Doelling, 2001; Doelling *et al.*, 2015; Zuchuat *et al.*, 2018; Kocurek *et al.*, in press). Note that the contemporaneous character between the Entrada Sandstone and the lower Curtis, as well as between the middle Curtis, upper Curtis, Moab Member, and Summerville Formation is not shown in this lithostratigraphic display.

TABLE 1 - FACIES DESCRIPTION FOR THE ENTRADA SANDSTONE, CURTIS FORMATION AND SUMMERSVILLE FORMATION

Facies	Description	Structures	Grain	Interpretation	Formation
A	Cross-stratified sandstone	Unidirectional tangential cross-bedded v-f graded sandstone, alternating grain flow and grain fall deposits, sharp base, rusty red or white, locally bleached, local occurrence of rhizoliths, varying bedform/bedform sets size, maximum individual dune thickness 15 m. Potential occurrence of counter-ripples at the toe of the foresets.	VF - F	Aeolian dune deposits, locally influenced by a dynamic and migrating water table/saturated level.	Entrada Ss Moab Mbr.
B	Plane parallel laminated to mottled mudstone with localized evaporites	Dark, red silty mudstone with pale yellow to white v-f graded sand lenses, plane parallel laminated to stratified or mottled, potential bleached patches around rhizoliths, localized evaporite-rich horizons, maximum individual horizon thickness 1 cm.	SI - CI	Aeolian interdune to coastal plain domain with occasional flooding with development of s abkha-type deposits and/or superficial vegetation.	Entrada Ss Summersville Fm.
C	Tangential cross-stratified sandstone	Trough cross-stratified v-f graded sandstone, common rippled reactivation surfaces, potential mud drapes and rip-up mud clasts, eventual desiccation cracks and/or evaporite-rich horizons. Thickness ranging between dm- to m values.	VF - M	Tidally-influenced migrating 3D-dunes.	Entrada Fm. Curtis Fm. Summersville Fm.
D	Structureless fluidised sandstone	Deformed to structureless fluidised of green to pink silt- to fine-grained sandstone, local fluid-escape and loading structures still visible, sometimes visually expressed as well rounded sandstone boulders with injected mudstone, maximum boulder ϕ 25 cm, maximum bed thickness 2 m.	SI - F	Destruction of original sedimentary structures due to fluids flowing through the sandstone bed or through liquefaction of water-saturated horizons.	Entrada Ss Curtis Fm.
E	Thoroughly bioturbated condensed sandstone	Rusty-red condensed, cemented, fine-grained sandstone, thoroughly bioturbated, maximum thickness 25 cm.	F	Sediment starvation in a semi-arid coastal plane setting.	Entrada Ss
F	Matrix-supported basal conglomerate	Rounded to well-rounded, matrix-supported basal conglomerate, no preferred clast orientation but their long axis tend to be parallel to the bedding plane, matrix consists of f- to m-grained sandstone, maximum clast ϕ 8 cm, maximum bed thickness 20 cm.	F-Pb	Flash flood deposits.	Curtis Fm. ?
G	Planar- to low angle cross-stratified sandstone	Plane-parallel- to low angle cross-stratified v-f graded gray to green to white sandstone, potential herringbone cross-lamination, unidirectional current, and oscillation ripple-lamination, as well as dm-scale soft sediment deformation, maximum individual bed thickness 60 cm.	VF - F	Upper shoreface to beach deposits with tidal influence.	Curtis Fm.
H	Tangential cross-stratified gravelly sandstone	Matrix-supported conglomeratic dune, hm-scale lateral extent, sub-horizontal erosive base, rip-up mud clasts, extra-basinal sub- to rounded clasts, maximum clast ϕ 2.5 cm, unidirectional-current trough cross-stratification, maximum individual dune thickness 2.50 m.	M - Gr	High energy, asymmetric tidal flow pattern within a laterally restricted embayment.	Curtis Fm.
I	Tidally-influenced cross-stratified conglomeratic sandstone	Matrix- to clast-supported lense-shaped intraformational conglomerate of restricted lateral extent, locally developed and amalgamated in tidal bundles, rip-up mud clasts, extra-basinal sub- to rounded clasts, maximum clast ϕ 2.5 cm, bidirectional cross-stratification with superimposed current-ripples, maximum bed thickness 60 cm.	F - Gr	High energy tidal channels-inlets.	Curtis Fm.
J	Planar to sigmoidal cross-stratified sandy conglomerate	Clast- to matrix-supported conglomerate, hm-scale lateral extent, convex-down erosive base, flat top, extra-basinal sub- to rounded clasts, maximum clast ϕ 2.5 cm, planar cross-stratification, maximum individual thickness 3.00 m.	M - Gr	Point bar lateral accretion within a migrating tidal channel.	Curtis Fm.
K	Plane parallel laminated mud- to siltstone	Plane parallel laminated mud- to siltstone, scattered bidirectional current ripple cross-stratifications gray to green, occasional desiccation cracks, sporadic bioturbations both parallel and normal to the bedding planes.	SI - CI	Gentle flow activity with tidally-related current reversals.	Curtis Fm.
L	Heterolithic silt- and sandstone with lenticular bedding	Rippled v-f graded sandstone, grayish lenses containing herringbone and current ripple cross-stratifications within a matrix of laminated gray to green mud- to siltstones, occasional desiccation cracks, sporadic bioturbations both parallel and normal to the bedding planes.	SI - F	Current reversals in lower subtidal zone.	Curtis Fm.

TABLE 1 - FACIES DESCRIPTION FOR THE ENTRADA SANDSTONE, CURTIS FORMATION AND SUMMERVILLE FORMATION

Facies	Description	Structures	Grain Interpretation	Formation
M	Heterolithic silt- and sandstone with wavy bedding	Ripple cross-stratified vf-f grained grayish sand layers, with bi-directional current indicators and interbedded with laminated gray to green siltstone, occasional desiccation cracks, sporadic bioturbations both parallel and normal to the bedding planes, varying amount of organic matter.	Si - F Current reversals in subtidal zone (shallower than Facies L).	Curtis Fm. Moab Mbr.
N	Heterolithic sandstone with flaser bedding	Ripple and herringbone cross-stratified vf-f gray to green to white sandstone, scattered mud lenses, as well as single and double mud drapes, varying amount of organic matter.	Vf - F Upper sub- to lower intertidal sandflat.	Curtis Fm.
O	Sandstone with climbing ripples	Climbing ripple cross-stratified vf-f grained sandstone, gray to green.	Vf - F Tidal channel overbank spill on tidal flat, Upper sub- to lower intertidal sandflat.	Curtis Fm.
P	Cross-stratified sandstone arranged in well-defined rhythmic tidal bundles	Vf-(f-m) grained gray to green to white sandstone, arranged in tidal bundles, with occasional anti-ripples documented from their toesets, varying amount of organic matter.	Vf - F(-M) Tidal inlets, lower energy than Facies I.	Curtis Fm.
Q	Structureless sandstone	Vf-f grained gray to green to white sandstone, massive, with potential scattered single and/or double mud drapes. Usually rounded and smoothly weathered.	Vf - F The nature of the lack of structure might only be due to intensive surface weathering. Presence of mud drapes indicate sub- or intertidal environment.	Curtis Fm.
R	Thoroughly bi-directional rippled cross-stratified sandstone	Thoroughly rippled silt- to vf-grained sandstone, dominated by herringbone cross-stratifications, potential climbing ripples.	S - Vf Deep subtidal environment with near equal flood and ebb tidal current conditions. Note that the weathering can in some cases erase most of the sedimentary structures.	Curtis Fm. Moab Mbr.
S	Plane parallel-stratified sandstone	Plane parallel-stratified vf-f grained sandstone with scattered current ripple lamination, white, pink or green. Note that the weathering expression of this facies varies between the different units of the Curtis Fm. Potential mud cracks and soft sediment deformations.	(S-) Vf - F Tidal sandflat, upper flow regime (to lower antitune-regime?). Documented mud cracks indicate short-lived subaerial exposure.	Curtis Fm. Moab Mbr.
T	Condensed sandstone	Thin, yellow structureless sandstone, occasionally displaying low-amplitude undulations, exclusively observed capping the Moab Tongue Member of the Curtis Fm. Maximum bed thickness 10 cm.	(Vf-F-) F Condensed horizon.	Moab Mbr.
U	Rippled cross-stratified sandstone	Undulated to rippled cross-stratified vf-f grained, gray to brown sandstone, with 3D current ripples, possible interference ripples, potential mud cracks and soft sediment deformations.	Vf - F 3D migrating ripples under unidirectional current conditions.	Entrada Ss Curtis Fm. Moab Mbr.
V	Plane parallel-laminated siltstone	Dark red soft slope forming siltstone, most probably plane parallel-laminated, scattered pale white bleached lenses and evaporites.	Si Supratidal plain.	Summersville Fm. Summersville Fm.
W	Iron rich ripple- and parallel-laminated sandstone	Dark red to brown cemented vf-f grained sandstone, gentle ripple cross-stratifications, potential desiccation cracks.	Vf - F Fluvial overbank deposits.	Summersville Fm.
X	Palaeosol	Dark purple mud or silt.	M-S sub-aerially exposed surface with superficial soil development.	Entrada Ss, Curtis Fm. Moab Mbr. Summersville Fm.

TABLE 2 - FACIES ASSOCIATIONS FOR THE ENTRADA SANDSTONE, CURTIS FORMATION AND SUMMERVILLE FORMATION

Facies Association	Depositional Environment	Facies Included	Formation
FA 1a	Coastal wet aeolian dune system (Kocurek and Havholm, 1993; Mountney, 2012), with episodic (marine) partial flooding of interdunes deposits and superficial development of soil- and vegetated horizons.	A, C, X	Entrada Sandstone Slick Rock Mbr.
FA 1b	Coastal wet aeolian interdune and lower coastal plain system (Kocurek and Havholm, 1993; Mountney, 2012), with episodic (marine) partial flooding of interdunes deposits and superficial development of soil- and vegetated horizons.	B, C, D, X	Entrada Sandstone earthy facies
FA 2	Beach deposits to upper shoreface deposits, with potential associated tidal channels cut-and-fill.	C, G, S, U	Curtis Fm.
FA 3a	Subtidal heterolithic mud-, silt- vf-grained sandstone, generally upward coarsening from laminated mudstone to wavy bedded sandstone, scarsely	H, I, J, K, L, M	Curtis Fm.
FA 3b	Subtidal heterolithic vf- to f-grained sandstone generally upward coarsening from wavy- to flaser bedded sandstone, scarsely bioturbated.	H, I, M, N	Curtis Fm.
FA 4a	Sandy tidal flat with correlative major tidal channels, with potential subaerial exposures.	S, U, X	Curtis Fm.
FA 4b	Tidal channel infills and splays, distal correlative of FA 4a in the northern areas.	C, H, I, L, M, N, S, U	Curtis Fm.
FA 5	High energy, sub- to intertidal sand -dominated environments, encompassing tidal flats, tidal channels, tidal dunes and tidal bars.	C, G, (K, L, M,) N, O, P, Q, R, S(, X)	Curtis Fm.
FA 6	Upper intertidal heterolithic channels and flats complex, upward fining, with intermittent prolonged subaerial exposures and rare bioturbation, indicator of a more stressed environment than FA 3.	K, L, M, N, Q, S, U, X	Curtis Fm.
FA 7	Coastal dry aeolian dune field (Mountney 2012), arranged in five sequences separated by supersurfaces, upon which transgressive water-carried sediments and/or palaeosol can be observed.	A, N, Q, S, T, U, X	Curtis Fm. Moab Mbr.
FA 8	Supratidal lower coastal plain, with episodic marine flooding.	U, V, W, X	Summerville Fm.

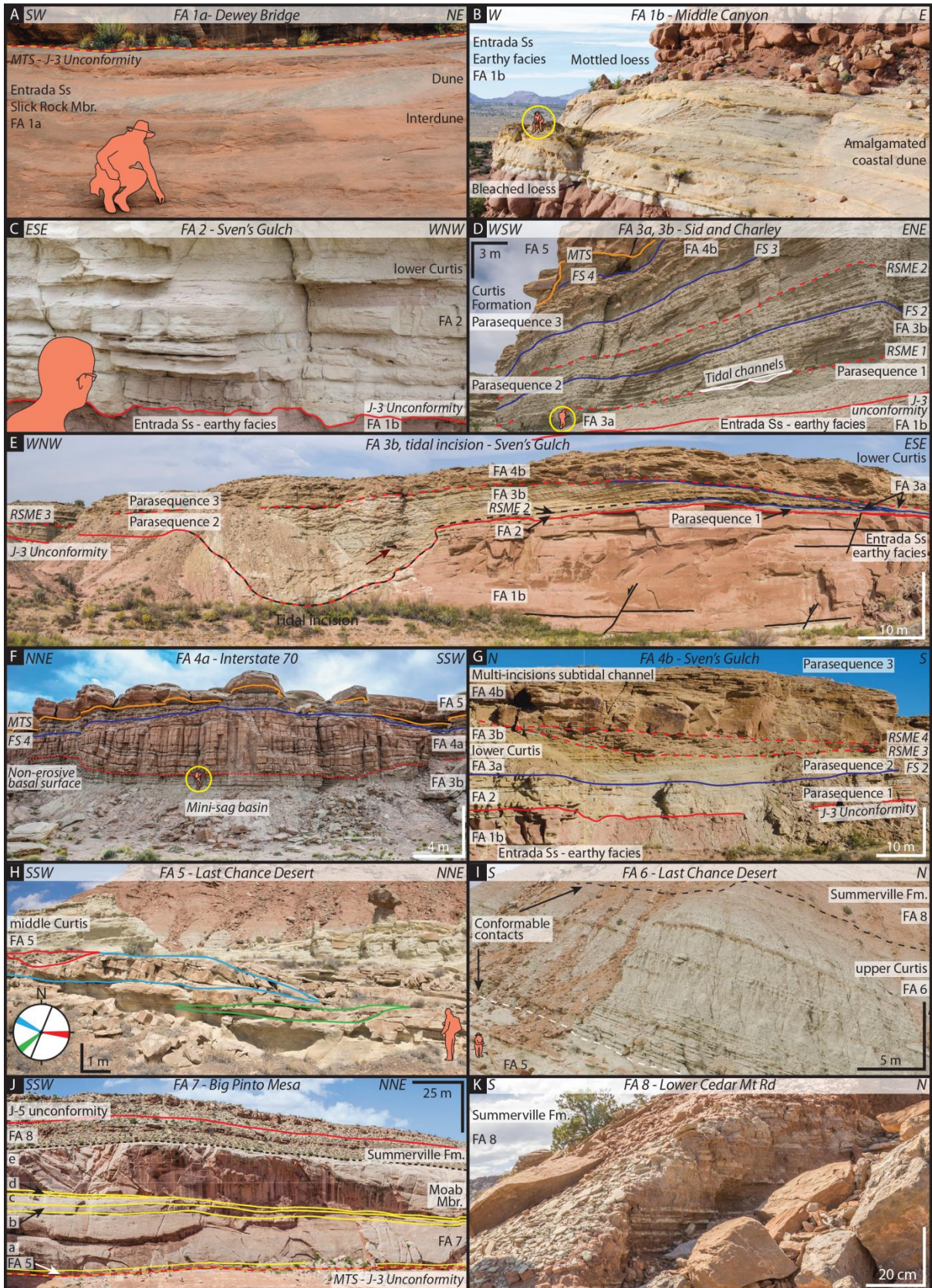


Fig. 3 (previous page) – Summary panel of the Facies Associations (FA) cropping out with in the study area. **A.** Example of wet coastal aeolian dunes of FA 1a (Entrada Sandstone, Slick Rock Member). **B.** Amalgamated aeolian coastal dunes within the fine-grained, marginal marine earthy facies of FA1b (Entrada Sandstone). Note the bleached horizon directly below the dunes. Geologist for scale. **C.** High-energy upper shoreface to beach deposits, with rip-up clasts and occasional mud-drapes. Note the loaded and eroded irregular geometry of the J-3 Unconformity. **D.** Typical stacking architecture of subtidal mud- (FA 3a) and sand-dominated heterolithic flat deposits (FA 3b). **E.** Major tidal incision observed at Sven's Gulch, carved during a short-lived regressive phase within Parasequence 2. The dark-red arrow points at a boulder of Entrada Sandstone within a matrix of FA 3b sand-dominated deposits. Note also the ravinement of Parasequence 2 deposits during the transgressive phase of Parasequence 3, followed by the development of a regressive and erosive, subtidal channel complex (FA 4b). **F.** Mini sag basin generated by the collapse of FA 3b deposits, as FA 4a sand-rich sub- to supratidal sandflat was being deposited. **G.** Two incision phases of FA 4b subtidal channel. **H.** Bidirectional tidal inlets (red and blue contours), and a third south-westward laterally accreting tidal channel (green contour) within a sub- to intertidal flat surrounding environment (FA 5). The respective migration direction of these three bedforms is color-coded on the rose-diagram, whereas the black line on the diagram illustrates the outcrop orientation. **I.** Conformable contact between the underlying FA 5 Sub- to intertidal channel-dune-flat complex, grading into the thinner and finer-grained FA 6 upper sub- to intertidal deposits, which are conformably overlain by FA 8 supratidal deposits of the Summerville Formation. **J.** Five aeolian sequences recorded in the Moab Member of the Curtis Formation. **K.** Close-up images of FA 8 supratidal deposits displaying regular episodes of marine flooding (white sandstone beds).

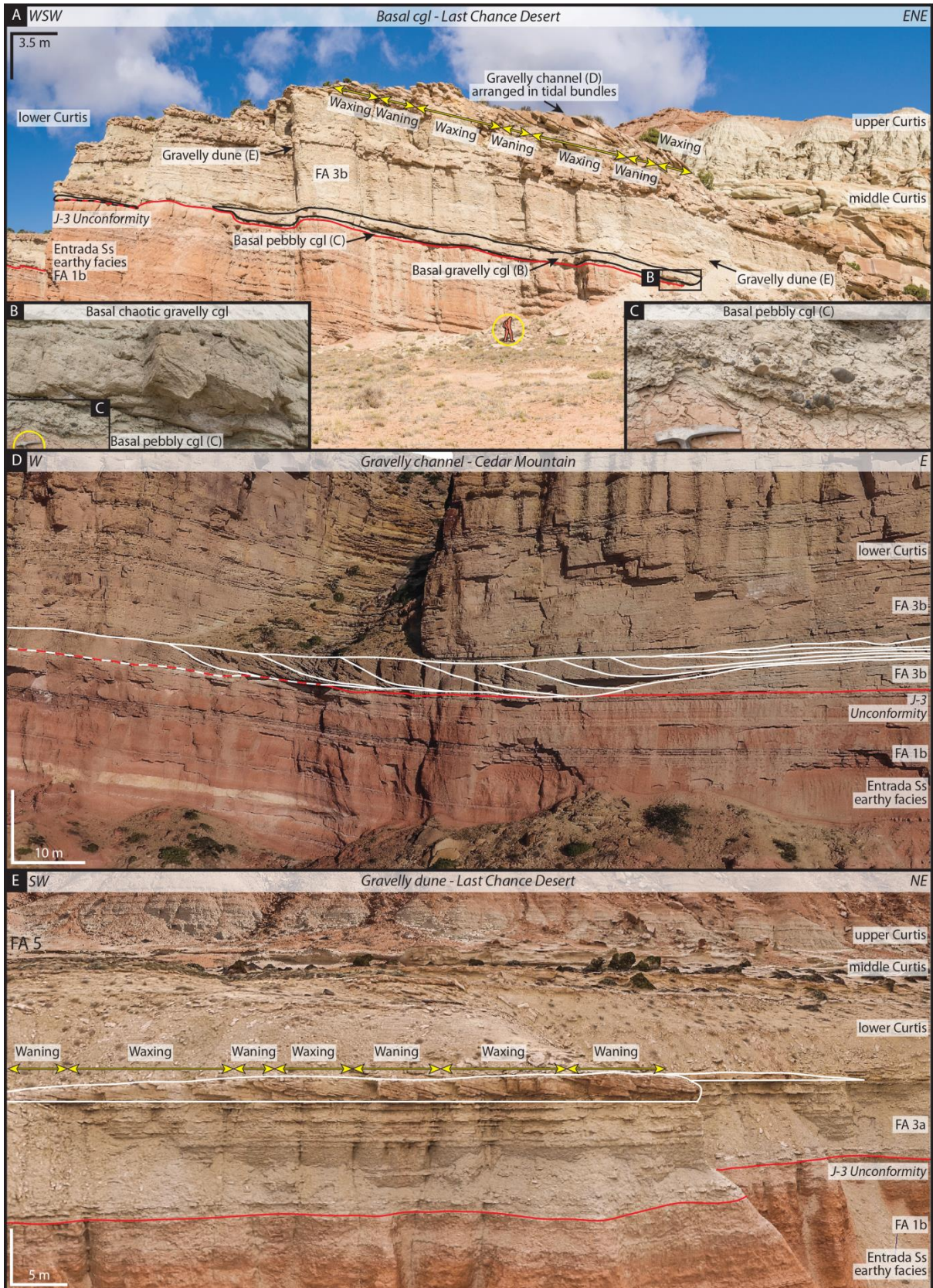


Fig. 4 (previous page) – **A.** Three different conglomeratic deposits observable within the lower Curtis unit. Note the waxing-waning bundle arrangement of the upper gravelly channel and the absence of similar structure in the gravelly dunes. **B-C.** Close-up of the basal flash flood pebbly conglomerate, overlain by a gravelly dune. **D.** lateral migration of a sinuous subtidal, gravelly channel. Note its concave up, erosive base and flat upper surface (see Fig. 10 for detail architectural arrangement of that subtidal channel). **E.** Gravelly dune, arranged in waxing-waning bundles, migrating over subtidal, mud-dominated heterolithic flat deposits (FA 3a).

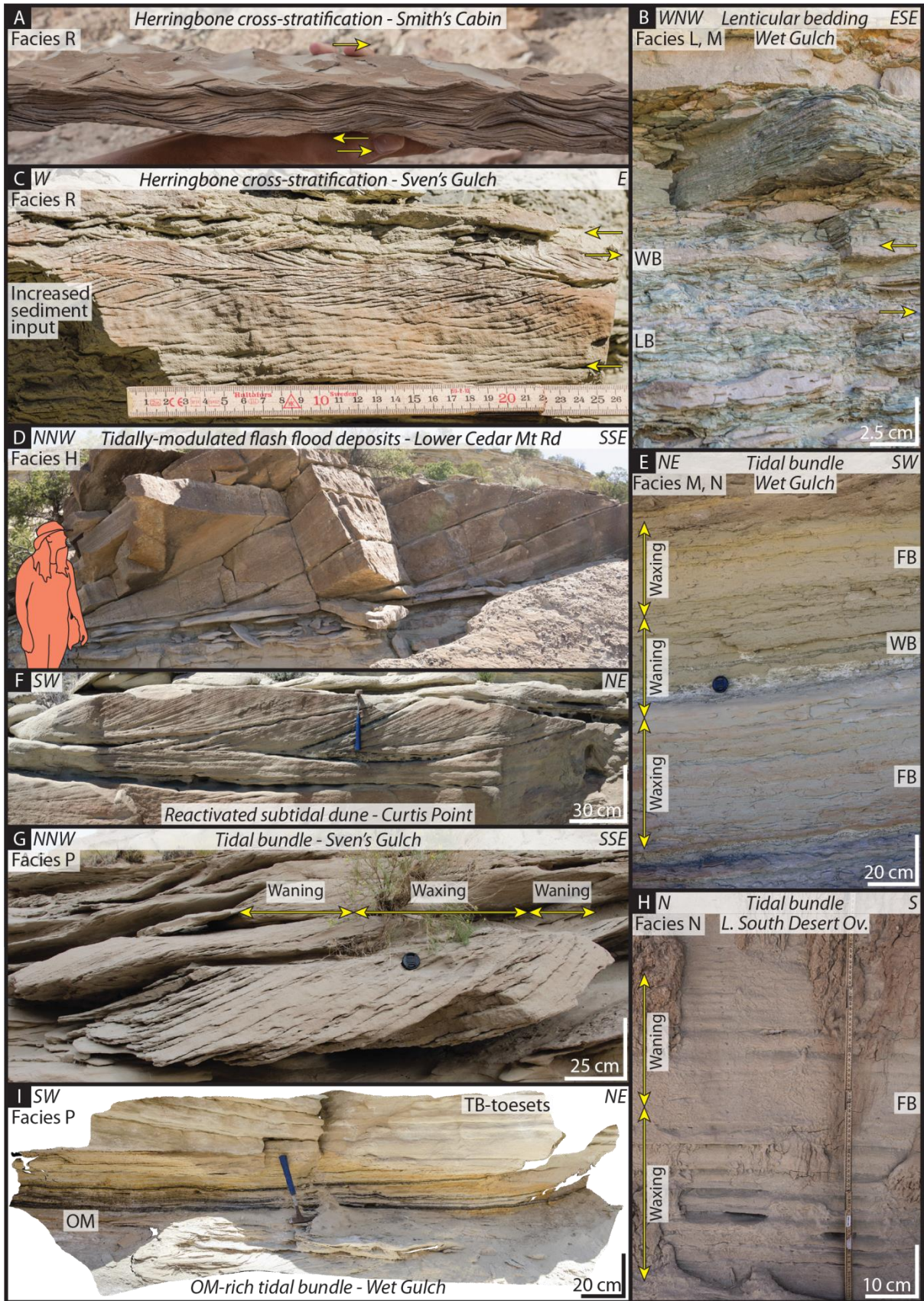


Fig. 5 (previous page) – Common tide-dominated and tidally-modulated bedforms present in the Curtis Formation. See Facies Table 1 for codes. **A.** Bi-directional rippled cross-stratified sandstone (Facies R). **B.** Heterolithic silt- and sandstone with lenticular (LB) and wavy bedding (WB) (Facies L, M). **C.** Bi-directional rippled cross-stratified sandstone with episodic climbing ripples (Facies R). **D.** Tangential cross-stratified gravelly sandstone (Facies H), thought to result from tidally-reworked flash flood deposits, migrating over a sole of mud- to sand-dominated heterolithic deposits (FA 3). **E.** Heterolithic silt- and sandstone with wavy and flaser bedding (FB) (Facies M, N), arranged in rhythmic tidal bundle. **F.** Tangential cross-stratified sandstone (Facies C), with rippled reactivation surfaces, mud drapes and rip-up mud clasts. **G.** Cross-stratified sandstone arranged in well-defined rhythmic tidal bundles (Facies P). **H.** Heterolithic sandstone with flaser bedding (Facies N), arranged in rhythmic tidal bundle. **I.** Organic-rich (OM) toesets of a cross-stratified sandstone arranged in well-defined rhythmic tidal bundles (TB) (Facies P).

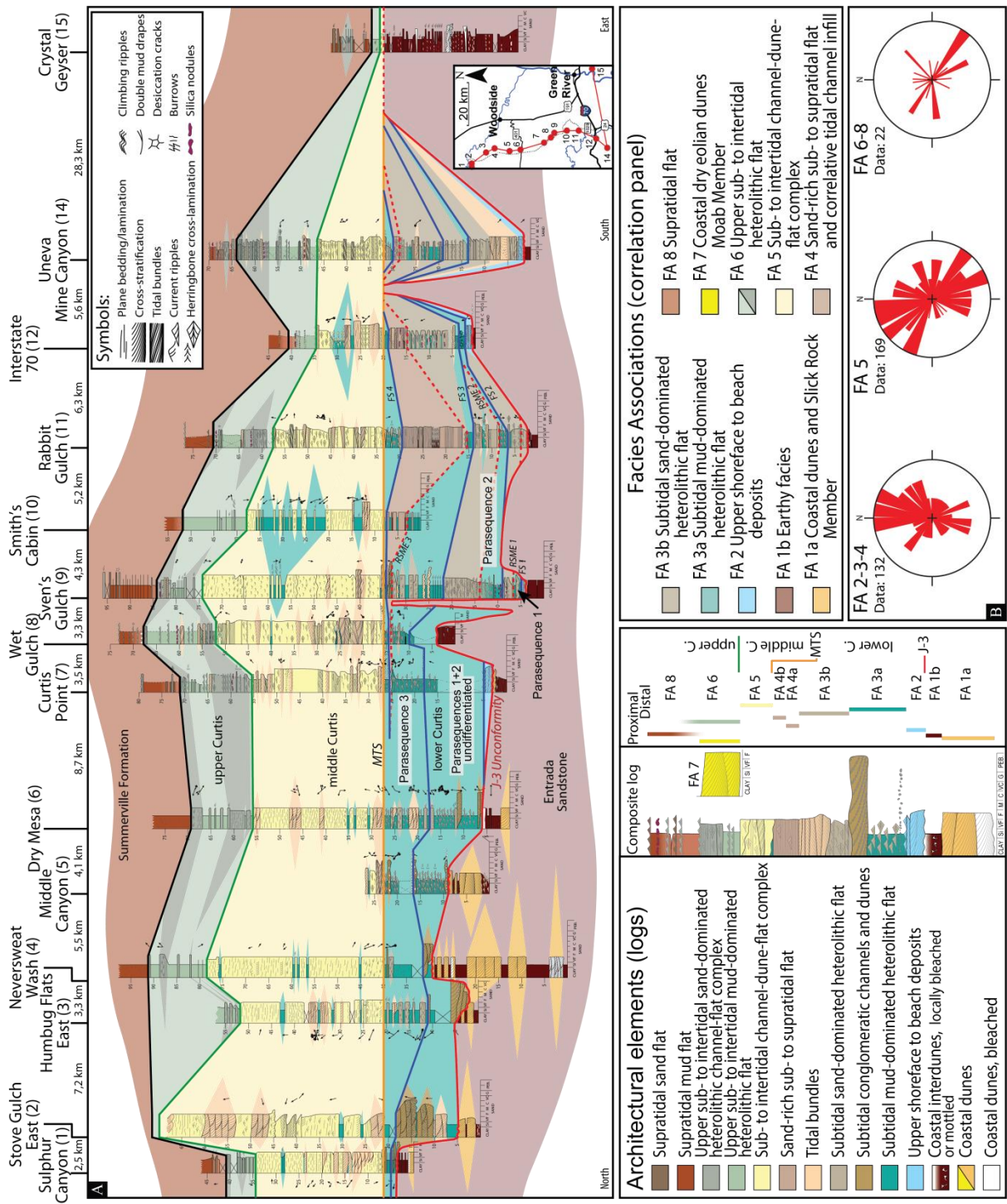


Fig. 6 – A. N-S-W oriented correlation panel along the NW margin of the San Rafael Swell, and the correlative spatial distribution of facies associations across the basin. The datum corresponds to the Major Transgressive Surface (MTS). **B.** Rose diagrams displaying the palaeocurrent measurements for the lower Curtis (FA 2, FA 3, and FA 4), the middle Curtis (FA 5), and the upper Curtis-Summerville Formation intervals (FA 6 and FA 8).

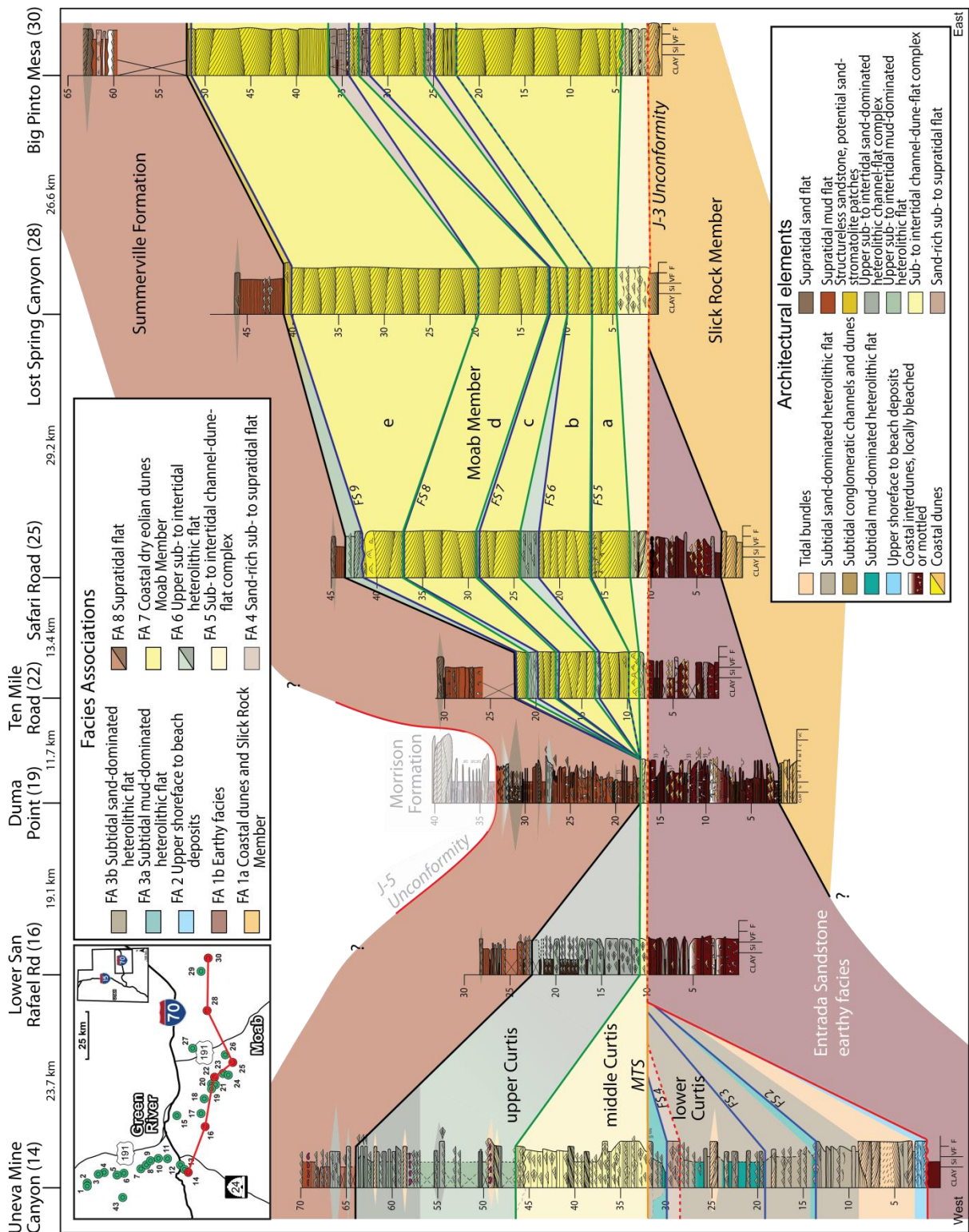


Fig. 7 – E-W oriented correlation panel across the marine part and the aeolian Moab Member of the Curtis Formation. The datum corresponds to the Major Transgressive Surface (MTS). Note that the five, cyclical aeolian sequences identified in the Moab Member of the Curtis Formation suggest that the contemporaneous Summerville Formation could have undergone, and most probably underwent, similar cycles as it was being deposited.

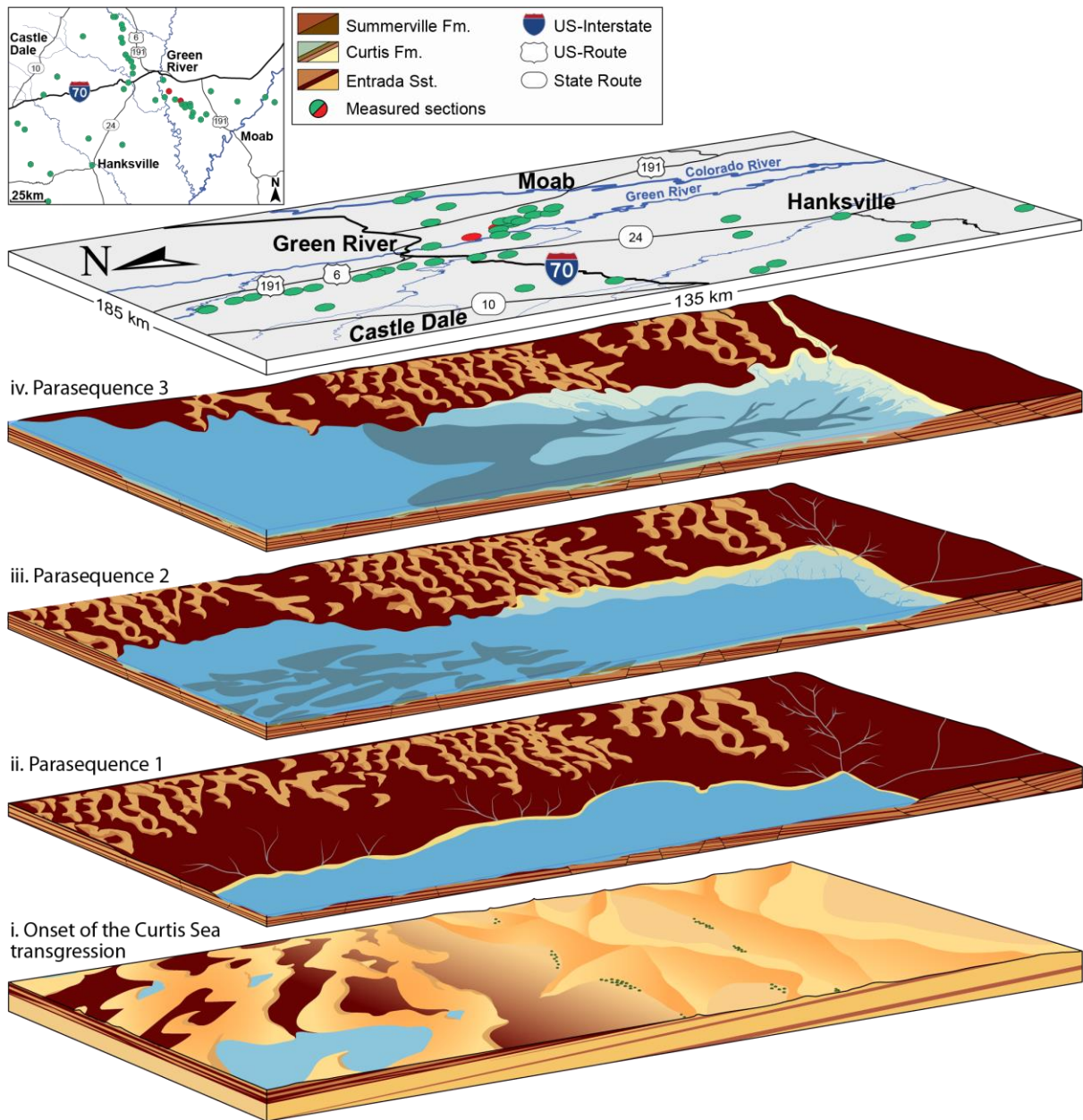


Fig. 8 – Summary basinal history for the Entrada-Curtis-Summerville interval.

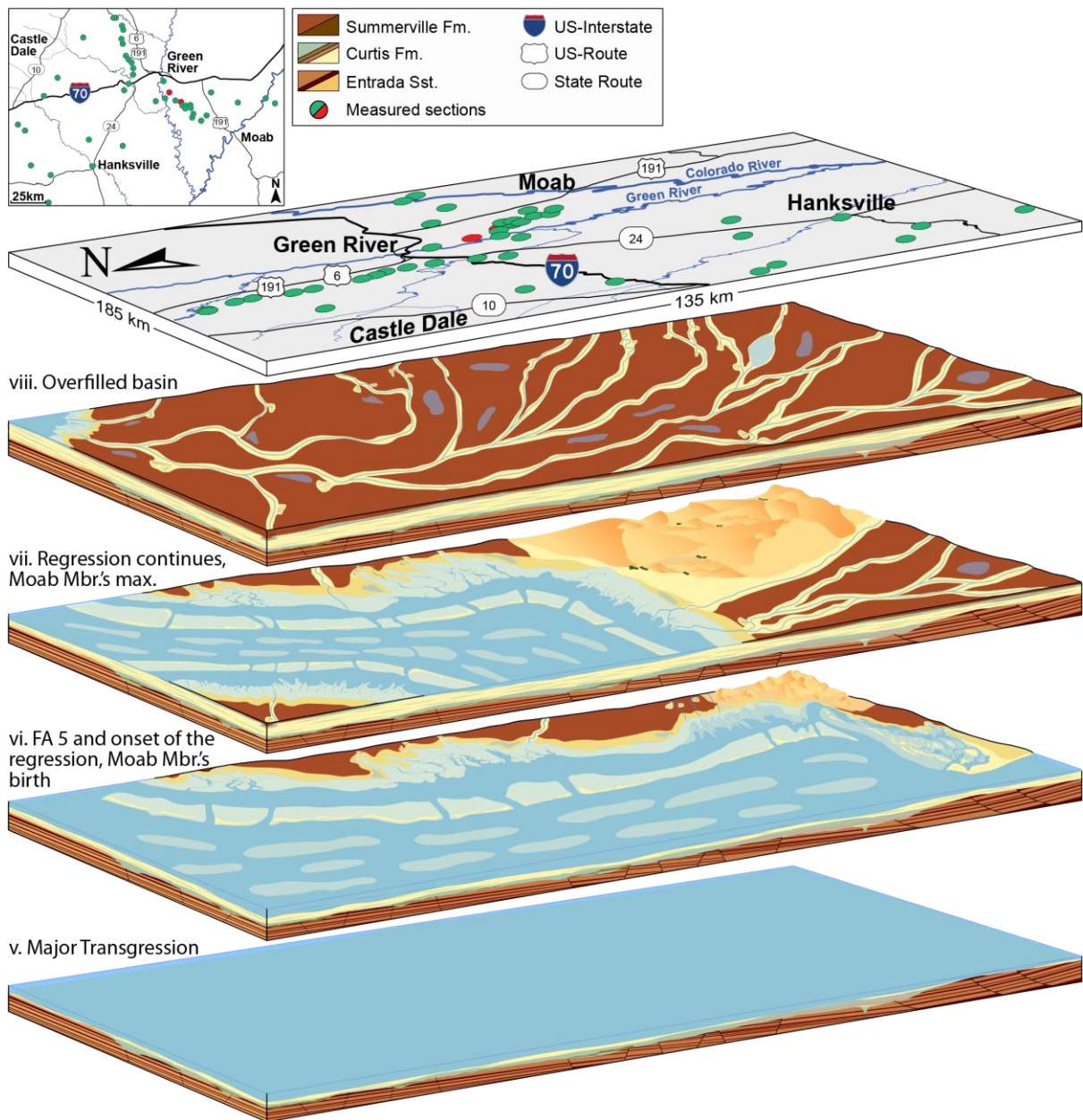


Fig. 8 (follow) – Summary basinal history for the Entrada-Curtis-Summerville interval.

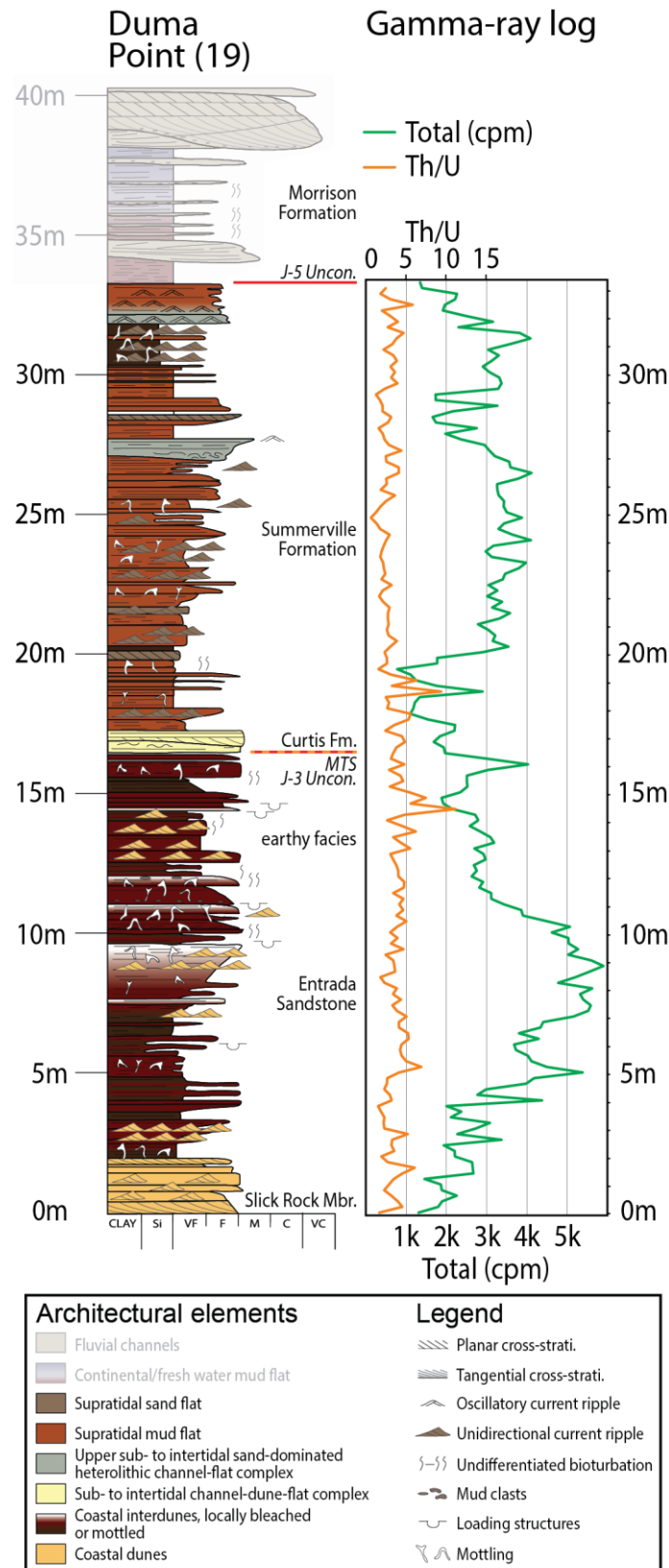


Fig. 9 – Duma Point sedimentary section and associated cyclical Gamma-ray log. The Thorium/Uranium (Th/U) values generally fall below 7 at approximately 5, which suggest a more prominent marine origin for these sediments, rather than a fully continental provenance (Fertl *et al.*, 1982). The Morrison Formation is shaded as it is not of interest for this study. See Fig. 2 for section location.

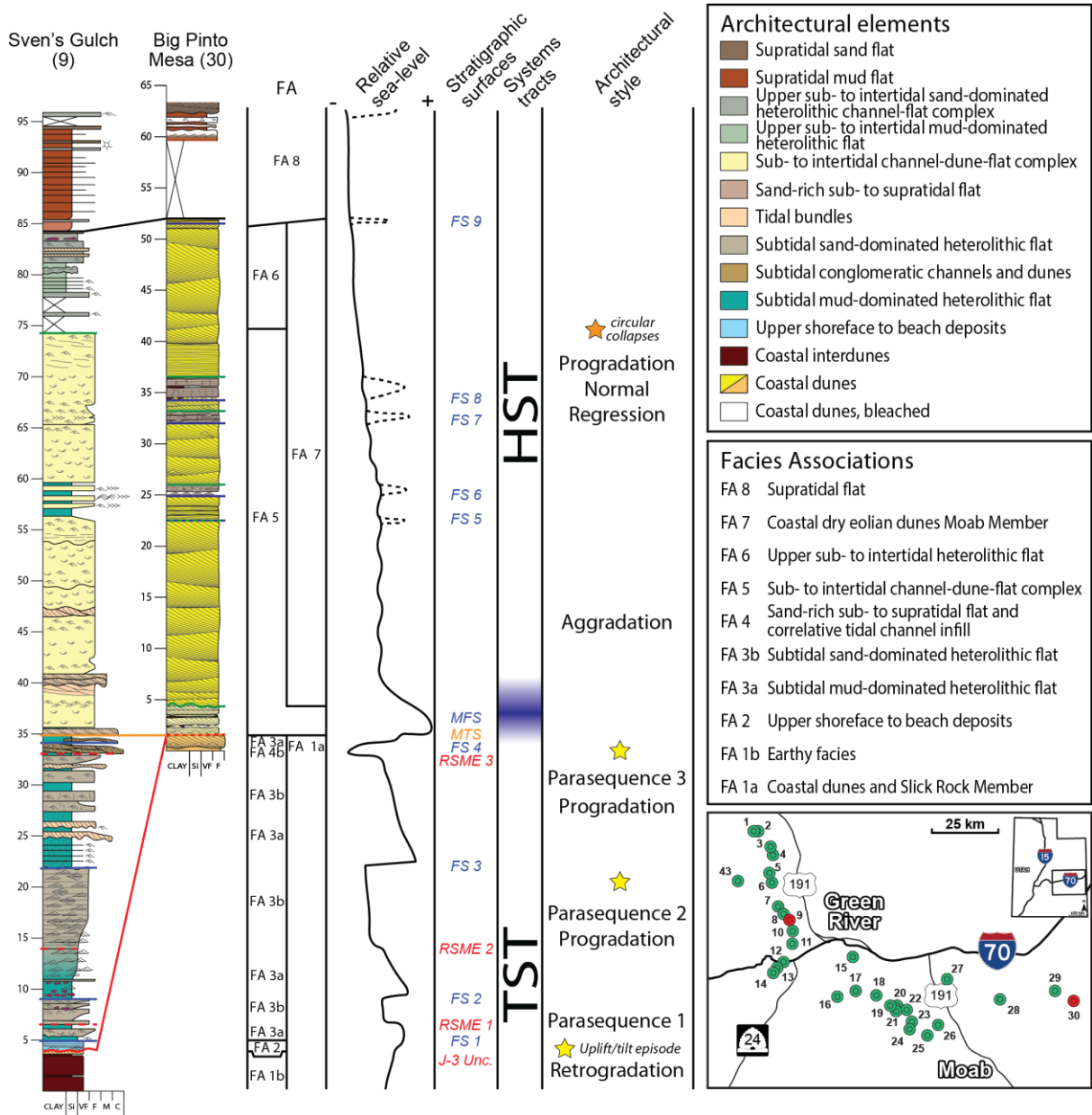


Fig. 10 – Comparison between the relative sea-level signal recorded by the marine part (Sven's Gulch, left red dot on the map) and the aeolian Moab Member of the Curtis Formation (Big Pinto Mesa, right red dot on the map), illustrating the overwriting of allocyclic signals by the tide-dominated system once it entered in resonance, accompanied by the deposition of the middle Curtis, whereas the contemporaneous continental deposits kept recording such allocyclicly-forced relative sea-level variations. See Fig. 11 for illustration of uplift phases.

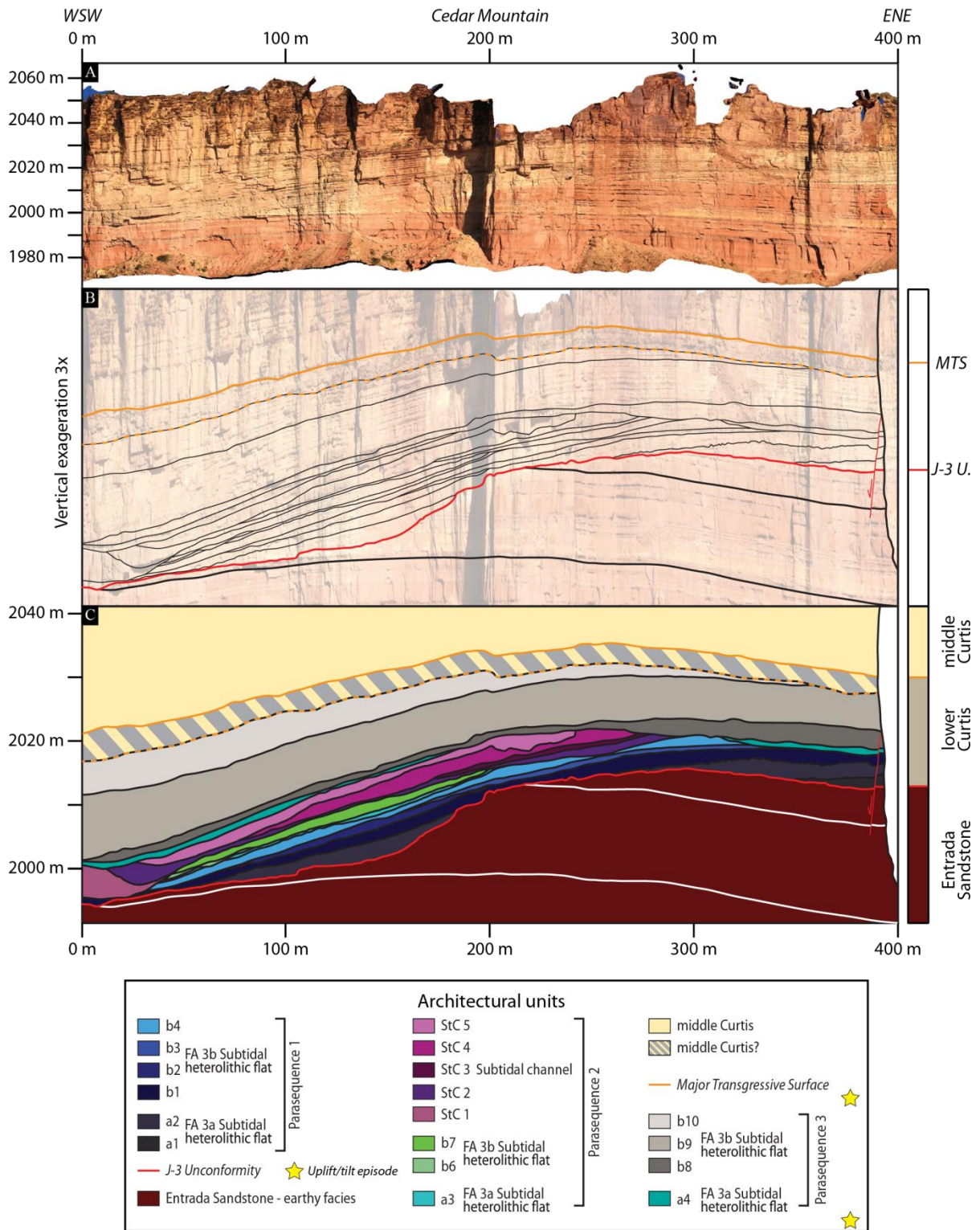


Fig. 11 – A. Photogrammetric model of Cedar Mountain showing the earthy facies of the Entrada Sandstone, the erosive relief developed at its top, as well as the lower and middle Curtis strata overlying the J-3 Unconformity. B-C. Vertically exaggerated interpreted model, which illustrates the impact of both allocyclic and autocyclic forcing on the system as the lower Curtis was developing. **Allocyclic forcing:** The angular relationship between the different strata indicates that a first tilting of the Entrada Sandstone strata occurred prior to the deposition of Parasequence 1 deposits, a second one occurred before Parasequence 3 developed, and the last one preceded the Major Transgression.

Further, the effect of relative sea-level variations, accompanied by the shift of the FAs belt, resulted in the development of the three parasequences. **Autocyclic forcing:** The minor spatio-temporal energy variations, as well as the WSE-ENE laterally migrating subtidal channel (pink-purplish tones) illustrate best the intrinsically dynamic behaviour of the tide-dominated system, but its multi-story incision-amalgamation also testifies of a potential impact of external forcing over the system. This contrasts with the middle Curtis' system and its behaviour, which was impacted and developed quasi exclusively as a response of autocyclic forcing.

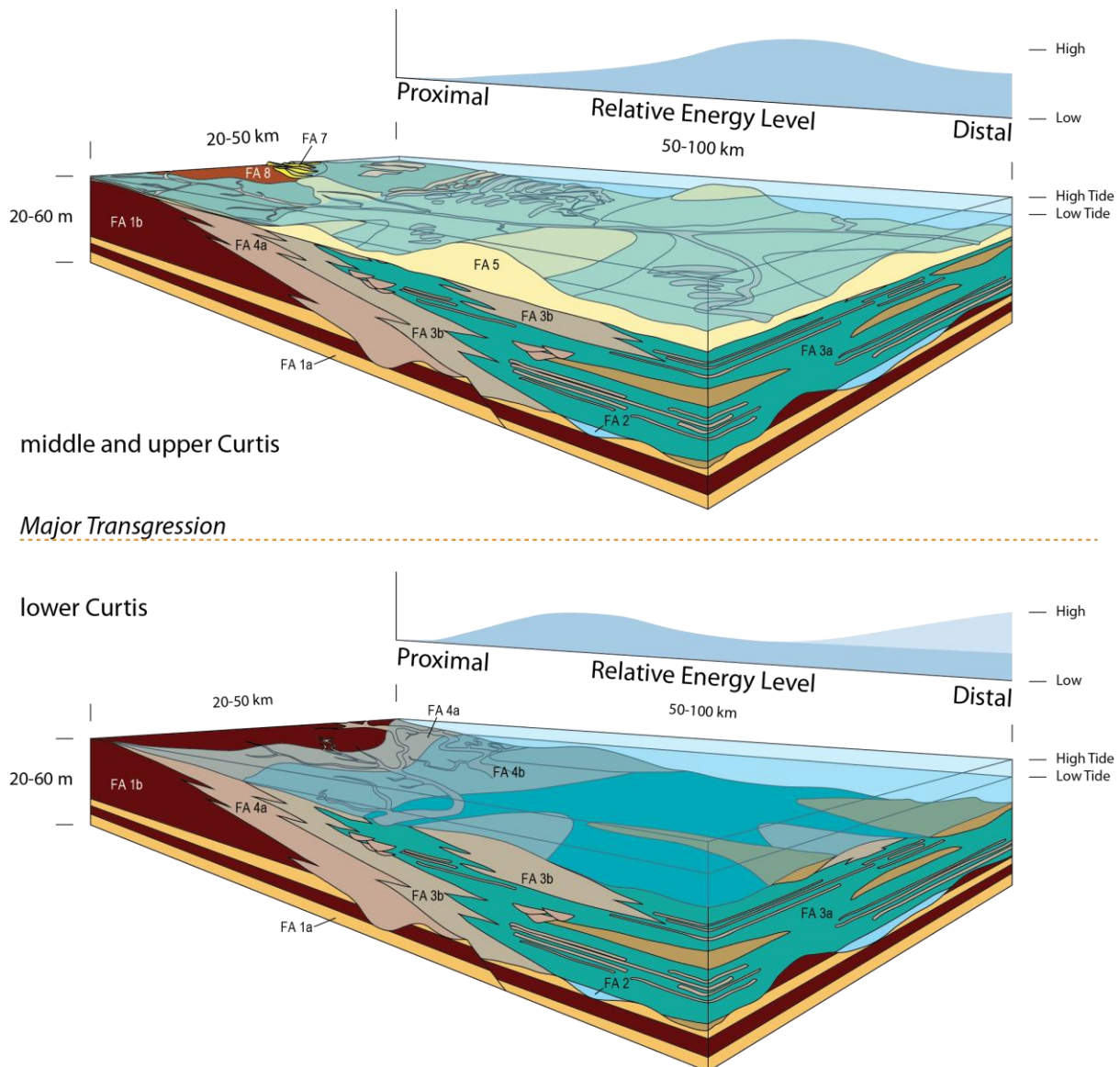


Fig. 12 – Models representing the spatial distribution of the different FA across and idealised Curtis-like basin during the lower Curtis, as well as the middle-upper Curtis intervals, and their correlative energy level's spatial distribution within the system. Note the coarsening trend from the distal parts of the basin and towards the shoreline in the lower Curtis, with the replacement of the mud-dominated FA 3a deposits, by FA 3b's and FA 4a's coarser-grained and cleaner sediments.

8. Appendix

8.1. Abstracts, first author

8.1.1. Zuchuat et al. (2017). *International Meeting of Sedimentology, Toulouse.*

Zuchuat, V.¹, Sleveland, A.R.N.¹, Rimkus, A.¹, Braathen, A.¹, and Midtkandal, I.¹ (2017). Modelling the Sequence Stratigraphic Development of the Upper Jurassic Curtis Formation along the NE Margin of the San Rafael Swell, Central-Eastern Utah, USA: an Example of a Low-Gradient Tidal Basin.

¹*Tectonostratigraphic Research Group, University of Oslo, Sem Sælands Vei 1, 0371 Oslo, Norway*

Accepted for a poster presentation

MODELLING THE SEQUENCE STRATIGRAPHIC DEVELOPMENT OF THE UPPER JURASSIC CURTIS FORMATION ALONG THE NE MARGIN OF THE SAN RAFAEL SWELL, CENTRAL-EASTERN UTAH, USA: AN EXAMPLE OF A LOW-GRADIENT TIDAL BASIN

Valentin ZUCHUAT^(1,@), Arve SLEVELAND⁽¹⁾, Algirdas RIMKUS⁽¹⁾, Alvar BRAATHEN⁽¹⁾, Ivar MIDTKANDAL⁽¹⁾

⁽¹⁾ Department of Geosciences, University of Oslo (Norway)

[@] valentin.zuchuat@geo.uio.no

This study focuses on the Middle and Upper Jurassic Entrada-Curtis-Summerville formations, following a 60 km north-south trending escarpment on the north-eastern margin of the San Rafael Swell, Central-Eastern Utah, USA. Based on sedimentary facies analysis and application of sequence stratigraphic principles, a reconstruction of depositional environments emphasises the highly dynamic interactions between depositional processes in low-gradient tidal basins. Intricate lateral and vertical distribution of facies is mapped, and correlation is linked to key sequence stratigraphic surfaces of regional significance. The collected data and its interpretation sustains that (i) the regional J-3 Unconformity displays evidence of preand syn-Curtis Formation erosional episodes, carving down ca. 15 m into the underlying strata of the Entrada Sandstone. (ii) Laterally restricted shoreface deposits, formed in topographic lows, represent the first stage of the Curtis Sea transgression over the Entrada Sandstone. (iii) The transgression of the Curtis Sea occurred in a backstepping manner, with the subsequent deposition of three coarsening-up parasequences, mainly consisting of subtidal mudand sand-dominated heterolithic deposits. (iv) Several episodes of relative sea-level variations, possibly linked to glacio-eustatic processes, occurred during the transgressive phase, leading to the development of a proximal, sand-dominated subto supratidal flat in the south and its correlative distal subtidal, multi-incised channels in the north. (v) The transgression reached its maximum extent with the deposition of sand-dominated high-energy tidal channels and bar complexes, which protected the backbarrier intertidal mix-flat. (vi) Suband intertidal strata represent an initial period of architectural aggradation, succeeded by the early stage of a prograding supratidal coastline during highstand. This study has shown that a sequence stratigraphic approach over a complex low-gradient tide-dominated basin is successful in correlating the highly heterolithic measured sections, as well as linking the development of such deposits to a relative base level history through the careful identification of the following sequence stratigraphic surfaces: flooding surfaces, tidal ravinement surfaces and regressive surfaces of marine erosion. It further enhances that facies distribution prediction still remain highly uncertain in such a complex low-gradient tide-dominated system.

8.1.2. Zuchuat et al. (2017). British Sedimentological Research Group, Annual General Meeting, Newcastle upon Tyne.

Zuchuat, V.¹, Da Costa, S.¹, Sundal, A.¹, Braathen, A.¹, and Midtkandal, I.¹ (2017). Schizophrenia in sedimentology: The J-3 Unconformity and the Curtis Formation, Central-Eastern Utah, USA.

¹*Tectonostratigraphic Research Group, University of Oslo, Sem Sælands Vei 1, 0371 Oslo, Norway*

Accepted for an oral presentation

Schizophrenia in sedimentology: The J-3 Unconformity and the Curtis Formation, Central-Eastern Utah, USA

Valentin Zuchuat¹, Sigrid Da Costa¹, Anja Sundal¹, Alvar Braathen¹, Ivar Midtkandal¹

¹University of Oslo, Sem Sælands Vei 1, 0371 Oslo, Norway; valentin.zuchuat@geo.uio.no

The tide-dominated, Upper Jurassic Curtis Formation crops out in Eastern-Central Utah, overlying the continental to marginal marine Entrada Sandstone. The contact between the two sedimentary formations is formally identified as the J-3 Unconformity, which can be traced over significant distances. It has since been regarded as a “simple” subaerial unconformity, followed by a third order transgression within an enclosed basin and the resulting deposition of the tide-influenced Curtis Formation. However, careful inspection of the different facies and their sub-regional correlation clearly shows that the essence of the J-3 Unconformity is not merely characterised by a long-lasting phase of subaerial exposure. It instead displays evidence of an intricate poly-erosional history, happening during short-lived syn-depositional transgressive and regressive periods. The initial bounding surface was locally altered by processes associated with development of the Curtis Formation, and the nature of their impact is strongly process-dependent. Pre-Curtis erosional processes mainly involved aeolian deflation and fluvial incision, creating a basinwide gentle relief. Syn-Curtis erosional mechanisms were controlled by the distribution and magnitude of tidal forces within the basin, resulting in a steeper and more localised relief in comparison with pre-Curtis widespread denudation. Furthermore, sedimentary processes alone can't explain the present-day relief observed with the J-3 Unconformity. Indeed, tectonic played, at various scale, a key role in the funnelling of the various erosional forces and the distribution of the depocentres, with (i) m-scale grabens and horsts structures, and (ii) hydroplastic sand remobilisation, both observed within the uppermost strata of the Entrada Sandstone, as well as (iii) syn-Curtis sub-regional tectonic uplift. This study shows that reducing an unconformity to a single process is insufficient. Instead, careful mapping and understanding of such a schizophrenic surface can provide a non-negligible amount of information regarding the dynamic of a basin and its subsequent infill.

8.1.3. Zuchuat et al. (2018). International Sedimentological Congress, Québec City, 2018.

Zuchuat, V.¹, Midtkandal, I.¹, Poyatos-Moré, M.¹, Da Costa, S.¹, Halvorsen, K.¹, , Sundal, A.¹, Cote, N.², and Braathen, A.¹ (2018). Unconformities matter: The spatial and temporal information contained in the J-3 Unconformity and the Curtis Formation, east-central Utah, USA.

¹*Tectonostratigraphic Research Group, University of Oslo, Sem Sælands Vei 1, 0371 Oslo, Norway*

²*Natural and Environmental Sciences Department, Western State Colorado University, 600 North Adams Street, Gunnison, CO 81231*

Accepted for an oral presentation

Unconformities matter: The spatial and temporal information contained in the J-3 Unconformity and the Curtis Formation, east-central Utah, USA.

V. Zuchuat^{1*}, I. Midtkandal¹, M. Poyatos-Moré¹, S. Da Costa¹, K. Halvorsen¹, A. Sundal¹,
N. Cote², A. Braathen¹

¹Department of Geosciences, University of Oslo, Sem Sælands vei 1, 0371 Oslo, Norway.

²Natural & Environmental Sciences Department, Western State Colorado University, 600 North Adams Street, Gunnison, CO 81231.

*e-mail: valentin.zuchuat@geo.uio.no

A spatio-temporal re-interpretation of a regionally significant unconformity is proposed to refine the depositional history of its basin, highlighting the fact that unconformities are dynamic sedimentary features and should not be considered as a simple "break in deposition". The Upper Jurassic (Oxfordian) Curtis Formation crops out in east-central Utah, and was strongly impacted by tide-related processes at the time of deposition. It unconformably overlies the Middle-Jurassic (Callovian) coastal eolian to marginal marine deposits of the Entrada Sandstone. The two formations are separated by Pipiringos & O'Sullivan¹ (1978) J-3 Unconformity, widely regarded as a "simple" subaerial unconformity representing a significant break in deposition between the Middle- and Upper Jurassic, followed a third order transgression within a semi-enclosed basin and the deposition of the tide-dominated Curtis Formation. This interpretation has been proven inaccurate by meticulous identification of the different types of relief characterizing this surface, by the careful inspection and by the sub-regional correlation of the various facies bounding it, both above and below the surface. The J-3 Unconformity displays an intricate poly-generational history as it was impacted by a range of erosional and depositional processes during short-lived transgressive and regressive episodes. The resultant J-3 Unconformity is thus a composite stratigraphic boundary that is not only diachronous from its distal to proximal reaches as is typical for single-generation surfaces of subaerial erosion, but also recorded episodes of erosion that are separated by larger temporal gaps. As the Sundance Sea started to transgress from the north, eolian deflation increased and slowly cannibalized the eolian deposits of the Entrada Sandstone when its sediment supply was drastically reduced. The transgression(s) was accompanied by an increased water table within continental sedimentary column over the study area. Contemporaneous fluvial erosion occurred locally as flash floods were flowing from neighboring highlands. While the Curtis Sea kept transgressing, sub-aqueous erosional and soft sediment deformational mechanisms were controlled by the distribution and magnitude of tidal forces within the basin, resulting in steeper and more localized incisions during short-lived regressive episodes, whereas transgressive phases lead to distinct and extensive, dm- to m-scale irregular relief. Sedimentary processes alone can't explain the present-day relief observed with the J-3 Unconformity. Steep faulting localizing depressions and horst-like shoulders can be linked to hydroplastic deformation by mobility of subsurface sand. Such surface expressions further shaped the J-3 Unconformity as it funneled the various erosional forces and impacted on the spatial distribution of depocentres. Typical features include; (i) m- to dm-scale graben-and-horst structures, (ii) sag basins juxtaposed with related sand-pillow uplifts, and (iii) syn-Curtis gentle folding and erosion linked to sub-regional uplift.

This study shows (i) such a poly-genetic surface is a dynamic sedimentary feature and cannot be regarded as unconformity *sensu stricto*, which will notably lead to lithostratigraphic paradoxes, and hence, such nomenclature shall be dealt with caution, but (ii) that careful mapping and understanding of such a multifaceted surface can provide valuable information regarding the dynamic of a basin and its subsequent infill.

References

¹ Pipiringos, G.N. & O'Sullivan, R.B., (1978). Principal unconformities in Triassic and Jurassic rocks, western interior United States: a preliminary survey. *U.S. Geological Survey, Professional Paper, 1035-A*, 1-29.

8.1.4. Zuchuat et al. (2018). British Sedimentological Research Group, Annual General Meeting, Edinburgh, 2018.

Zuchuat, V.¹, Sleveland, A.R.N.¹, Pettigrew, R.², Dodd, T.², Clarke, S.², Sundal, A.¹, and Braathen, A.¹, Midtkandal, I.¹ (2018). Why you should care about neighbouring sedimentary systems: Overprinted allocyclic processes by tidal resonance in the Upper Jurassic Curtis Formation, Utah, USA.

¹*Tectonostratigraphic Research Group, University of Oslo, Sem Sælands Vei 1, 0371 Oslo, Norway*

²*Basin Dynamics Research Group, Keele University, ST5 5BG, Keele, Staffordshire, United Kingdom*

Accepted for an oral presentation

Why you should care about neighbouring sedimentary systems: Overprinted allocyclic processes by tidal resonance in the Upper Jurassic Curtis Formation, Utah, USA.

Zuchuat, V.¹, Sleveland, A.R.N.¹, Pettigrew, R.², Dodd, T.², Clarke, S.², Sundal, A.¹, and Braathen, A.¹, Midtkandal, I.¹ (2018). Why you should care about neighbouring sedimentary systems: Overprinted allocyclic processes by tidal resonance in the Upper Jurassic Curtis Formation, Utah, USA.

¹*Tectonostratigraphic Research Group, University of Oslo, Sem Sælands Vei 1, 0371 Oslo, Norway*

²*Basin Dynamics Research Group, Keele University, ST5 5BG, Keele, Staffordshire, United Kingdom*

Some tide-dominated sedimentary units and basins in the rock record do not correspond to any modern, tide-dominated and/or tide-influenced coastlines such as deltas, estuaries, and lagoons. The semi-enclosed, shallow, Utah-Idaho Trough foreland basin that the Curtis Sea transgressed during the earliest Upper Jurassic is one of these exceptions. It was transgressed from today's Wyoming, south-westwards into Utah. A severe starvation of perennial fluvial input due to the persistent aridity, which reigned over and around the basin prior, during, and after the Curtis Sea's transgression, characterises this basin, in which the lower, middle, and upper Curtis, and the Summerville formations were deposited. The shallow basin's protected nature, as well as its elongated morphology (ca. 800x150 km), allowed for efficient wave energy dissipation. Consequently, the semi-enclosed, shallow marine system was dominated by amplified tidal forces, resulting in an intricate arrangement of heterolithic deposits.

Intrinsic autocyclic processes acting upon the system were strongly impacted by allocyclic forcing, during the deposition of the lower Curtis. Relative sea-level variations, as well as uplift and deformation episodes, resulted in three parasequences, separated by traceable flooding and ravinement surfaces. The subsequent transgression defines the base of the middle Curtis, and its basal compound transgressive/ravinement surface can be traced throughout the study area, and beyond. The shallow-marine part of the system entered into tidal resonance, which overprinted any evidence of allocyclic forcing and related traceable stratigraphic surfaces, because the basin reached the optimal length-to-width configuration as a consequence of this transgression. However, the contemporaneous Moab Member of the neighbouring coastal aeolian dune field, characterised by five stacked aeolian sequences, as well as the Summerville Formation's supratidal deposits, continued to register allocyclic signals, as the Curtis Sea regressed.

This study shows that (i) if the tide-dominated basin reaches its ideal configuration, it can enter into a resonant stage, in which autocyclic behaviours can overprint the impact of otherwise dominant allocyclic processes, and hence, (ii) if the system is alternatively dominated by auto- or allocyclic processes, it is necessary to study neighbouring and contemporaneous depositional systems if one aims at obtaining the researched basin's most complete sequence stratigraphic history.

Key word: Tidal resonance, autocyclic and allocyclic processes, stratigraphic surfaces, aeolian sequences, Curtis Formation

8.1.5. Zuchuat et al. (2019). Vinterkonferansen, Bergen 2019.

Zuchuat, V.¹, Sleveland, A.R.N.¹, Pettigrew, R.², Dodd, T.², Clarke, S.², Sundal, A.¹, and Braathen, A.¹, Midtkandal, I.¹ (2019). Why you should care about neighbouring sedimentary systems: Overprinted allocyclic processes by tidal resonance in the Upper Jurassic Curtis Formation, Utah, USA.

¹*Tectonostratigraphic Research Group, University of Oslo, Sem Sælands Vei 1, 0371 Oslo, Norway*

²*Basin Dynamics Research Group, Keele University, ST5 5BG, Keele, Staffordshire, United Kingdom*

Accepted for an oral presentation

Why you should care about neighbouring sedimentary systems: Overprinted allocyclic processes by tidal resonance in the Upper Jurassic Curtis Formation, Utah, USA.

Zuchuat, V.¹, Sleveland, A.R.N.¹, Pettigrew, R.², Dodd, T.², Clarke, S.², Sundal, A.¹, and Braathen, A.¹, Midtkandal, I.¹ (2018). Why you should care about neighbouring sedimentary systems: Overprinted allocyclic processes by tidal resonance in the Upper Jurassic Curtis Formation, Utah, USA.

¹*Tectonostratigraphic Research Group, University of Oslo, Sem Sælands Vei 1, 0371 Oslo, Norway*

²*Basin Dynamics Research Group, Keele University, ST5 5BG, Keele, Staffordshire, United Kingdom*

Modern, tide-dominated and/or tide-influenced coastlines correspond to deltas, estuaries, and lagoons. However, some tide-dominated basins and related sedimentary units in the rock record, such as the semi-enclosed, shallow, Utah-Idaho Trough foreland basin that the Curtis Sea transgressed south-westwards during the earliest Upper Jurassic, do not correspond to any of these modern systems. Persistent aridity caused the characteristic severe starvation of perennial fluvial input throughout this basin, in which the informal lower, middle, and upper Curtis, as well as the Summerville Formation were deposited. Wave energy was efficiently dissipated by the shallow basin's elongated morphology (ca. 800x150 km), as well as its protected nature. Consequently, the semi-enclosed, shallow marine system was dominated by amplified tidal forces, resulting in a complex distribution of heterolithic deposits.

In the early stage of the transgression, as the lower Curtis was deposited, allocyclic forcing was strongly impacting upon the system's intrinsic autocyclic processes. Short-lived relative sea-level variations, as well as uplift and deformation episodes, resulted in three parasequences, separated by traceable flooding and ravinement surfaces. The subsequent transgression, which defines the base of the middle Curtis, flooded the entire study area, and beyond, allowing for the shallow-marine part of the system to enter into tidal resonance because the basin reached the optimal length-to-width configuration. This resonant system overprinted any evidence of allocyclic forcing and related traceable stratigraphic surfaces. However, the contemporaneous and neighbouring Summerville Formation's supratidal deposits, as well as the Moab Member's coastal aeolian dune field, characterised by five stacked aeolian sequences, lingered to record allocyclic signals, as the Curtis Sea regressed.

This study shows that (i) a tide-dominated basin can enter into resonance as it reaches its optimal morphological configuration, leading to the overprinting of otherwise dominant allocyclic processes by autocyclic behaviour. (ii) It is therefore required to extend the research focus to neighbouring and contemporaneous depositional systems in order to fully understand the dynamic stratigraphic history of a basin alternatively dominated by auto- and allocyclic processes.

Key word: Tidal resonance, autocyclic and allocyclic processes, stratigraphic surfaces, aeolian sequences, Curtis Formation

8.2. Extended abstracts, co-author

8.2.1. *Midtkandal et al. (2018). International Conference on Greenhouse Gas Control Technologies, Melbourne.*

Midtkandal, I.¹, Sundal, A.¹, Braathen, A.¹, Petrie, E.², Evans, J.³, Zuchuat, V.¹, Skurtveit, E.¹⁻⁴, Tveranger, J.⁵, Torabi, A.⁵, Gutierrez, M.⁶, and the COPASS team (2018). CO2 seal bypass – a multidisciplinary approach to CO2 migration and storage.

¹*Tectonostratigraphic Research Group, University of Oslo, Sem Sælands Vei 1, 0371 Oslo, Norway*

²*Natural and Environmental Sciences Department, Western State Colorado University, 600 North Adams Street, Gunnison, CO 81231*

³*Department of Geology, Utah State University, 4505 Old Main Hill, Logan, UT 84322-4505*

⁴*Norwegian Geotechnical Institute, Sognsveien 72, 0855 Oslo, Norway*

⁵*Uni Research, Centre for Integrated Petroleum Research, Allegaten 41, 5007 Bergen, Norway*

⁶*Civil and Environment Engineering Department, Colorado School of Mines, 1500 Illinois St., Golden, CO 80401*

Accepted for an oral presentation



14th International Conference on Greenhouse Gas Control Technologies, GHGT-14

21st -25th October 2018, Melbourne, Australia

CO₂ seal bypass – a multidisciplinary approach to CO₂ migration and storage

Ivar Midtkandal^a, Anja Sundal^a, Alvar Braathen^a, Elizabeth Petrie^b, James Evans^c, Valentin Zuchuat^a, Elin Skurtveit^{a,d}, Jan Tveranger^e, Anita Torabi^c, Marte Gutierrez^f and the COPASS team

^aTectonostratigraphic Research Group, University of Oslo, Norway

^bWestern Colorado State University, Gunnison, CO, USA

^cUtah State University, Logan, UT, USA

^dNorwegian Geotechnical Institute, Oslo, Norway

^eUni Research CIPR, Bergen, Norway

^fColorado School of Mines, Golden, CO, USA

Abstract

A multi-disciplinary project that targets a naturally occurring CO₂ plume and its interaction with the overlying sedimentary succession is summarized. The Navajo Sandstone – Page Sandstone – Carmel Formation – Entrada Sandstone – Curtis Formation – Summerville Formation is a largely sandstone-dominated succession which is naturally fed by mantle-derived CO₂ in central Utah. The succession has received an influx of CO₂-charged groundwater from below at times prior to its present-day state of erosion into cliff-forming strata that allow close inspection and sampling. Visually striking red rocks stained by Fe³⁺ are bleached by reducing CO₂-charged groundwater, creating pale yellow plumes, and striations through strata, and represent readily identifiable reservoirs and migration conduits for fluids, respectively. Typical field expressions are sandstone-dominated reservoir rocks that once hosted CO₂, whereas fracture corridors in low-permeability rocks such as marls and mudstones represent the main migration pathways (exceptions exist for both types). The study area displays a high-resolution record of entrapment, seal integrity and fluid flow in a multi-storied, CO₂-filled paleo-reservoir. As such, it provides a valuable analogue for understanding and forecasting geologically controlled effects and mechanisms likely encountered during future CO₂-capture and - storage efforts.

Keywords: CO₂, Jurassic, Utah, reservoir, modelling, sedimentology, structural geology

1. Introduction

Capture and storage of CO₂ is reliant on the presence of suitable sedimentary reservoir intervals that contain the appropriate sedimentary architecture, structural modifications, chemistry, porosity, and permeability. Any approaches to reservoir modelling include constraining the reservoirs inherent sedimentary heterogeneities, as well as their internal structural deformation, if any. A common approach to improving modelling and reducing risk is to visit geologic outcrop areas with rocks that share key traits with the target reservoir, such as origin of sedimentary strata or structural deformation history. The CO₂ Seal and Bypass (COPASS) project has approached a naturally occurring CO₂ reservoir in Utah (Fig. 1) that has been exhumed since the fluids migrated through the rocks. The Navajo Sandstone – Page Sandstone – Carmel Formation – Entrada Sandstone – Curtis Formation – Summerville Formation is a largely sandstone-dominated succession, which is naturally fed by mantle-derived CO₂.

Visually striking red rocks stained by Fe^{3+} are bleached by reducing CO_2 -charged groundwater, creating pale yellow plumes, and striations through strata, and represent readily identifiable reservoirs and migration conduits for fluids, respectively. Typical field expressions are sandstone-dominated reservoir rocks that once hosted CO_2 , whereas fracture corridors in low-permeability rocks such as marls and mudstones represent the main migration pathways (exceptions exist for both types).

The aforementioned cliff sections and subsurface strata represent an outstanding natural laboratory to target fundamental understanding of CO_2 plumbing systems covering aspects such as temporal impact of CO_2 plumes on flow and model forecasting capability. The study area provides unparalleled opportunities to study a real-world CO_2 fluid flow and storage scenario where lessons learned can be applied to other analogous areas where suitable. In contrast, analogous studies address outcrop sites where one or more parameters are deemed similar to one or more target reservoirs, whereas other dissimilarities must be adjusted for. This facilitates sensitivity studies on parameters impacting reservoir quality, integrity and responses, thus providing a tool for forecasting suitability of a given site for CO_2 storage. The work has included: (i) High-resolution field studies, (ii) assessment of scaling from mm-cm scale outcrop observations to high-resolution, representative element volume reservoir models, (iii) analyses of diagenetic effects, (iv) investigation of geomechanical properties of fault rocks and tight caprocks, (v) investigation around how reservoir pressure and time-dependent diagenetic impacts caused by CO_2 migration affect geomechanical properties, and (vi) education.

The project integrates observations from actively leaking and former, exhumed reservoir-seal systems employing field, laboratory and reservoir modelling studies. The aim is to implement observed flow and leakage patterns combined with observed diagenetic status and rock strength assessments in 3D simulation models. The outcome will be valuable for CO_2 storage site assessment by aiding containment planning, leakage prevention and

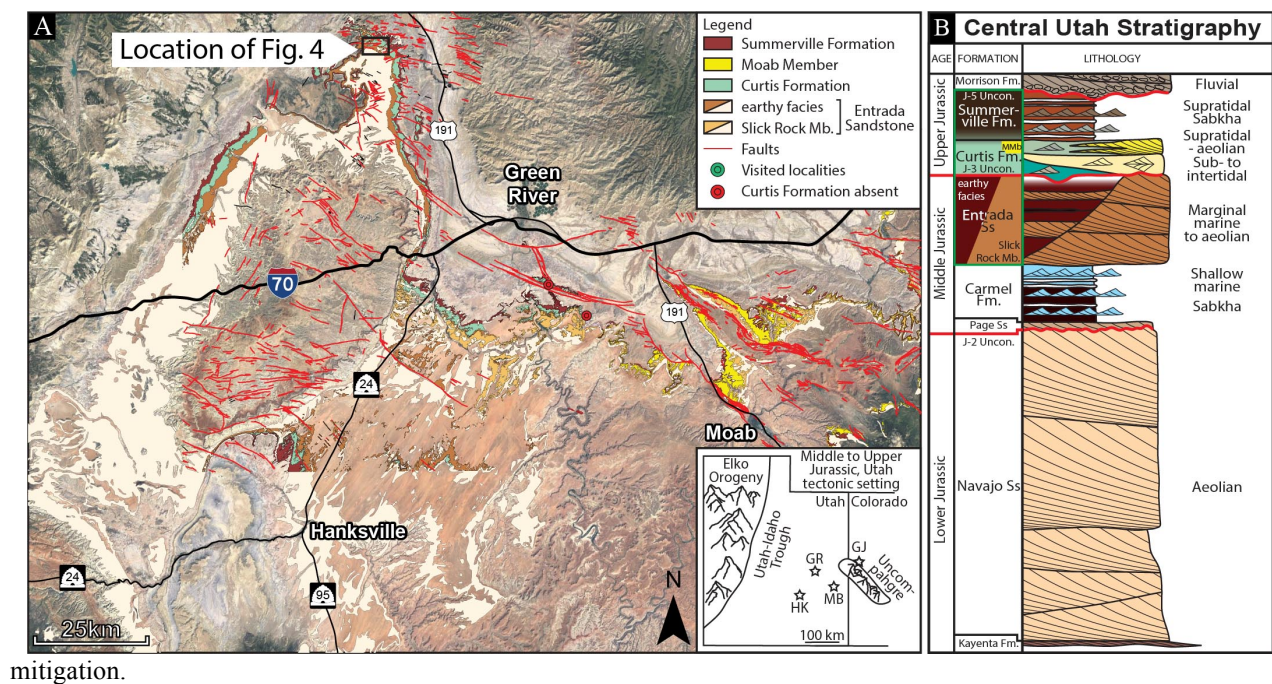


Figure 1. A: Map of field area, with insert map of Utah, with regional tectonic setting. B: Generalised stratigraphy of the study area, with main reservoir units shown as relative coarse-grained units.

1.1. Sedimentology of reservoir succession

Detailed characterization of sedimentary architecture and distribution of the reservoir interval has been among the primary scientific targets for the COPASS project. The sedimentary succession overall records several cycles of sea level variation that has intermittently submerged the region in a shallow sea, and/or exposed the area to air. Both scenarios include sedimentation in a warm and arid climate similar to today's Sahara, which resulted in carbonate and evaporite deposition in subaqueous sub-environments, and aeolian conditions on land, expressed as sand dunes and structureless loess strata. A preliminary distinction was made to determine which intervals represent significant reservoirs, and which are potential reservoir seals and/or intervals that may be bypassed through faults or fractures created by tectonic forces. A regional summary of reservoir and seal intervals is given in [1, 2], which identifies primary reservoirs in the aeolian Navajo and Entrada sandstones. The widespread desert dune intervals within the Navajo and Entrada sandstones represent nearly ideal reservoir intervals due to their homolithic and well-sorted nature. As such, these intervals contain valuable information on how fluids flow in these types of reservoirs, but present somewhat limited challenges with respect to distribution of reservoirs in heterolithic strata. These units are, however, subject to internal deformation during compaction from burial and structural stresses, as discussed in section 1.2 below. Other units within the exposed strata in the target area are heterolithic in nature and are prioritised scientific targets in this study.

Of special interest is the shallow marine succession represented by the Callovian Curtis Formation, which is identified as secondary reservoir succession. This unit is especially well exposed along accessible cliffs within and around the San Rafael Swell in central Utah, allowing high-quality 2D and 3D reconstructions of depositional development in space and time. This unit revealed a distribution of reservoir-grade sandstone that was systematically organized according to palaeo-water depth and the capacity of tidal currents to re-distribute sand during sedimentation [2]. The detailed investigation describes how sub-regional syn-sedimentary tectonic disturbance is recorded in the strata along with several short-lived pulses of relative sea level rise and fall, which in turn resulted in highly complex intra-Curtis Formation reservoir intervals, punctuated by mudstone. Up to 45 m of reservoir-grade sandstone intervals are documented in the Curtis Formation (Fig. 2), which display excellent reservoir properties, in part due to the early chlorite cementation typical of tidally dominated sedimentary environments. The resultant compartmentalisation of reservoir volumes is detailed in [2]. Furthermore, a sub-regional breakdown of architectural complexity allows construction of a depositional model that in turn can populate a realistic numerical model for fluid flow through the succession (discussed below). An improved understanding of how sedimentary sub-environments are distributed and stacked in widespread shallow basins in general has resulted from this study, as well as increased knowledge about Utah's Jurassic history

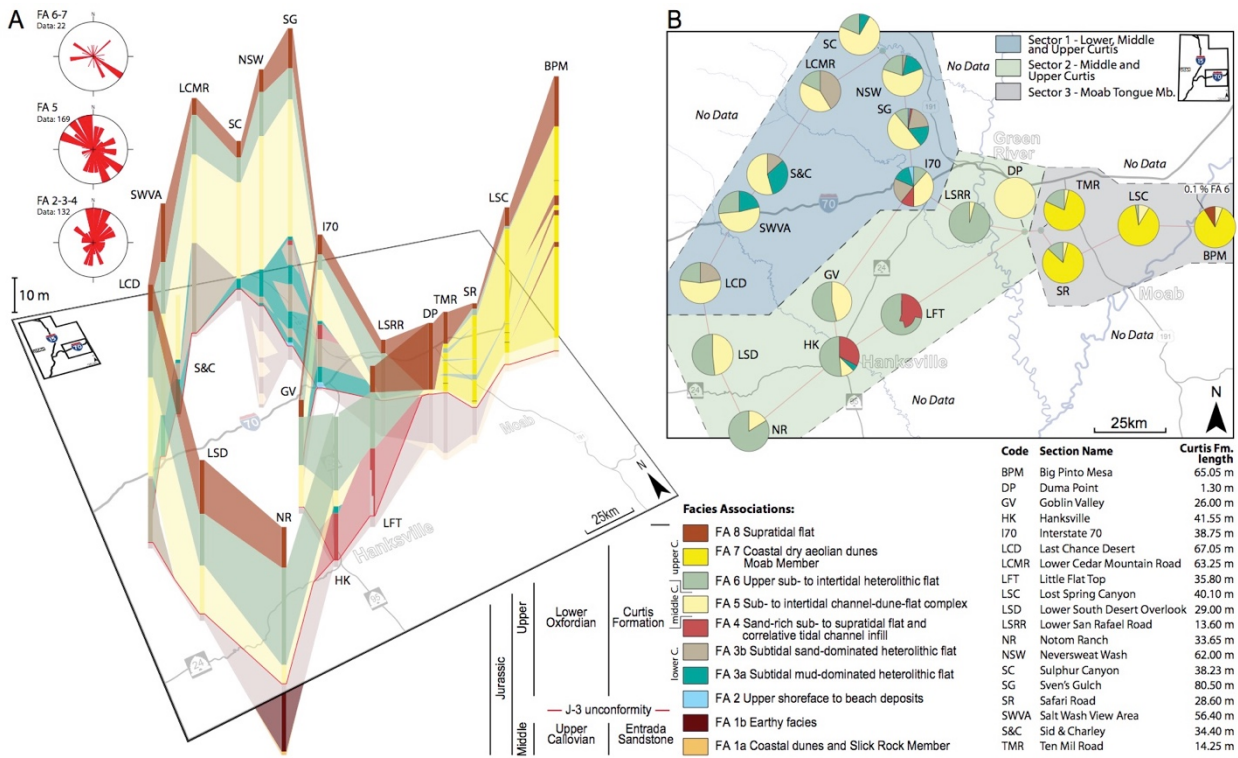


Figure 2. Regional distribution of reservoir, and non-reservoir units within the heterolithic Curtis Formation. The mapped thickness variations from [2] provide a base for further modelling of reservoir behaviour.

1.2. Structural geology and geomechanical properties of reservoir succession

Utah's geological record shows evidence of several major tectonic events occurring since the early Mesozoic, linked to the development of the North American Cordillera [3]; The Middle Jurassic - Lower Cretaceous Nevadan Orogeny; the Middle Jurassic Elko Orogeny, marked by an alternating extensional- and contractional stress regimes and the development of successive regional foreland basins; the Lower Cretaceous to Paleogene Sevier Orogeny, which resulted in thin-skinned contractional structures; and the Upper Cretaceous to Paleogene Laramide Orogeny, featuring notable basement-rooted monoclines, such as the San Rafael Swell – considered the most significant structural inheritance within the studied succession. Curtis Formation was buried to a depth of between 2.45 km and 2.86 km in the San Rafael Swell area [4].

Three main populations of structures have been investigated, in order to identify distribution, domineering deformation mechanism and potential impact on fluid flow; (i) deformation linked to Jurassic aeolian sandstones in the San Rafael Swell monocline, (ii) seismic scale normal faults, and (iii) fracture corridors (for ii and iii, see Ogata et al. 2014). Both folding and faulting of thick-bedded fine-grained aeolian sandstones triggered formation of deformation bands and fractures [5]. Larger, steep normal faults in the same sandstones show typical core and damage zones, as described in [1]. Within the several hundred meter wide west-verging monocline forelimb of the San Rafael Swell, in total 4 populations of deformation bands can be identified and ascribed to a given chronology. Common small-scale structures are shear-compaction cataclastic bands but there are also some shear-isochoric and shear-dilation bands. Further, certain locations host en-echelon fracture systems and isolated fractures with similar kinematics as the bands they are superimposed on. For all 4 populations, the band and fracture populations record progressive sub-simple shear of beds during folding, revealing cases where bands are either compactional or

dilatational depending on their orientation in the strain field. The high frequency of bands in the folded beds, with limited contribution from short fractures, transform the highly permeable host rock into an aquitard.

In addition to structures associated with normal faults and the fold-limb of the San Rafael Swell, the homolithic sandstones in the Navajo and Entrada sandstones contain systematic sets of deformation bands that stem from their burial and tectonic deformation history. These deformation bands' influence on fluid flow and compartmentalisation is documented and discussed in other studies (e.g. [6, 7]). The mechanical strength of reservoir-grade sandstone beds that have been subject to extensive stresses, expressed by dense deformation band sets in certain layers, was investigated in laboratory to test whether reservoir layers are weakened after expulsion of CO₂-charged water as a result of changing reservoir plumbing conditions. A relationship between layer porosity and uniaxial as well as tensile strength was documented for the Entrada Sandstone unit [6], where higher porosity leads to reduced strength. Testing for strength reduction caused by removal of load-bearing minerals within the reservoir layer proved inconclusive, in part due to enigmatic stratal relationships within the Entrada Sandstone reservoir zones, and thereby uncertain interpretations of sedimentary origin.

Further efforts have investigated seal integrity variables in the same successions, by laboratory-testing fine-grained samples from the Entrada Sandstone interval. This rock type responds to stress by fracturing, in contrast to the porous sandstone. Field samples and well data have been tested for strength variation between Fe-stained rocks that are bleached by CO₂-charged groundwater flow through the strata, and un-altered rocks. Calcite coats the fracture planes in places, suggesting precipitation during fluid flow, and the potential for clogging and thereby re-sealing of reservoir compartments during groundwater migration [7]. The only observed clogging, however, is identified as precipitated pyrite within a CT-imaged fracture.

1.3. Reservoir properties

Parts of the reservoir succession (i.e. Navajo, Carmel, Curtis, Entrada formations) has been subject to detailed petrographic studies, with an aim to evaluate dynamic reservoir and seal properties. A key target has been to constrain how they evolve under the influence of different pressure and temperature regimes (i.e. during burial, uplift, deformation), and are affected by reactive fluid flushing.

The red, aeolian sandstones, abundant and typical of the study area, are generally quartz and K-feldspar rich and fairly well sorted. The amount of fine grained, pore-filling clay, mainly illite and sericite, is facies dependent and more abundant in inter-dune settings. Carbonate cementation (i.e. calcite and recrystallized dolomite) is commonly pervasive, both pre- and post-dating quartz and feldspar overgrowths [9].

Fe-oxides and hydroxides are abundant, commonly appearing as fibrous, hematite aggregates [9]. Previous studies suggest that chemical removal of as little as 0.1 wt% Fe can cause evident bleaching of red sandstones [10]. As the observed Fe-aggregates are highly porous, however, with low density per area and volume fraction, it is difficult to quantify chemical mass removal by means of XRD and SEM. Paleo-fluid migration patterns are easily recognisable in the field, however, as bleached patches along fracture zones and reservoir/seal boundaries, and provide information of dynamic reservoir behaviour. Less carbonate cement is recorded in bleached, diagenetic facies, and more carbonate cement in fine grained, less permeable layers, suggesting carbonate dissolution by a migrating fluid [9].

Precipitates on fracture surfaces in bleached Entrada Sandstone were found to comprise gypsum and pyrite, indicating alternating red-ox conditions [7,11]. Evidence of multiple fluid expulsions into surrounding host rock is also recorded, with advective transport and subsequent precipitation along reaction fronts as Mn and Fe-oxides []. Diffusive bleaching along fractures, faults and along layer boundaries are common. Fluid front geometries and sharpness is indicative of reactive fluid density and reactivity. Bleaching patterns along the base of a sealing unit (Carmel Fm.) was found indicative of advective flow, as intrusion was induced by overpressure during deformation, illustrating how the capillary seal of a cap rock can be overcome [9]. Transient in-situ pressures and temperature variation in the reservoir causes temporal changes in fluid viscosity and thereby relative permeability. One and the same geological unit may behave as a conduit during some parts of burial/uplift-history, while sealing the unit at other times and physical conditions [9].

Porosity varies with facies and degree of cementation, from $< 5\%$ in sealing layers and muddy inter-beds, to $> 20\%$ in aeolian dune deposits. Permeability depends both on clay content and cementation, as well as on structural and sedimentological meso-scale heterogeneities. Permeable units between low-permeability layers are prone to over-pressurization during burial, and establishment of fluid escape routes during regional tectonic events may have caused de-pressurization and weak layer collapse. Very porous (and weak) beds would appear as excellent reservoirs in well data; while they may in fact display reduced horizontal and vertical permeability locally due to deformation band density. Facies-related differences in geomechanical properties, pressure distribution and selective structural collapse have significant implications for injectivity and reservoir behavior [6,7,9,12,13].

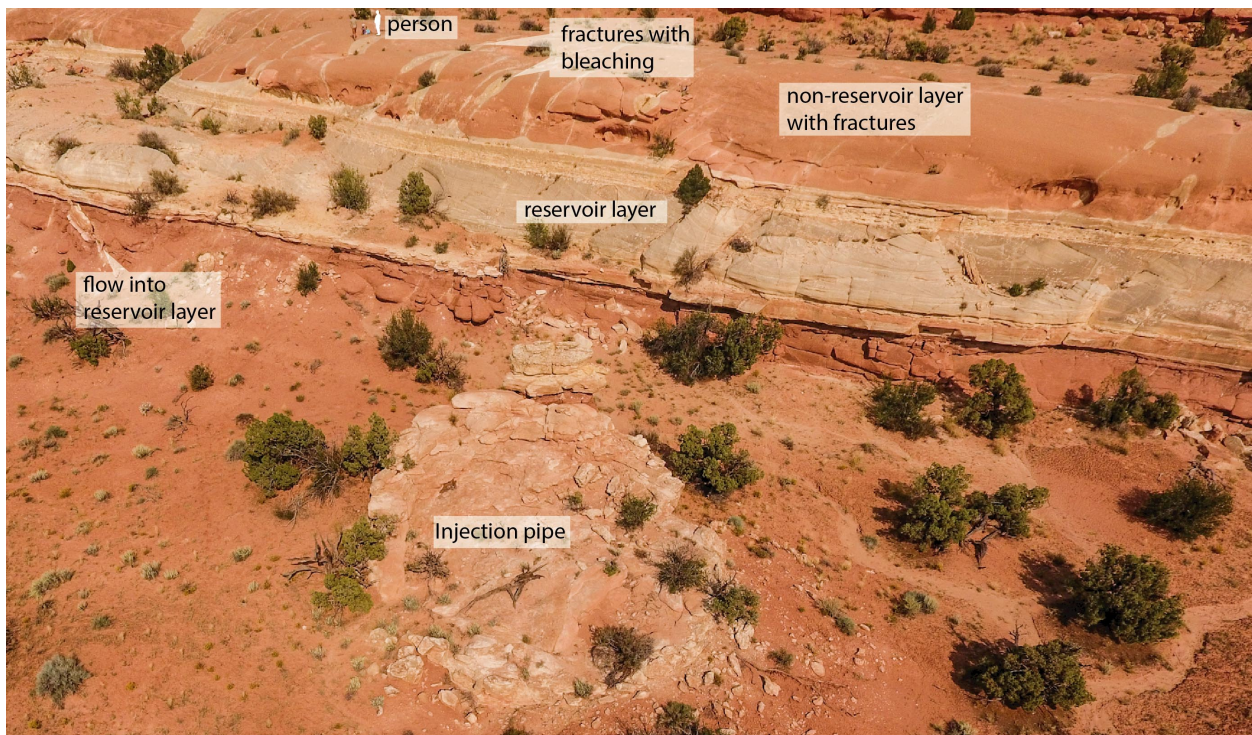


Figure 3. Field example of an aeolian reservoir layer, with fine-grained non-reservoir layers above and below. The circular feature in the foreground is one of many pipes that are considered fluid conduits in the area. Note the fracture sets with bleaching above the reservoir layer.

1.4. Reservoir modelling

Elements of the collected structural and sedimentological data are integrated in a reservoir model centered on the Entrada Sandstone – Curtis Formation interval in the Humbug Flat area NW of Green River. The model is based on an interpreted 3D, ground-based lidar scan draped with high-resolution digital images and linked to a series of sedimentary logs inside the model area. (Fig. 4)

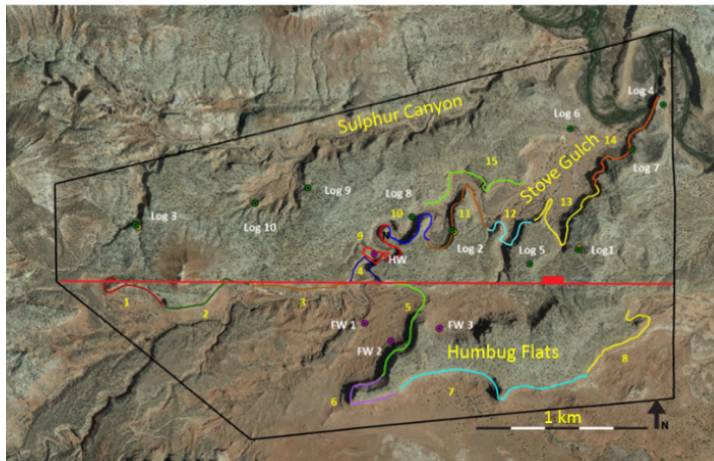


Figure 4. Location of the Humbug Flats site from Google Earth. The right image shows the extent of the modelled area (black line), Coloured lines show Outcrops scanned using lidar. Coloured dots and white labels show the position of the sedimentary logs. Note the East-West running normal fault crossing the area.

The sedimentary logs are included as “pseudo-wells” in the model, i.e. following the actual round-surface trace of the log rather than being vertical. The model area is bisected by an E-W oriented fault dipping around 60 degrees towards North with 40 m displacement. Interpretation of the lidar images was based on identifying and tracing key surfaces, including the J-3 unconformity separating the Entrada Sandstone and the Curtis Fm. and boundaries between facies associations identified in the sedimentary logs (Fig. 5).

	Zone	Facies association labels	Interpretation
Curtis Formation	11	C_FA5	Upper intertidal
	10	C_FA4	Sub-intertidal
	9	C_FA3	Subtidal
	8	C_FA2	Tidal transition
	7	C_FA1	Sub-tidal shelf
J-3 unconformity			
Entrada sandstone	6	E_FA2_1	Wet eolian dune
	5	E_FA3_1	Floodplain deposits
	4	E_FA1_1	Wet interdune
	3	E_FA2_2	Wet eolian dune
	2	E_FA3_3	Floodplain deposits
	1	E_FA4	Wet eolian dune

The resulting outcrop traces were compiled as points and used to reconstruct pre-erosion depositional and structural geometries. The surface together with the mapped fault form the framework for the model grid. Resolution XY is 20 m x 20 m; vertical resolution varies depending on thickness of the individual facies (cm to decameter).

The facies model set-up employs a combination of object and pixel-based methods employing geometric and spatial constraints mainly derived from the sedimentological work in the area (Fig. 6).

Petrophysical measurements for facies and fracture-related petrophysics from the outcrop are unevenly distributed, and in some cases most likely not representative for properties at the time of fluid migration (e.g. the Curtis Fm is presently pervasively cemented). The database is still in the process of being worked up ahead of carrying out flow simulations. The aim is to employ the model to simulate vertical and lateral movement of fluids in the Entrada – Curtis succession and compare results to bleaching patterns as observed in the field area.

Figure 5. Vertical structuring of the model is based identification of key stratigraphic surfaces. The thickness of the Entrada and Curtis are about 115 and 77 m respectively

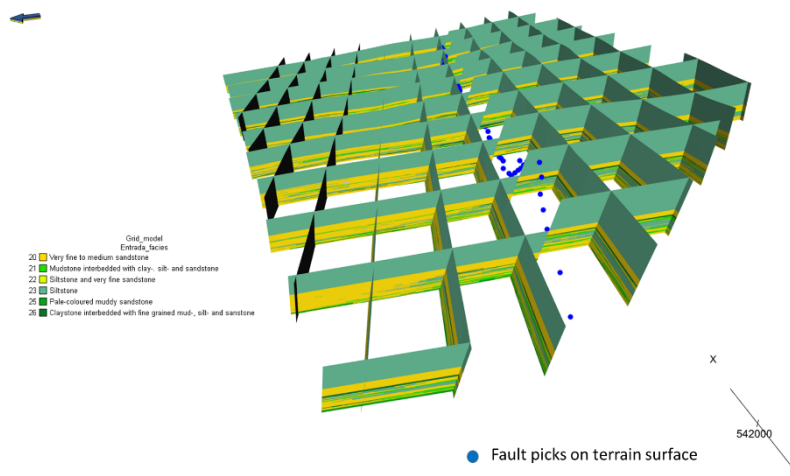


Figure 6. Row & column mesh showing a facies realization of the Entrada Sandstone. Blue dots indicate surface picks of the E-W trending fault.

1.5. Discussion

The exhumed (palaeo) CO₂ reservoir in central Utah lends itself to detailed, in-situ studies of a heterolithic reservoir succession that has been subject to structural deformation. The field data are naturally closely spaced where accessibility of outcrops is good, whereas other areas contain scarce or no information. Sedimentary architecture is well documented in outcrops with good exposure but limited accessibility by aerial

imagery, whereas sampling is reliant on both accessibility and outcrop quality. The shortcomings of field studies such as this cannot be accurately assessed simply due to the unknown entity represented by data that was never collected in the field. However, the high-resolution datasets that were amassed represent, as a collection or individually, potentially important input parameters for understanding reservoir behaviour and fluid flow when assessing other injection targets.

The lowermost portion of the reservoir succession studied in COPASS received CO₂-charged brine from a mantle, derived plume in the subsurface, and can be regarded as a poor analogue to injection strategies today. However, this project has shown that fractures in low-permeability strata higher in the stratigraphy acted as fluid conduits during vertical migration [8, 9], and thereby representing realistic fluid flow and reservoir behaviour scenarios in these intervals.

1.6. Conclusions

The multi-disciplinary approach to investigating a once functioning, naturally occurring CO₂ flow and storage reservoir has revealed a diversity in complexities which is expected to mirror challenges faced when planning and initiating CO₂ injection elsewhere. This study provides new insights into specific, geologically anchored data that goes into populating a numerical reservoir simulation, including a selection of the upscaling filters that are required in order to realistically simulate flow and storage without compromising complexity that has been documented from field studies. When comprehensively integrating complexities revealed by detailed studies that address specific sub-disciplines on a single reservoir, subsets of challenges can be addressed when targeting other injection sites in the future. The full complexity of the targeted exhumed palaeo-reservoir remains greater than this study can unravel within the budget and timeframe at present, and a similar level of complexity should be expected from subsurface targets upon investigating their feasibility from a geological perspective. The exhumed reservoir succession in Utah offers potential for resolving specific challenges that may arise from new targets sites in the future.

1.7. Scope for further work

New opportunities for investigation the behaviour of this naturally occurring CO₂ reservoir was uncovered during COPASS field campaigns. A number of apparent palaeo-seeps are expressed as landscape depressions and as remnant pipes in the landscape of CO₂ seal bypass-systems addresses:

- 1) What is the detailed footprint of CO₂ flow along faults and fractures?
- 2) Can seepage (leak) out of the storage compartment be identified by seismic imaging?
- 3) Will pressure-driven reactivation of faults and fractures create recordable micro-seismic events?
- 4) Can case-true synthetic seismic imaging of vertical CO₂ seep, consistent with geological flow paths, inform our interpretation of seismic chimneys?
- 5) Can detailed geological datasets and related geophysical models verify the existence of and quantify CO₂ volumes (saturation) required to create offshore geophysical chimneys, and thereby improve confidence in subsurface CO₂ reservoirs?

(1)

Acknowledgements

This work forms part of the CO₂ seal bypass project (COPASS), funded by the Research Council of Norway (RCN) under grant number 244049. We acknowledge cooperation with the SUCCESS research centre (grant number 193825/S60, RCN), and thank Schlumberger for software license-grants. The COPASS team members (in addition to the listed authors) include Nikoline Bromander, Sigrid Østmo daCosta, Nathan Cote, Kristine Halvorsen, Anette Harneshaug, Ida Hope, Eivind Larsen, Ole Rabbel, Algirdas Rimkus, Arve Sleveland, Susanne Tvetveterås, Fredrik Wesenlund.

References

- [1] Ogata K, Senger K, Braathen A, Tveranger J. 2014. Fracture corridors as seal-bypass systems in siliciclastic reservoir-cap rock successions: Field-based insights from the Jurassic Entrada Formation (SE Utah, USA). *J Struct Geol* [Internet];66:162–87. Available from: <http://dx.doi.org/10.1016/j.jsg.2014.05.005>
- [2] Zuchuat V, Sleveland AR, Sprinkel DA, Rimkus A, Braathen A, Midtkandal I. 2018. New insights on the impact of tidal currents on a low-gradient, semi-enclosed epicontinental basin - the Curtis Formation, East-Central Utah, USA. *Geol Intermt west.*;5:131–65.
- [3] Yonkee WA, Weil AB. 2015. Tectonic evolution of the Sevier and Laramide belts within the North American Cordillera orogenic system. *Earth-Science Reviews.*
- [4] Petrie ES, Sundal A, Gutierrez M, Braathen A. 2017. Deformation band formation and reactivation associated with a Laramide fault propagation fold. In: *Geological Society of America Abstract with Programs*. Seattle, Washington; p. 289–299 #303868.
- [5] Zuluaga LF, Fossen H, Rotevatn A. 2014. Progressive evolution of deformation band populations during Laramide fault-propagation folding: Navajo Sandstone, San Rafael monocline, Utah, U.S.A. *J Struct Geol* 68:66–81.
- [6] Larsen EB. 2015. Geomechanical and structural characteristics of a paleoreservoir-caprock succession - Sandstones of Humbug Flats, Central Utah. University of Oslo;. 90p.
- [7] Skurtveit E, Braathen A, Larsen EB, Sauvin G, Sundal A, Zuchuat V. 2017. Pressure Induced Deformation and Flow Using CO₂Field Analogues, Utah. *Energy Procedia*.114(1876):3257–66. <http://dx.doi.org/10.1016/j.egypro.2017.03.1457>
- [8] Sundal A, Skurtveit E, Midtkandal I, Hope I, Larsen EB, Kristensen RS, Braathen, A. 2016. Facies-controlled fluid migration patterns and subsequent reservoir collapse by depressurization - the Entrada Sandstone, Utah. In: *AGU Fall Meeting Abstracts*. San Francisco; 2016. p. Abs. ID H53D-1742. <https://agu.confex.com/agu/fm16/meetingapp.cgi/Paper/178654>
- [9] Sundal A, Miri R, Hellevang H, Tveranger J, Midtkandal I, Zuchuat V, Aagaard, P, Braathen, A. 2016. Movement of CO₂ charged fluids in low permeability rocks during deformation: migration patterns in the Carmel Formation, Utah. In: *13th International Conference on Greenhouse Gas Control Technologies*. Lausanne, Switzerland; 2016.
- [10] Parry WT, Chan MA, Beitler B. 2004. Chemical bleaching indicates episodes of fluid flow in deformation bands in sandstone. *Am Assoc Pet Geol Bull.* 88(2):175–91. <http://doi.aapg.org/bulletns/2004/02feb/175/175.htm>
- [11] Sundal A, Petrie ES, Hellevang H, Midtkandal I, Braathen A. 2016. Reactive Fluid Expulsion During Progressive Deformation In The Fold Limb Of The San Rafael Swell, Utah, Usa. In: *GSA Annual Meeting*. Denver, CO; no. 171-7.

[12]Hope I. 2015. Deformation bands in collapsed sandstone reservoirs. University of Oslo; 99p.

[13]Bromander N. Facies-controlled reservoir quality and preferential deformation in sandstone reservoirs; a case study from the Entrada Sandstone, Utah, USA. University of Oslo. 134p.

8.2.2. Skurtveit et al. (2017). International Conference on Greenhouse Gas Control Technologies, Lausanne.

Skurtveit, E.¹⁻², Braathen, A.², Larsen, E.B.², Sauvin, G.¹, Sundal, A.², and Zuchuat, V.² (2017). Pressure induced deformation and flow using CO₂ field analogues, Utah. *Energy Procedia*, 114, 3257-3266.

¹Norwegian Geotechnical Institute, Sognsveien 72, 0855 Oslo, Norway

²Tectonostratigraphic Research Group, University of Oslo, Sem Sælands Vei 1, 0371 Oslo, Norway

Accepted for an oral presentation



Available online at www.sciencedirect.com

ScienceDirect

Energy Procedia 114 (2017) 3257 – 3266

Energy

Procedia

13th International Conference on Greenhouse Gas Control Technologies, GHGT-13, 14-18
November 2016, Lausanne, Switzerland

Pressure induced deformation and flow using CO₂ field analogues, Utah

Skurtveit, Elin^{a*}, Braathen, Alvar^b, Larsen, Eivind B.^b, Sauvin, Guillaume^a, Sundal,
Anja^b and Zuchuat, Valentin^b

^aNorwegian Geotechnical Institute, PO Box 3930 Ullevaal Stadion, 0806 Oslo, Norway

^bUniversity of Oslo, PO Box 1047 Blindern, 0316 OSLO, Norway

Abstract

Exhumed reservoirs providing evidence of CO₂ accumulation and transport in geological history offer a unique possibility to supplement our knowledge on leakage processes observed along faults and fractures. A field location and drill core from Central Utah, USA has been used to characterize mechanical properties and fracture distributions in multiple reservoir-caprock couplets where bleaching pattern around fractures provides evidence of fluid flow. Analysis shows that fractures are mainly observed in low porosity units corresponding to layers with high strength and stiffness. Microstructural characterization substantiates evidence of fracture aperture separated by areas with mineral precipitation clogging aperture. Minerals observed filling fractures are calcite, gypsum and pyrite, suggestive of precipitation from reducing fluids. Fracture aperture distribution and identification of mineralogical changes along the fracture surface provides important input for improved, novel analyses of CO₂ transport properties of fractures and faults.

© 2017 The Authors. Published by Elsevier Ltd. This is an open access article under the CC BY-NC-ND license (<http://creativecommons.org/licenses/by-nc-nd/4.0/>).

Peer-review under responsibility of the organizing committee of GHGT-13.

Keywords: geological sequestration; leakage; faults; fractures; flow.

* Corresponding author. Tel.: +47 47893848

E-mail address: elin.skurtveit@ngi.no

1. Introduction

Geological sequestration of CO₂ is steadily maturing towards a stage where it may provide a significant means for mitigating global emissions. A key concern of the general public, potential investors, insurance companies and sequestration site operators is the risk of leakage of injected CO₂ from the reservoirs into nearby/overlying groundwater aquifers or hydrocarbon pools, or even to the surface. Existing sequestration sites are generally small and have not been operational for sufficient time to fully forecast and assess leakage scenarios of laterally extensive reservoirs on the time scales relevant for subsurface CO₂ storage. Thus the study of exhumed reservoirs showing evidence of CO₂ accumulation in geological history offer a unique possibility to supplement our knowledge on leakage processes observed along faults and fractures, and to understand the relevant spatial and temporal scales of CO₂ leakage in order to better constrain the threats of injection-induced pressure buildup.

In this paper we present the results from ongoing mapping and characterization of an exhumed reservoir and seal section in the Entrada Formation, central Utah. This site is of particular relevance to CO₂ storage studies due to natural subsurface CO₂ plumes, for instance underneath the Little Grand Wash Fault (Fig. 1). A research well drilled into the footwall damage zone of Little Grand Wash fault in 2012 retrieved a complete core of a multi-storied succession of reservoirs and caprocks [1, 2], and experimental characterization of core samples from this well is used to supplement field mapping datasets from the exhumed analogue at Humbug Flats. This site provides insight into a well exposed reservoir caprock succession of a fault and footwall anticline, where there is bleaching both along certain layers and up along faults and fractures. For the combined dataset, detailed mapping of stratigraphy and fracture distribution combined with mechanical testing and characterization of geochemical reactions and fracture flow properties, form our basis for discussion of fluid transport along fractures. This demonstrates the importance of in-depth assessment of faults and fracture corridors into seal integrity analysis, and emphasizes a demand for better understanding of controlling mechanism for fracture flow properties.

2. Study area

The study area in Central Utah (Fig. 1) is located at the northern end of the San Rafael desert, east and NE of the San Rafael Swell monocline, and above the NW termination of the Paradox Basin with its source rocks. The region offers multiple reservoirs and seal units, and has accordingly been the site for extensive hydrocarbon exploration and some production. Further, there are several reservoirs with CO₂ accumulation mainly charged from a mantle source. The local stratigraphy is described in Fig. 1d with the Jurassic eolian Navajo Sandstone and lower Entrada Formation as the two reservoirs of interest. The upper part of the Entrada Formation is a mixed (supra-) tidal to shallow marine succession where the low permeable layers of the Entrada Earthy facies, locally mottled, provide local seals to intraformational eolian sandstone reservoirs. Fluid migration and secondary trapping is controlled by faults and anticlines [e.g. 3], as seen for Little Grand Wash fault and Salt Wash graben, both truncating the Green River Anticline. These sites show ongoing CO₂-leakage with travertine, and extensive bleaching and mineralized veins in older exhumed parts. There are hydrocarbon strains documenting paleo-fluid flow [4].

In the study area, the approximately WNW-ESE trending Little Grand Wash fault has normal, down-south throw of 150-250 meters. Dated travertine documents 400.000 years of CO₂ expulsion and the Crystal Geyser is still active erupting CO₂-charged ground water [5]. Recently, a research well, CO2W55, was drilled into the footwall damage zone of the Little Grand Wash fault [1] covering a succession from the upper Entrada Formation, through Carmel Formation and into the Navajo Sandstone. Element and isotope geochemistry of fluid samples from the drilling project show a complex mixing of CO₂ saturated brine as inflow from faults and flow of CO₂ undersaturated meteoric groundwater in the Navajo Sandstone reservoir. Further, reacted CO₂-charged brines were found in the overlying fractures and reservoirs zones [1].

Humbug Flats is located to the NE side of the San Rafael Swell, the latter a regional asymmetric anticline (Fig. 1c). The study site is intersected by an E-W trending normal fault with displacement of tens to hundred meters.

Extensive structural and stratigraphic mapping of the Entrada Formation in this area show fault related fracture corridors comprising joint swarms and subordinate shear fractures with extensive bleaching within the fault tip process-zones [6].

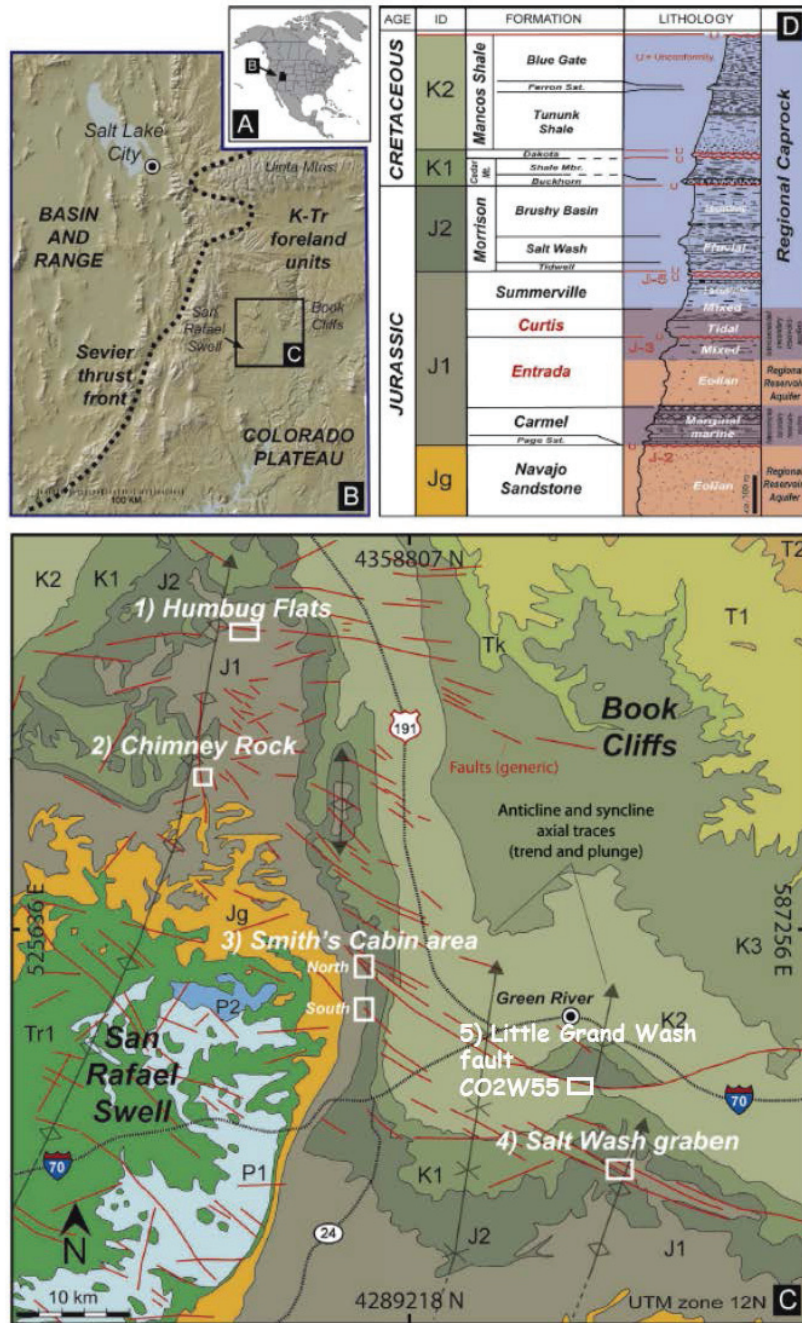


Fig. 1. Field location, Utah (A, B), geological map (C) and stratigraphy for the area (D), after Ogata et al. [6]. The locality at Humbug Flats and the well CO2W55 along the Little Grand Wash fault is marked on the geological map.

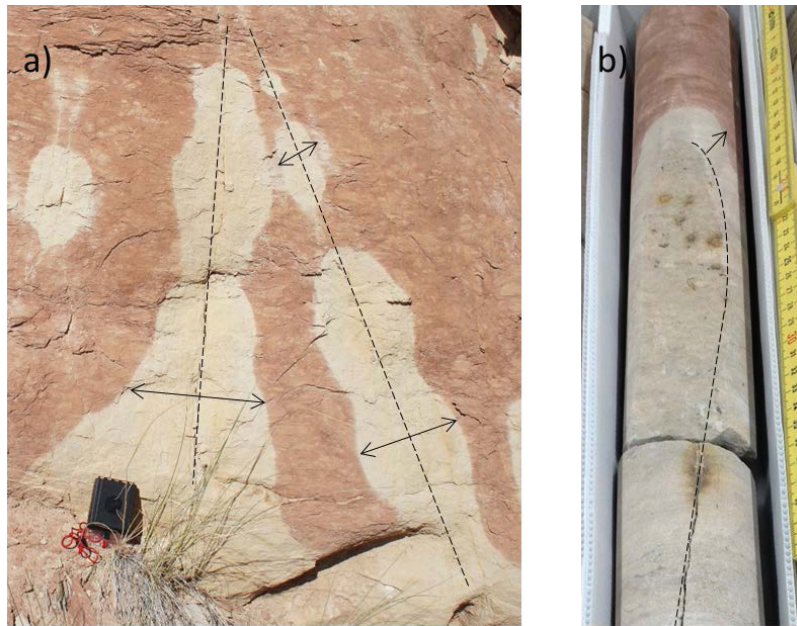


Fig. 2. Fractures (dotted lines) showing varying width of bleached, altered zone marked by arrows. Fractures observed in the Humbug Flats site (a) and in drill core from well CO2W55 (b).

3. Methods

In the field, 1d scan lines were used to collect statistical data on fracture distribution for selected sandstone layers within the upper Entrada Formation. These units vary in porosity. Fracture orientation (strike-dip), layer appearance (bed-confined or through-going) and bleaching patterns were recorded. Plugs for mechanical testing was prepared in the laboratory from blocks sampled in the field. The test program for the field samples from Humbug Flats comprised unconfined compressional strength tests (UCS) and indirect tensile strength tests (Brazil test). All tests were performed using equipment located at the Norwegian Geotechnical Institute (Oslo, Norway). Standard sized plugs of 25 mm diameter and around 55 mm height were prepared for the UCS tests. For the Brazil tests discs of 25 mm diameter and height of 12.5 mm were used. All plugs were tested in dry conditions. The porosity of the investigated layers were calculated from the plug bulk density and particle density. Since the layers all have a quartz-dominated mineralogy, the theoretical particle density of quartz, 2.65 g/cm^3 , were used in the calculations.

Natural fractures from well CO2W55 targeting Little Grand Wash fault were logged and sampled at the Shell core storage in Rijswijk, Nederland. Fractures orientation, bleaching, mineral fill, displacement and depth were recorded. Additionally the fracture roughness (joint roughness coefficient, JRC) was measured for open fractures following the method suggested by Barton and Choubey [7]. Fracture aperture was recorded using a Nikon Metrology industrial high-resolution 3-D computer tomography (CT) scanner, which images processed into three-dimensional reconstructions of the 3D aperture distribution of fractures. In addition, microstructure and mineral composition of fracture surfaces were characterized using a HITACHI SU 5000 (Field Emission) scanning electron microscope (SEM).

4. Data of Humbug Flats

4.1. Field observations

The field location at Humbug Flats shows a reservoir-caprock succession (Fig. 3a and b) of which layers with four characteristic facies, L1-L4, has been studied in detail. Work targeted layer-mechanical properties and fracture frequencies in transects toward a one m-displacement fault (Fig. 3c) with a distinct slip surface. Facies L1 and L4 is fluvial plain/overbank deposits with porosity ranging from 8-14 %, L2 is a fluvial sandstone with porosity around 20 % and L3 is a bleached eolian sandstone with 30 % porosity. The latter unit is clearly visible as a "white" layer in the succession.

The fractures were recorded in the vicinity of a fault cutting layer L1-L4. The three most competent layers, L1, L2 and L4 is dominated by bed confined fractures, although some through going fractures are observed for each layer. Fracture frequencies listed in Table 1 is from around the small fault zone. The highest fracture frequency of 5 fractures per meter is found for L1. Layer L3 differs from the three other layers by the presence of deformation bands and deformation band swarms and slightly fewer fractures. Background fracture frequencies are found to be an average of 0.7 fractures per meter. The fractures measured outline two fracture populations, respectively NNW-SSE and WNW-ESE, both with a high angle to bedding.

4.2. Geomechanical characterization

The geomechanical characterization includes a total of 11 UCS tests and 71 indirect tensile strength measurements for four characteristic facies L1-L4. The tensile strength is in the order of 0.5 to 3.5 MPa, whereas the uniaxial compressive strength (UCS) is 30-40 MPa for L4 and 60-70 MPa for L1. UCS was not measured for L2 whereas for the weak L3 facies, tensile fractures split the plug vertically and a strength of 2 MPa were measured. The results show a good correlation between tensile strength and porosity, with the highest porosity corresponding to the lower strength. The mechanical strength and elastic properties are listed in Table 1 together with porosity and fracture data from the scanlines.

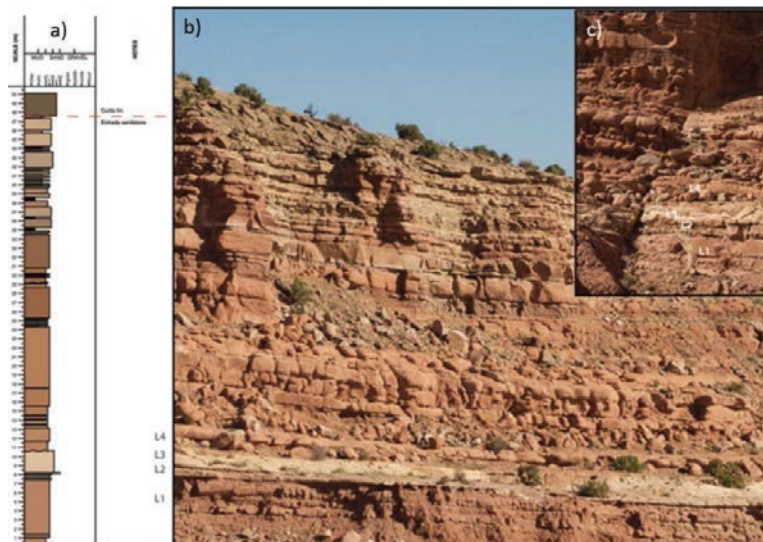


Fig. 3. Humbug Flats sedimentary log (a) outcrop photo showing the position of layer L1 to L4 in the lower part of the logged section (b) and photo of the 1 m displacement fault where scanlines for fracture frequencies are recorded (c).

Table 1. Layer description and strength measurements for location at Humbug Flats.

Humbug Flats	Description	Porosity (%)	Fracture distribution (maximum #/meter)	Young's Modulus (GPa)	UCS strength (MPa)	Indirect tensile strength (MPa)
Layer L4	Quartz dominated, some plagioclase and iron oxides	13-16	4	2-3	38	1.6
Layer L3	Quartz dominated, bleached color and extensively deformed by deformation bands	26-30	2	0.1-0.2	2	0.4
Layer L2	Quartz dominated, with carbonate crystals	16-20	4	-	-	1.2
Layer L1	Quartz dominated, some plagioclase and iron oxides	7-10	5	4-5	65 MPa	2.7

5. Data of Little Grand Wash Fault

5.1. Fracture distribution

Sedimentary log and fractures in the Entrada Formation of well CO2W55 from depth interval 20-100 m is presented in Fig. 4 and show a fracture frequency of 0-3 fractures per meter. The fractures logged are all natural sub-vertical fractures. Irregular fractures typical for degassing of CO₂ during coring is not included in the log. Deformation bands are also not included. The logged fracture are all classified as tensile (mode I) fractures with no indications of shear movement. Most fractures were found in bleached parts of the core, only four fractures were from unbleached parts. JRC was measured for all the open fractures and give an average coefficient of 8-9, with the smoothest fractures offering JRC of 6 and the roughest a JRC of 13. Comparison of the fracture log with the sedimentary log show that fractures are mostly observed within the low permeable horizons, whereas the thick reservoir sections at 35-45 m depth and 80-88 m depth is unfractured.

5.2. Fracture aperture

Preliminary results from the fracture characterization using computer tomography (CT) show that there is a distinct difference between fractures with extensive bleaching contrary to non-bleached fractures of the Entrada Formation (Fig. 5). The unbleached fracture show a small fracture aperture, with several contact points along the fracture and limited mineral growth, whereas bleached fractures have a wider fracture aperture, more complex fracture pattern and precipitation of calcite and some heavy minerals. Fracture aperture distribution was mapped using the 3D CT volume of plugs from the fractures in the core, as shown in Fig. 6. The maximum fracture aperture mapped is 1.2 mm. High aperture pathways can be interpreted as continuous zones across the plug and one high aperture zone can be correlated with an intersecting fracture. The dark blue represents areas where the fracture is completely clogged by precipitated oxides seen as high density (black) CT values.

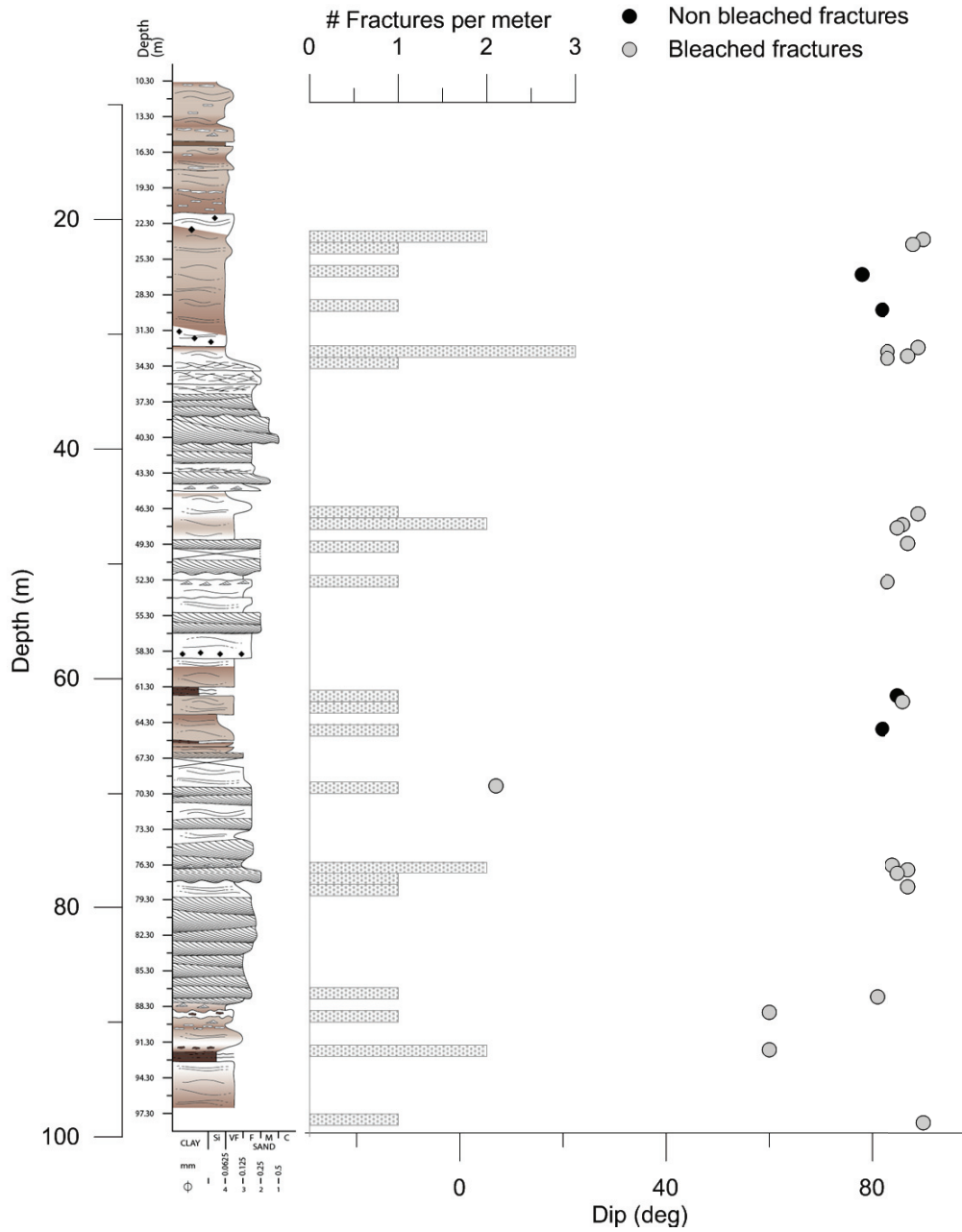


Fig. 4. Sedimentary and fracture log from well CO2W55 in the footwall damage zone of Little Grand Wash fault. Bars show natural fractures per meter of logged core (top axis). Dots show dip of fractures (lower axis) and indicate the relative amount of fractures in bleached or unbleached host rock.

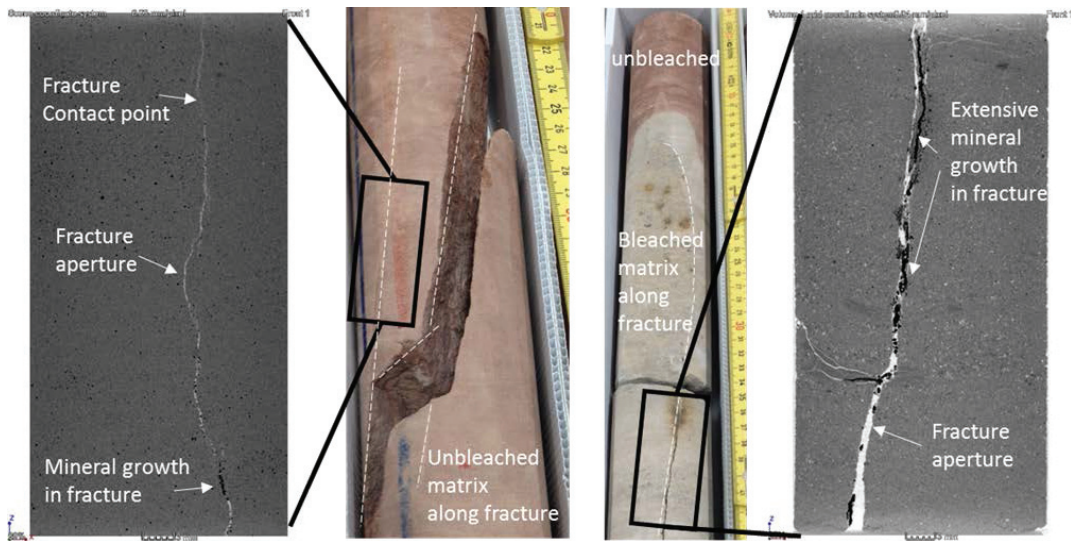


Fig. 5. Example of unbleached (sample 1) and bleached (sample 7) fractures in core from the Entrada Formation, Utah (see Fig. 4). Computer tomography (CT) images from plugs cored along the fracture show fracture aperture (white), dense minerals as fracture fill (black) and contact points along the fracture where there is no aperture.

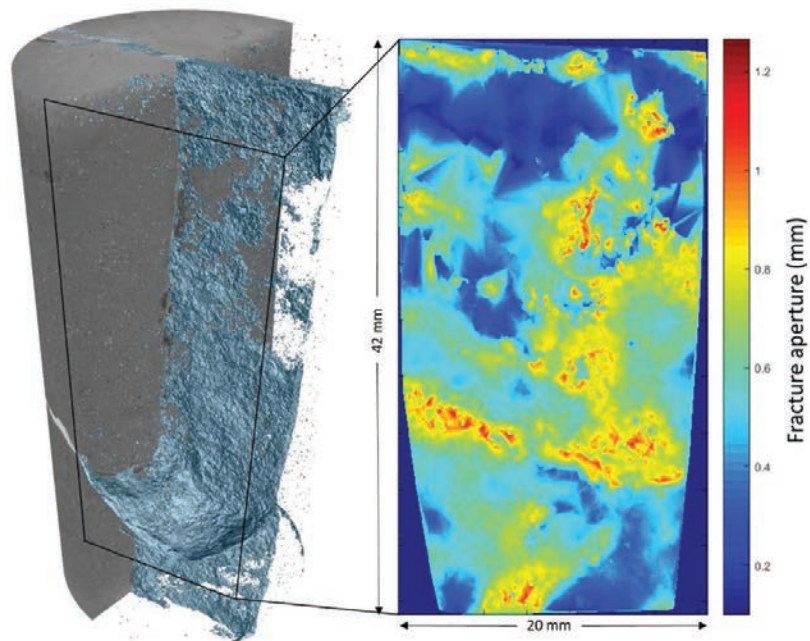


Fig. 6. Fracture aperture visualization based on the 3D CT volume of plug from bleached fracture at depth 45.75 m in well CO₂W55. A section of the main fracture surface is mapped and coloured based on aperture. Red is the highest aperture (1.2 mm), whereas dark blue is the lowest detectable aperture from the CT pixel resolution (0.1 mm) and completely clogged areas.

5.3. Fracture microstructure and geochemical characterization

Fractures from the core were sampled from bleached and unbleached Entrada Formation. From each sampling interval one fractured and one intact/unfractured plug were sampled. Table 2 show the preliminary results from the fracture and matrix characterization. On the fracture plane of sample 1, representing red coloured diagenetic facies of Entrada Sandstone, large, euhedral calcite crystals are observed. Barite crystals are relatively abundant as well. These may have precipitated from saline pore-fluids, but may also be a sample pollutant sourced from drilling mud (barite appears to postdate calcite). The calcites are interpreted as precipitated in situ from a carbonate saturated solution. Grains making up a quartz-rich sandstone matrix are coated with illite. The red color characteristic for aeolian deposits is commonly found to stem from hematite (often mixed with illite) coating [8]. The fracture surface of sample 4, representing a bleached zone, is rougher compared to sample 1. Dark, scattered mineral growth (sparse) in light grey sandstone matrix is pyrite, interpreted to have precipitated from reducing fluids. Fe-reduction with resultant bleaching, with associated sulphate (aqueous) reduction may form pyrite [8]. Clay coatings are not observed, however pore filling clays (illitic) are present. K-feldspars appear leached. Sample 7 matrix comprises porous, light coloured quartz rich sandstone with evident overgrowths. Dark patches on the fracture surface are made up of gypsum with abundant pyrite. Gypsum appears as fibrous crystals in rosettes, with scattered euhedral, cubic pyrite crystals. Their coexistence is indicative of varying redox-conditions, consistent with Ca and S in gypsum that is sourced from carbonate weathering and pyrite oxidation [9, 10].

Table 2. Description for selected fractured intervals within the core from the drill hole CO₂W55, Little Grand Wash fault.

Core depth (m)	Sample (#)	Description	Host rock porosity (%)
24.71 - .77	1-3	Unbleached zone with sub-vertical fracture. The matrix is quartz-rich with illite as grain coating. Calcite and barite crystals are observed on the fracture surface.	5-6
32.02 - .37	4-6	Bleached zone with sub-vertical fracture. Quartz rich matrix with pore filling clays. Pyrite scattered on the fracture surface.	8-9
45.75 - .94	7-10	Bleached zone with sub-vertical fracture. Quartz rich sandstone. Fracture surface show patches of gypsum and pyrite.	8-10

6. Discussion and conclusions

The mapped fracture distribution of Humbug Flats and the core from well CO₂W55 show that fractures are mainly found within the low porosity Earthy facies sections of the Entrada Formation. The current strength data available for Entrada Formation at Humbug Flats suggests a relationship between mechanical strength and porosity, where the layer L1 is found to have the highest fracture frequency and the lowest porosity together with the highest stiffness and strength. The fractured samples from the core logging in well CO₂W55 is from intervals with similar matrix porosity as layer L1, suggesting a similar strength and stiffness for these layers. Overall, the dominant failure mode observed within the core is mode I joints. Our interpretation is that the logged section of Entrada Formation can be described as the damage zone of Little Grand Wash fault and that the sub-vertical fractures define a fracture corridor seal bypass system as described by Ogata et al. [6].

Microstructural and geochemical observations from the fracture surfaces sampled indicate transport of reducing fluids along the fractures. The fluid is most likely a reacted CO₂ charged brine as described by Kampman et al. [1] resulting from the complex mixing of CO₂ saturated brine and groundwater within the Navajo reservoir sandstone and migrating upwards and along the fracture corridors. The CT imaging of the fractures and following aperture mapping indicate that the fracture is a mixture of open fracture providing distinct pathways for flow (Fig. 6) and

contact points where the fracture has been clogged by a dense mineral phase identified as pyrite precipitated from the in-situ fluid within the fracture.

The fracture mapping and characterization provided in this study provide important background data needed for the design and interpretation of planned fracture flow tests. Controlling parameters for fracture flow is the fracture aperture, whereas the sensitivity of a fracture to open or close due to changes in normal stress or shear stress is controlled by the fracture stiffness. The fracture stiffness can be related to the distribution of contact areas versus aperture and further visualization and quantification of the fracture aperture and contact points will be important aspect together with measurements of fracture flow properties under varying stress conditions.

Acknowledgements

We thank to Shell for access to core samples. Funding for the research is awarded from the Research Council of Norway to the CO₂ seal bypass project (no 244049).

References

- [1] N. Kampman, M. Bickle, A. Maskell, H. Chapman, J. Evans, G. Purser, Z. Zhou, M. Schaller, J.C. Gattacceca, P. Bertier, Drilling and sampling a natural CO₂ reservoir: Implications for fluid flow and CO₂-fluid-rock reactions during CO₂ migration through the overburden, *Chemical Geology*, 369 (2014) 51-82.
- [2] A. Busch, N. Kampman, S. Hangx, J. Snippe, M. Bickle, P. Bertier, H. Chapman, C. Spiers, R. Pijenburg, J. Samuelson, The Green River Natural Analogue as A Field Laboratory To Study the Long-term Fate of CO₂ in the subsurface, *Energy Procedia*, 63 (2014) 2821-2830.
- [3] I. Garden, S. Guscott, S. Burley, K. Foxford, J. Walsh, J. Marshall, An exhumed palaeo - hydrocarbon migration fairway in a faulted carrier system, Entrada Sandstone of SE Utah, USA, *Geofluids*, 1 (2001) 195-213.
- [4] B. Dockrill, Z.K. Shipton, Structural controls on leakage from a natural CO₂ geologic storage site: Central Utah, USA, *Journal of Structural Geology*, 32 (2010) 1768-1782.
- [5] J.P. Evans, J. Heath, Z.K. Shipton, P.T. Kolesar, B. Dockrill, A. Williams, D. Kirchner, T.E. Lachmar, S.T. Nelson, Natural leaking CO₂-charged systems as analogs for geologic sequestration sites, in: *Third Annual Conference on Carbon Capture and Sequestration*, Alexandria, VA, 2004.
- [6] K. Ogata, K. Senger, A. Braathen, J. Tveranger, Fracture corridors as seal-bypass systems in siliciclastic reservoir-cap rock successions: Field-based insights from the Jurassic Entrada Formation (SE Utah, USA), *Journal of Structural Geology*, 66 (2014) 162-187.
- [7] N. Barton, V. Choubey, The shear strength of rock joints in theory and practice, *Rock Mechanics*, 10 (1977) 1-54.
- [8] B. Beitler, W.T. Parry, M.A. Chan, Fingerprints of fluid flow: Chemical diagenetic history of the Jurassic Navajo Sandstone, southern Utah, USA, *Journal of Sedimentary Research*, 75 (2005) 547-561.
- [9] C. Ritsema, J. Groenenberg, Pyrite oxidation, carbonate weathering, and gypsum formation in a drained potential acid sulfate soil, *Soil Science Society of America Journal*, 57 (1993) 968-976.
- [10] Z. Lin, X. Sun, Y. Lu, L. Xu, J. Gong, H. Lu, B.M. Teichert, J. Peckmann, Stable isotope patterns of coexisting pyrite and gypsum indicating variable methane flow at a seep site of the Shenhu area, South China Sea, *Journal of Asian Earth Sciences*, 123 (2016) 213-223.

8.2.3. Sundal et al. (2017). International Conference on Greenhouse Gas Control Technologies, Lausanne.

Sundal, A.¹, Miri, R.¹, Hellevang, H.¹, Tveranger, J.², Midtkandal, I.¹, Zuchuat, V.¹, Aagaard, P.¹, and Braathen, A.¹ (2017). Movement of CO₂ charged fluids in low permeability rocks during deformation: migration patterns in the Carmel Formation, Utah. *Energy Procedia*, 114, 4537-4544.

¹Tectonostratigraphic Research Group, University of Oslo, Sem Sælands Vei 1, 0371 Oslo, Norway

²Uni Research, Centre for Integrated Petroleum Research, Allegaten 41, 5007 Bergen, Norway

Accepted for an oral presentation



13th International Conference on Greenhouse Gas Control Technologies, GHGT-13,
14-18 November 2016, Lausanne, Switzerland

Movement of CO₂ charged fluids in
low permeability rocks during deformation:
migration patterns in the Carmel Formation, Utah
Anja Sundal^{1*}; Rohaldin Miri¹; Helge Hellevang¹; Jan Tveranger²;
Ivar Midtkandal¹; Valentin Zuchuat¹; Per Aagaard¹ and Alvar Braathen¹.

¹Department of Geosciences, University of Oslo, Sem Saelands vei 1, 0371 Oslo, Norway

²Uni Research, Centre for Integrated Petroleum Research, Nygårdsgaten 112-114, 5020 Bergen, Norway

Abstract

Understanding geodynamic reservoir and seal performance is important in order to ensure safe storage of CO₂. In Utah leakage from natural gas reservoirs through sandstones and along faults may be observed as diagenetic alteration traces. Aeolian deposits, stained red by iron oxides, have commonly been bleached by reducing fluids of varying density. At the study site, bleaching is observed within and along the base of a low-permeability, regionally sealing unit; the lowermost Carmel Formation. Compactional stress during progressive deformation in the San Rafael monocline induced pressure gradients driving flow through the seal and towards venting fractures. Chemical transport processes are interpreted to be a combination of diffusion and advection. Capillary barriers may be overcome as transient *in situ* pressures and temperatures affecting fluid properties. The same geological unit may behave as a conduit during some parts of burial/uplift-history and as a sealing unit at other times.

© 2017 The Authors. Published by Elsevier Ltd. This is an open access article under the CC BY-NC-ND license (<http://creativecommons.org/licenses/by-nc-nd/4.0/>).

Peer-review under responsibility of the organizing committee of GHGT-13.

Keywords: fluid flow; CO₂; CCS; leakage; advection; diffusion; siltstone; seal;

* Corresponding author. Tel.: +47 40 88 53 80

E-mail address: anja.sundal@geo.uio.no

1. Introduction

Reservoir characterization including evaluation of fluid properties and behaviour in different parts and depths of a reservoir is of importance to ensure safe, long term CO₂ sequestration. Our study targets well exposed and accessible sedimentary rocks as reservoir and seal analogues for CO₂ storage in Utah, USA (Fig. 1). These reservoirs display evidence of progressive deformation, diagenesis and CO₂ fluid flushing both prior to - and after exhumation, and present a unique outcrop analogue in which to study fluid phase behaviour, flow in fractures and porous media and their associated geochemical alterations.

One aim of the COPASS project is to investigate the effect of fluid density on plume geometries and escape routes during deformation of the reservoir and cap rocks, as well as the relative contribution of advective versus diffusive chemical mass transport. Our chosen field locality in the Carmel Formation (Fig.1), exhibits a puzzling pattern of fluid migration within and along the base of a low-permeability unit, as well as displaying evidence for upwards flow towards and through fracture corridors. The plume imprint can be observed in outcrop as bleached sections of otherwise red siltstone, interpreted as reducing fluids (e.g. CO₂ charged brine) that dissolved and removed iron through reactive transport [1].

2. Geological setting

2.1. Sedimentology and rock texture

The Carmel Formation was deposited during the Middle Jurassic (ca. 160 Ma) and forms part of the San Rafael Group; overlying aeolian deposits of the Page and Navajo Sandstones and succeeded by the Entrada Sandstone. It comprises a 50-300 m thick succession of sandstone, shale, limestone and gypsum beds [2], reflecting a transition from aeolian to restricted marine conditions [2, 3, 4] The investigation targets the lowermost 2 m interval of the Carmel Formation [5], which in the study site comprises deep red/brown/purple coloured sandy mudstone (Fig. 1).

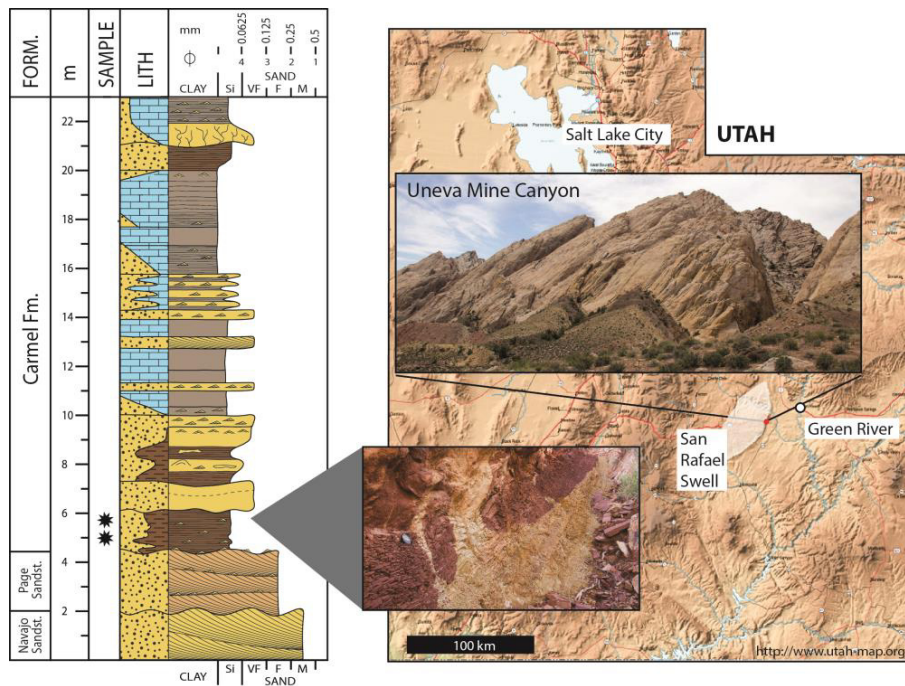


Fig. 1. Sedimentary log (left) through the upper Navajo and Page sandstones and into the studied unit; the Carmel Formation. Sample locations are marked with stars. Map showing the location of the field study site in Uneva Mine Canyon crosscutting the San Rafael Swell in SE Utah.

Bleached parts of the unit appear yellow/white and are likely formed through Fe-removal by reducing fluids [1]. The red, finely laminated intervals are interpreted as coastal sabkha deposits, with coarser grained, lighter coloured and rippled sandstone layers representing fluvial input, with possible marine incursions and reworking. The deposits become progressively more marine upwards, comprising fully cemented, sandy limestones. These appear completely impermeable.

In a thin-section sample cut perpendicular to bedding (at about 5 m in the log shown in Fig. 1), it is evident that the bed is finely laminated, with mean grain sizes varying from silt ($< 62.5 \mu\text{m}$) to clay (Fig. 2). The porosity is very low, in the order of 1 to 5 % as estimated with simple image analysis (color pixel count with ImageJ software). Some apparent moldic pores (lower right, Fig. 2) may be due to damage during sample preparation.

Carbonate cementation is pervasive (Fig. 2), and clay pore filling is dense, thus permeability in this part is extremely low to non-existent; typically $< 1 \text{ mD}$, contrasting with the underlying high permeability Page and Navajo sandstone aquifers. From a reservoir modeler's perspective the Carmel Formation is commonly considered a sealing unit.

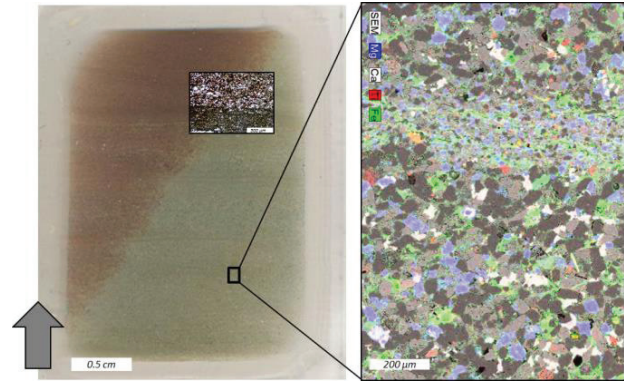


Fig. 2. Thin section cut perpendicular to layering and spanning a reaction front (bleaching). Arrow shows stratigraphic up. Insert photo from optical microscope (plane light, 5x). Right: photomicrograph from SEM showing rock texture and carbonate cement distribution as blue dolomite (Mg) + white calcite (Ca). Porosity is black, Fe is green and Ti is red.

2.2. Structural deformation

When modeling fluid migration, the structural setting and burial history are important elements to consider. The San Rafael Swell forms a large (km scale), N-S striking monocline ascribed to fault-propagation folding above basement-rooted thrusts as part of the Laramide Orogeny. Later uplift and erosion has exposed the Jurassic stratigraphy which now can be investigated in numerous gullies cutting at right angles through the monocline ("flat irons" Figs. 1, 3). At the study site, the layer of interest is dipping 52° , consistent with an overall fold axis that trends 012° . The growth of the San Rafael monocline may have started in the Late Cretaceous, and ends in the Eocene with termination of the Laramide orogeny. Non-decompacted maximum burial is estimated to 4.1 km using regional stratigraphic thickness and borehole data within the San Rafael Swell [6].

Progressive deformation during monocline growth can be established from cross cutting relationships of deformation bands, fluid intrusions and fractures in the underlying, porous and well sorted sandstones [7, 8]. These authors advocate that sedimentary bed and lamina-parallel deformation bands formed early in the folding phase, while E-W striking fractures, perpendicular to the fold axis, are interpreted to have formed in the later stages of deformation.

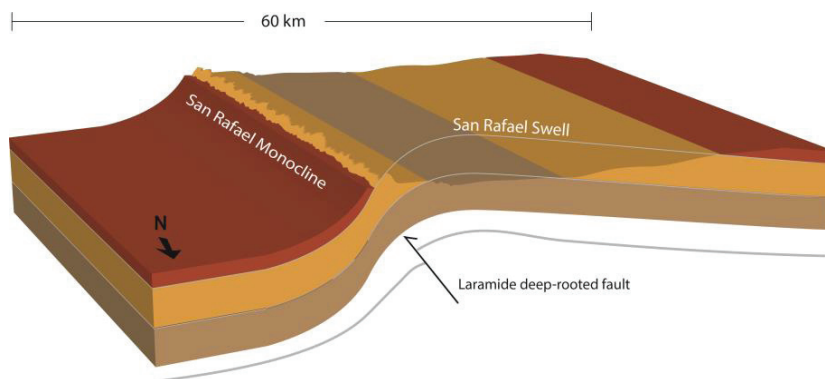


Fig. 3. Conceptual sketch of the structural setting in the study area. The top of the monocline (indicated, white line) is eroded, creating "flat irons" along the eastern flank. The Jurassic stratigraphy (i.e. the Kayenta, Navajo, Page, Carmel Entrada and Curtis formations) is exposed in cross cutting gullies perpendicular to the N-S striking fold axis. Simplified here, indicating only the contact between seal (Carmel Fm.) and underlying aquifer (Page). An ault propagation fold and subsurface geometries after Zuluaga et al. [8].

3. Geochemistry

The sand- and silt-fraction framework grains in the Carmel Formation at the study site mostly consist of quartz and K-feldspar. In the clay fraction sericite (micro-mica) and illite are dominant. Illite also occurs as grain coatings. Furthermore, pore filling, fibrous hematite aggregates are abundant (Fig. 4a). Accessory minerals are plagioclase, ilmenite, rutile, apatite and sylvite. Rare-earth elements are found in the shape of monazite and gibbsite. The sample is pervasively carbonate-cemented. Dolomitization of calcite is observed as rhombic alterations (Fig. 4b). The relative volumetric proportions are similar, as illustrated in Fig. 2: white (Ca) versus blue overprint (Mg + Ca). Quartz and feldspar overgrowths predate the last generation of carbonate cementation.

Element maps from SEM analysis are used as proxy for the spatial volumetric distribution of minerals in the sample. Mg and Ca (blue) are mainly carbonate-cemented areas (calcite and dolomite). Ti (red) is present in rutile and ilmenite. Ilmenite appears as yellow due to overlap with Fe (green). Remaining Fe distribution is mostly oxides (hematite), but also some minor clay (e.g. chlorite). In hand specimen the reaction front is very evident (Fig. 2). However, in SEM it is not obvious, making sample navigation difficult. Comparison of definitely red areas and definitely bleached areas reveals small differences in Fe (oxide) content in SEM images, however evident in thin section. The aggregates are porous and have low density per area (Fig. 4a). There are, however, noticeably smaller amounts of carbonate cement in bleached samples (Fig. 5). There is a clear correlation between grain size and carbonate cementation, fine grained strata are more cemented (Figs. 3b, 5c).

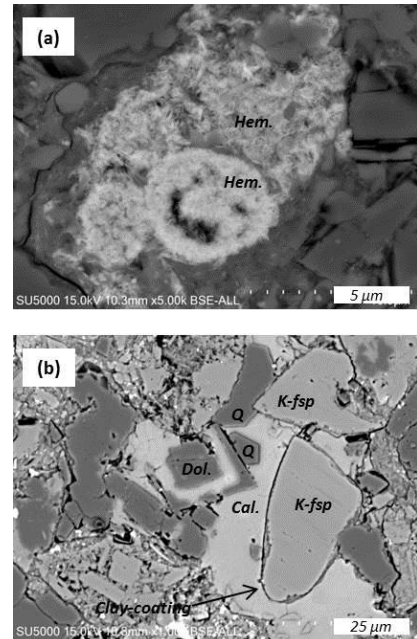


Fig. 4 Photomicrographs from SEM analysis of thin section (Fig. 2) (a) Pore filling hematite aggregate. (b) Poikilotopic calcite cement, dolomitization, quartz overgrowth, illite coated K-feldspar framework grains.

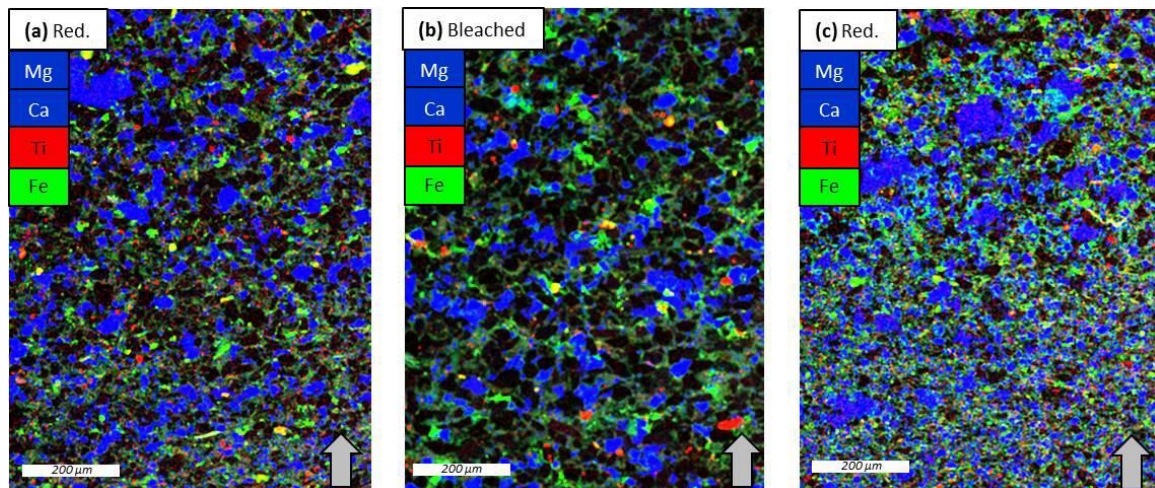


Fig. 5. Element analysis by SEM. Images are oriented according to stratigraphic up (arrow). Element coloration is used as proxy for volumetric mineral content (%) in the sample points. Mg and Ca (blue) are mainly carbonate cemented areas (calcite and dolomite). Ti (red) is present in rutile and ilmenite. Ilmenite appears as yellow due to overlap with Fe (green). Remaining Fe distribution is mostly oxides (hematite), but also some minor clays (e.g. chlorite). (a) Sample from red area 26 % carbonate cement (blue) (b) Sample from bleached area 19 % carbonate cement (blue) (c) Sample from fine grained red area, more patchy cement distribution.

Petrographic studies support deposition in a sabkha environment [3], with salt precipitation and earth profile minerals. Further, diagenetic evidence of quartz overgrowth is indicative of deep burial as proposed by Petrie [6].

4. Fluid migration

Reducing fluids that circulated through permeable layers, fractures and faults in the Jurassic strata of Utah are interpreted to originate from deeper seated natural gas accumulations and also from mantle sourced CO₂ [9, 10]. Dissolution of methane and/or CO₂ in water produces acid which increases the reduction potential of fluids. Both light (CH₄ enriched) and dense (CO₂ enriched) reducing fluids are observed to cause bleaching in reservoirs and along faults in Utah [10]. However, for bleaching to occur, chemical dissolution and subsequent mass removal of solid phase Fe must be facilitated, by advection and/or diffusion. The plume migration into the Carmel Formation predicted from bleaching displays an inverted funnel shape, indicating fluid flow along the base of the Carmel Formation and upwards through an E-W striking fracture (Fig. 1). Evidence of flow along the base of the low permeability layer indicates that the fluid was denser than resident formation water, which would be consistent with a CO₂ charged brine, sourced laterally and/or from below. The question posed is how a dense fluid was driven upwards into and along the fracture (bleaching wall rock), perpendicular to very fine grained, low permeability strata. One possible explanation is that the observed fracture, interpreted to have formed late in the folding phase [8], opened by compressive stress that also compacted pore space and thereby forced fluid escape. In the case of a buoyant fluid there would also be an advective flow component towards a conductive vertical fracture.

4.1 Modeling

We examined a convective-diffusive process in the porous media, considering mixing in a two-component system composed of water and CO₂. The simulation study was performed using the commercial multicomponent simulator Eclipse 300 [11] with fully implicit solution method and the CO2STORE option. The diffusion process is restricted to the gas phase with a diffusion coefficient of 1.15×10^{-8} m²/s. The calculations of liquid- and gas-phase partitioning for CO₂ and H₂O are performed using a 2-component Soave-Redlich-Kwong (SRK) cubic equation of state (EOS) in the numerical simulator.

The model domain is a 2D synthesis Cartesian block-center grid with a length of 1 and 0.5 m in x and y direction respectively. The model comprises three distinct regions: Region # 1 is composed of a low permeability (0.01 mD) block initially saturated with water. Region # 2 represents a fracture domain of high conductivity (100 D). Region # 3 has similar rock properties as region # 2 but initially saturated with CO₂ at connate water saturation. The domain is divided into 204 grid blocks with grid refinement close to the fracture to avoid abrupt changes of the fluxes. A schematic illustration of the domain is shown in Fig 6.

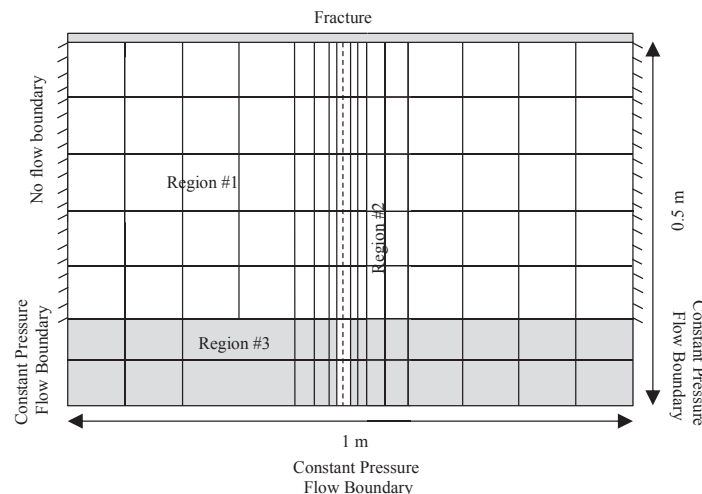


Fig. 6: Model set up for numerical modelling tests. Grid domain has 250 cells. The reactive plume is represented in region #3 (Carmel Fm.). Overlying region #1 is inactive, whereas the fluid conducting fracture (Fig. 1) is represented by a high permeability zone in region #2.

Simulation was run over a period of 200 hours. However, the simulator reported to be unable to solve the system of equations. This problem can be caused by varying pore volumes, but more likely due to small compressibility of fluids and the boundary conditions applied in the simulation set-up. In fact, these boundary conditions require a geomechanical model capable of capturing pore volume variations. Lacking this feature, the pressure tensor cannot be solved properly as the volume of entering/passing from one grid cell to the grid cell adjacent is not balanced.

5. Discussion

At the study site, bleaching, chemical mass removal and migration of reducing fluids in the Carmel Formation is interpreted to have taken place during the last phase of San Rafael Swell folding at the study site, corresponding temporally to the opening of E-W trending fracture corridors (joint swarms). Previous studies have proposed that reducing fluids originated from diffusive leakage charged by underlying units. We propose a structurally induced pressure gradient during deformation as the main driving force for advective transport. Reducing fluids may have been sourced both from below and laterally (Fig. 7). During folding, compressive stress compacted pore space and thereby forced migration of fluids. Without a geomechanical reasoning, recreating the inverted funnel fluid plume geometry by numerical modelling, whether denser or lighter than connate water, does not seem feasible.

Impact of reducing fluids are observed in over- and underlying strata, as extensive bleaching of entire beds or associated with fractures. Several tectonically driven events of fluid migrations may have occurred before complete uplift and erosion [12]. The properties of CO₂ charged brine in a high temperature, high pressure regime would be less viscous and lighter, and the chemical reactivity higher in a deep, compressed reservoir/seal-system compared to surface conditions or a tectonically dormant setting. *In situ* fluid properties may have facilitated migration into and within a low permeability unit. The Carmel Formation is commonly considered a regional sealing unit above permeable aquifers [13, 14], and also considered a suitable cap rock for CO₂ storage [15]. It seems, however, that under high pressure leakage may occur into this unit not only through fractures, but into sealing lithologies. This requires that the capillary pressure is overcome.

The reaction fronts are very sharp, indicating relatively rapid net removal of Fe. This conforms to lateral, advective transport as the dominant mechanism rather than vertical diffusion in the low permeability host rock. However, reaction fronts are cutting straight across sedimentary lamina (Figs. 2 and 8), which is more typical of diffusion driven transport. Either advection dominance or rapid reactions depleting the diffusive front of Fe created a sharp front. Flow separation may have been introduced by a density difference between formation water and reducing fluid during venting as the fracture opened, with diffusion zoning extending beyond the advective front, given rapid diffusion rates and high reactivity.

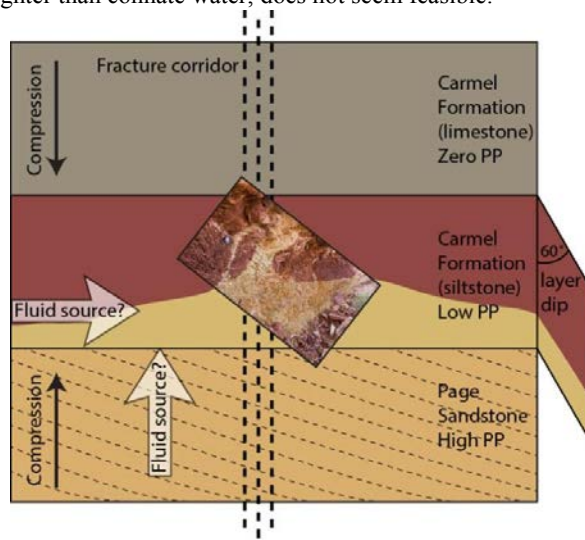


Fig. 7. Conceptual model of fluid migration within the Carmel Formation from plume geometries observed in the study area (Fig. 1). Flow towards and upwards in fracture corridor, diffusive and advective transport through and along the base of low permeability strata.



Fig. 8. Detail photo from the field locality, showing upwards and/or outwards moving "blobs" along small fractures. Sharp reaction fronts mostly cut straight across sedimentary strata. Grey arrow points to stratigraphic up. One layer parallel front is seen (encircled).

On macro-scale (field location and hand specimen) bleaching is obvious, clearly indicating that that pore-filling and grain-coating iron oxides have been removed. But the mass fraction difference of Fe is very small. However, previous studies suggest that as little as 0.1 wt. % Fe-removal can cause bleaching, so image analysis (SEM) or XRD may not be sufficiently accurate. There is work in progress for more precise mineral estimates across the interphase in order to solve the chemical mass balance. However, we document less carbonate cement in bleached, diagenetic facies, and more carbonate cement in fine grained, less permeable layers, indicating carbonate dissolution by a migrating fluid.

5. Conclusion

Reservoir conductivity and cap rock efficiency are not only a question of spatial properties (i.e. porosity and permeability in pores and fractures) linked to sedimentary facies. Transient *in situ* pressures and temperatures of the reservoir will cause temporal changes in fluid viscosity and relative permeability. The same geological unit may behave as a conduit during some parts of burial/uplift-history and as a sealing unit at other times.

In order to better understand this system, advanced analyses of couple geochemical models for diffusion with multiphase flow in advective transport and fluid separation are required. Further, geomechanical models for pore space reduction triggering pressure gradients are of importance. This work is in progress within the COPASS project and will serve as a valuable analogue in research targeting CO₂ storage and potential seal bypass.

Acknowledgements

This work forms part of the CO₂ seal bypass project (COPASS) which is funded by the Research Council of Norway (RCN) under grant number 244049. Also we acknowledge cooperation with the SUCCESS research centre (grant number 193825/S60, RCN), and thank Schlumberger for software license-grants. We are grateful for the help by Berit Løken Berg in SEM analyses. The scanning electron microscope used was JEOL JSM 6460LV at the University of Oslo.

References

- [1] Beitler, B., Parry, W. T., and Chan, M. A. (2005). Fingerprints of fluid flow: chemical diagenetic history of the Jurassic Navajo Sandstone, southern Utah, USA. *Journal of Sedimentary Research*, 75(4), 547-561.
- [2] Gilluly, James, and Reeside, J.B., Jr., 1928, Sedimentary rocks of the San Rafael Swell and some adjacent areas in eastern Utah, IN Shorter contributions to general geology, 1927: U.S. Geological Survey Professional Paper, 150-D, p. D61-D110.
- [3] Blakey, R.C., Peterson, F., Caputo, M.V., Geesaman, R.C., and Voorhees, B.J. (1983), Paleogeography of Middle Jurassic continental, shoreline, and shallow marine sedimentation, southern Utah, in Reynolds, M.W., and Dolly, E.D., eds., *Mesozoic Paleogeography of West-Central United States*: Society of Economic Paleontologists and Mineralogists. Rocky Mountain Section, Symposium, v. 2, p. 77-100.
- [4] Jones, L. S., and Blakey, R. C. (1993). Erosional remnants and adjacent unconformities along an eolian-marine boundary of the Page Sandstone and Carmel Formation, Middle Jurassic, south-central Utah. *Journal of Sedimentary Research*, 63(5).
- [5] Thompson, A.E., and Stokes, W.L., (1970), Stratigraphy of the San Rafael Group, southwest and south central Utah: *Utah Geological and Mineral Survey Bulletin*, no. 87, 53 p.
- [6] Petrie, E.S., Evans, J.P. and SJ Bauer, (2014), Failure of cap-rock seals as determined from mechanical stratigraphy, stress history, and tensile-failure analysis of exhumed analogs. *AAPG Bulletin*, v98 no 11 pp 2365-2389
- [7] Fossen, H., Schultz, R.A. Shipton, Z.K. and Mair, K. (2007) Deformation bands in sandstone: a review. *Journal of the Geological Society* 164, no. 4: 755-769.
- [8] Zuluaga, L. F., Fossen, H., and Rotevatn, A. (2014) Progressive evolution of deformation band populations during Laramide fault-propagation folding: Navajo Sandstone, San Rafael monocline, Utah, USA. *Journal of Structural Geology*, 68, 66-81.

- [9] Loope B., Kettler M., and Weber K. (2010), Follow the water: Connecting a CO₂ reservoir and bleached sandstone to iron-rich concretions in the Navajo sandstone of south-central Utah, USA: *Geology*, v. 38, p. 999–1002, doi: 10.1130/G31213.1.
- [10] Wigley, M., Kampman, N., Dubacq, B., and Bickle, M. (2012). Fluid-mineral reactions and trace metal mobilization in an exhumed natural CO₂ reservoir, Green River, Utah. *Geology*, 40(6), 555-558.
- [11] Schlumberger (2012) Eclipse 300 Compositional. <http://www.software.slb.com/products/eclipse/>
- [12] Sundal, A., Petrie, E., Hellevang, H., Midtkandal, I and Braathen, A. (2016) Reactive fluid expulsion during progressive deformation in the fold limb of the san rafael swell, utah, usa. GSA Annual Meeting in Denver, Colorado, USA. Session No. 171, 26.09.2016, T212. Multifaceted Approaches to Understanding Fluid-Fault Interactions in Natural Resources and Geologic Hazards (Posters)
- [13] Trimble, L.M. and Doelling H.H. (1978) *Geology and uranium-vanadium deposits of the San Rafael River mining area; Emery County, Utah. Utah Geol. Mineral. Surv. Bull.*, 113 (1978), p. 112
- [14] Rocam X.A. (2003) Tectonic and sequence stratigraphic implications of the Morrison Formation-Buckhorn Conglomerate transition, Cedar Mountain, East-Central Utah. Unpublished Master Thesis Ohio University. 222 pp.
- [15] Payne, W.G., Mozley, P.S., Sprinkel, D.S., and Campbell, A.R. (2011) Controls on Porosity and Permeability Within the Carmel Formation: Implications for Carbon Sequestration* Search and Discovery Article #80185 *Adapted from oral presentation at AAPG Annual Convention and Exhibition, Houston, Texas, USA, April 10-13, 201 http://www.searchanddiscovery.com/documents/2011/80185payne/ndx_payne.pdf

8.3. Abstracts, co-author

8.3.1. Bromander et al. (2018). Vinterkonferansen, Copenhagen.

Bromander, N.¹, Da Costa, S.¹, Skurtveit, E.¹⁻², Evans, J.³, Midtkandal, I.¹, Braathen, A.¹, Zuchuat, V.¹, and Sundal, A.¹ (2018). Regional evaluation of structural collapse in sandstone reservoirs and impact on reservoir quality, a case study from the Entrada Sandstone, Utah, USA.

¹*Tectonostratigraphic Research Group, University of Oslo, Sem Sælands Vei 1, 0371 Oslo, Norway*

²*Norwegian Geotechnical Institute, Sognsveien 72, 0855 Oslo, Norway*

³*Department of Geology, Utah State University, 4505 Old Main Hill, Logan, UT 84322-4505*

Accepted for a poster presentation

POSTER

Regional evaluation of structural collapse in sandstone reservoirs and impact on reservoir quality, a case study from the Entrada Sandstone, Utah, USA

Nikoline Bromander¹, Sigrid Østmo da Costa¹, Elin Skurtveit², James Evans³, Ivar Midtkandal¹, Alvar Braathen¹, Valentin Zuchuat¹ and Anja Sundal¹

¹University of Oslo, Norway, ²Norges Geotekniske Institutt (NGI), Norway, ³Dept. of Geology, Utah State University, Logan, Utah, USA

In this study we examine exhumed paleo-reservoirs showing evidence of past CO₂-charged fluid accumulation to better understand processes related to geological sequestration of CO₂ in subsurface siliciclastic reservoirs. Field data was collected from the wet aeolian dune system in the Jurassic Entrada Sandstone in Utah, USA, and in particular the reservoir characteristics of the light-coloured fluvial and aeolian dune interlayers have been evaluated. Bleaching in red rocks is interpreted to have developed in response to reduction and/or dissolution of iron oxides as CO₂-charged fluids from underlying reservoirs escaped through the sedimentary succession. Some light-coloured, highly porous layers contain extensive amounts of deformation bands, which may be associated with structural collapse.

The working hypothesis is that observed reservoir collapse structures (deformation bands) in specific layers is a regional feature related to sedimentary facies. Deformation band distributions and orientations are used to document reservoir collapse. Deformation bands occur in different structural settings; clusters connected to faults cutting the stratigraphy, single deformation bands exclusively in fluvial and aeolian dune interlayers dying out in the over/underlying facies forming small scale faults in the reservoir, as well as in major meter-scale circular collapse structures. Deformation bands were present in some specific layers throughout the field area, with frequencies from 0 to 18 per meter and the degree of structural

collapse increased towards zones of high deformation, e.g. faults. Preliminary results show that collapse structures are regional features exclusively occurring in two types of facies, with the degree of collapse locally determined by structural parameters.

8.3.2. Da Costa et al. (2018). Vinterkonferansen, Copenhagen.

Da Costa, S.¹, Bromander, N.¹, Zuchuat, V.¹, Braathen, A.¹, Sundal, A.¹, and Midtkandal, I.¹ (2018). Topographic Development as a result of regional incision, faulting, and deposition at the onset of relative sea-level rise; The upper Entrada Sandstone and the lower Curtis Formation, Utah, USA.

¹*Tectonostratigraphic Research Group, University of Oslo, Sem Sælands Vei 1, 0371 Oslo, Norway*

Accepted for a poster presentation

POSTER

Topographic Development as a result of regional incision, faulting, and deposition at the onset of relative sea-level rise; The upper Entrada Sandstone and the lower Curtis Formation, Utah, USA.

*Sigrid Østmo da Costa¹, Nikoline Bromander¹,
Valentin Zuchuat¹, Alvar Braathen¹, Anja Sundal¹
and Ivar Midtkandal¹*

¹University of Oslo

A 43 km North-south section on the North-Eastern margin of the San Rafaell Swell has been studied, focusing on the Upper Jurassic eolian Entrada Sandstone, the J-3 regional Unconformity, and the overlying Curtis Formation of Oxfordian age. Emphasis is on the distribution of sedimentary facies in direct contact with the unconformity, and those affected by erosional topography during deposition.

The J-3 Unconformity displays at least 3 generations of erosive incision, possibly 6. The composite unconformity has been subaerially eroded by eolian and fluvial action, besides tidal denudation postdating the onset of regional deposition. Present-day erosional relief, magnitude, and wavelength contribute to multi-phase erosional processes resulting in inconsistent erosional patterns, and distribution of sedimentary facies above and below the unconformity. Tectonic activity has influenced the development concerning substratum fluidisation and brittle deformation.

Generations of J-3s erosive incision varies regionally and locally across the section. A series of 5-10 m deep channel-like scours linked to a stratigraphic level several meters above the J3 Unconformity, erode to a deeper stratigraphic level than J3s original level. Intra-formational faults in Entrada Sandstone suggest contribution to focused erosion at the Entrada-Curtis boundary.

Similarly, erosive lower boundaries of tidal sandstone bodies in direct contact with J3 suggest that repeated relative sea-level changes lead to deeper stratigraphic erosion of the J3 Unconformity.

The on-going investigation will improve constraints on how reservoir-quality sandstone volumes are affected by erosional topography in tidal environments, by determining distributional factors. Distinguishing between local and regional variability is a target, to filtrate basin-specific anomalies.

8.3.3. Halvorsen et al. (2018). Vinterkonferansen, Copenhagen.

Halvorsen, K.¹, Tveterås, S.¹, Braathen, A.¹, Midtkandal, I.¹, and Zuchuat, V.¹ (2018). Sand tectonics - sand mobility linked to faulting and the influence on depositional systems.

¹*Tectonostratigraphic Research Group, University of Oslo, Sem Sælands Vei 1, 0371 Oslo, Norway*

Accepted for an oral presentation

ORAL

Sand tectonics - sand mobility linked to faulting and the influence on depositional systems

Kristine Halvorsen¹, Susanne Tveterås¹, Alvar Braathen¹, Ivar Midtkandal¹ and Valentin Zuchuat¹

¹*University of Oslo*

Mobility of sand by fluidisation, so-called sand tectonics, can drive surface movements and implicitly have a significant impact on sediment distribution and sand body geometries. Although similarities between sand- and salt tectonic-related structures exist, substantial differences in deformation style and geometries occur. We address the understanding of sand tectonic processes. Three outcrops in the Upper Jurassic Entrada Sandstone and Curtis Formation in Utah (USA) have been used to characterise the structural and sedimentary response to the underlying mobilisation of sand. Key observations are assembled from mapping of sag-upwarp and fault geometries, as well as from logging and description of growth succession. The latter deposits attest to channelised sub- to inter-tidal depositional environments. Data show that mild sand mobilisation results in meter-scale gentle sag and upwarps (sand pillows). Increased sand mobility leads to progressively higher and steeper relief between upwarps and sags, which links to nucleation of faults and thereby development of small fault-bound grabens. During fault activity, growth sequences attest to repeated fault movement events, demonstrating the strong structural control on the basin fill. After graben formation, many of the faults in higher positions of the grabens are truncated and removed by erosion. Subsequent lenticular-shaped basin fill reflects a wider channelized depositional body than that of the grabens. However, the grabens seem important in locating

these channels. The result from our analysis may provide important input applicable to both CO₂ storage operations and the petroleum industry.

8.3.4. Midtkandal et al. (2017). International Meeting of Sedimentology, Toulouse.

Midtkandal, I.¹, Zuchuat, V.¹, Braathen, A.¹, Sundal, A.¹, and Evans, J.² (2017). Syn-sedimentary Subsurface Liquefaction and Collapse; Injectites, Pseudo-Channels and Pseudo-Clinoforms in the Jurassic Entrada and Curtis Formations, Utah, USA.

¹*Tectonostratigraphic Research Group, University of Oslo, Sem Sælands Vei 1, 0371 Oslo, Norway*

²*Department of Geology, Utah State University, 4505 Old Main Hill, Logan, UT 84322-4505*

Accepted for an oral presentation

SYN-SEDIMENTARY SUBSURFACE LIQUEFACTION AND COLLAPSE; INJECTITES, PSEUDO-CHANNELS AND PSEUDO-CLINOFORMS IN THE JURASSIC ENTRADA AND CURTIS FORMATIONS, UTAH, USA

Ivar MIDTKANDAL^(1,@), Valentin ZUCHUAT⁽¹⁾, Alvar BRAATHEN⁽¹⁾, Anja SUNDAL⁽¹⁾, James EVANS⁽²⁾

⁽¹⁾ Department of Geosciences, University of Oslo (Norway)

⁽²⁾ Utah State University (United States)

[@] ivar.midtkandal@geo.uio.no

Intra-formational collapse features and sand injectites in the Jurassic Entrada Sandstone are linked to unusual channel-and clinoform-like features in cliff sections belonging to the overlying Curtis Formation. At first sight, large-scale features appear to represent conventional sedimentary architecture such as channel incision and clinoform development. Close inspection reveals syn-sedimentary subsurface collapse and sag of intra-Entrada Sandstone and/or Curtis Formation beds caused the features, rather than a sedimentary response to channelized transport and basin deepening.

The middle to upper Jurassic succession in eastern Utah is composed of widespread units with moderate lateral variation on a regional scale. Above the well-known Navajo Sandstone, the Page Sandstone, the Carmel Formation, the Entrada Sandstone, and the Curtis and Summerville formations follow in successive order. Recent years' field campaigns has revealed a number of intra-formational collapse features, injectites and faults within the Entrada and Curtis formations, which may be explained by liquefaction of water-laden subsurface strata at the time of collapse. The collapse features and sand-injectites in the Entrada Sandstone are contained within its upper Earthy Facies, a wet aeolian/inter-dune depositional unit with immature soil profiles. These are preserved as towering sandstone pillars in today's landscape, due to their differential cementation that resulted in increased resistance to weathering and erosion.

Intra-Curtis Formation features resemble channels and clinoforms (hence the pseudo-prefix), but formed in response to local syn-sedimentary sagging, driven by mobilization/liquefaction of older marine mud within the same unit, or by the same mechanisms as in the underlying Entrada Sandstone. A combination of the two is possible. The channel-like features do not show erosion into older beds, but appear to be passively draping a miniature sag basin. Either side of the sag feature is characterized by a dense set of 5-15 cm offset faults with several syn-sedimentary features such as small growth packages and intense climbing ripple lamination across small escarpments. Asymmetric fault geometries on opposing sides indicate slight lateral tectonic rafting during development. A clinoform-like succession resembles sedimentary architecture normally associated with delta mouth-bar deposition, but is actually a series of faulted sand-and mudstone beds with sediment transport "upstream", which appears to represent a larger-scale version of the aforementioned channel-like feature. Both depositional environments are interpreted to represent sub-to intertidal sand flats.

On-going efforts to characterize and date cement in the collapse breccia is expected to improve constraints on timing of events, and thus strengthen or contradict the working hypothesis that suggests linked mechanisms.

8.4. External collaborations

8.4.1. *Petrarc project* (same affiliation address for all three entries)

Sleveland, A.R.N.¹, Zuchuat, V.¹, Midtkandal, I.¹, van Soelen, E.E.¹, Twitchett, R.J.², Hammer, Ø.³, Planke, S.¹⁻⁴⁻⁵, and the Deltadalen Study Group (in prep.). High-resolution stratigraphic analyses of Permian-Triassic core material in Deltadalen, Central Spitsbergen.

¹*Tectonostratigraphic Research Group, University of Oslo, Sem Sælands Vei 1, 0371 Oslo, Norway*

²*Earth Sciences Department, Natural History Museum, Cromwell Road, London SW7 5BD, UK*

³*Natural History Museum, University of Oslo, Sars gate 1, 0562 Oslo, Norway*

⁴*CEED, Department of Geosciences, University of Oslo, Sem Sælands Vei 1, 0371 Oslo, Norway*

⁵*Volcanic Basin Petroleum Research, Oslo Science Park, Gaustadalléen 21, 0349 Oslo, Norway*

Sleveland, A.R.N.¹, Zuchuat, V.¹, v. Soelen, E.E.¹, Twitchett, R.J.², Midtkandal, I.¹, Svensen, H.⁴, Planke, S.¹⁻⁴⁻⁵ (2018) Sedimentation across the end-Permian mass extinction event and the recovery of benthic biota, revealed by two shallow cores from Central Spitsbergen, Svalbard, International Sedimentological Congress, Québec City.

Sleveland, A.R.N.¹, Planke, S.¹⁻⁴⁻⁵, Zuchuat, V.¹, Franeck, F.¹, Svensen, H.⁴, Midtkandal, I.¹, Hammer, Ø.³, Twitchett, R.², & the Deltadalen Study Group (2017). High-resolution stratigraphic analyses of Permian-Triassic core material recovered in central Spitsbergen, EGU, conference abstract, Vienna.

8.4.2. *Trias North project*

Three dimensional sedimentary architecture of a prograding tide-influenced deltaic system on SW Edgeøya, Svalbard

Anell, I.¹, Røhnert, D.², Zuchuat, V.¹, Smyrak-Sikora., A.³, Ogata, K.⁴, Osmundsen, P.T.⁵, Olaussen, S.³, K., Maher, H.⁶, Klausen, T.K.⁷, Husteli, B.⁵, Midtkandal, I.,¹ Braathen, A.¹ (in prep.)

¹*Tectonostratigraphic Research Group, University of Oslo, Sem Sælands Vei 1, 0371 Oslo, Norway*

²*Faculty of Geosciences, University of Bremen, Klagenfurter Str. 2-4, 28359 Bremen, Germany*

³*Arctic Geology Department, The University Centre in Svalbard, Svalbard Science Centre, N-9171 Longyearbyen, Norway*

⁴*Department of Earth Sciences, VU University Amsterdam, De Boelelaan 1085, 1081 HV Amsterdam, The Netherlands*

⁵*Norges Geologiske Undersøkelse, Leiv Eirikssons vei 39, 7040 Trondheim*

⁶*Department of Geography & Geology, 6001 Dodge Street, Durham Science Center, Omaha, NE, USA*

⁷*Department of Earth Science, University of Bergen, Allégaten 41, 5007 Bergen, Norway*

8.5. Teaching and supervision

8.5.1. Master thesis co-supervision, University of Oslo:

Da Costa S. (2018). The complexity of regional erosion; incision, faulting, and deposition during the development of the J-3 unconformity, Utah, USA. University of Oslo.

Halvorsen, S. (2018). Sand tectonics – sand mobility linked to faulting and the influence on depositional systems. University of Oslo.

Tveterås, S. (2018). Fault style and deformation mechanisms caused by sand mobility in the Entrada Sandstone and Curtis Formation, Utah, USA. University of Oslo.

8.5.2. Guest lecturer, University of Oslo:

GEO4280: Sequence Stratigraphy and Basin Dynamics

GEO4216: Sedimentology and Sequence Stratigraphy